國立台灣大學工學院土木工程學系
碩士論文
Department of Civil Engineering
College of Engineering
National Taiwan University
Master Thesis

# 傾斜地層場址的
# 地盤反應之數值模擬
# Numerical Modeling of Ground Response for Sites with Inclined Soil Layers

楊致榮
Zhi-Rong Yang

指導教授: 郭安妮 博士
Advisor: Annie On-Lei Kwok, Ph.D.

中華民國 108 年 7 月
July, 2019

**doi:10.6342/NTU201903794**

# 誌謝

在這兩年進入台大大地組之後，學到了許多東西也交到了許多朋友，感謝郭安妮老師一路上細心的指導，充實我關於大地地震工程的專業知識，也透過老師的指教讓我的英文論文一點一滴的產生，非常謝謝老師的指導，另外也感謝一路陪伴到研究所的朋友們以及大地組的夥伴們，修課的時候一起奮鬥，放鬆的時候也一起歡笑，令我在學習之路上跟大家一起成長了許多，謝謝大地組夥伴們這兩年來的陪伴，祝我們都未來順利、一帆風順。

doi:10.6342/NTU201903794

# 摘要

在大地工程中，地震所造成由下往上的波傳往往對地面上造成嚴重的災害，振動波傳經過不同地地層條件，例如: 土層密度、土壤剪力波速、不同土層間的傾斜角度...等等，都會造成放大或是縮小的效果，對原本預期的結果產生了更為嚴重災害危害我們的安全，此種效應被稱之為場址效應，本研究主要是探討不同的地形幾何條件、傾斜角度，邊界條件下所造成的場址效應以探討土壤的線性以及非線性行為。

在真實地盤中，土壤的性質極為複雜，為了簡化模擬時獲取土層參數的困難性，我們將土層視為好幾區均質土壤的結合，當土壤材料在小應變的情形下，我們將土壤的行為視為線彈性體，土體仍然保持著線彈性行為，當我們進行動態分析的模擬時，雷利阻尼通常被設置在土體材料模擬土壤的消能反應，然而，當土體的剪力變變形過大的時候，土體由線彈性轉換為塑性，除了雷利阻尼以外也需要利用遲滯阻尼來模擬非線性的土壤消能行為，以便數值模擬的分析，本研究透過上述的不同土層材料條件，經由 FLAC 2D 7.0 軟體配合 DEEPSOIL 軟體驗證，歸納出場址效應所造成對地表面的影響以及在地震時後，所可能發生災害的危險區域。

關鍵字: 場址效應、傾斜地盤、邊界條件、剪力波速、放大因子

doi:10.6342/NTU201903794

# Abstract

In geotechnical engineering practice, the seismic wave propagation from bottom to the ground surface often cause damaging disasters on the ground. Vibration waves pass through different stratigraphic conditions, such as soil layer densities, soil shear wave velocities, and tilt angle between different soil layers etc., would cause amplification or declination of site response. The effect is so-called site effect.

This study mainly discusses different geological conditions to explore the tendency of ground motion. In the real site, the nature of the soil is extremely complicated. In order to simplify the difficulty of obtaining soil parameters during the simulation, we regard the soil layer as a combination of several homogeneous soils. With small shear strain of soil material, the behavior is regarded as a linear elastic body, and the soil performs elastic linearity. In dynamic analysis, Rayleigh damping is usually assigned in the soil material to simulate the energy dissipation of soil. However, with larger deformation, the behavior of soil convert linear elasticity into plasticity. It is also necessary to use hysteretic damping to simulate nonlinear soil energy dissipation in numerical simulation.

The study summarizes the results of different soil conditions, developing the trend affected by the influence of site effect. Also, evaluating the most dangerous region of the basin while earthquake occurred.

**Keywords**: site effect, Basin effect, inclined soil layers, shear-wave velocity, amplification factor

doi:10.6342/NTU201903794

# Table of Contents

doi:10.6342/NTU201903794

# List of Figures

doi:10.6342/NTU201903794

doi:10.6342/NTU201903794

doi:10.6342/NTU201903794

doi:10.6342/NTU201903794

doi:10.6342/NTU201903794

# List of Tables

doi:10.6342/NTU201903794

# Chapter 1 Introduction

## 1.1 Motivation

Taiwan is located at Pacific Rim Seismic Belt, and this is reason why Taiwan had suffered such many earthquake catastrophes. Ground motion would be affected by directly wave propagation pass through different soil conditions, such as soil properties, local site geometry, boundary conditions. It is so-called site effect. Due to site effect, ground response might be amplified or de-amplified, caused much more severe results harmful to our life. So evaluate ground site response is an important part of predicting how ground motion works. In the research, applying different site geometry, inclination of soil layers and boundary conditions, like rigid base and compliant base to analysis soil linear elastic and nonlinear soil behaviors of site response.

## 1.2 Research Objective and Methodology

The objective of this study is to evaluate the influence of different boundary conditions and soil layers inclinations on site response. Soil model parameters that are required for specification in site response analysis include shear wave velocity, unit weight of subsurface material, Poisson’s ratio, strain-dependent material curves (modulus reduction and damping ratio), etc… In time domain analysis, Rayleigh damping was used in the analysis of linear elastic continua to damp the natural oscillation modes of the system in dynamic analysis when small shear strain occurred.

doi:10.6342/NTU201903794

Element tests are executed with different soil parameters of numerical simulation model for fitting the modulus reduction and damping curve to figure out the coefficient of nonlinear soil model. To quantify the amplification factors, we consider different types of inclined angles, boundary conditions, and input motion. Specify Nahanni earthquake seismic motion to the bottom boundaries (rigid, compliant base) to perform upward wave propagation pass through different inclined soil intersection. To conduct the site response, FLAC 2D 7.0, which is a finite difference method (FDM) commercial methodology, is executed in the research to construct the two-dimensional plane-strain numerical models. Lastly, we develop the method to predict most dangerous region of inclined basin when earthquake arose.

# Chapter 2 Literature Review

In chapter 2, previous studies on local site effect of the basin or inclined ground geometry would be reviewed. Therefore, the method of analyzing seismic site response would be performed in literature review. Furthermore, the concepts of amplification factors might be introduced.

## 2.1 Site effect on ground motion and amplification factors

Site effect has significant influence on ground motion induced by seismic wave. When directly wave propagation passes through different underground components, the amplitude of site response might be changed. Moreover, frequency content and acceleration history of soil model wouldn’t be equal as previous prediction. And it is so-called site effect. This phenomena might increase the strength of incident seismic motion and strengthen the impact on affected region and structures (J.F. Semblat et. al, 2004). Simple definition of the amplification factors of site effect is comparing the response of underground through surface caused by directly seismic wave propagation. By using the method of Fourier transform and response spectrum analysis of spectral acceleration, the influence of site effect can be demonstrated distinctly.

In engineering practice, the magnitude of earthquake is correlated to local site effect. Different ground topography and soil densities would lead to significant amplification and remarkable energy dissipation of wave propagation. This is the reason why in the

doi:10.6342/NTU201903794

current studies, we had pay much more attention on the influence of local site conditions on the seismic ground motion like inclination intersection of soil, different shear-wave velocity and site geometry after strong earthquake occurred. For instance, Meinong earthquake, 2016, due to the site effect, the vibration of ground surface in the Jianan plain is much more intense than that in the adjacent area of Meinong district. In addition, the earthquake source itself accompany with seismic wave radiation, which be one kinds of wave conduction. There wouldn’t be same vibration in each direction of the earthquake source, however, the radial distribution of vibration energy. In Meinong earthquake, the region located at the western side had been severely damaged.

Furthermore, take ChiChi earthquake, 1999, for example, which was one of severe natural catastrophes in Taiwan history, the epicenter located in Nantou, Chichi, and magnitude was the seven point five level. Normally, as approach as the epicenter, the intensity of ground motion and damage would be larger. However, seismic intensity, recorded in Taipei, was stronger than adjacent city. The significant reason is the ground geometry and subsurface properties of the underlying material in Taipei basin. Even though Taipei is far away from epicenter of ChiChi earthquake, as a result of site effect, seismic wave propagation had transmitted from stiffer rock layer to softer soil of basin. This indication amplifies site response of motion, also have been correlated to damage distribution during destructive earthquakes occurred.

doi:10.6342/NTU201903794

## 2.2 Previous studies on impact of subsurface geometry on ground motion

### 2.2.1 Observations/Empirical Studies

The earthquake-induced ground motion depends on the shake intensity, distance of epicenter and fault of the earthquake. Generally, local site effects researches suppose that geometry of soil layers were horizontal. However, the site response is sensitive to combinations of impedance contrast, thickness of sedimentary layers, and inclination of plane intersection and side boundary conditions. Gouveia (2016) had mentioned the impact of stiffness and interface of slope between layers on seismic response of the soil. Two types of bi-dimensional simulation model were introduced: horizontal stratification and dipping soil interface between layers (shown as Figure 2.1), for evaluating that how site response and ground motion strongly depend on soil properties, inclined intersection layers and soil stiffness. The results of the study demonstrate that soils with the non-horizontal stratification accompany with higher amplification factors, however, the response in transfer functions wouldn’t strengthen as the tilt angles increase (Figure 2.2). And it also verifies the declination of resonance frequencies and amplitude of transfer functions with increasing PGA of input motion (Figure 2.3). Gouveia also mentioned this phenomenon might be one kinds of soil nonlinearity. The research cases with lower shear-wave velocity, mean softer layers, are relatively insensitive to the variation of the

doi:10.6342/NTU201903794

ground parameters and site geometry, essentially due to the filtering effect of the waves in the softer soil.

### 2.2.2 Numerical modeling

Dynamic properties of the subsurface soil are intensively dependent on the level of deformation induced by the seismic wave. With small levels of element deformation, such as in seismic dynamic analysis, soils perform linear elastic behavior, otherwise, for higher levels of distortion the site response is nonlinear and dependent of the number of stress loading cycles. In geotechnical engineering practice, finite difference method is a common numerical method used for dynamic analysis. This method can be easily constructed than finite element method does. The theory of FDM (finite different method) is based on mathematical discretization of the equations of boundary problems. By this method, continuous calculate process can be applied in series of short durations. In these intervals, the function is approximated by approximate expressions. Therefore, each interval of finite element would be the integration, with the results in the previous interval are considered as initial for the next time interval.

To describe the finite difference method, the example of one-dimensional wave propagation is performed in the following figure. The difference elements are illustrated in Figure 2.4. The differential equations for a solid, one-dimensional soil bar of density (ρ) and Young’s modulus (E) are given as constitutive law follows:

doi:10.6342/NTU201903794

$$\sigma_{xx} = E\frac{\partial u_x}{\partial x} \tag{2.1}$$

The law of motion is

$$\rho\frac{\partial^2 u_x}{\partial t^2} = \frac{\partial \sigma_{xx}}{\partial x} \tag{2.2}$$

The bar is assumed to be unconfined laterally and is discretized into several equal finite difference elements. The central finite difference equation correlates to Equation 2.1 for a typical element *i* given by Equation 2.3.

$$\sigma_{xx}^{i}(t) = E\frac{u_x^{i+1}(t) - u_x^{i}(t)}{\Delta x} \tag{2.3}$$

Whereas t represents the time at which quantities are evaluated and the superscript, *i*, means the element number. The equation of the element motion is similarly discretized for grid point *i* that shows the velocity and displacement in Equation 2.4 and 2.5 respectively.

$$\dot{u}_x^{i}\left(t + \frac{\Delta t}{2}\right) = \dot{u}_x^{i}\left(t - \frac{\Delta t}{2}\right) + \frac{\Delta t}{\rho\Delta x}\left[\sigma_{xx}^{i}(t) - \sigma_{xx}^{i-1}(t)\right] \tag{2.4}$$

$$u_x^{i}(t + \Delta t) = u_x^{i}(t) + \dot{u}_x^{i}\left(t + \frac{\Delta t}{2}\right)\Delta t \tag{2.5}$$

In this method, the quantities on the right-hand sides of all difference equations are performed. Therefore, the Equation 2.3 must be applied to all grid zones before calculating the Equation 2.4 and 2.5, which are evaluated for all grid points. Conceptually, this process for computation is equivalent to a simultaneous update of material variables.

## 2.3 Ground response analysis

doi:10.6342/NTU201903794

### 2.3.1 Ground response in one-dimensional analysis vs. multi-dimensional analysis

Seismic wave propagation induced by earthquake from the bedrock to ground surface would pass through underground deposit. This is reason from how site response of ground surface arise. However, softer soil material perform as wave filter and rebuild site response characteristics, including change of response amplitude, resonant frequencies, and shake duration, etc… Because of filtering effect, strength of wave propagation would be modified as amplification or reduction of intensity.

In reality, earthquake induced motion would be multi-dimensional purpose. Complex local geology may generate site amplification in soft soils significantly larger than what would be expected. Taking multi-dimensional effect into account seems to have a special practical interest and they should be included in the earthquake engineering practice for analysis of real site response. However, if we consider multi-dimensional effect into numerical simulation, the computation step might extremely increase and cost a lot of time for program computation. To simplify the calculation process of the program, one-dimensional analysis is usually conducted in geotechnical engineering practice. 1D isotropic analysis only allows wave propagation in one-direction and confines another orientation to construct the influence on specific site of direct wave propagation.

Compare one-dimensional with multi-dimensional effect on ground motion, the results in multi-dimensional simulation might be much more in accordance with real site than

doi:10.6342/NTU201903794

1D results. Also, the interaction of multi-dimensional effect to 1D may amplify the isotropic site response in consequence. Although the methods of one-dimensional ground response analysis are easily constructed for the complicated geology with parallel material boundaries, such conditions are not commonly met in reality. Therefore, multi-dimensional seismic response analysis techniques are significantly required for characterizing the real site effect by nature (K.D. Pitilakis et.al, 2015).

### 2.3.2 Response spectrum

In engineering practice, response spectrum method is usually developed for seismic analysis. By this method, we could estimate the variation of wave propagation passing through different soil media and determine the maximum amplitude of site response in time or frequency domain, and the prediction of how great damage occurred. The response spectrum method for vibration of analysis in linear, degree-of-freedom systems has been developed in the dynamic equilibrium equations, which is defined as:

$$m\ddot{u} + c\dot{u} + ku = -m\ddot{u}_g \qquad (2.6)$$

Whereas $m$ is the mass, $c$ is viscous dashpot representing damping, and $k$ is the stiffness of single degree of freedom system. $u$ is the relative displacements of the nodal, and $\dot{u}$ and $\ddot{u}$ are the first and secondary order different of $u$, evaluated as the relative velocities and relative accelerations.

To evaluate the response spectrum, the frequency-domain solution, Newmark β method (Newmark, 1959) is mostly common employed to estimate the response of single degree of freedom (SDOF) systems. This method calculates the nodal relative velocity $\dot{u}_{i+1}$ and relative displacement $u_{i+1}$ during the oscillation time by following equations:

$$\dot{u}_{i+1} = \dot{u}_i + [(1-\gamma)\Delta t]\ddot{u}_i + (\gamma\Delta t)\ddot{u}_{i+1} \tag{2.7}$$

and

$$u_{i+1} = u_i + (\Delta t)\dot{u}_i + [(0.5-\beta)(\Delta t)^2]\ddot{u}_i + [\beta(\Delta t)^2]\ddot{u}_{i+1} \tag{2.8}$$

The parameters $\beta$ and γ define the assumption of the acceleration variation over a time step (Δt) and determine the stability and accuracy of the integration of the method. The values, β and γ are assumed 0.25 and 0.5 respectively because of the integration is unconditionally stable for any time step (Δt) without numerical damping ratio. And this is the reason why Newmark β method with average acceleration parameters is commonly used to model the dynamic response of single and multiple degree of freedom systems in numerical simulation.

### 2.3.3 Frequency-domain and time-domain analyses

In geotechnical engineering practice, most studies express equivalent linear analysis in frequency domain and nonlinear analysis in time domain. Studying seismic vibration response from the category of time is called the time domain. The solution in time domain for prediction of earthquake ground motion is based on the 1D viscoelastic shear-wave

doi:10.6342/NTU201903794

equation presented. The derivation in a time-domain equation is performed as an infinite impulse response filter. Conducting analysis in the time domain has several advantages including causality of whole oscillation duration, and direct modeling of impulsive processes. The time-domain solution is intuitively more suitable for estimating earthquake ground motions and ease of inclusion of nonlinear soil behavior.

By methodology of Fourier Transform, time domain data could be represented as a sum of a series of both sine and cosine waves, which could be converted into the frequency domain to observe its seismic energy distribution at each frequency. The Fourier Transform is expressed in form of angular frequencies as follow:

$$A(\omega) = \int_0^{\infty} a(t) e^{i\omega t} dt \tag{2.9}$$

In which *A(ω)* is Fourier Transform spectra, *a(t)* is acceleration history during whole oscillation. *A(ω)* is the function in complex number, can be express as follow:

$$A(\omega) = C(\omega) - iS(\omega) = E(\omega) e^{-i\phi(\omega)t} \tag{2.10}$$

$C(\omega) = \int_0^{\infty} a(t) cos(t) dt$ : Cosine transform function.

$S(\omega) = \int_0^{\infty} a(t) sin(t) dt$ : Sine transform function.

$E(\omega) = \sqrt{C(\omega)^2 + E(\omega)^2}$ : Fourier Transform amplitude spectra.

These equations could evaluate energy distribution in frequency domain. Equivalent linear analysis usually be conducted in frequency domain. The advantages of frequency

doi:10.6342/NTU201903794

domain analysis is that it's much more convenient for figuring out the energy content of higher frequencies and lower frequencies, and for observing the maximum response amplitude in specific frequency. By Fourier Transform, we could determine the resonant frequencies which might cause the significant damage.

### 2.3.4 Hysteresis damping

As we mentioned in previous sections, dynamic analysis, the equivalent-linear method has been utilized for calculating the wave propagation and response spectra in soil and rock at sites subjected to seismic excitation. However, the method couldn't directly perform nonlinear effect because it only assumed linearity during computation process. The strain-dependent modulus and damping curves are taken into account in an average sense. Therefore, the nonlinear model is usually expressed to account for soil column effects on strong ground motion which caused large deformation of the material.

The hyperbolic model for nonlinearity is defined by two types of functions shown as follows:

$$\tau = \frac{\gamma G_0}{1+\beta(\gamma/\gamma_r)^s} \tag{2.11}$$

$$\tau = \frac{2G_0((\gamma-\gamma_{rev})/2)}{1+\beta((\gamma-\gamma_{rev})/2\gamma_r)^s} + \tau_{rev} \tag{2.12}$$

Whereas $\gamma$ is the given shear strain, $\gamma_r$ is reference strain, $\beta$ is dimensionless factor, $G_0$ represents maximum shear modulus and $s$ represents dimensionless exponent. Equation

doi:10.6342/NTU201903794

2.11 defines the stress-strain relationship which means backbone curve for loading, and Equation 2.12 defines the stress-strain relationship for unloading-reloading cycles. Hysteretic damping ($\xi_{hysteretic}$) is proportional to the energy dissipation in each oscillation cycle and the area of the hysteretic loop. In the other words, hysteretic damping is proportional to the ratio of the area enclosed by the hysteretic loop. The relationship of hysteretic damping can be expressed as:

$$\xi_{hysteretic} = \frac{A}{4\pi B} \tag{2.13}$$

Where *A* correlates to the area enclosed by the loading-unloading curve, and *B* represent the triangular area shown in Figure 2.5 (Camilo Phillips, 2009). In the equivalent-linear formulation applied in numerical simulation, the shear modulus and damping ratio are iteratively tried and error for fitting the effective level of shear strain in soil and rock material. Then the converged values of *G* and $\xi$ are used in site response calculation respectively.

doi:10.6342/NTU201903794

### 2.3.5 Viscous damping

Generally, for numerical simulation, damping is assumed into the geotechnical model to express seismic energy dissipation in real condition of soil layers. While soil material is under small strain, viscous damping usually be applied in dynamic analysis for absorbing energy in linear soil behavior. Rayleigh damping was originally used in elastic continua structures. The equation of Rayleigh damping is expressed in the matrix form to perform as proportional damping model, shown as Equation 2.14:

$$C = \alpha M + \beta K \tag{2.14}$$

Where *C* is components proportional to the mass (*M*) and stiffness (*K*) matrices, and $\alpha$ is the mass-proportional damping constant, $\beta$ is the stiffness-proportional damping constant. For the multiple degree-of-freedom system, the critical damping ratio in the soil system, $\xi_i$, in any other angular frequency, can be determined by the Equations as (Bathe and Wilson 1976):

$$\alpha + \beta {\omega_i}^2 = 2\omega_i \xi_i \tag{2.15}$$

or

$$\xi_i = \frac{1}{2}\left(\frac{\alpha}{\omega_i} + \beta \omega_i\right) \tag{2.16}$$

$\xi_i$, also known as critical damping ratio, is the fraction of critical damping for the soil mode with angular frequency $\omega_i$. The normalized critical damping is in variation with angular frequency $\omega_i$, shown as in Figure 2.6. The curve is given in three components,

doi:10.6342/NTU201903794

mass and stiffness only (α, β equals zero) and the combination of both curves. As shown, mass-proportional damping is dominant at range of lower angular frequency, however, stiffness-proportional damping be at higher angular frequencies. It is noted that each mass and stiffness damping supply half damping force of all. The combination curve represents that the sum of both component reaches minimum value at:

$$\xi_{min} = (\alpha \;\; \beta)^{1/2} \tag{2.17}$$

$$\omega_{min} = (\alpha/\beta)^{1/2} \tag{2.18}$$

The constants α and β could be derived by solving the simultaneous programs of Equation 2.8. Lastly, the center frequency of the numerical model is defined as:

$$f_{min} = \omega_{min}/2\pi \tag{2.19}$$

doi:10.6342/NTU201903794

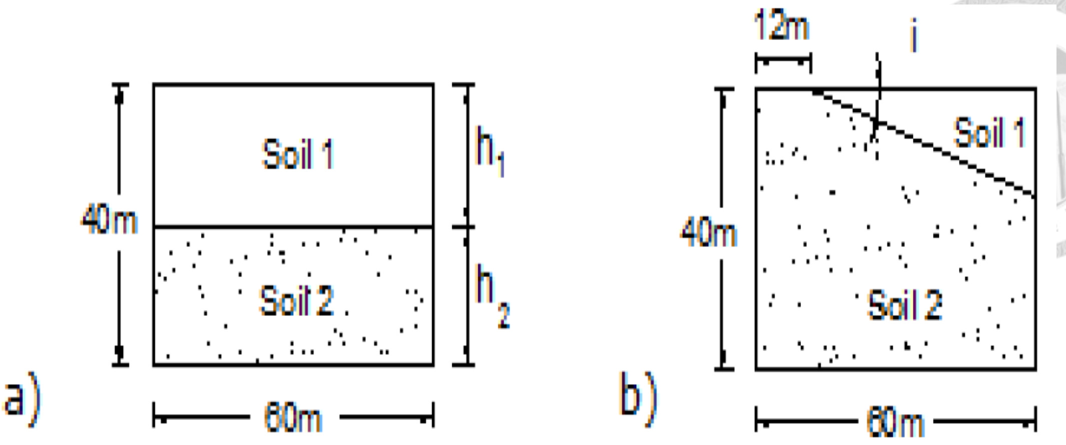

**Figure 2.1** *Models: (a) Type 1- horizontal interface, (b) Type 2- non-horizontal interface* **(Gouveia 2012)**

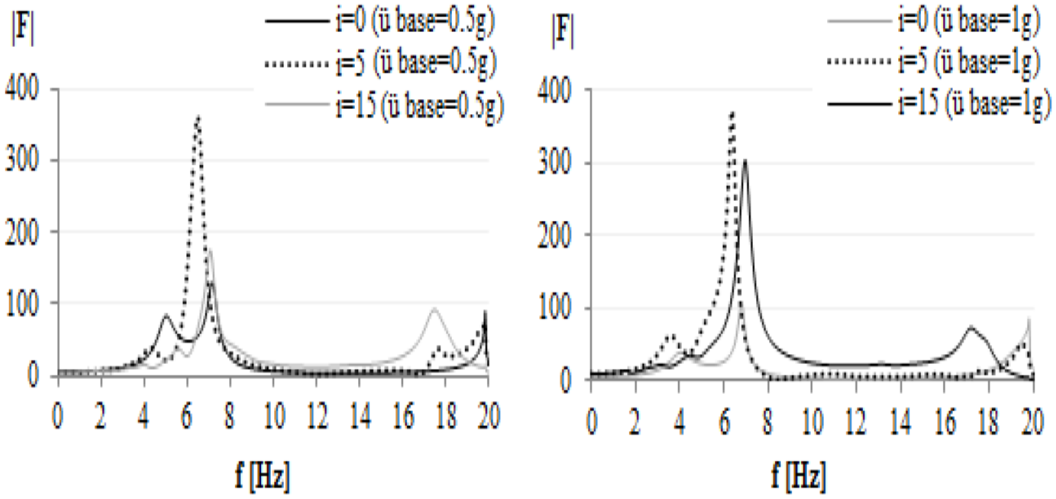

**Figure 2.2** *Transfer functions associated to the control points* **(Gouveia 2012)**

doi:10.6342/NTU201903794

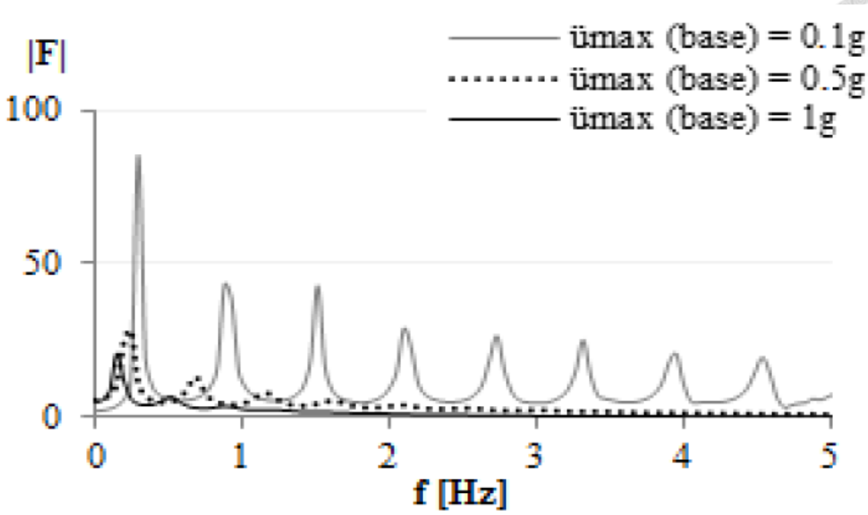

**Figure 2.3** *Amplification factors of different PGA of input motion* **(Gouveia 2012)**

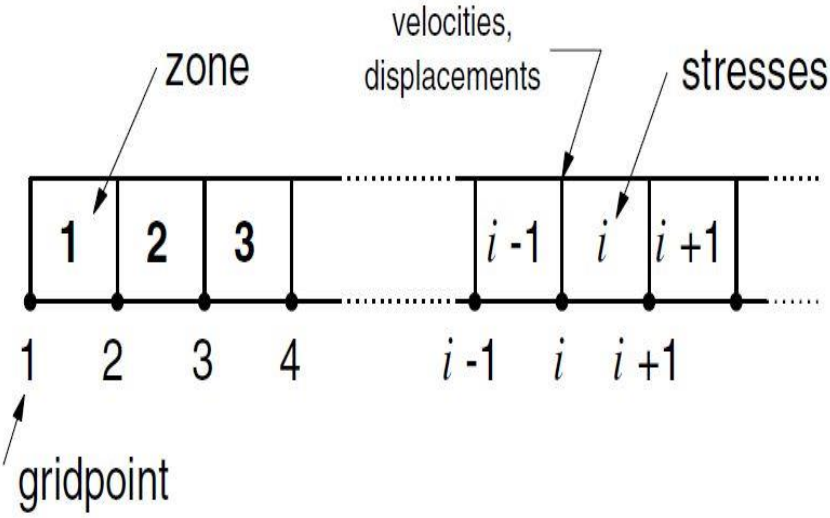

**Figure 2.4** *Numbering scheme for elements and the grid points (FLAC 2D7.0 manual)*

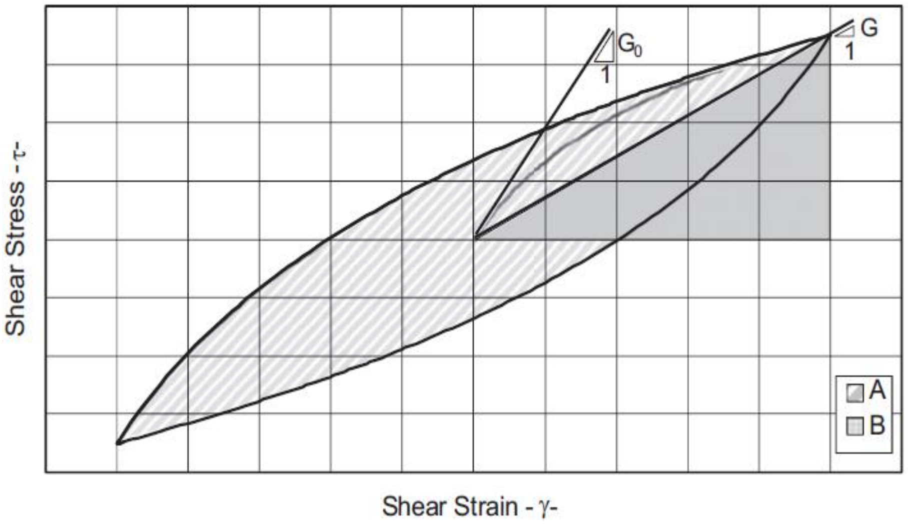

**Figure 2.5** *Stress-strain relationship (Camilo Phillips 2009)*

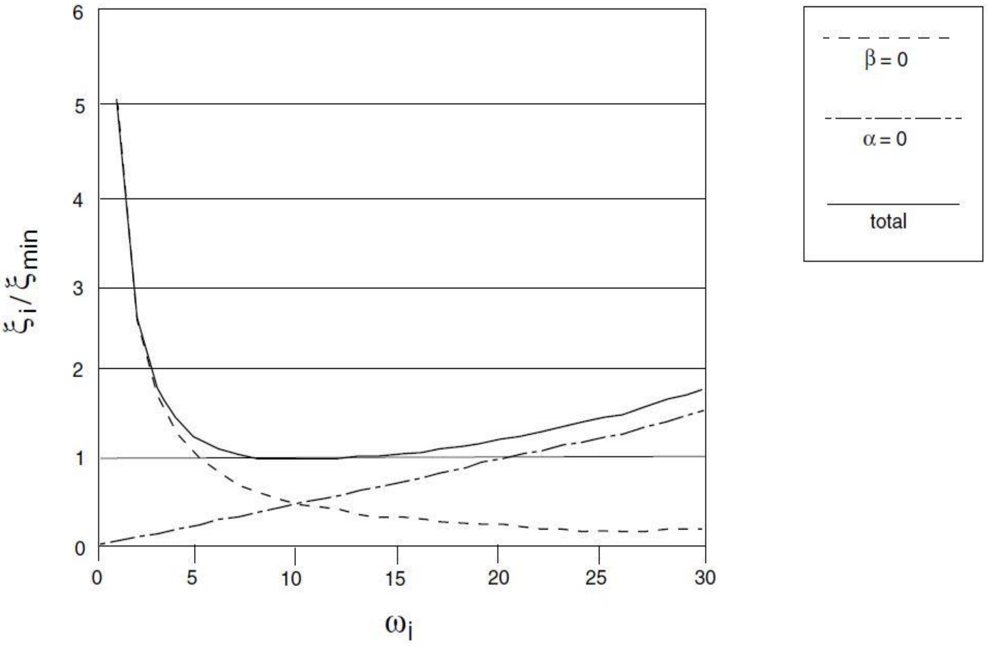

**Figure 2.6** *Variation of normalized critical damping ratio with angular frequency (FLAC2D 7.0 Manual)*

doi:10.6342/NTU201903794

# Chapter 3 Research Methodology

The objective of this research is to identify the trend of ground response for sites with non-one-dimensional wave propagation. Effect of layer inclination, half-space condition, thickness of sediment, impedance between different sediments and soil nonlinearity on ground response would be examined. All numerical simulations would be conducted in FLAC 2D 7.0, which is a finite different method (FDM) computational program. Numerical results would be compared with the ground response computed by using one-dimensional (1D) soil column model in FLAC 2D 7.0, as well as the 1D model from DEEPSOIL 7.0.

## 3.1 Analysis methodology

### 3.1.1 FLAC 2D 7.0

‘FLAC’ stands for Fast Lagrangian Analysis of Continua. FLAC 2D 7.0 is a finite difference method numerical software. For dynamic analysis, it permits two-dimensional, plane-strain, or plane-stress simulation. With the assigned initial and boundary conditions, the finite difference method could be applied to solve the equations of motion. For the finite difference method, each derivative of the governing equation at the spatial discrete element is directly replaced by the algebraic expression of the field variable (stress, displacement), however, these variables aren’t defined inside the elements.

doi:10.6342/NTU201903794

## 3.2 Model Calibration

### 3.2.1 Model size and grid size

To minimize the effect of reflections from the side boundary, free field boundary is used. However, the model should still be wide enough because there would still be reflections near the boundary. In this study, there is an underground basin structure with width of 150 m. the area of interest is in the middle 150 m. By trial and error, it has been determined that the total width of the model needs to be at least 5 times of the basin size ( Figure 3.1 ). With this model width, the ground response at a distance of 0.25 basin width from the side boundaries would approach free-field one-dimensional response(which is shown in Figure 3.2). In addition, the model width can be used for both rigid and compliant bottom boundaries.

The size and amounts of element grids would affect the computational time. In FLAC, there is a limitation on the number of elements that can be specified for each numerical model. Besides, size of the mesh grids can affect the accuracy of the simulation results. Hence, three grid sizes were tested: 2m x 2m, 1m x 1m, and 0.5m x 0.5m. By comparing the computational time and the accuracy of the numerical results obtained from models with these grid sizes, 1m x 1m is determined to be the most appropriate grid size for current study (which is shown in Figure 3.3).

### 3.2.2 Boundary condition

For dynamic analysis, several types of boundary conditions are available in FLAC. To minimize seismic wave reflection at model boundaries, free-field boundary can be used for vertical boundary while quiet boundary can be used for horizontal boundary (See Figure 3.4). In addition, external dynamic loading can be applied at the model boundary while internal dynamic loading can be applied at the internal grid points. The types of dynamic loading and boundary conditions are shown schematically in Figure 3.2.

When the half-space is made of very stiff material (e.g. seismic bedrock) or input motion is a within motion (i.e. motion recorded by at-depth seismometer), the rigid base condition should be used at the bottom boundary of the numerical model. In this way, downward propagating wave would be fully reflected. (Figure 3.5) To simulate the rigid base condition in FLAC2D, the nodes at the bottom boundary need to be fixed against y-direction and the acceleration history should be applied at these bottom nodes. Alternatively, when the input motion is an outcropping motion, the compliant base condition should be used at the bottom boundary. In this way, the downward propagating waves would be partially refracted to the half-space. In FLAC2D, in order to model a compliant base condition, the quiet boundary, which can absorb the seismic waves that approach the boundary (Figure 3.6), should be applied. This concept of compliant base boundary was developed by Lysmer and Kuhlemeyer (1969), which

doi:10.6342/NTU201903794

was based on the application of independent dashpots in the normal and shear directions of the model boundaries. The dashpots could provide viscous normal and shear tractions which can be evaluated by the equations below:

$$t_n = -\rho \ C_p \ v_n \qquad (3.1)$$

$$t_s = -\rho \ C_s \ v_s \qquad (3.2)$$

where $v_n$ and $v_s$ are velocities in normal and shear directions. $C_p$ and $C_s$ are P-wave and S-wave velocities and ρ is the element mass density. Using these equations, the input acceleration history can be converted into shear stress history. It should be noted that a thin layer (e.g. 1 m in thickness) must be added to the bottom of the model to represent the half-space material when a compliant base condition is desired.

For the left and right boundaries, free-field boundary can be used to absorb the waves that are propagating to the sides. If no special boundary is applied on the sides, the width of the model needs to be very large such that the reflection would not affect the response in the region of interest. When the material damping is low, the required model width may lead to an impractical model size. For soils with high material damping, the required width can be relatively small (Seed et al. 1975). In FLAC2D, when the free-field boundary is specified at the side boundaries (which isshown in Figure 3.7), two dashpots would be applied in the normal and shear directions along the lateral sides. The application of free-field boundary allows user to reduce the model

doi:10.6342/NTU201903794

width and decrease the number of mesh girds, hence the computational time can be reduced.

### 3.2.3 Material model

In this study, two material models are used to represent the behavior of sediment. They are the linear elastic model and the nonlinear model with hysteretic damping. For the linear elastic models, the parameters are estimated using some correlation relationships. Based on Gardner's equation (1974) and Brocher's empirical function (2005) as indicated below, the soil density and pressure wave velocity can be estimated from shear-wave velocities in the range of 0.3 km/s to 3.55 km/s.

Gardner's equation:

$$\rho = 1.74 \ V_p{}^{0.25} \tag{3.3}$$

Brocher's empirical equation:

$$V_p = 0.9409 + 2.0947 \ V_s - 0.8206 \ V_s{}^2 + 0.2683 \ V_s{}^3 - 0.0251 \ V_s{}^4 \tag{3.4}$$

Besides, we can evaluate the Poisson's ratio by using Lindseth's equation and linear elastic formulae as follow:

Lindseth's equation:

$$V_p = \mathit{0.308}\,\rho \ V_p + 3460 \ (\mathrm{V_p} \ \text{in} \ \mathrm{ft/s}, \rho \ \text{in} \ \mathrm{g}/cm^3 \ ) \tag{3.5}$$

Linear elastic formulas:

$$V_s = \sqrt{\frac{G}{\rho}} \tag{3.6}$$

$$V_p = \sqrt{\frac{\lambda + 2G}{\rho}} \tag{3.7}$$

$$\lambda = \frac{vE}{(1+v)(1-2v)} \tag{3.8}$$

$$G = \frac{E}{2(1+v)} \tag{3.9}$$

With the methodology mentioned above, the values of the material parameters are estimated and summarized in

.

In this study, viscous damping ratio is assumed to be 5% for soil and 2% for bedrock material. The Rayleigh damping parameters in FLAC2D are the minimum damping ratio $\xi_{min}$ and center frequency $f_{min}$, which could be obtained by Equation 2.8 to Equation 2.10. To determine the target frequencies for the FLAC2D model, we should ideally perform modal analysis to determine the fundamental frequencies for the 2D model. However, to simplify the calculation, we estimate the fundamental frequencies for different (1D) soil columns in the model by using Equation 3.10.

$$f_{1D} = \frac{V_s}{4H} \tag{3.10}$$

where $V_s$ represents the shear-wave velocity in m/s and $H$ is the thickness of soil layers. Since two target frequencies are needed for full Rayleigh damping formulation, the first target frequency would be selected as the lowest site frequency among the 1D soil columns and the second target frequency would be five times of the highest fundamental frequency among the 1D soil columns.

To incorporate soil nonlinearity in the analysis, nonlinear stress-strain model needs to be specified. In FLAC, Hardin and Drnevich’s model can be used to represent this nonlinear behavior. In addition, Masing’s rules are utilized by FLAC to describe the unloading and reloading behavior. To identify the appropriate values for the parameter

doi:10.6342/NTU201903794

in Hardin and Drneivch's model, target curves for the sediments are first selected. Then, element testing is performed. Figure 3.5 and 3.6 show the results of element testing.

## 3.3 Input motion

In this study, input motion recorded during Nahanni earthquake is used. For this recording, the duration is 19.05 seconds. The predominant period is 0.06 second while the peak ground acceleration is 0.17 g. To examine the effect of soil nonlinearity on the ground response, the amplitude of the input motion is scaled up such that soil nonlinearity can be "activated" in the analysis. The acceleration history and response spectra of the input motion are shown in Figure 3.8 and Figure 3.9 respectively.

## 3.4 Model Validation

### 3.4.1 Comparison to 1D model for ground response of sites with horizontal layering

To show that FLAC2D is capable of predicting the ground response for the simplest site condition, a plane strain 2D linear elastic model is created in FLAC2D to simulate the ground response for a horizontally layering site. The exact solution for this problem can be obtained by performing the frequency-domain linear analysis in DEEPSOIL. For this validation exercise, both rigid base and compliant base conditions are tested. As shown in Figure 3.10 and Figure 3.11, the results from FLAC2D match well with those from the frequency domain analyses from DEEPSOIL.

### 3.4.2 Comparison to theoretical solutions for ground response of semi-circular basin

As shown in previous sub-section, 2D plane strain model from FLAC2D can capture the ground response for sites with horizontal layering. In order to show that FLAC2D is capable of modeling 2D wave propagation, we simulate the ground response of a linear elastic semi-circular basin whose theoretical solution is presented by Wen (1995). The model parameters and geometry are shown in Figure 3.12, and the parameters ratio for FLAC simulation were chosen from Table 3.2. In Table 3.2, ρ, α, β, represent the soil densities, P-wave velocities and S-wave velocities respectively. We choose the parameter of model C to compare the results in FLAC and theoretical solution from Wen (1995). The comparison of the ratio of peak ground acceleration between the FLAC2D simulation and Wen (1995) are shown in Figure 3.13. The amplitude of PGA ratio and the variation of this ratio with x (horizontal) location of the basin are similar for the FLAC2D simulation and the theoretical solution from Wen (1995). The reason for the difference might be the numerical simulation in different software. In FLAC2D, we couldn’t perfectly generate the theoretical model from Wen (1995). Besides the semi-circular basin, we need to apply additional half space as the media for wave propagation. And we only can generate the 0 angle upward propagation in FLAC2D.

doi:10.6342/NTU201903794

## 3.5 Simulation cases

The focus of this study is to examine the ground response for sites with an underground basin structure by means of 2D numerical models and to compare these 2D results with those predicted by 1D analyses. Different basin geometry, in terms of different inclination angle of the lateral side (10°, 20°, 30°) is considered. In addition, different impedance ratios of materials outside and within the basin are used. Also, different half-space conditions (rigid or compliant) are considered.

doi:10.6342/NTU201903794

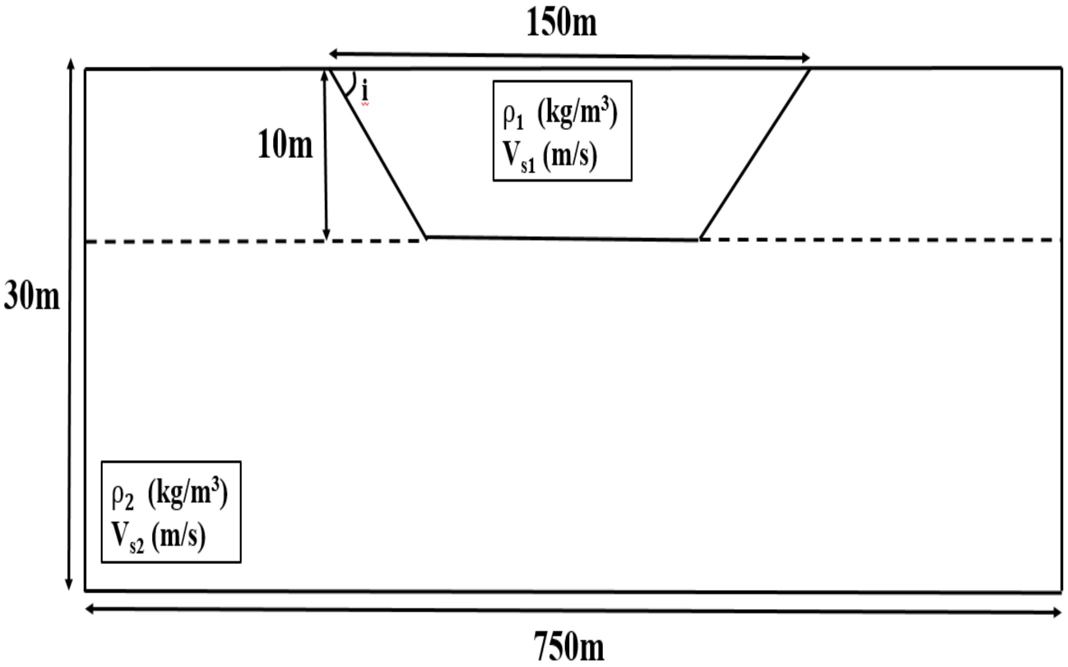

**Figure 3.1** *Model size for numerical simulation*

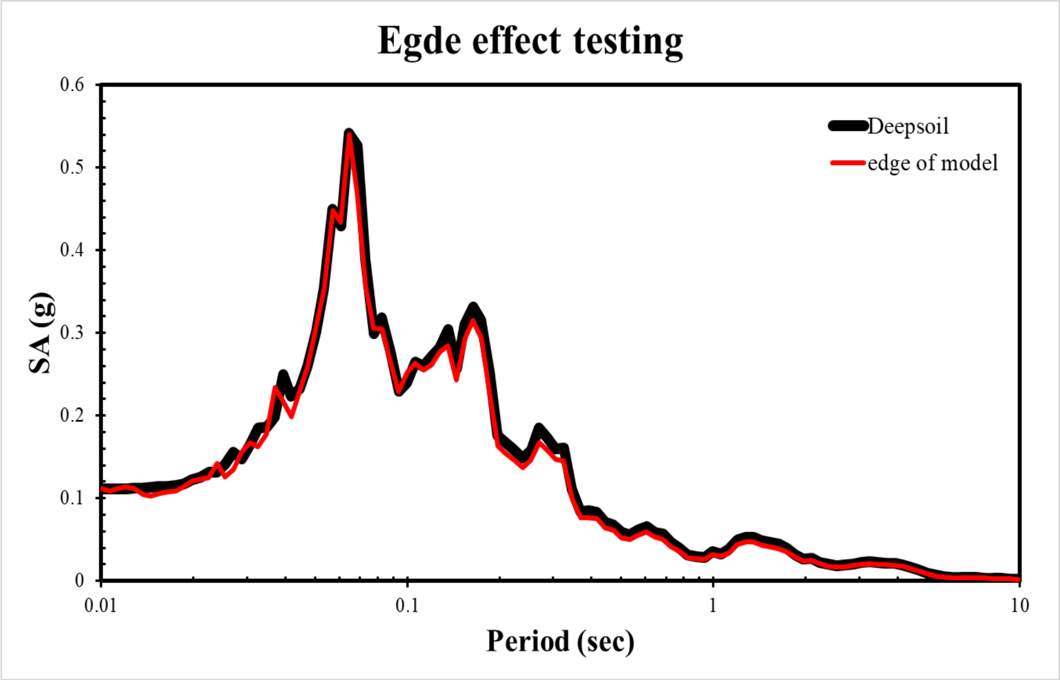

**Figure 3.2** *Testing of model size for eliminating the edge effect*

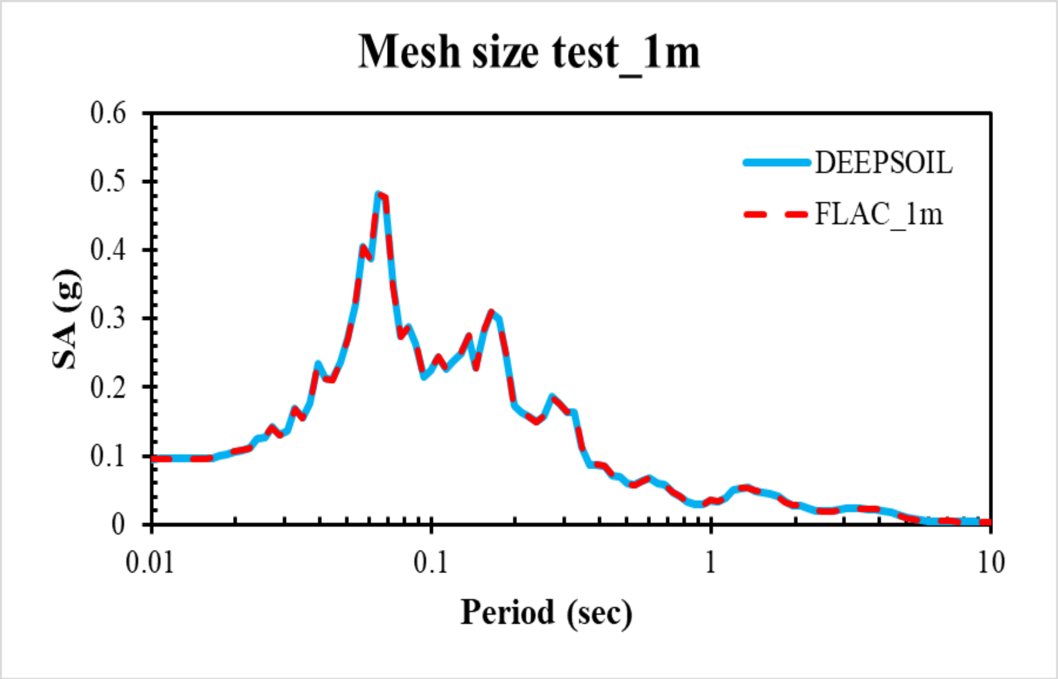

**(a)** ***1m gridpoints case***

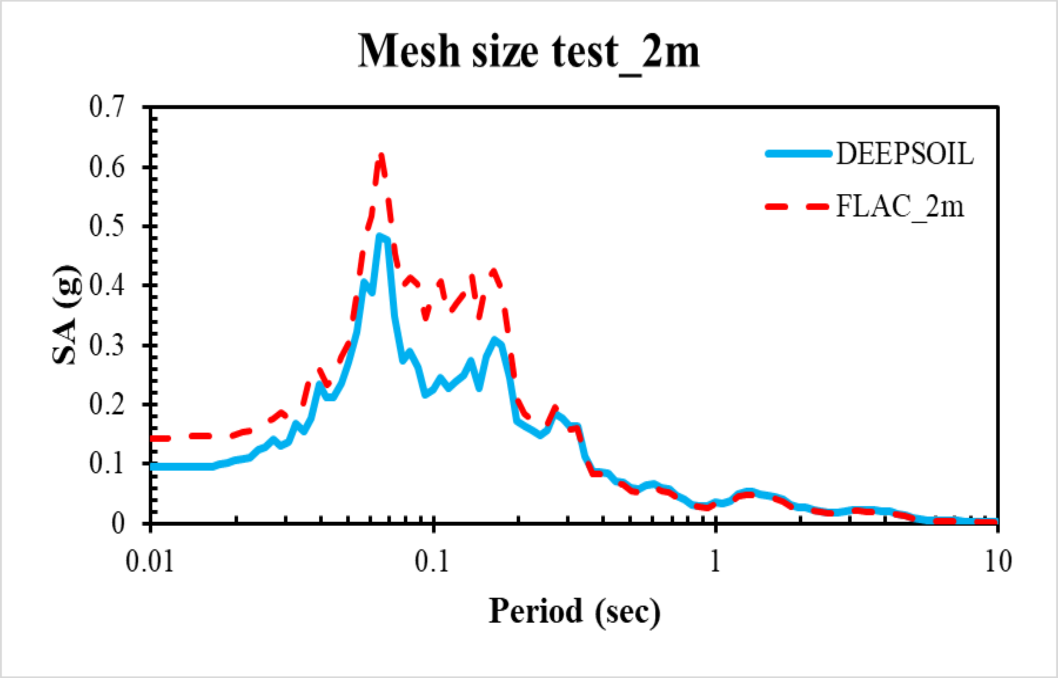

**(b)** ***2m gridpoints case***

**Figure 3.3** *Model size test of 1m grid & 2m grid*

doi:10.6342/NTU201903794

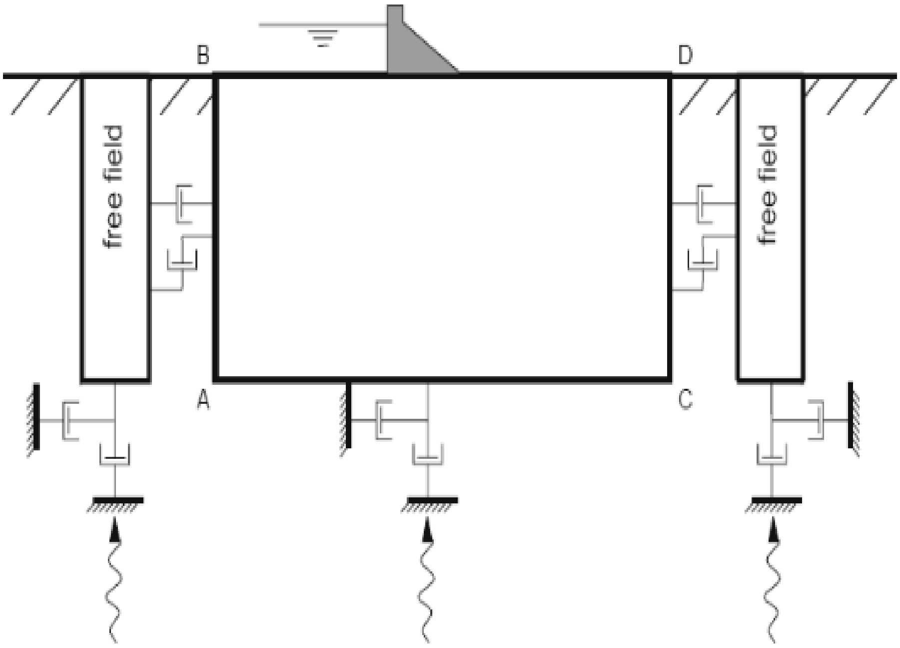

Figure 3.4 *Free-field boundary condition for seismic analysis (FLAC Manual)*

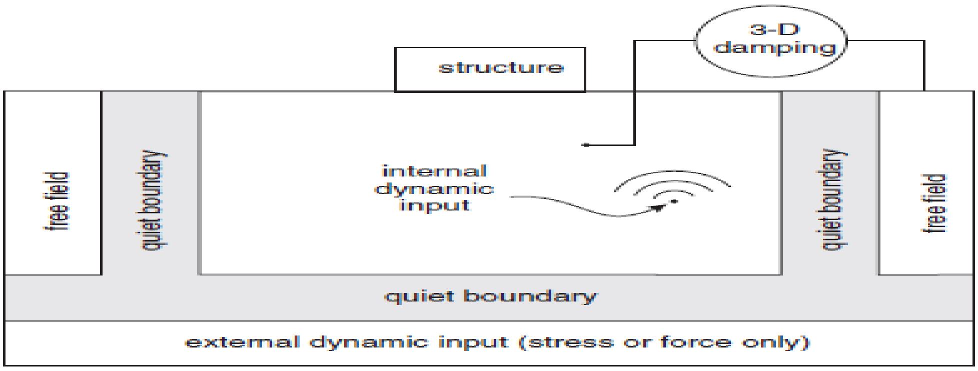

(a) Flexible base

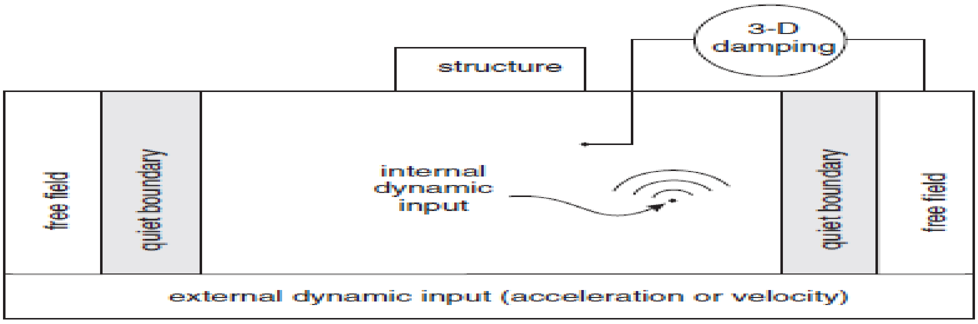

(a) Rigid base

Figure 3.5 *Types of dynamic loading boundary conditions available in FLAC (FLAC Manual)*

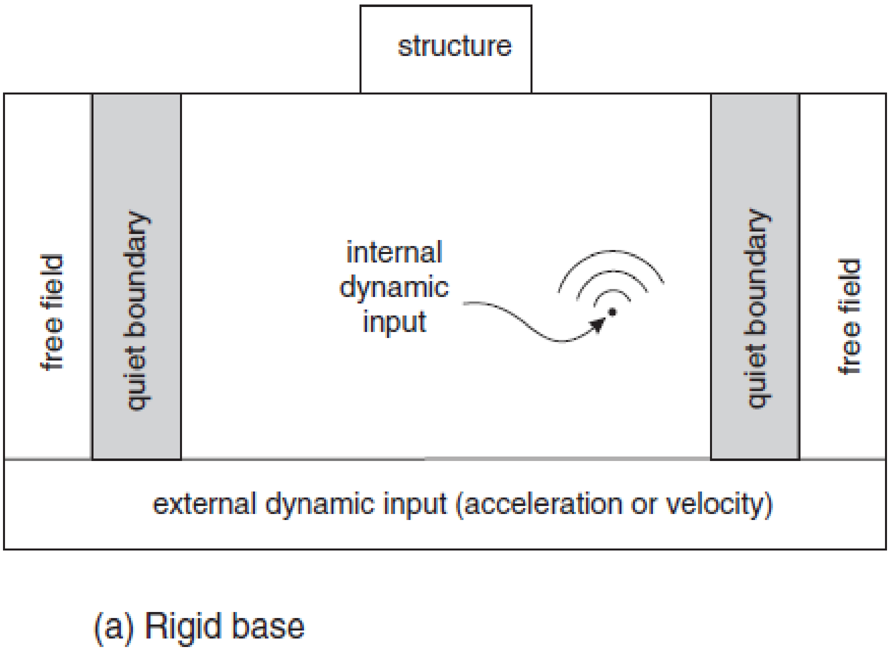

**Figure 3.6** *Types of dynamic loading and rigid boundary conditions*

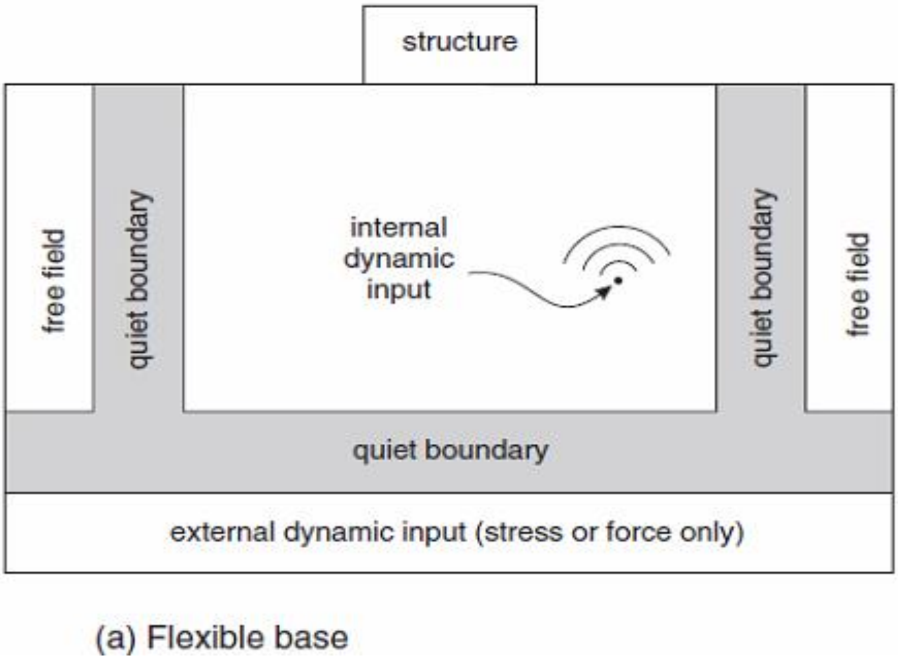

**Figure 3.7** *Types of dynamic loading and quiet boundary conditions*

doi:10.6342/NTU201903794

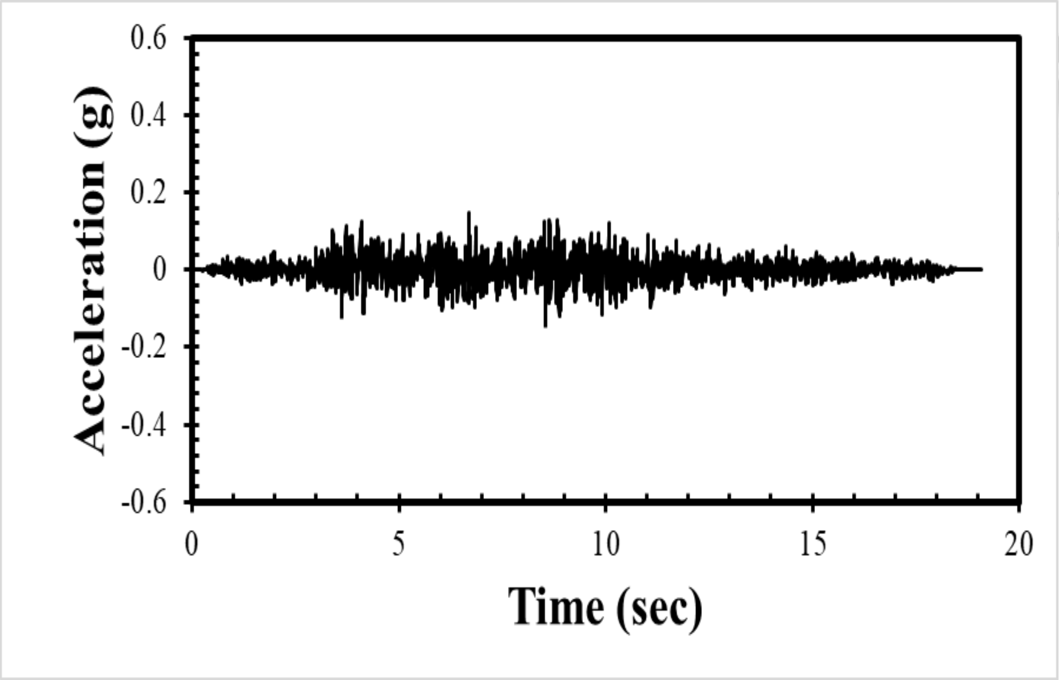

**(a) Earthquake Nahanni**

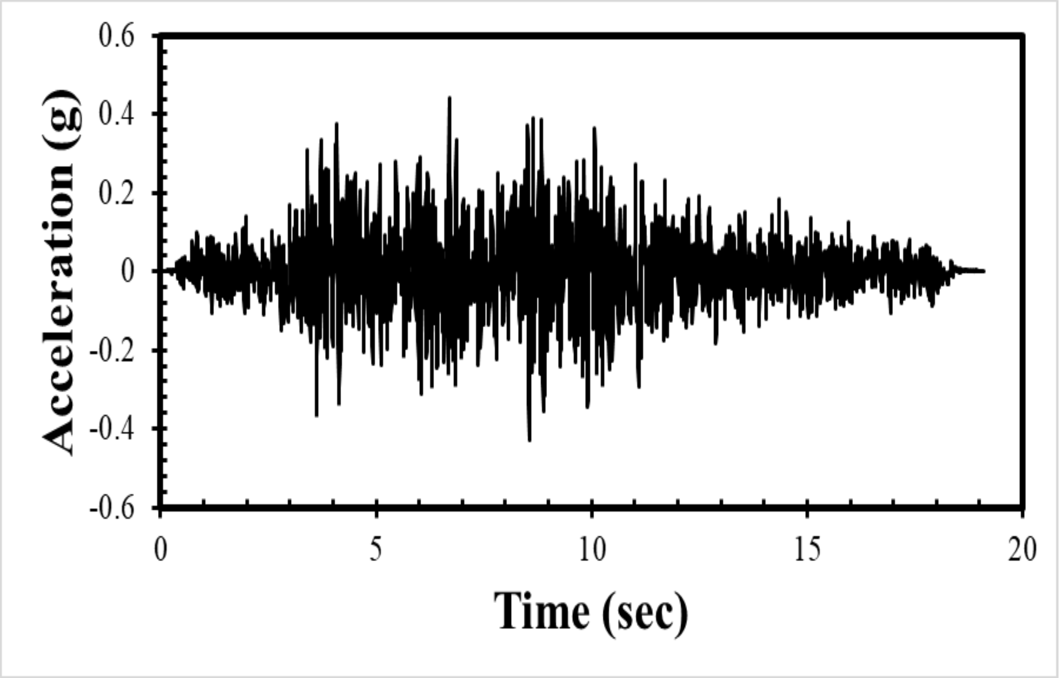

**(b) 3 times intensity of Nahanni**

**Figure 3.8** ***Acceleration history of input motion for numerical simulation***

doi:10.6342/NTU201903794

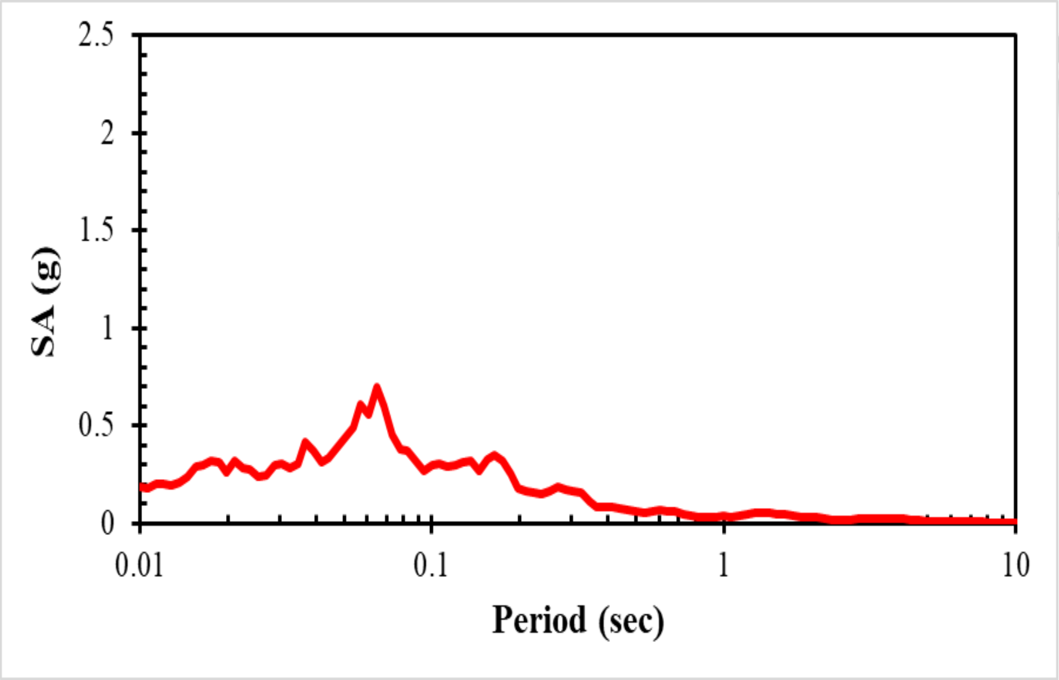

(a) Spectral acceleration spectrum of Nahanni

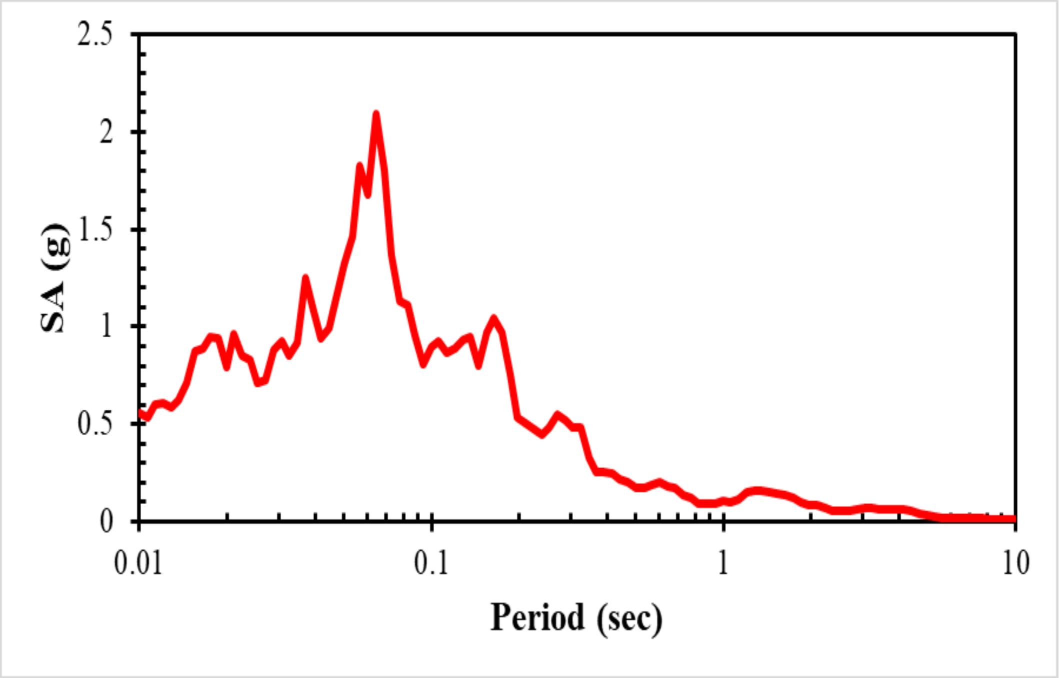

(b) Spectral acceleration spectrum of 3 times intensity of Nahanni

Figure 3.9 Spectra acceleration spectrum of input motions

doi:10.6342/NTU201903794

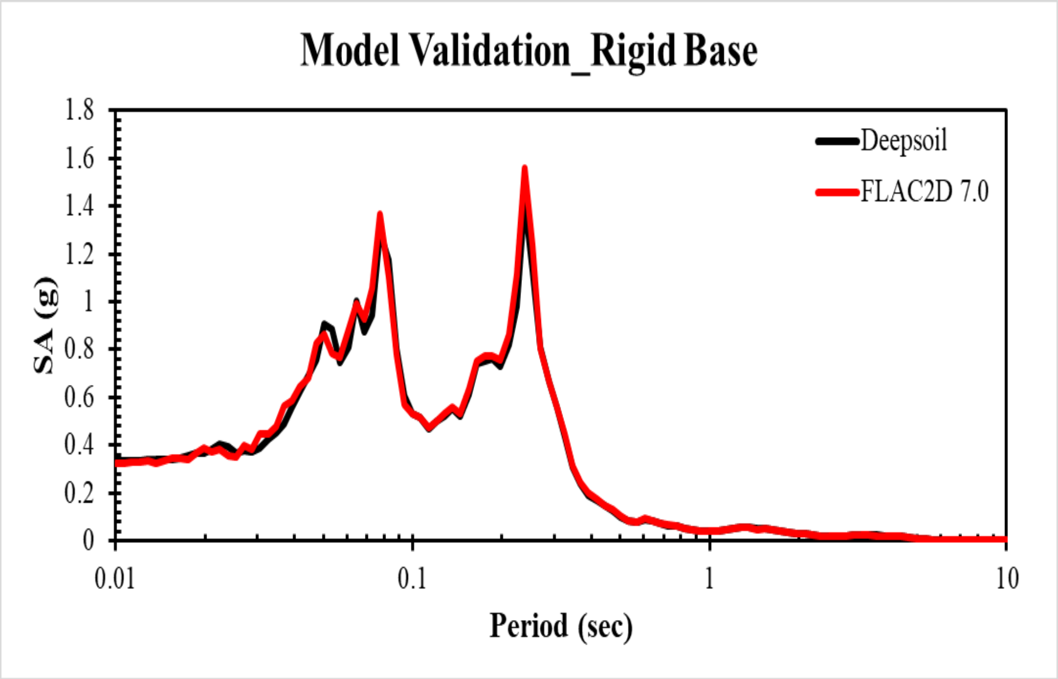

**Figure 3.10** *Model validation of rigid base in both FLAC and DEEPSOIL*

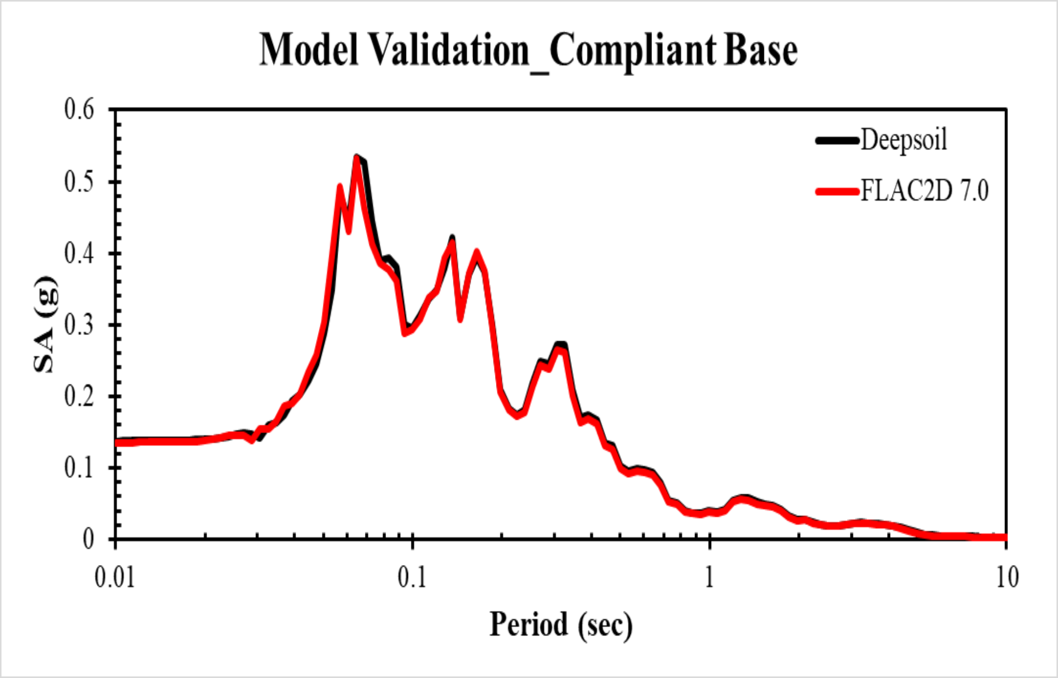

**Figure 3.11** *Model validation of compliant base in both FLAC and DEEPSOIL*

doi:10.6342/NTU201903794

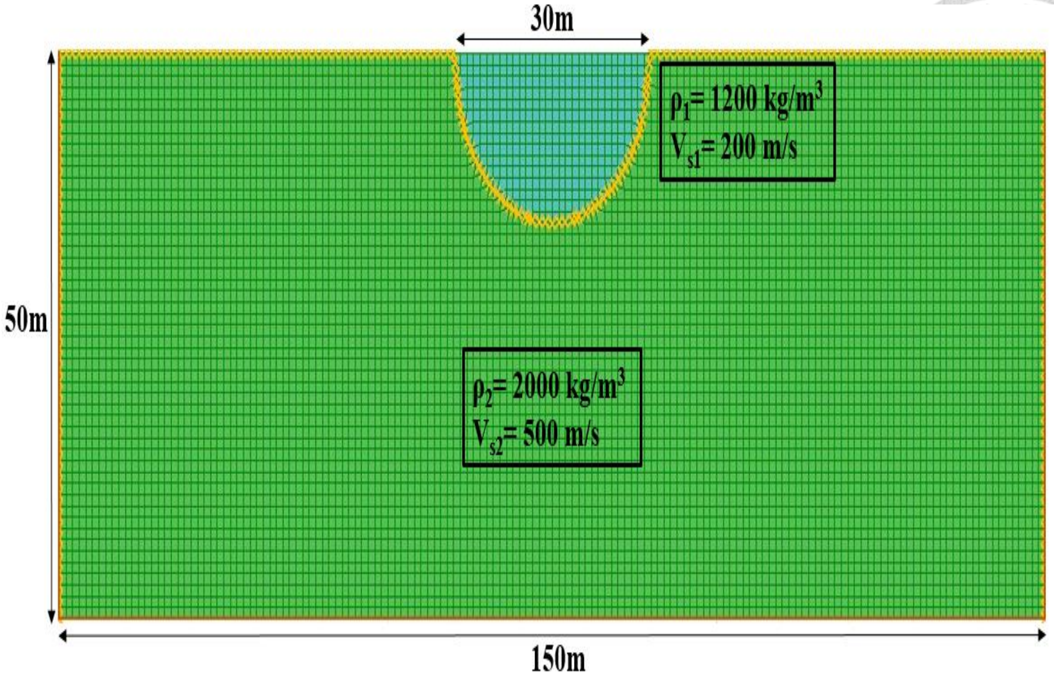

**Figure 3.12** *Geometry of theoretical semi-circular model*

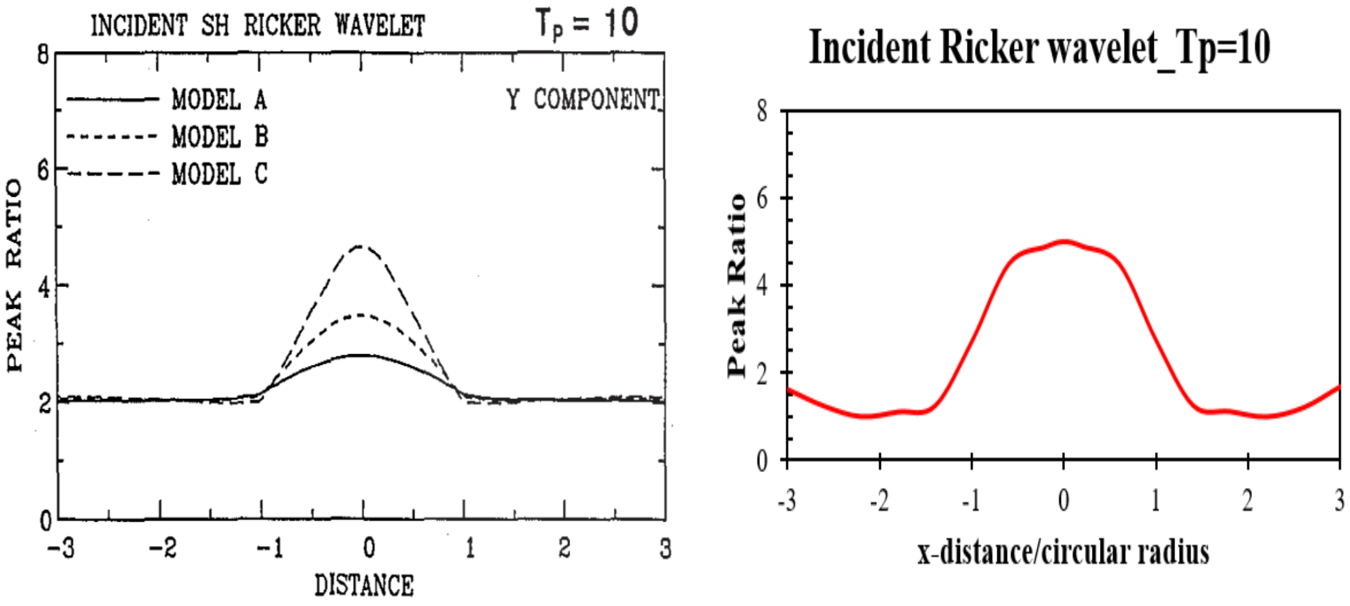

**Figure 3.13** *Comparison of two-dimensional peak ground acceleration ratio*

**Table 3.1** ***Properties of numerical simulation models***

| Shear-wave velocity, Vs | Material density ρ | Poisson's ratio v | Shear modulus G | Bulk modulus K |
|---|---|---|---|---|
| 300 m/s | 1900 kg/m$^3$ | 0.476 | 171000000 (Pa) | 3505500000 (Pa) |
| 500 m/s | 2000 kg/m$^3$ | 0.4553 | 500000000 (Pa) | 5426174497 (Pa) |
| 760 m/s | 2100 kg/m$^3$ | 0.426 | 1212960000 (Pa) | 7791355676 (Pa) |
| 1500 m/s | 2300 kg/m$^3$ | 0.3407 | 5175000000 (Pa) | 14517937850 (Pa) |

**Table 3.2** ***The model parameters for two-dimensional theoretical solution***

| **MODEL** | **DOMAIN 1** | | | **DOMAIN 2** | | |
|---|---|---|---|---|---|---|
| | **ρ1** | **α1** | **β1** | **ρ2** | **α2** | **β2** |
| **Model A** | **1** | **1** | **-** | **0.8** | **0.6** | **-** |
| **Model B** | **1** | **1** | **2** | **0.668** | **0.5** | **1** |
| **Model C** | **1** | **1** | **-** | **0.6** | **0.4** | **-** |

# Chapter 4 Simulation Results and Analyses

## 4.1 General description

The majority of this chapter is studying the results of the numerical simulation cases. Usually, the variation of site response is attributed to the different local site conditions, like boundary conditions and impedance contrast of underlying material. By spectral acceleration spectrum in time domain, we could evaluate the PSA of ground motion at specific period during seismic oscillation. To evaluate the seismic energy distribution in frequency domain, we change the acceleration output history into Fourier transform. It could help us to obtain the intensity of amplitude during whole frequency, and determine the predominant frequency. By cross comparison of these properties, we could develop the influence tendency which might cause amplification of site response and evaluate the affected local region of near basin edge which might be suffered great damage of the earthquake.

There are several cases of numerical simulation in this research and five major parts in these spectral acceleration figures. Black line represents the 1D results conducted in DEEPSOIL, blue lines represent the response of left edge away from the basin region, green lines represent the response occurred at left region of basin, red and orange lines are the opposite site where blue and green lines represent, and gray line represents the response at center of basin. Even though the symmetrical model

doi:10.6342/NTU201903794

geometry performed, the response occurred at the same distance to the middle of the model would be similar but not exactly equal. The reason for that phenomenon might be the asymmetry of real seismic wave propagation. Resonance frequency is a very important parameter to realize the earthquake damage in an alluvium site. The two-dimensional fundamental frequency of the model could be estimated by Bard & Bouchon's empirical functions as follow:

$$f^{SH} = f_h^S \sqrt{1 + (2h/l)^2} \tag{4.1}$$

Where $f^{SH}$ is defined as two-dimensional fundamental frequency of the model, $f_h^S$ is the one-dimensional fundamental frequency ($f_h^S$=Vs/4h, Vs represent shear-wave velocities and h is thickness of the alluvial layer), and h/l is expressed as the ratio of maximum thickness to the total width over which the valley's depth is more than one half the maximum thickness. With the empirical functions, we could estimate the fundamental frequencies of the numerical models in this study. The values are shown in Table 4.1. However, the estimated values of fundamental frequencies are different from those of the ground surface response. The reason for that phenomenon is because Bard & Bouchon's empirical functions are based on the theoretical semi-circular basin model. Therefore, we should figure another empirical functions to perfectly predict the predominant frequencies of the numerical model.

doi:10.6342/NTU201903794

For numerical simulation results for different ground geometry and boundary conditions, there are several aspects of analysis in this chapter. First, we could develop the spectral acceleration spectrum to demonstrate the spectra acceleration amplitude induced by seismic wave in time domain and the strength increase and declination in different vibration period. Second, the ratio of 2D and 1D peak spectral acceleration, one of amplification types could be attributed to the effect of considering 2D motion into 1D response and the tendency of amplification factors. This phenomenon might also strengthen the site response as expected in the 1D homogenous results. Third, the ratio of 1D and 2D smooth Fourier transform in frequency domain. Fourier transform could evaluate the seismic energy distribution in distinct frequency and the specific frequency accompanied with maximum response. Due to the additional 1m bedrock layer we assigned to the bottom complaint base to represent the properties of half-space, the wave propagation had been affected by properties in half-space and the site response wouldn't be equal in the bottom of the model. On the contrary, the bottom response in the model with rigid base is same as consequence. Therefore, in rigid base, we could define the amplification factors as the ratio of response on the ground surface to the bottom response induced by directly propagation. In cases for compliant base, spectral acceleration of Nahanni input motion is considered as base to demonstrate the ratio of output and input motion which performed as amplification effect. In cases for rigid base,

doi:10.6342/NTU201903794

the site response at the bottom is equal as the input motion response. The reason for that consequence is that the wave propagation of the input motion is applied to the defaulted rigid base without additional 1m bedrock, therefore, in the moment the seismic wave directly passed through the bottom boundary, the response of the input motion haven’t be interfered by the geological material properties. As consequence, we take the bottom response of the rigid base as the base to develop the amplification factors. Lastly, the PGA values are expressed with x-direction coordinate to perform the influence of the peak ground motion on different geological conditions at each location of the numerical model.

Generally, the response in y-direction is much lower than those in x-direction. The reason for this phenomenon is attributed to that the energy of secondary wave distributed to the response in x-direction is much more than the response in y-direction. To perform the dependent influence on different geological conditions, there are few results of numerical cases shown in each section.

doi:10.6342/NTU201903794

## 4.2 Ground response near basin edge

The observed difference in Fourier amplitude of seismic ground motion within different location is defined as spatial variation of earthquake ground motions. Spatial variation of earthquake ground motion has been recognized in previous seismic studies. A large number of empirical coherency functions have been developed (Harichandran, 1986; Ancheta et al., 2011). By definition, coherency evaluates the variation in Fourier phase and express the correlation between two ground motions, as exponentially decaying functions of frequency and site separation distances. It is a common practice to choose the shear-wave because it’s considered as the most damaging component from engineering practice. The lagged coherency, $\left|\overline{\gamma_{jk}}(\omega)\right|$, of the seismic motion between station j and k is defined as follows:

$$\left|\overline{\gamma_{jk}}(\omega)\right| = \frac{\left|\overline{S_{jk}}(\omega)\right|}{\sqrt{\left|\overline{S_{jj}}(\omega)\right|\left|\overline{S_{kk}}(\omega)\right|}}$$

The priority of this section is discussing the influence of different geological conditions on lagged coherency. This work investigates the phase variability of the ground motion by estimating lagged coherency from the numerical simulation results. There are five specific situations chosen to develop the lagged coherency correlated to the side edge, the edge of the numerical model, the ground surface of 1/4, 2/4, 3/4 intersection slope, and the middle surface of basin. All lagged coherency of different cases are shown in appendix. As higher values of lagged coherency, the site response would be highly dependent on the location chosen as reference point. From the results of lagged coherency, the tendency of compliant base in both soil linearity and nonlinearity is similar, and this phenomenon illustrated that the behavior of geological material wouldn’t affect the correlation of different local site. In rigid boundary condition, distinct difference exists in coherency curves. Due to the nonlinear soil behavior, the correlation between each site and reference point would decline. The reason for the observation could be attributed to the plasticity of soil material with large deformation, decreasing the linearly correlated process.

## 4.3 Influence of impedance contrast

With higher shear-wave velocity, it would represent soil layers become stiffer. In this study, there are four different shear-wave velocities applied to the soil material. In the region of the soil basin, S-wave 300 m/s is determined as velocity of the soil. Generally, rock layers, shown in Figure 3.1 $\rho_2$, accompany with higher shear-wave velocity. Therefore, we develop 500 m/s, 760 m/s, and 1500 m/s to be the shear-wave velocities of rock layers. Impedance contrast usually be utilized in engineering practice to represent the stiffness degree of the geological material. The equation of impedance contrast is shown as follow:

$$Impedance\ \ Contrast, IC = \frac{\rho_1 V_{s1}}{\rho_2 V_{s2}} \tag{4.1}$$

doi:10.6342/NTU201903794

Whereas $\rho_1$ and $V_{s1}$ are the density and shear-wave velocity of the soil basin, $\rho_2$ and $V_{s2}$ are the density and shear-wave velocity in the rock layering. By converting site response of the acceleration history outputs into spectral acceleration and Fourier transform, it might help us to evaluate the trend of influence varied with impedance contrast. With spectral acceleration spectrum in time domain, we could construct the amplitude of PSA during oscillation period. However, with Fourier transform in frequency domain, we could explore the energy distribution at specific frequency as we mentioned previously. For the comparison with the results of numerical simulation, we could evaluate some summary. Take the comparison of Figure 4.1, Figure 4.4 and Figure 4.7 and some results of y-direction response for example, as the increase shear-wave velocity which means the decrease impedance contrast occurred, both x and y spectral acceleration response would become more intense. As consequence, it might cause severe damage for ground surface.

From all figures shown follows, there would be an obvious trend. In the analysis of spectral acceleration aspects, the maximum response of the compliant base in both linear and nonlinear behavior cases change from the upward surface of 1/2 soil layer intersection to the middle surface of the basin with decreasing impedance contrast, like Figure 4.1 to Figure 4.9 In the other hand, the maximum response of rigid base would change the site from central surface of basin to the outward edge of the soil model, as

doi:10.6342/NTU201903794

you can see Figure 4.10 to Figure 4.18. In y-direction spectral acceleration spectrum, the response occurred at basin center is relative weak than the nearby region of basin, as the figures of SA in specific period shown in appendix.

In aspect of ratio of 2D peak spectral acceleration to 1D peak spectral acceleration, the results in both linearity and nonlinearity highlight the increase PSA ratio proportional to the higher shear-wave velocities, in other words, lower impedance contrast. As the response in y direction, we compare the site response with response of model edge to develop the amplification spectral affected by the different impedance contrast. Similar trend demonstrates in the spectral acceleration ratio in y direction, as the figures shown in appendix. The results of Fourier transform ratio varied with impedance contrast also demonstrates same tendency as we discussed in previous sections. And maximum Fourier ratio, represented maximum two-dimensional Fourier amplitude, occurred at about 10 Hz frequency distinctly as impedance contrast decreasing. The contrast results are shown in Figure 4.45. And the PGA curves in specific period are shown in the Appendix.

## 4.4 Influence of inclination angle

Due to site effect, different inclination angles would cause different response of ground motion. In this section, the influence of tilt angles on site response would be discussed. There are few cases of numerical simulation taken as representation to develop the tendency of site response. As you can see linear elastic compliant case in Figure 4.1 to Figure 4.9, due to higher tilt angles, the results might accompany with lower amplitude of spectral acceleration spectrum in x-direction. For the linear elastic rigid cases (Figure 4.10 to Figure 4.18), the maximum response in x-direction occurs at near the central region of the basin. However, in y-direction results, both spectral acceleration spectrum and ratio of spectral acceleration to the spectral acceleration at model edge, the phenomenon mentioned above isn’t distinct. Due to the influence of impedance contrast, at lower shear-wave velocity, the amplitude of y-SA increases as increasing tilt angles. At higher shear-wave velocity, the intensity of y-SA would decline as increasing tilt angles. All the results of y-SA spectrum are shown in appendix. For both nonlinear compliant and rigid cases (Figure 4.19 to Figure 4.27, Figure 4.28 to Figure 4.36), like linear cases for x-direction response, inclination angles may decrease the response. However, in nonlinear behavior, the location of maximum response would change from the central region to the district nearby the surface of intersection soil layering in the basin. All these results are attributed to the variation of inclination angles.

In Fourier transform analysis, as the tilt angles increase, the ratio of smooth Fourier amplitude would decline at lower frequency about 10 Hz. However, Fourier transform would diverge at higher frequency made the response unstable. Few results are shown in Figure 4.46. In PGA curves expressed in appendix, the maximum response would no

doi:10.6342/NTU201903794

longer occurred at central location of the basin as inclined angles increasing in few cases, shown in Figure 4.47.

## 4.5 Influence of depth of basin

In this research, we increase the depth of the numerical model to figure out the influence of the model size. We increase the vertical size of basin to 30 meters and remain the 20 meters underlying soil region, in the other word, enlarge the model size to 50 meters thickness. We choose the cases with shear-wave velocity 760 m/s and compliant base boundary because they are mostly like the real site condition. Therefore, there are two results of spectral acceleration spectrum as shown in Figure 4.43 and Figure 4.44.

Due to site effect, the site response would be amplified while seismic wave propagation passed through softer soil components. In these depth expanding cases, the proportion of soil material region would increase in whole numerical model. This phenomenon leads to lower stiffness than cases in 10 meters thickness basin. The results performed in Figure 4.43 and Figure 4.44 demonstrate higher site response as in comparison with Figure 4.6 and Figure 4.24. The maximum response would change the situation from nearby the middle ground surface of basin to the district far away from central ground surface. In Figure 4.50, we could obtain the variation of basin depth expanding cases. The maximum amplitude of Fourier transform would be induced at

doi:10.6342/NTU201903794

lower frequencies about 3 to 4 Hz in both linear and nonlinear cases while the results in 10 meters depth cases occurred at about 10 Hz.

## 4.6 Influence of boundary condition

There are two major boundary conditions applied to the bottom of numerical models, compliant base and rigid base. Also, free-field boundary is assigned to the lateral direction of model edge for eliminating lateral half-space wave reflection. To explore the influence of the boundary conditions, we could compare the results in compliant base with those in rigid base in contrast. The consequence points out that the amplitude of spectral acceleration in rigid base is much more intense than in compliant base. As the comparison shown in Figure 4.1 and Figure 4.10. The primary reason is fully upward seismic wave reflection may conducted in rigid base cases. However, complaint base would absorb the partial seismic energy by propagating the wave radiation to the downward half-space and refract residual energy to soil components. This effect demonstrates the difference of amplification factors and the site response between compliant base and rigid base.

Theoretically, rigid base is basically defaulted in the FLAC2D. However, in engineering practice, the reality of bedrock performs more likely compliant base. Therefore, the influence of compliant base is much more significant in the study. In linear elastic numerical cases, as applied compliant base alternated by rigid base, the location

doi:10.6342/NTU201903794

of maximum response would change from the nearby region of the basin edge to the middle of the basin. For mostly soil nonlinearity cases, the variation of boundary conditions leads to opposite consequence in linear cases. The maximum response would be induced at the site nearby model edge, shown in a series cases, Figure 4.19 to Figure 4.36.

For PSA ratio analysis, the values of the ratio in rigid base become larger than values in compliant base. This phenomenon also be attributed to the combination of two-dimensional effect and fully wave reflection of rigid base, shown in Figure 4.48. In the aspect of amplification factor. Site response of both linearity and nonlinearity in rigid base is strengthened intensively than in compliant base. These results are expressed in appendix.

## 4.7 Influence of soil nonlinearity

Generally, in geotechnical engineering, we consider assumption of linear elastic soil behavior for numerical analysis. Due to larger shear strain, the soil behavior would convert from elasticity to plasticity, turned soil linearity into nonlinearity. Rayleigh damping is used for dynamic analysis for linear elastic simulation. However, hysteresis damping curve should be considered for the soil nonlinearity. By conducting element test,

doi:10.6342/NTU201903794

we could determine the parameters for fitting reference curves of shear modulus and specific damping, like those we discussed in chapter 3.

In this section, we will discuss the influence of soil behavior. There are several cases shown in chapter 4. Take several cases for example, as Figure 4.1 to Figure 4.18 in comparison with Figure 4.19 to Figure 4.36 are the linear results versus nonlinear ones. In spectral acceleration aspect in both x and y direction, the amplitude of nonlinear response is lower than that of elastic linearity. The reason for this consequence is that the hysteresis damping is higher when large strain of soil material occurred. Therefore, more seismic energy should be damped, and the resulting response should be smaller than that in elastic linearity. With compliant base, the location of maximum response would occur at the region nearby the middle of the basin. And it also suggest that the ground surface of basin center would be the most dangerous region as soil behavior performed nonlinearity. In the contrast, rigid base condition, maximum response of mostly cases would change the site from the middle of the model to the side edge, as shown in Figure 4.31 to Figure 4.36 in comparison with Figure 4.13 to Figure 4.18. For the site response in y direction, the amplitude in linear cases is higher than in nonlinear cases, however, the spectrum in both is similar. This results would be expressed distinctly as shear-wave velocity increases. In the spectral ratio in y direction, the ratios in nonlinear cases are much higher than linear ones. The reason is attributed to the smaller response occurred

doi:10.6342/NTU201903794

at the model edge for nonlinear cases than for linear cases, causing higher spectral acceleration ratios.

The results performed in Fourier amplitude and peak spectral acceleration are expressed similar influence of soil behavior. The reason for that phenomenon is attributed stronger damping ratio induced by larger shear strain which causing small Fourier amplitude and PSA ratios. These simulation results are performed in appendix as follows.

## 4.8 Influence of input motion

In this study, we apply different types of seismic motion to the numerical model to evaluate the influence of different input motion. As we mentioned in chapter 3.3, we develop three times intensity of Nahanni earthquake as new input motion to perform the effect of different PGA while same vibration duration 20 seconds. And we choose the cases of compliant base with 760 m/s shear-wave velocity in both linear and nonlinear behavior as contrast because the properties in those cases are much more in accordance with material components in real site.

As shown in Figure 4.37 to Figure 4.42, even if we increase the strength of input motion, the site generated maximum response would be equal as the cases in Figure 4.4 to Figure 4.6 and Figure 4.22 to Figure 4.24. The amplitude of site response is also be strengthened as consequence. The results also demonstrate that the trend of these cases

doi:10.6342/NTU201903794

would be equal to the cases applied Nahanni input motion. However, the magnification of site response isn’t equal to multiple values of the input motion.

Additionally, we develop the trend of different input motion for site response. We choose ChiChi earthquake as new input motion because the predominant period of ChiChi (about 0.7 sec) is larger than Nahanni earthquake (about 0.08 sec). We choose the cases of compliant base with angle 30° in both linear and nonlinear behavior as the comparison shown in Figure 4.51 and Figure 4.52. As the results, the figures show the phenomenon that the maximum response would occur at specific dominant period. With lower shear-wave velocities (about 500m/s, 760 m/s), the predominant periods in both ChiChi and Nahanni earthquake cases are similar to the predominant period of input motion which applied to each case respectively. However, with higher shear-wave velocity (about 1500 m/s), the predominant periods in both ChiChi and Nahanni cases are similar about 0.1 second. All the comparisons are shown as follows.

doi:10.6342/NTU201903794

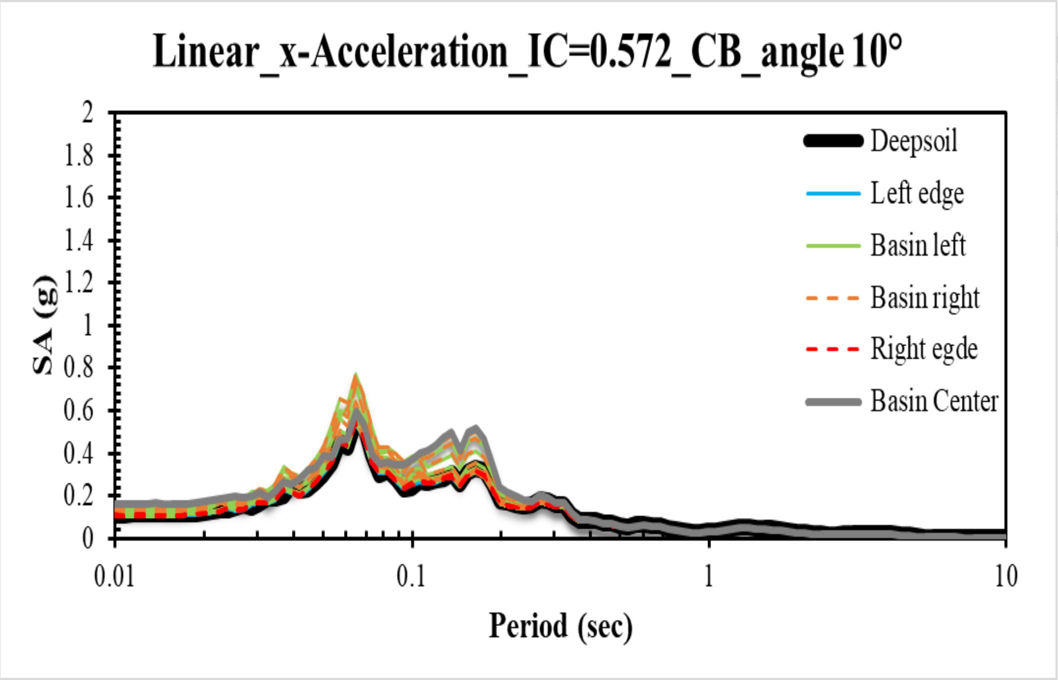

**Figure 4.1** *Spectral acceleration spectrum of x-acceleration for linear elastic case Vs=500 m/s _angle 10° with compliant base*

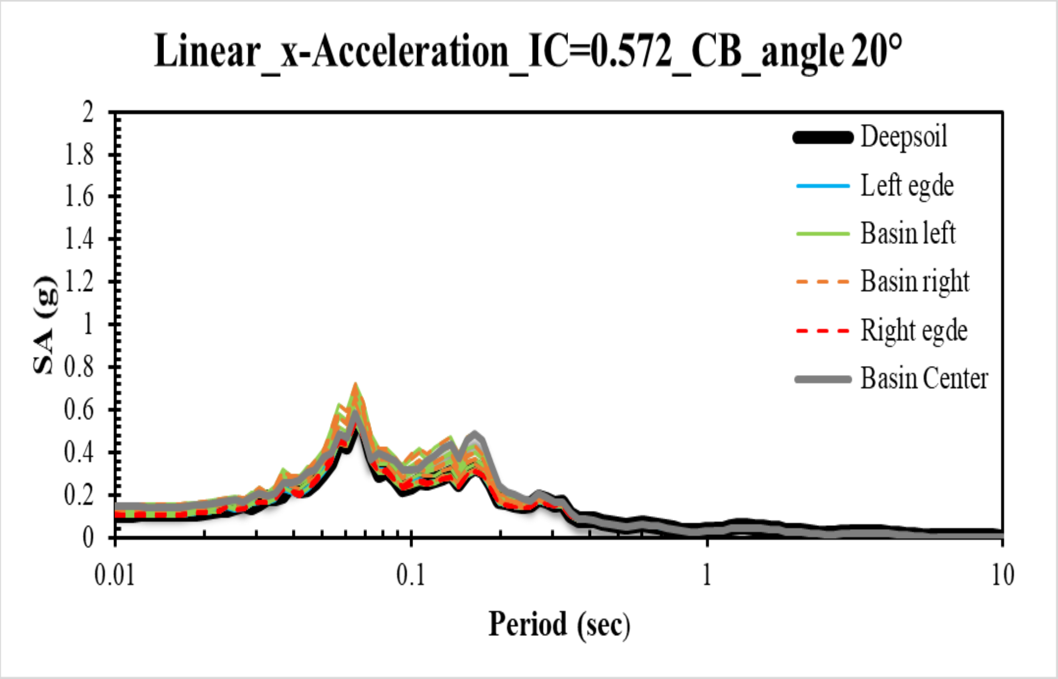

**Figure 4.2** *Spectral acceleration spectrum of x-acceleration for linear elastic case Vs=500 m/s _angle 20° with compliant base*

doi:10.6342/NTU201903794

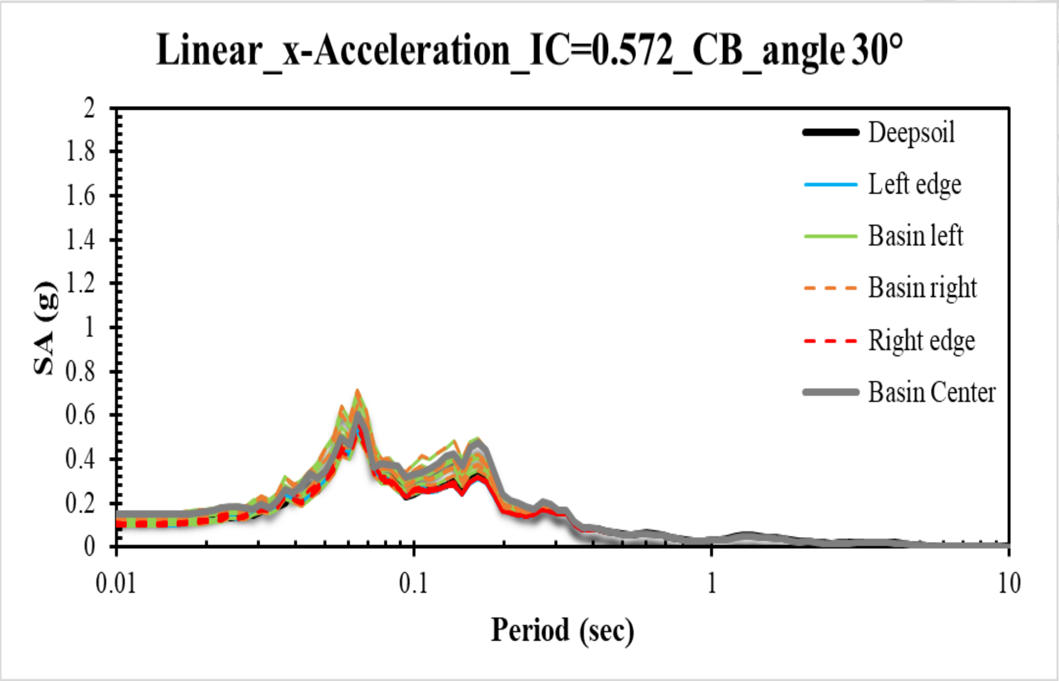

**Figure 4.3** *Spectral acceleration spectrum of x-acceleration for linear elastic case Vs=500 m/s _angle 30° with compliant base*

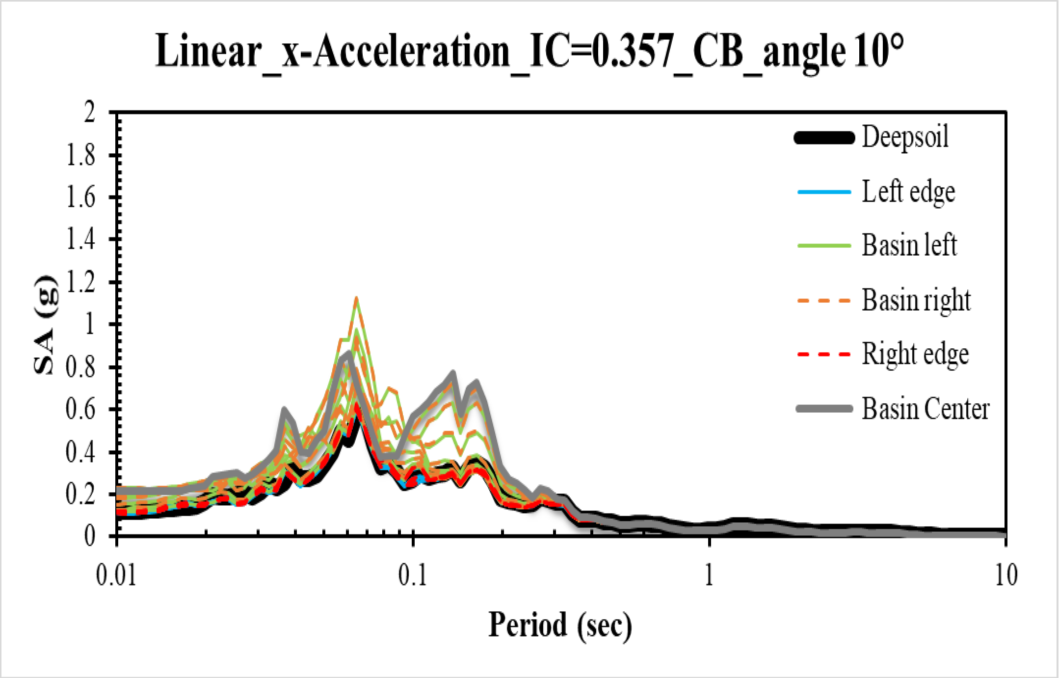

**Figure 4.4** *Spectral acceleration spectrum of x-acceleration for linear elastic case Vs=760 m/s _angle 10° with compliant base*

doi:10.6342/NTU201903794

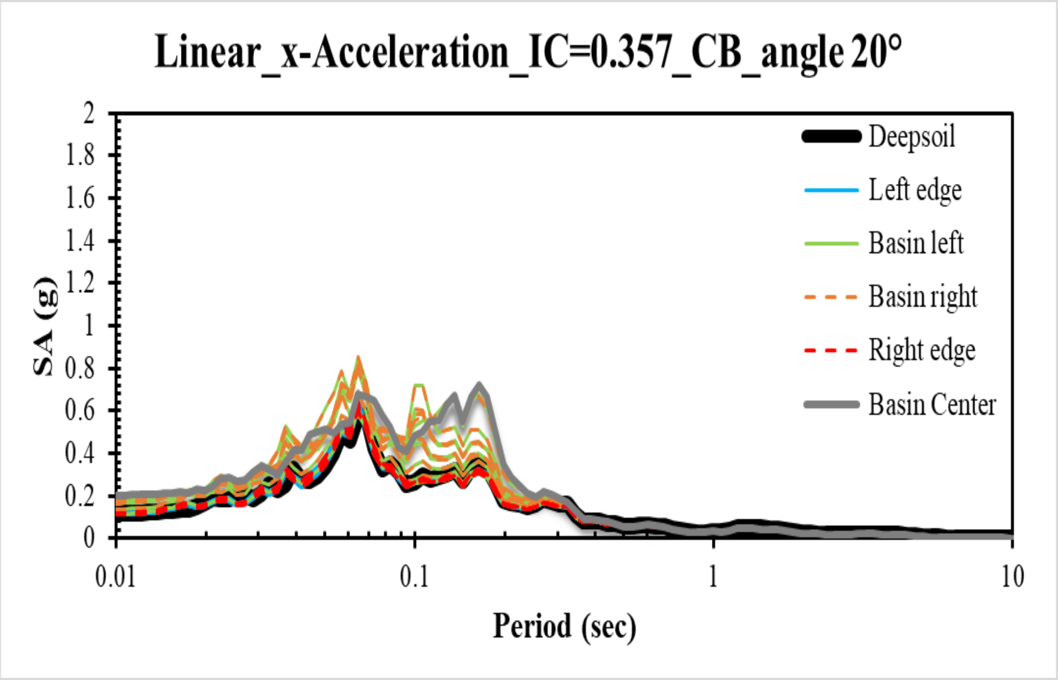

**Figure 4.5** *Spectral acceleration spectrum of x-acceleration for linear elastic case Vs=760 m/s _angle 20° with compliant base*

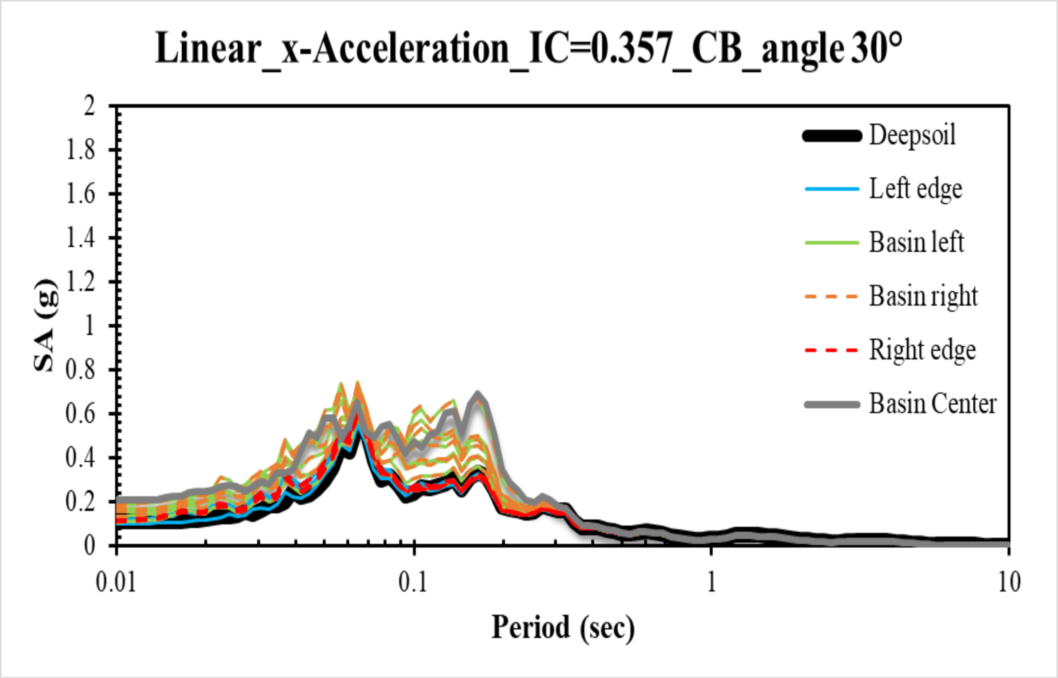

**Figure 4.6** *Spectral acceleration spectrum of x-acceleration for linear elastic case Vs=760 m/s _angle 30° with compliant base*

doi:10.6342/NTU201903794

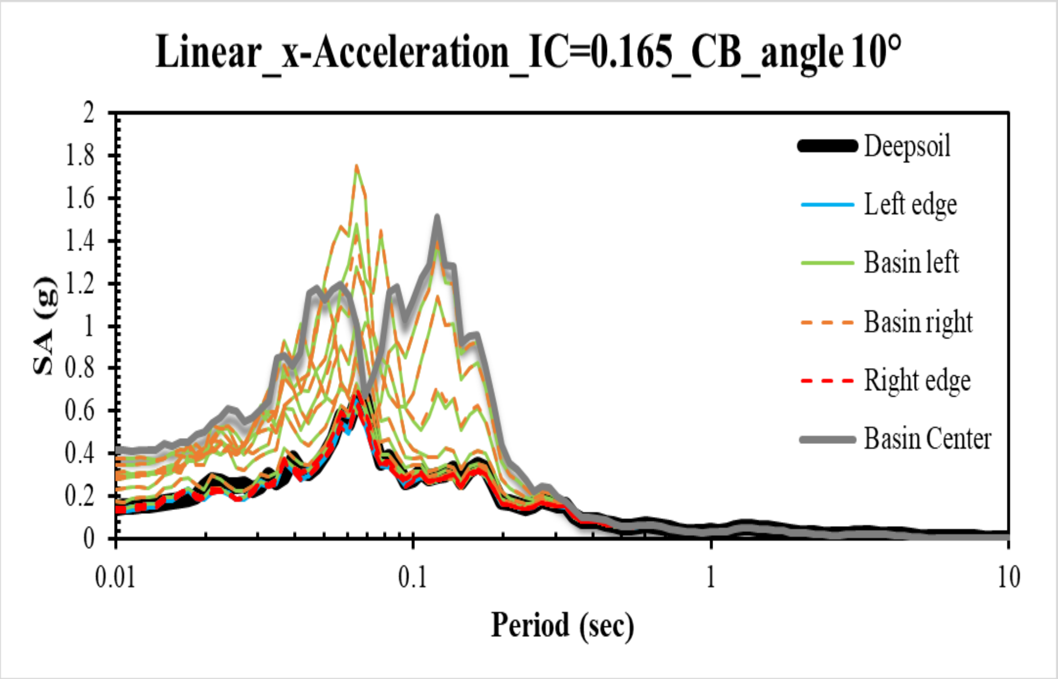

**Figure 4.7** *Spectral acceleration spectrum of x-acceleration for linear elastic case Vs=1500 m/s _angle 10° with compliant base*

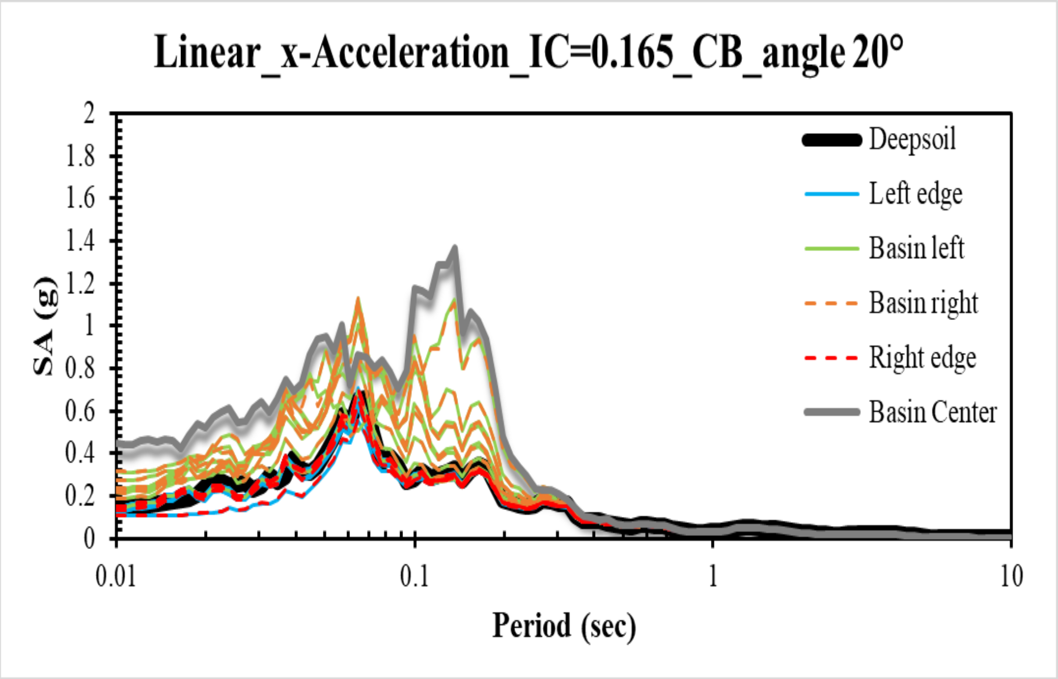

**Figure 4.8** *Spectral acceleration spectrum of x-acceleration for linear elastic case Vs=1500 m/s _angle 20° with compliant base*

doi:10.6342/NTU201903794

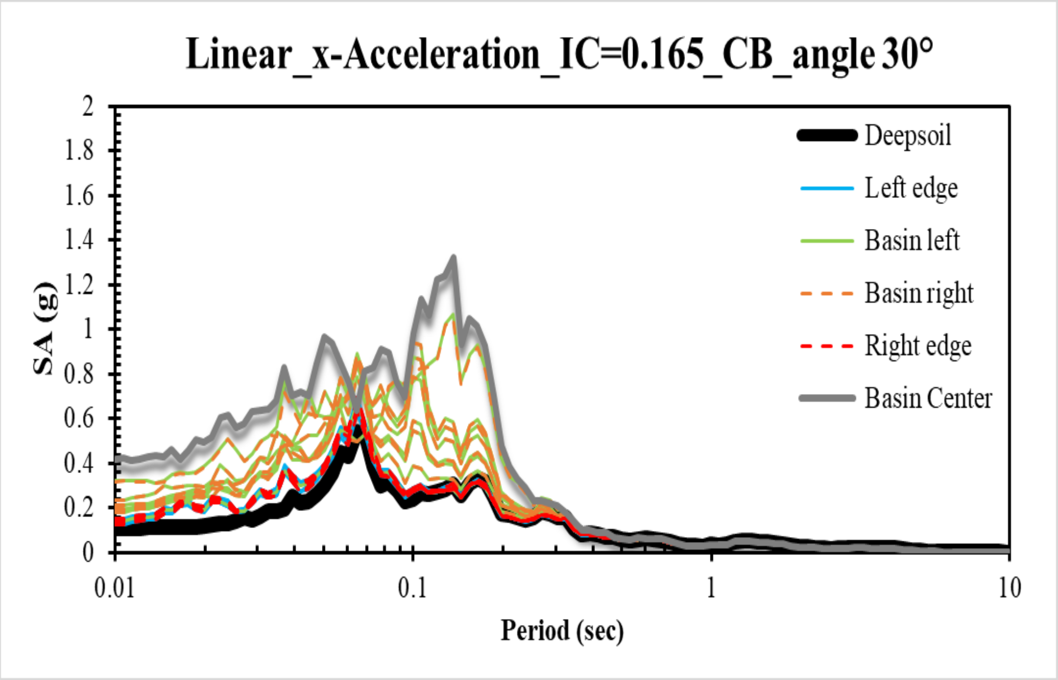

**Figure 4.9** *Spectral acceleration spectrum of x-acceleration for linear elastic case Vs=1500 m/s _angle 30° with compliant base*

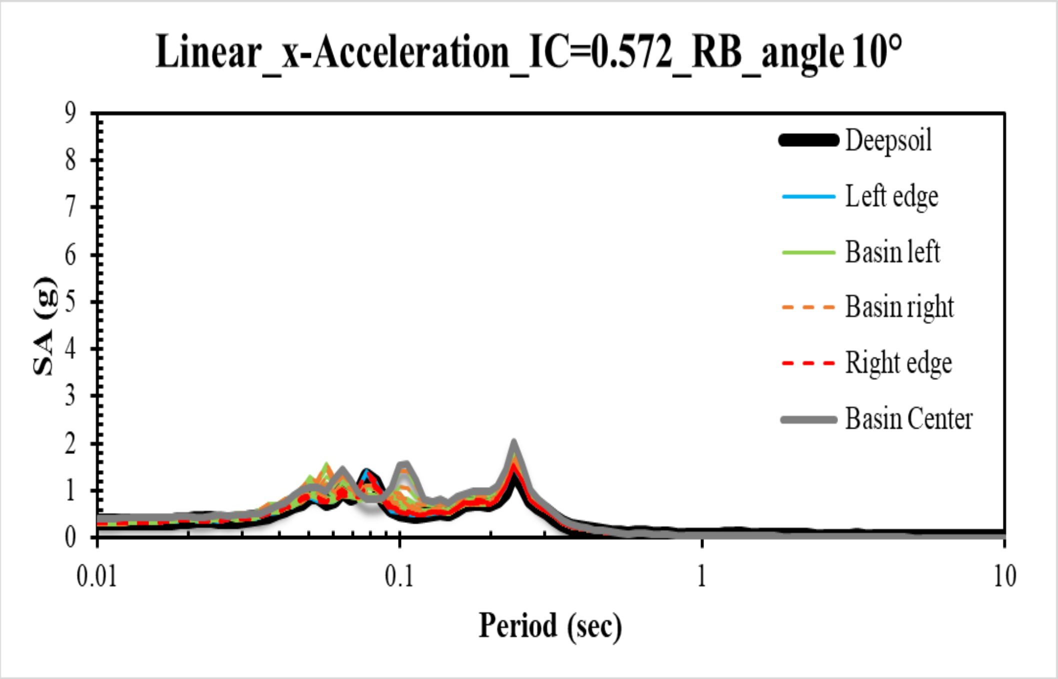

**Figure 4.10** *Spectral acceleration spectrum of x-acceleration for linear elastic case Vs=500 m/s _angle 10° with rigid base*

doi:10.6342/NTU201903794

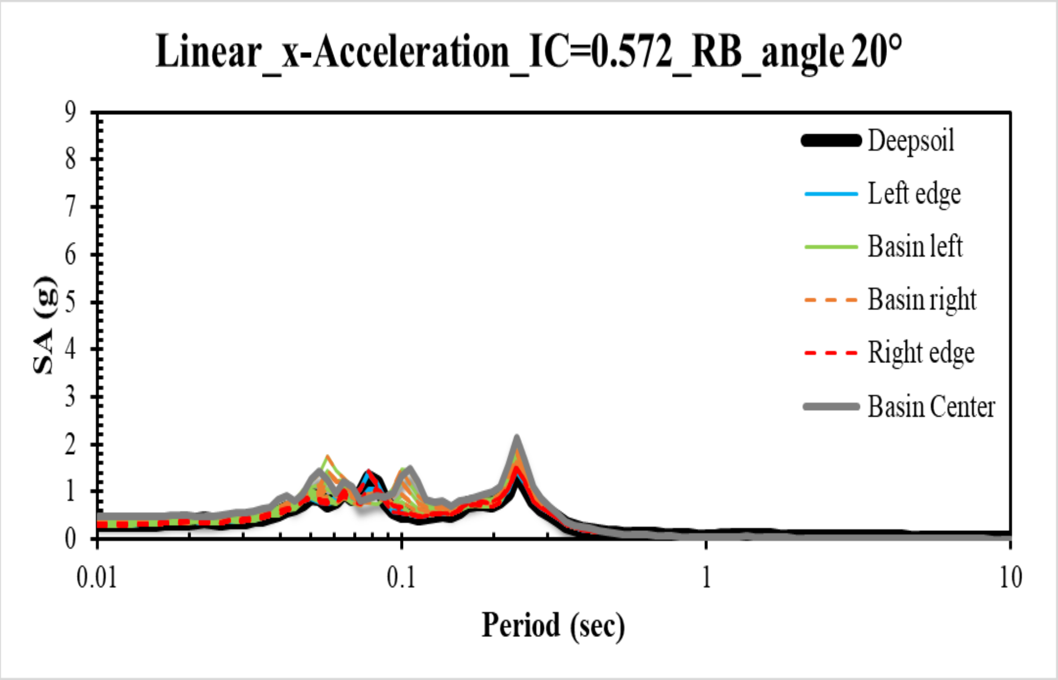

**Figure 4.11** *Spectral acceleration spectrum of x-acceleration for linear elastic case Vs=500 m/s _angle 20° with rigid base*

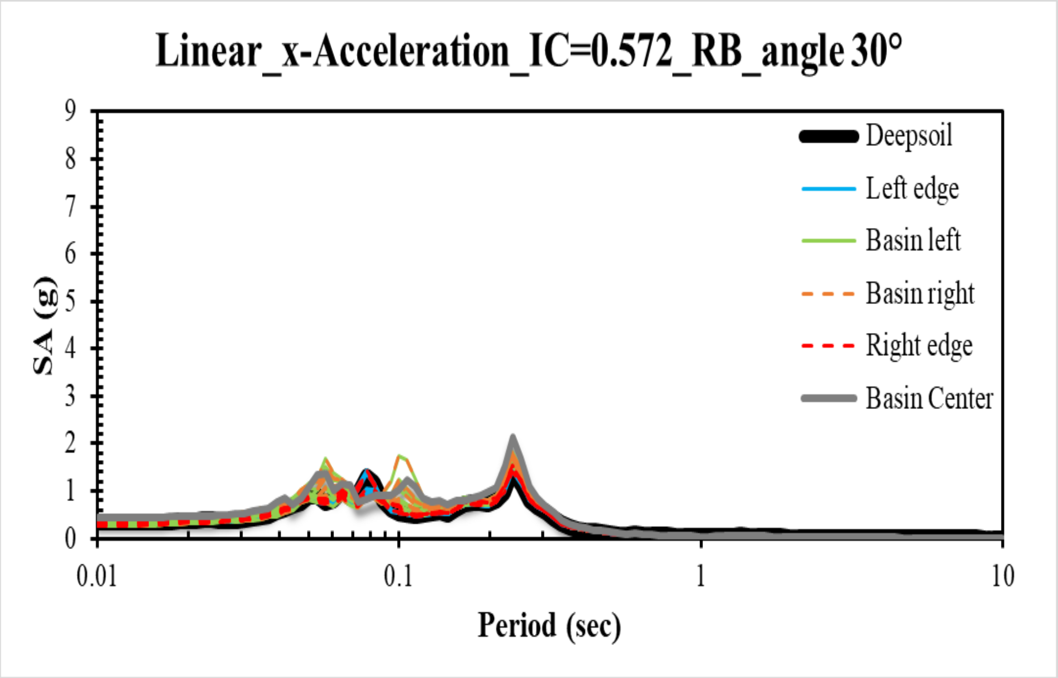

**Figure 4.12** *Spectral acceleration spectrum of x-acceleration for linear elastic case Vs=500 m/s _angle 30° with rigid base*

doi:10.6342/NTU201903794

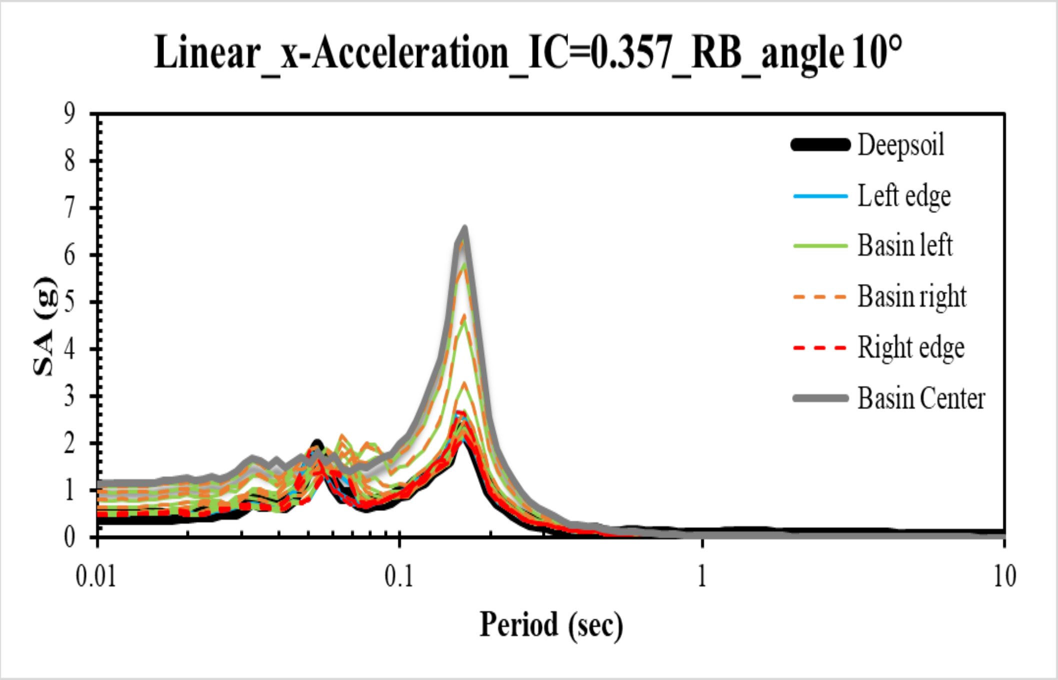

Figure 4.13 *Spectral acceleration spectrum of x-acceleration for linear elastic case Vs=760 m/s _angle 10° with rigid base*

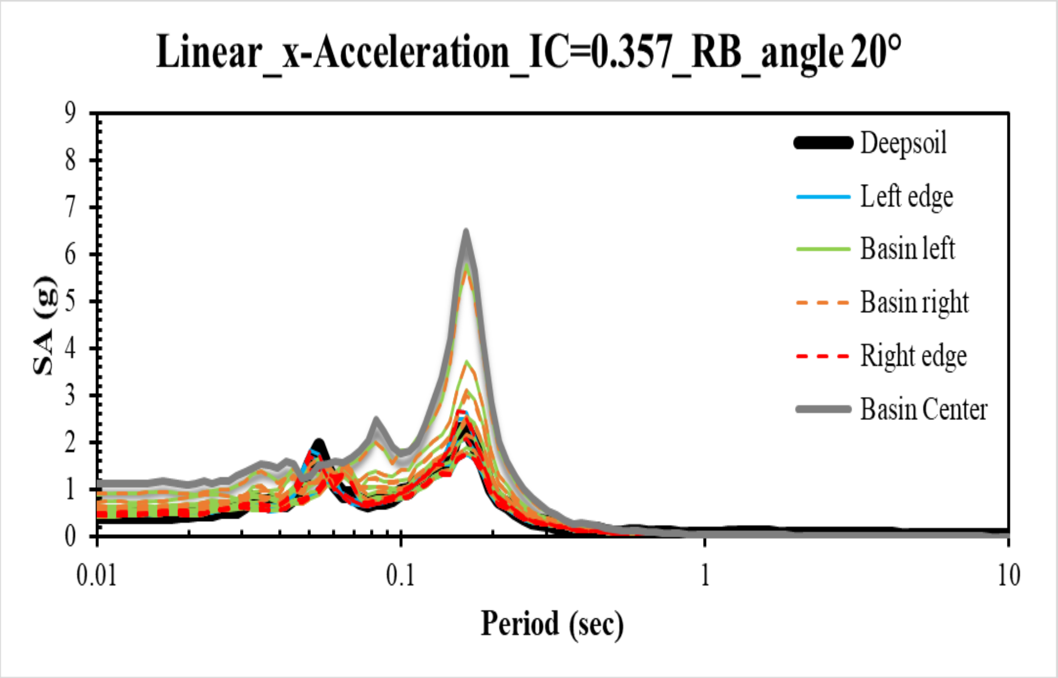

Figure 4.14 *Spectral acceleration spectrum of x-acceleration for linear elastic case Vs=760 m/s _angle 20° with rigid base*

doi:10.6342/NTU201903794

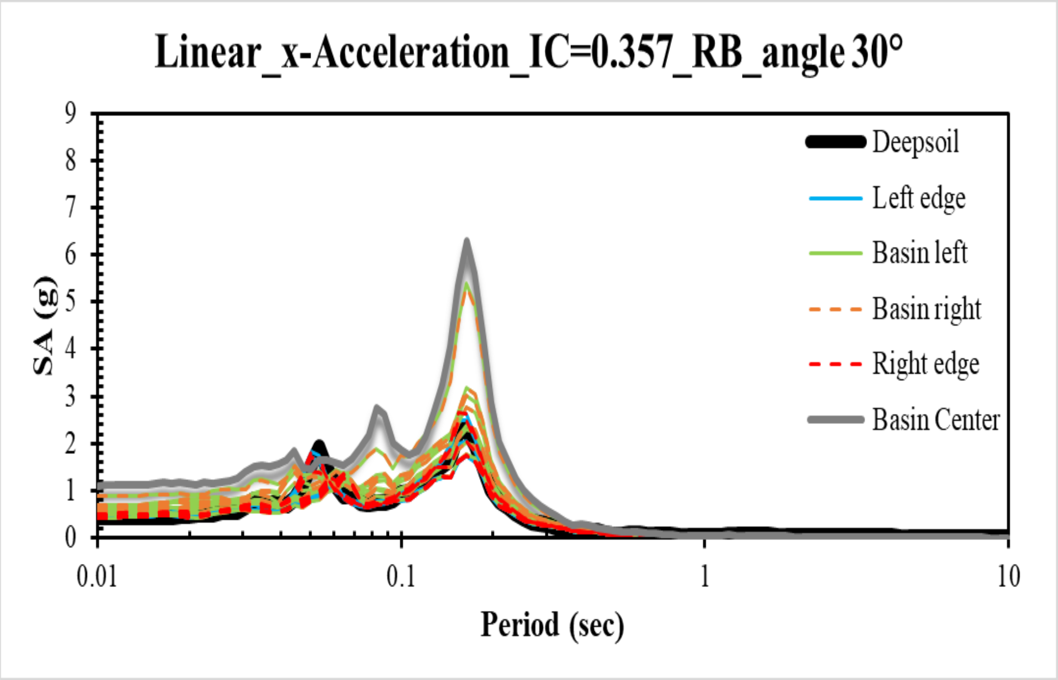

**Figure 4.15** *Spectral acceleration spectrum of x-acceleration for linear elastic case Vs=760 m/s _angle 30° with rigid base*

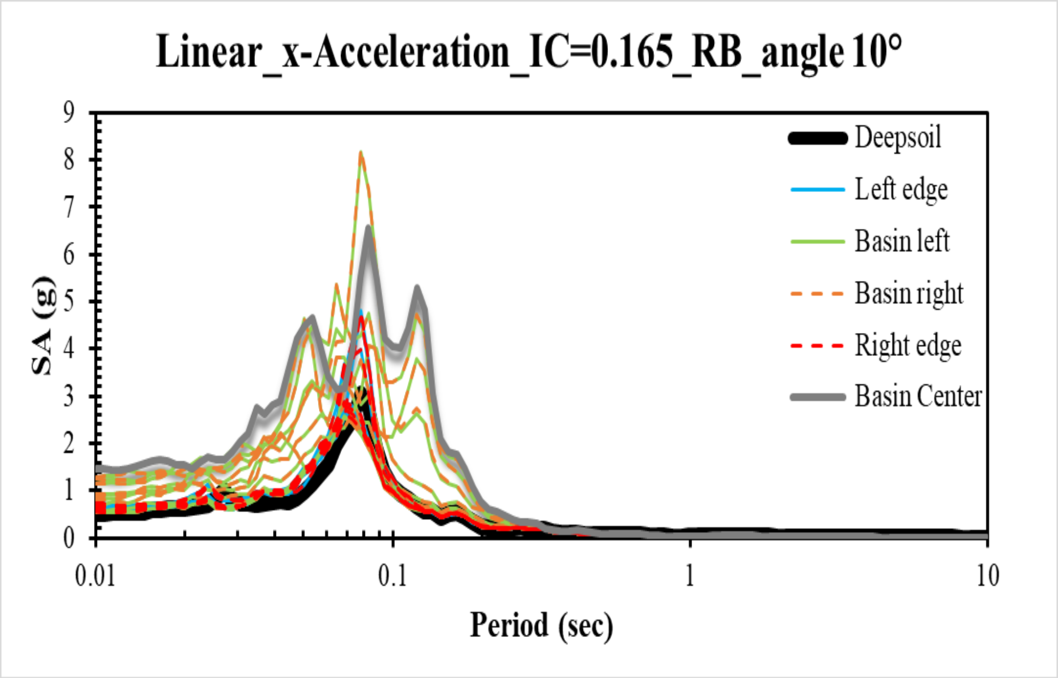

**Figure 4.16** *Spectral acceleration spectrum of x-acceleration for linear elastic case Vs=1500 m/s _angle 10° with rigid base*

doi:10.6342/NTU201903794

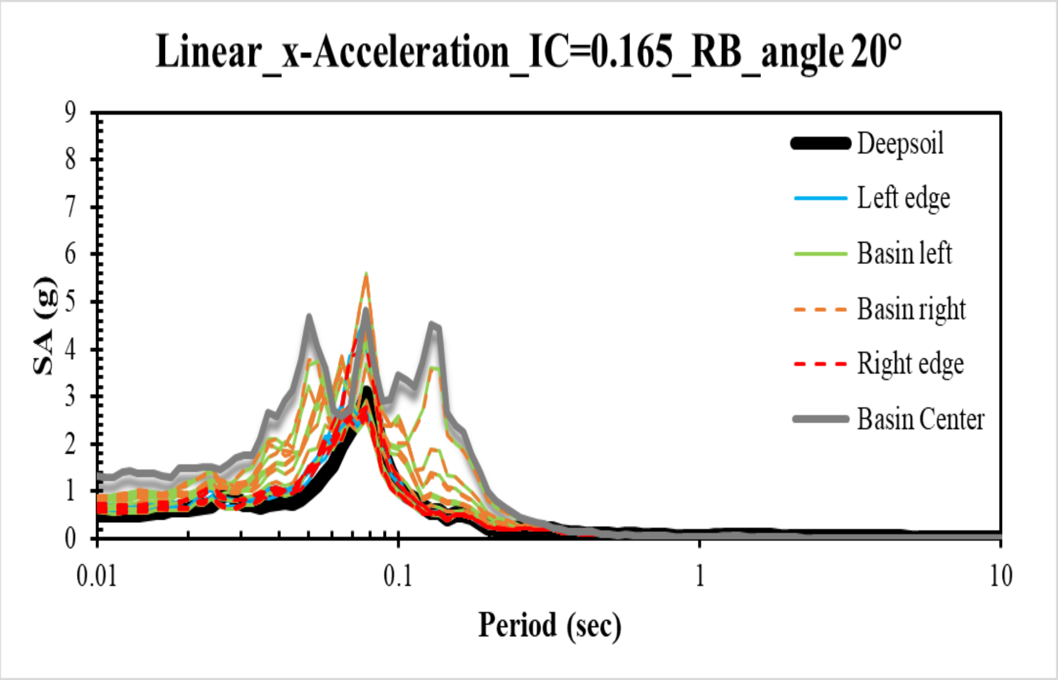

**Figure 4.17** *Spectral acceleration spectrum of x-acceleration for linear elastic case Vs=1500 m/s _angle 20° with rigid base*

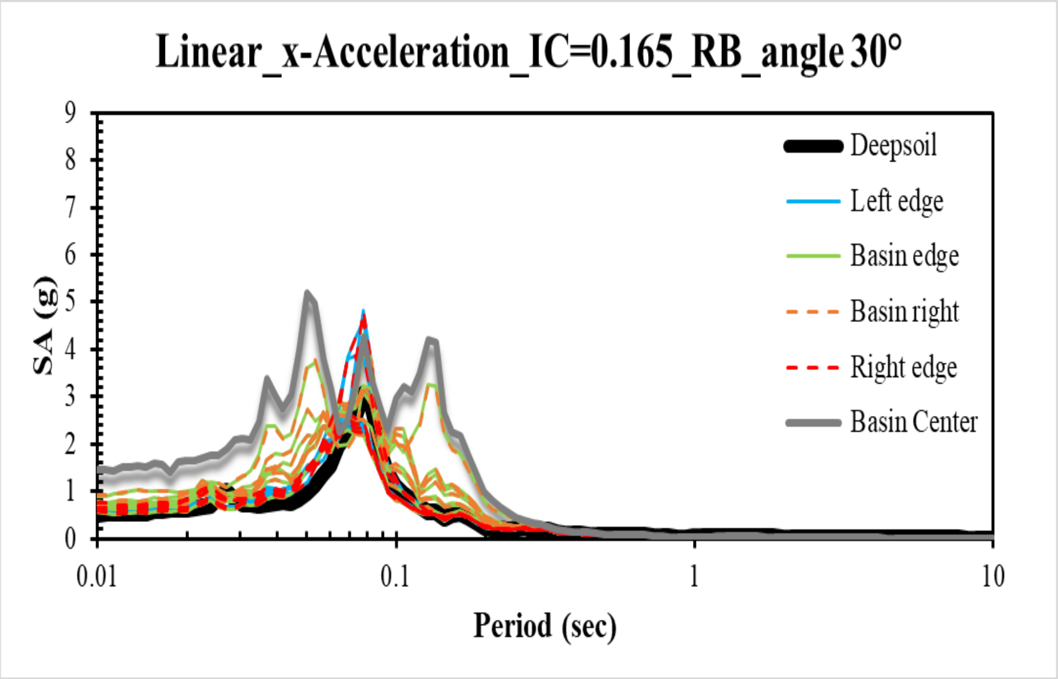

**Figure 4.18** *Spectral acceleration spectrum of x-acceleration for linear elastic case Vs=1500 m/s _angle 30° with rigid base*

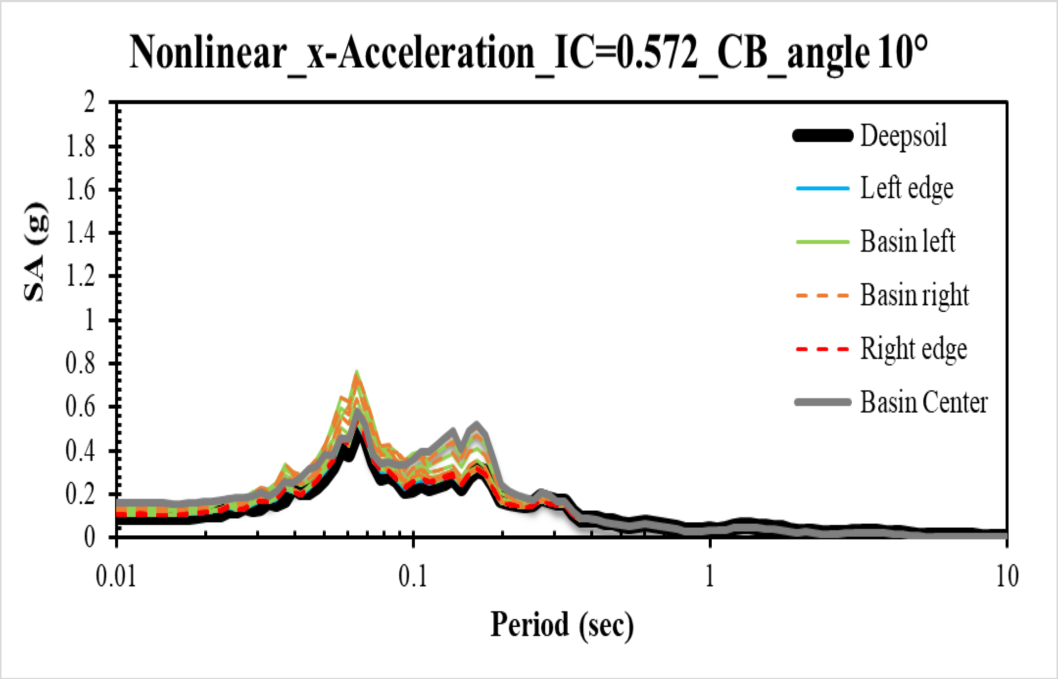

**Figure 4.19** *Spectral acceleration spectrum of x-acceleration for case Vs=500 m/s _angle 10° with compliant base*

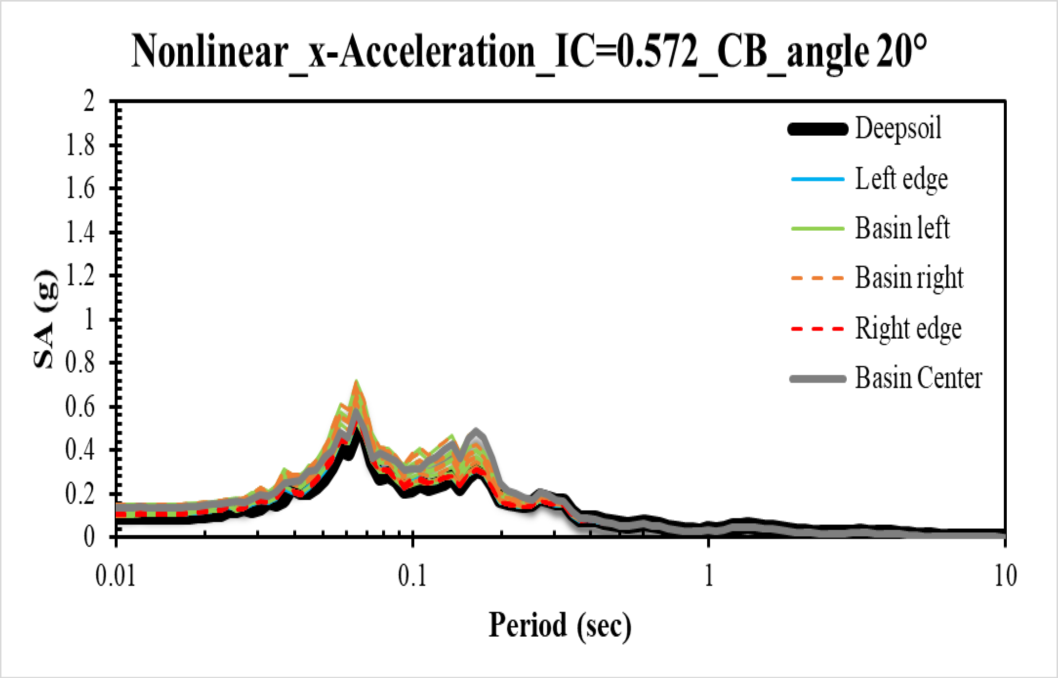

**Figure 4.20** *Spectral acceleration spectrum of x-acceleration for nonlinear case Vs=500 m/s _angle 20° with compliant base*

doi:10.6342/NTU201903794

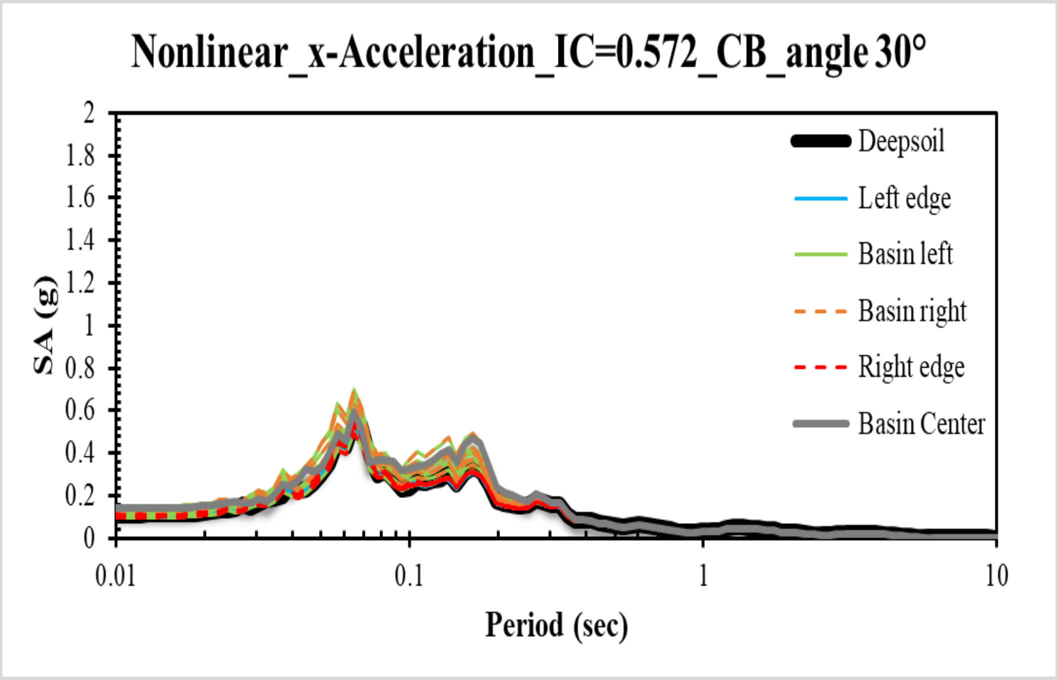

**Figure 4.21** *Spectral acceleration spectrum of x-acceleration for nonlinear case Vs=500 m/s _angle 30° with compliant base*

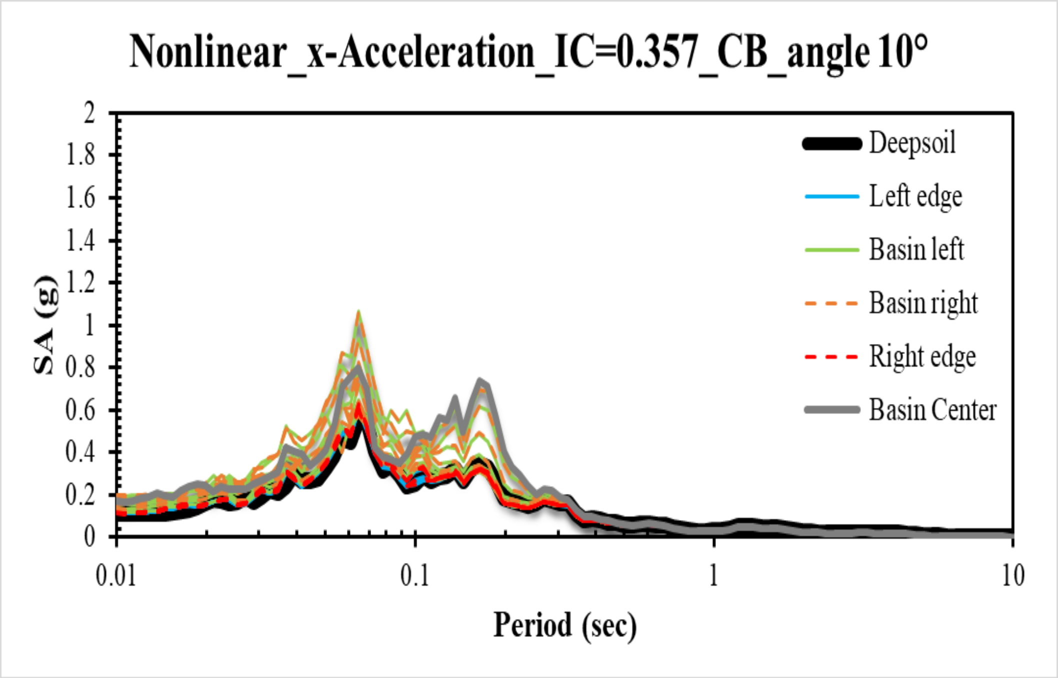

**Figure 4.22** *Spectral acceleration spectrum of x-acceleration for nonlinear case Vs=760 m/s _angle 10° with compliant base*

doi:10.6342/NTU201903794

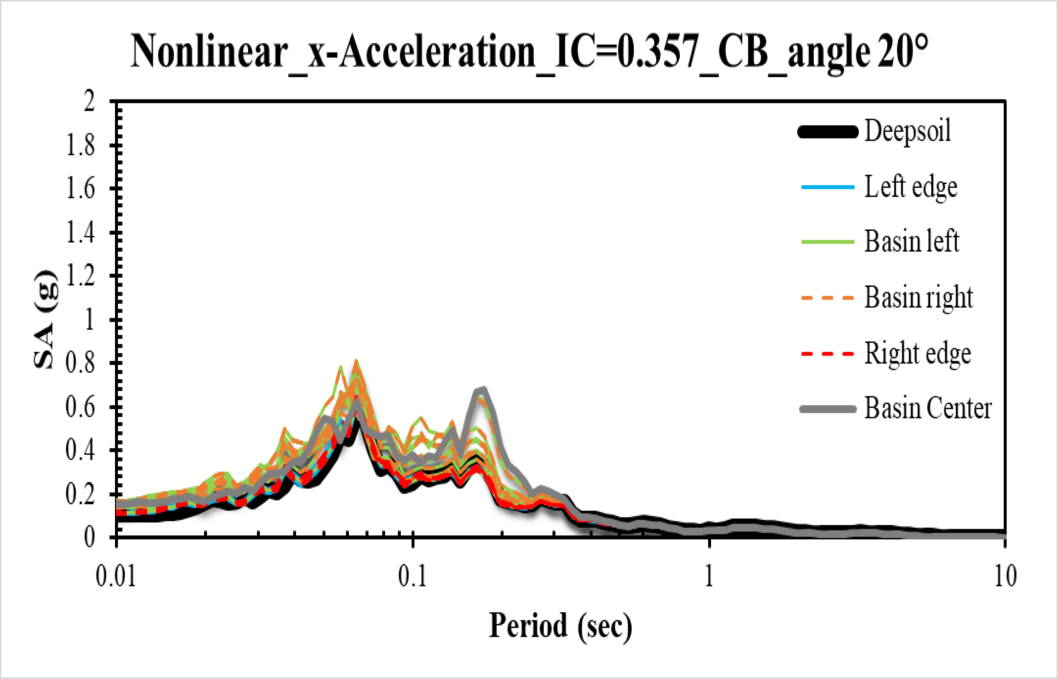

**Figure 4.23** *Spectral acceleration spectrum of x-acceleration for nonlinear case Vs=760 m/s _angle 20° with compliant base*

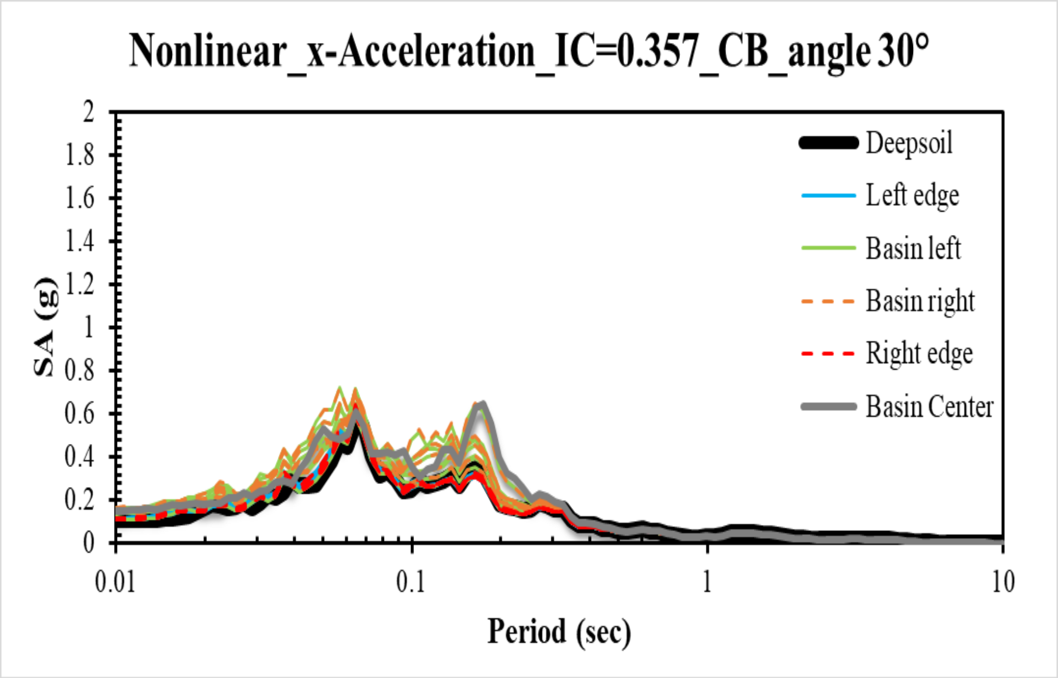

**Figure 4.24** *Spectral acceleration spectrum of x-acceleration for nonlinear case Vs=760 m/s _angle 30° with compliant base*

doi:10.6342/NTU201903794

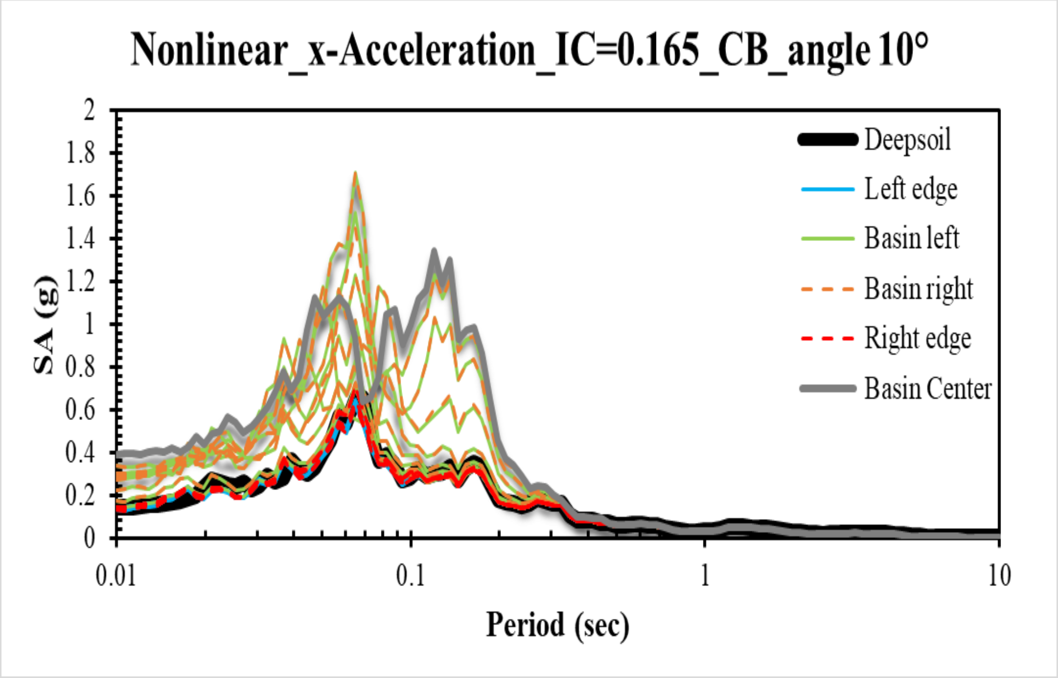

**Figure 4.25** *Spectral acceleration spectrum of x-acceleration for nonlinear case Vs=1500 m/s _angle 10° with compliant base*

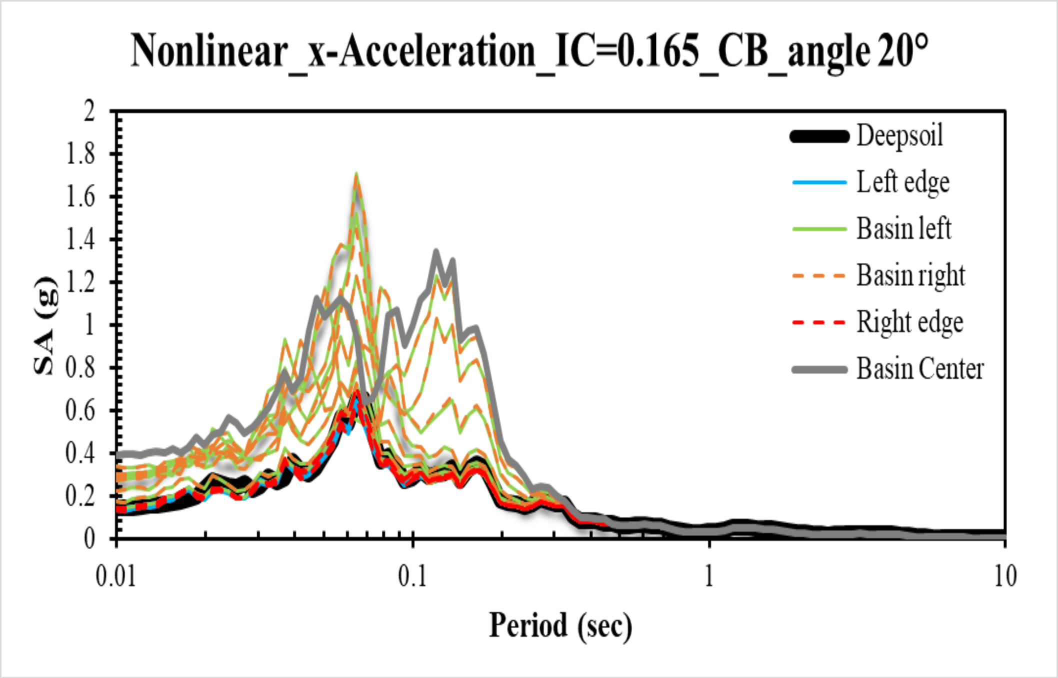

**Figure 4.26** *Spectral acceleration spectrum of x-acceleration for nonlinear case Vs=1500 m/s _angle 20° with compliant base*

doi:10.6342/NTU201903794

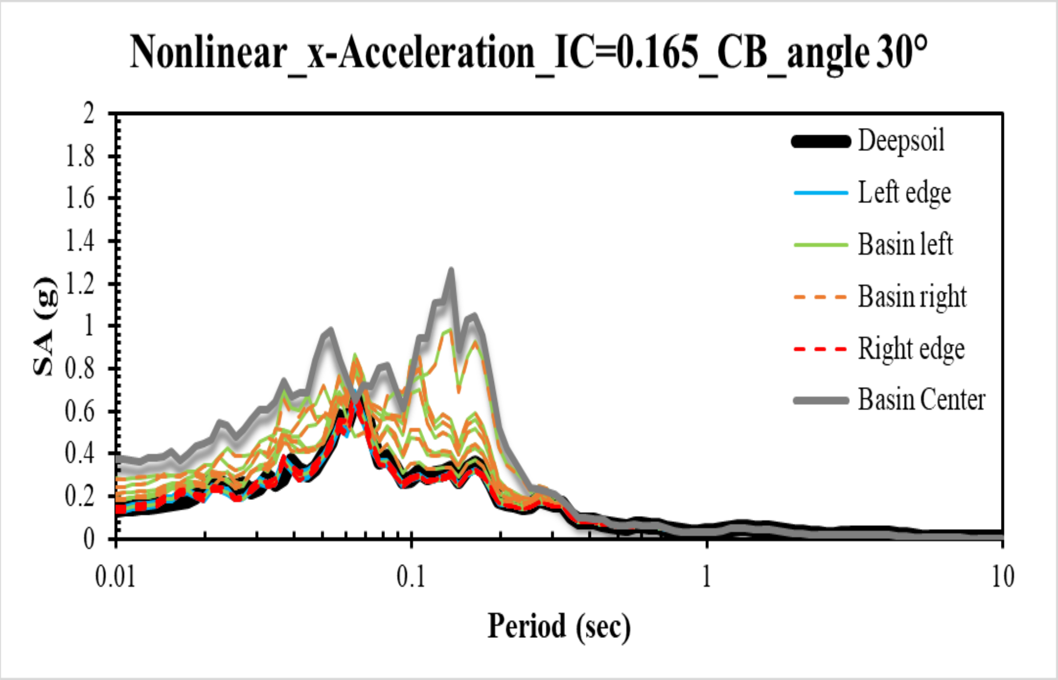

**Figure 4.27** *Spectral acceleration spectrum of x-acceleration for nonlinear case Vs=1500 m/s _angle 30° with compliant base*

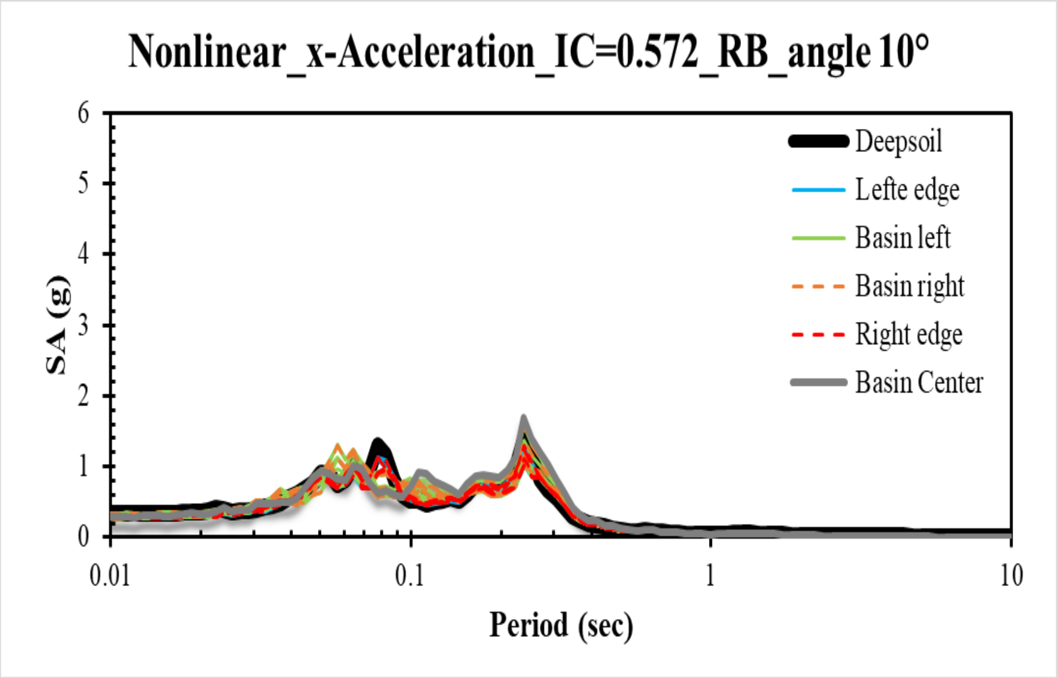

**Figure 4.28** *Spectral acceleration spectrum of x-acceleration for nonlinear case Vs=500 m/s _angle 10° with rigid base*

doi:10.6342/NTU201903794

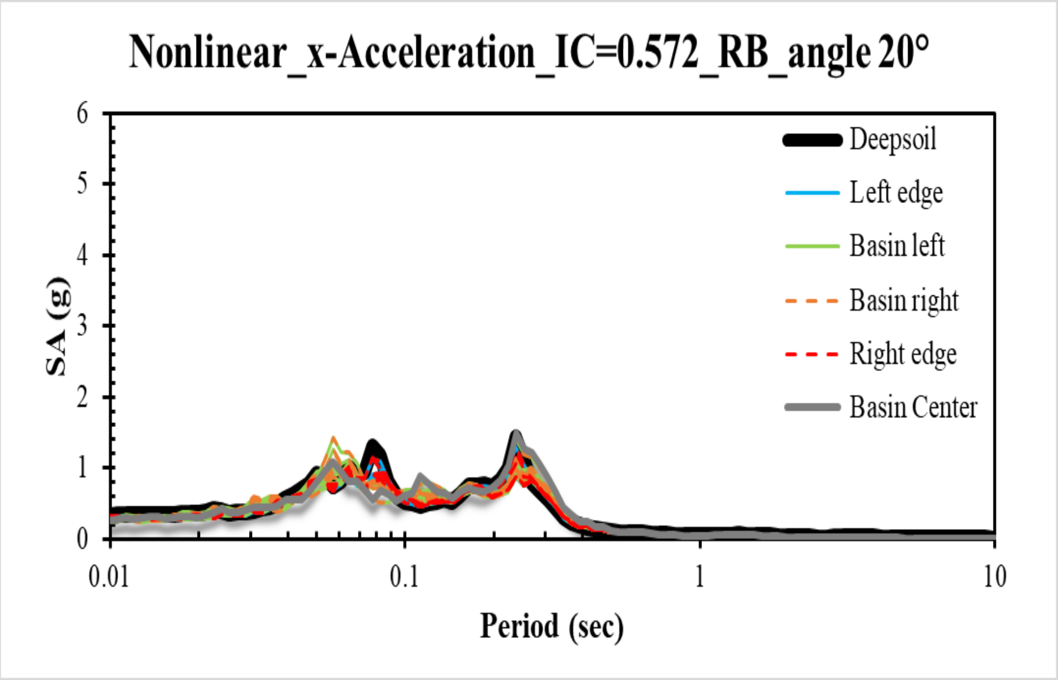

**Figure 4.29** *Spectral acceleration spectrum of x-acceleration for nonlinear case Vs=500 m/s _angle 20° with rigid base*

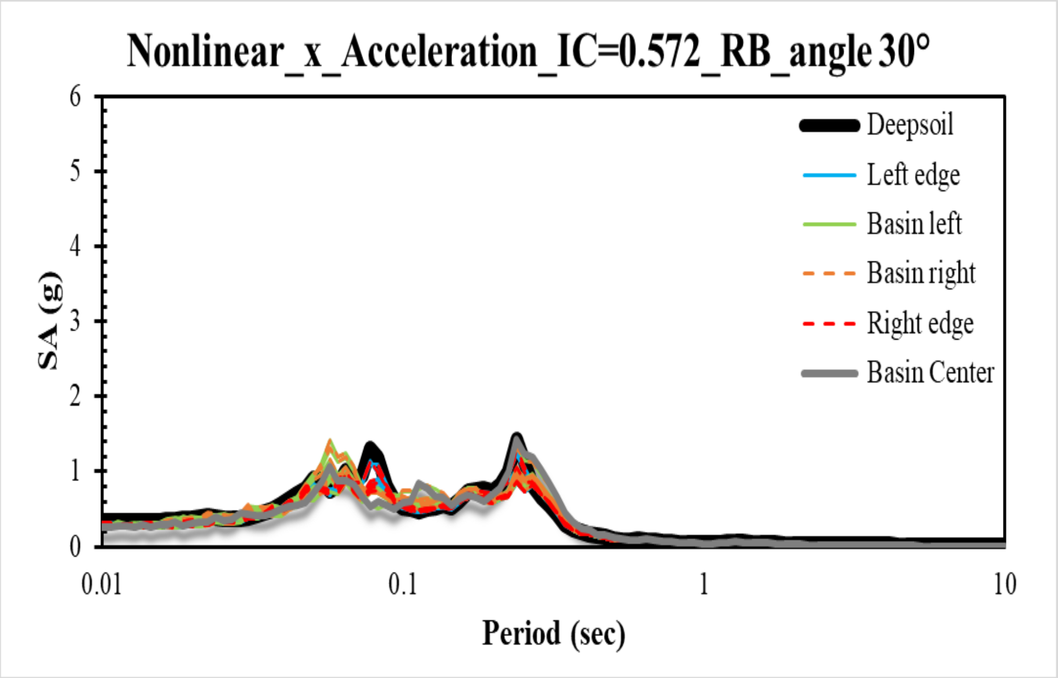

**Figure 4.30** *Spectral acceleration spectrum of x-acceleration for nonlinear case Vs=500 m/s _angle 30° with rigid base*

doi:10.6342/NTU201903794

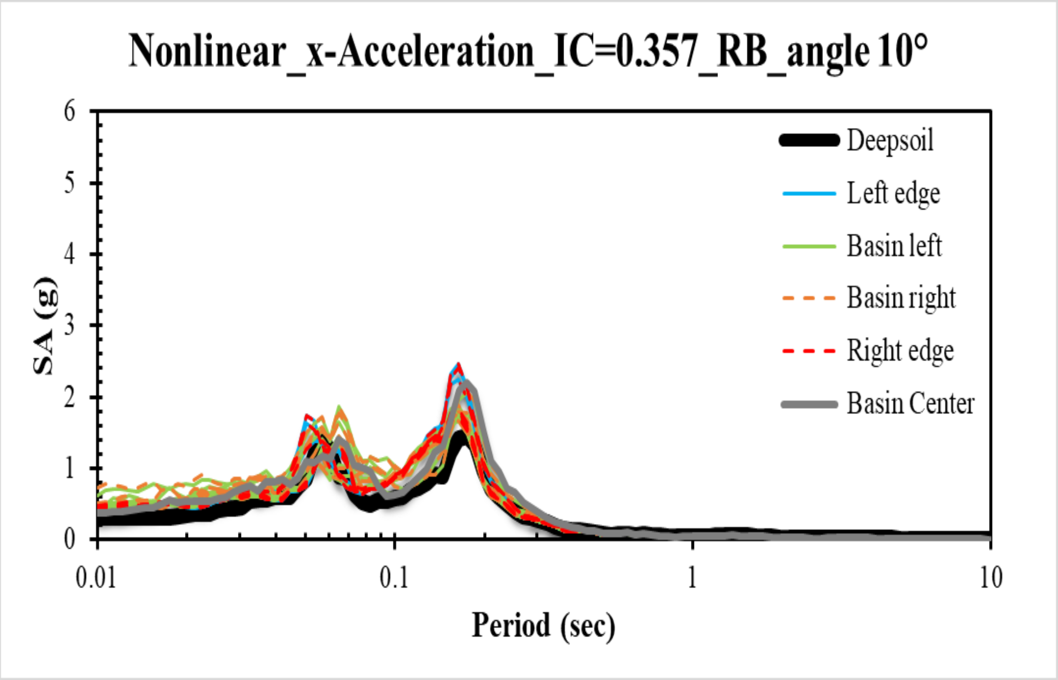

**Figure 4.31** *Spectral acceleration spectrum of x-acceleration for nonlinear case Vs=760 m/s _angle 10° with rigid base*

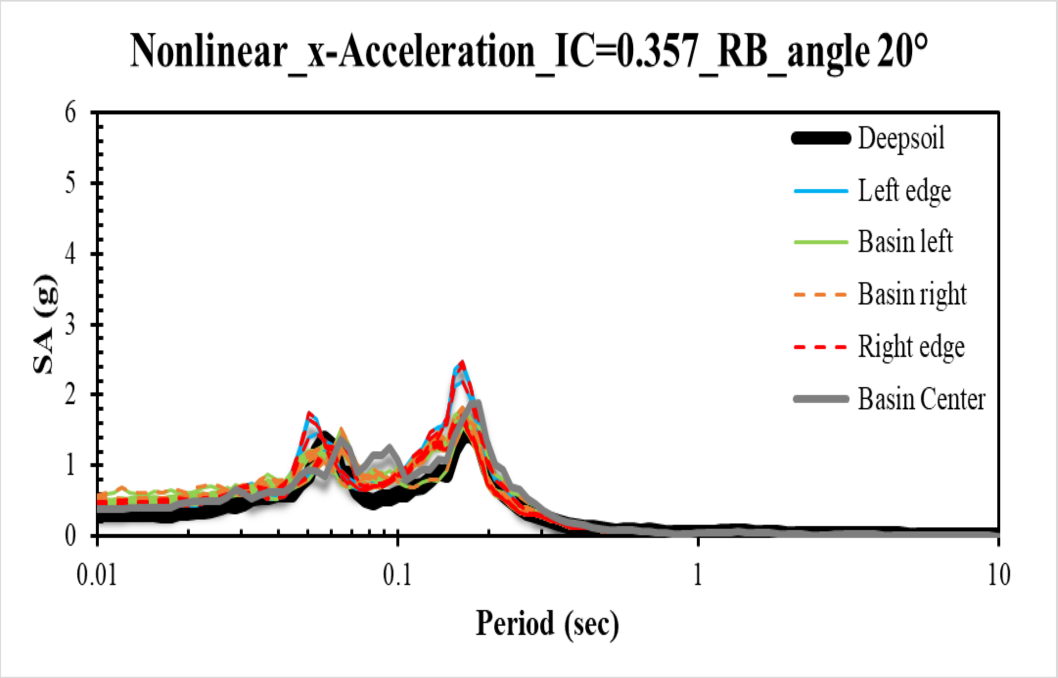

**Figure 4.32** *Spectral acceleration spectrum of x-acceleration for nonlinear case Vs=760 m/s _angle 20° with rigid base*

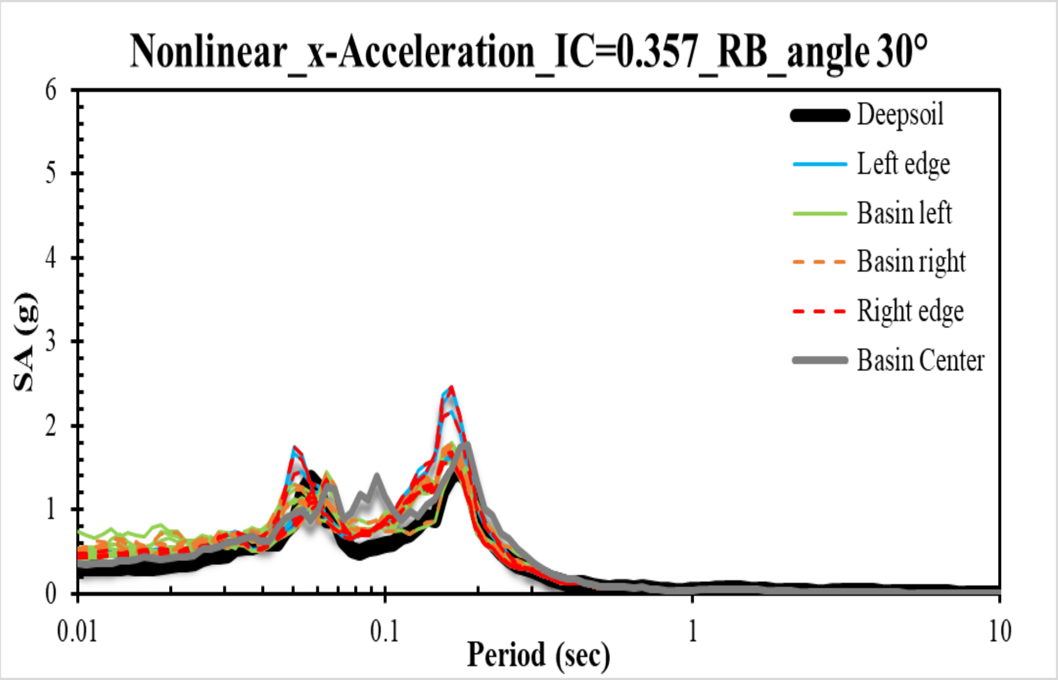

**Figure 4.33** *Spectral acceleration spectrum of x-acceleration for nonlinear case Vs=760 m/s _angle 30° with rigid base*

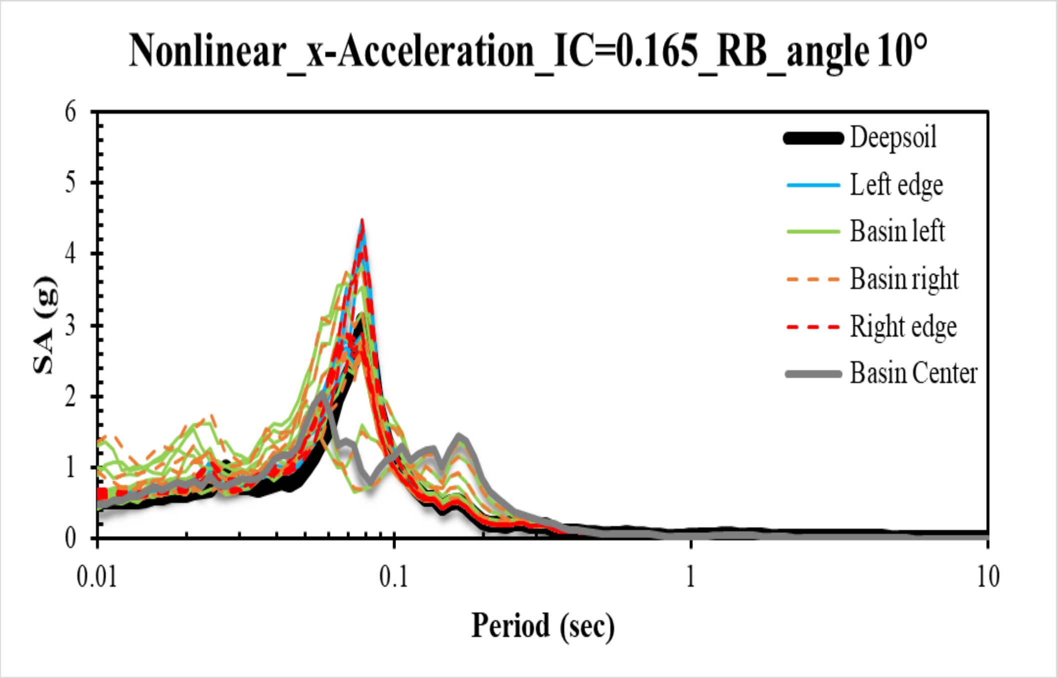

**Figure 4.34** *Spectral acceleration spectrum of x-acceleration for nonlinear case Vs=1500 m/s _angle 10° with rigid base*

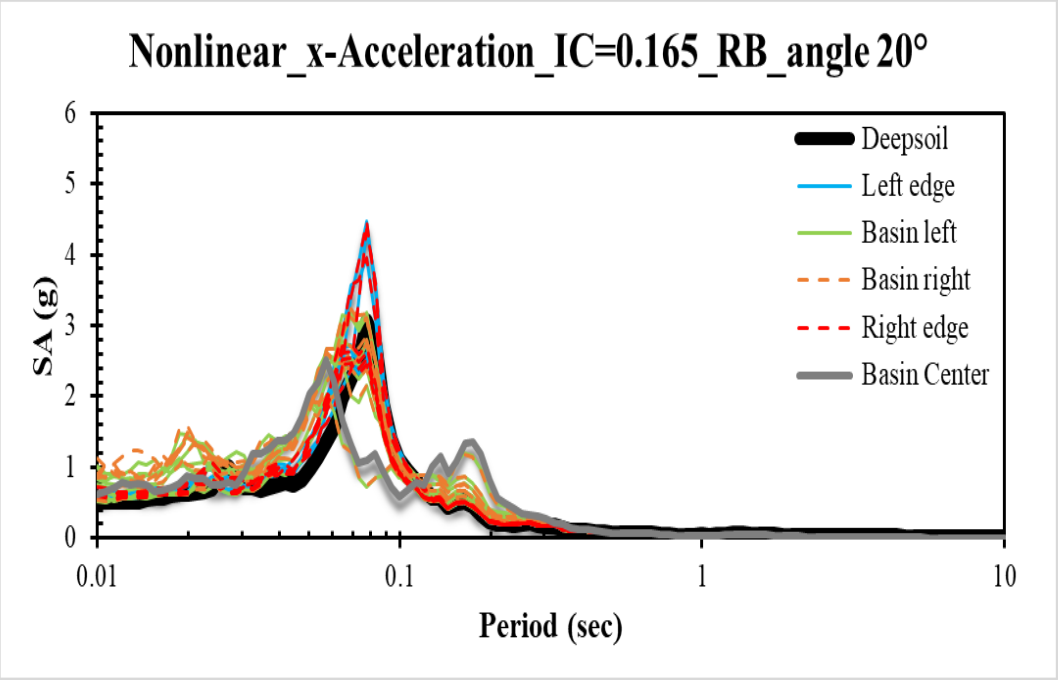

**Figure 4.35** *Spectral acceleration spectrum of x-acceleration for nonlinear case Vs=1500 m/s _angle 20° with rigid base*

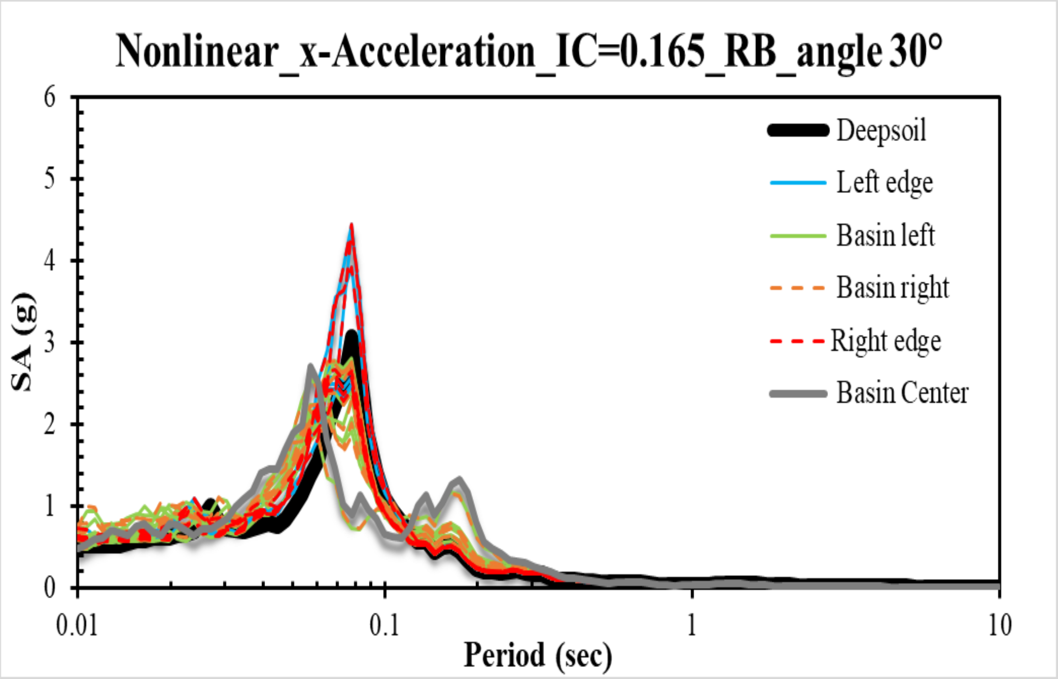

**Figure 4.36** *Spectral acceleration spectrum of x-acceleration for nonlinear case Vs=1500 m/s _angle 30° with rigid base*

doi:10.6342/NTU201903794

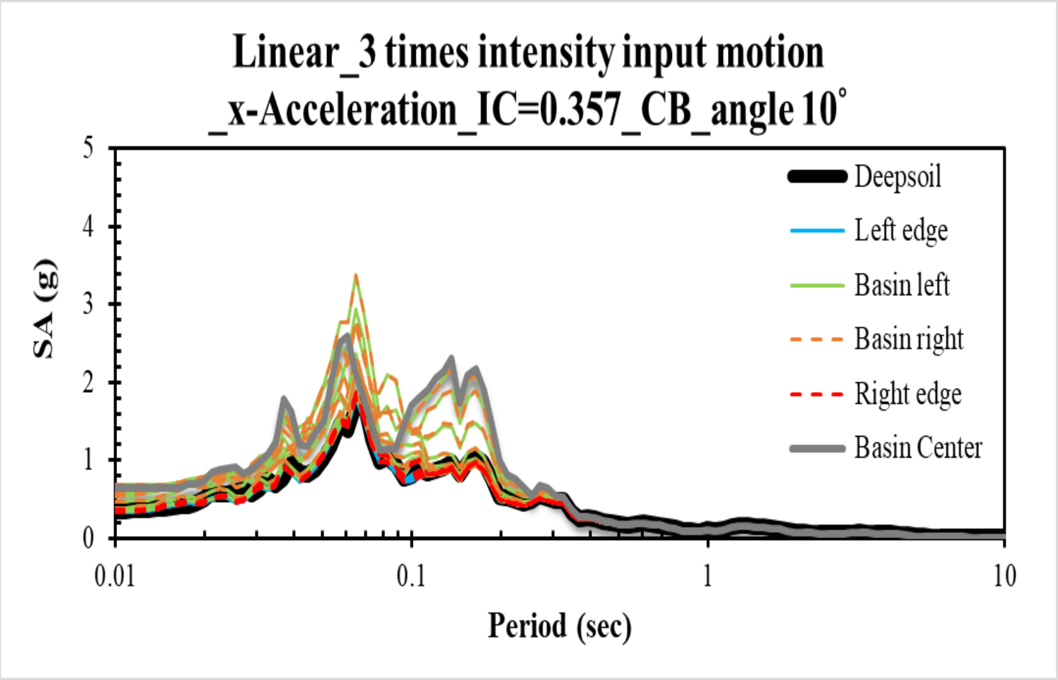

**Figure 4.37** *Spectral acceleration spectrum of 3 times intensity input motion for linear case Vs=760 m/s _angle 10° with compliant base*

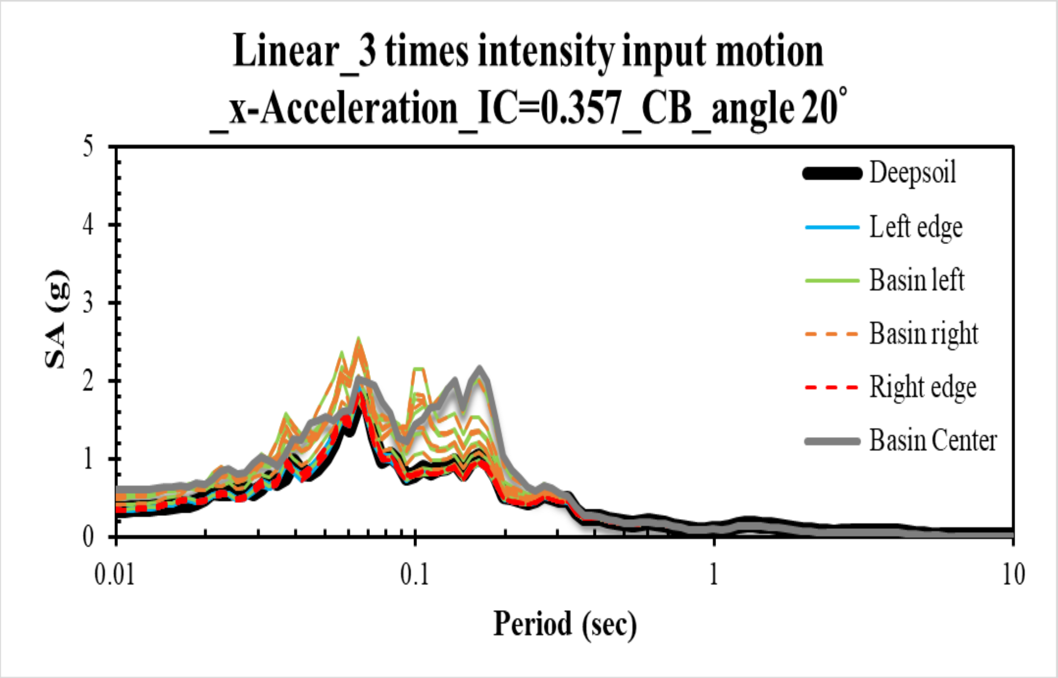

**Figure 4.38** *Spectral acceleration spectrum of 3 times intensity input motion for linear case Vs=760 m/s _angle 20° with compliant base*

doi:10.6342/NTU201903794

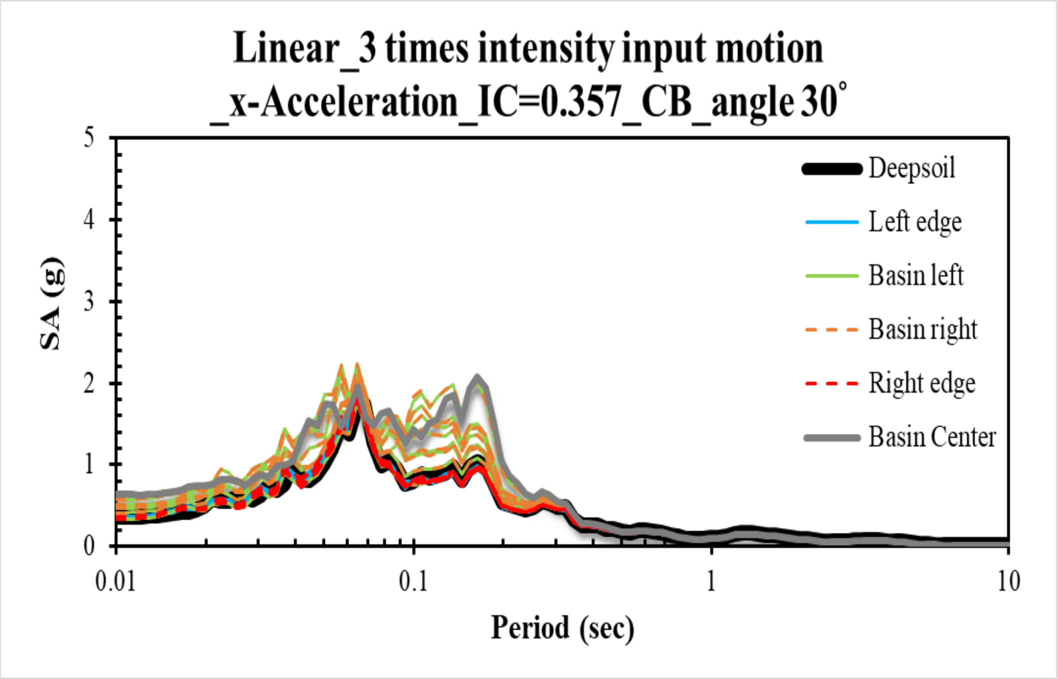

**Figure 4.39** *Spectral acceleration spectrum of 3 times intensity input motion for linear case Vs=760 m/s _angle 30° with compliant base*

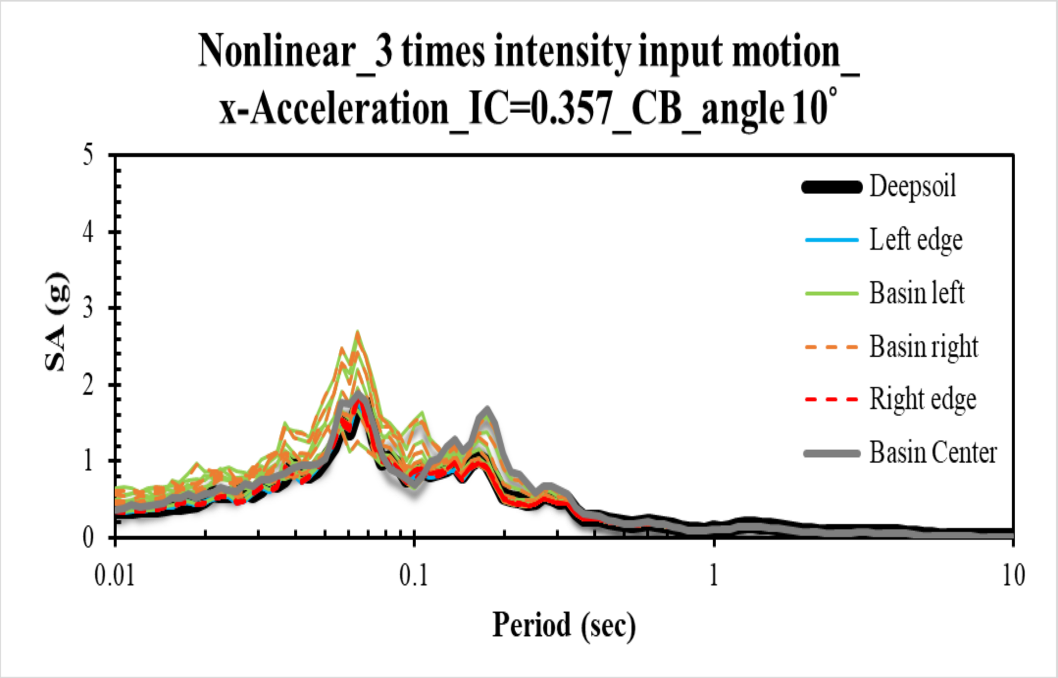

**Figure 4.40** *Spectral acceleration spectrum of 3 times intensity input motion for linear case Vs=760 m/s _angle 10° with nonlinear compliant base*

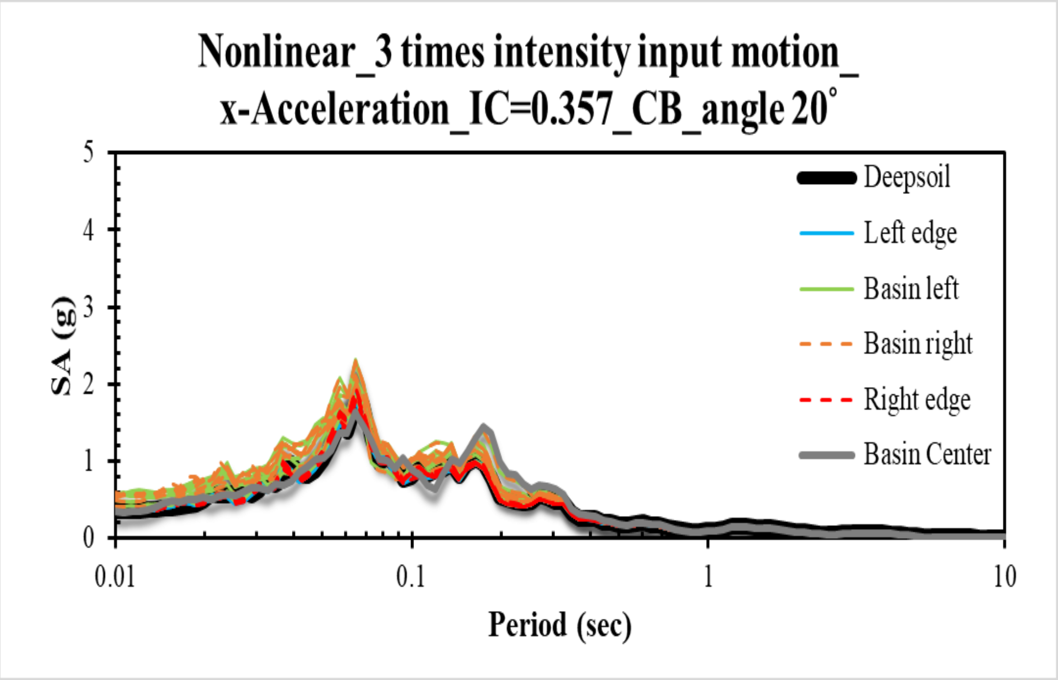

**Figure 4.41** *Spectral acceleration spectrum of 3 times intensity input motion for linear case Vs=760 m/s _angle 20° with nonlinear compliant base*

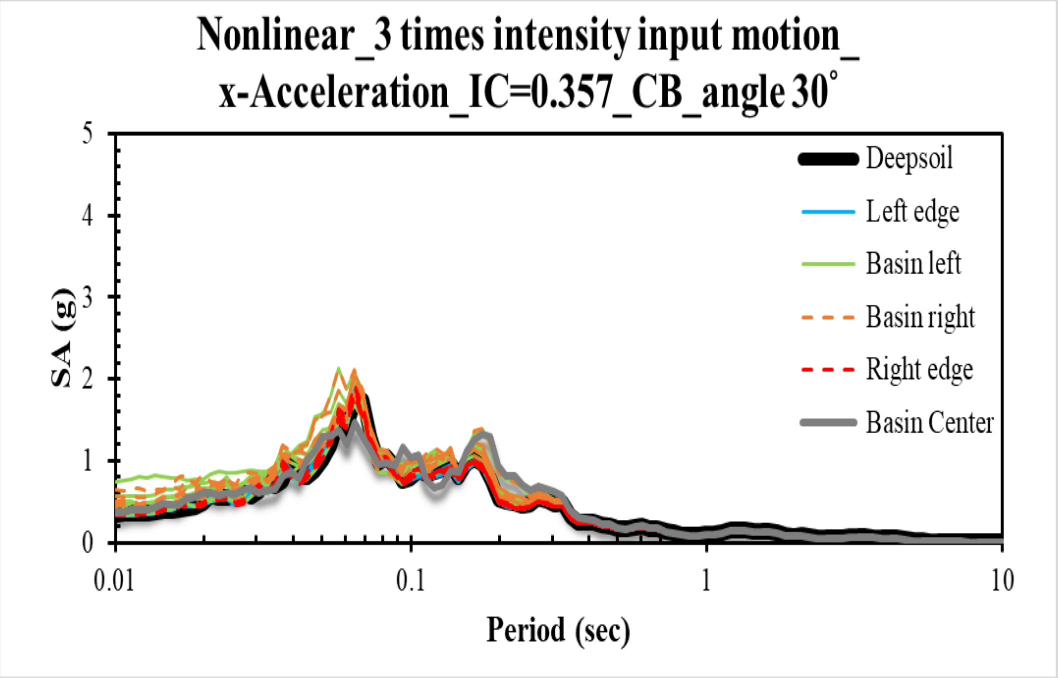

**Figure 4.42** *Spectral acceleration spectrum of 3 times intensity input motion for linear case Vs=760 m/s _angle 30° with nonlinear compliant base*

doi:10.6342/NTU201903794

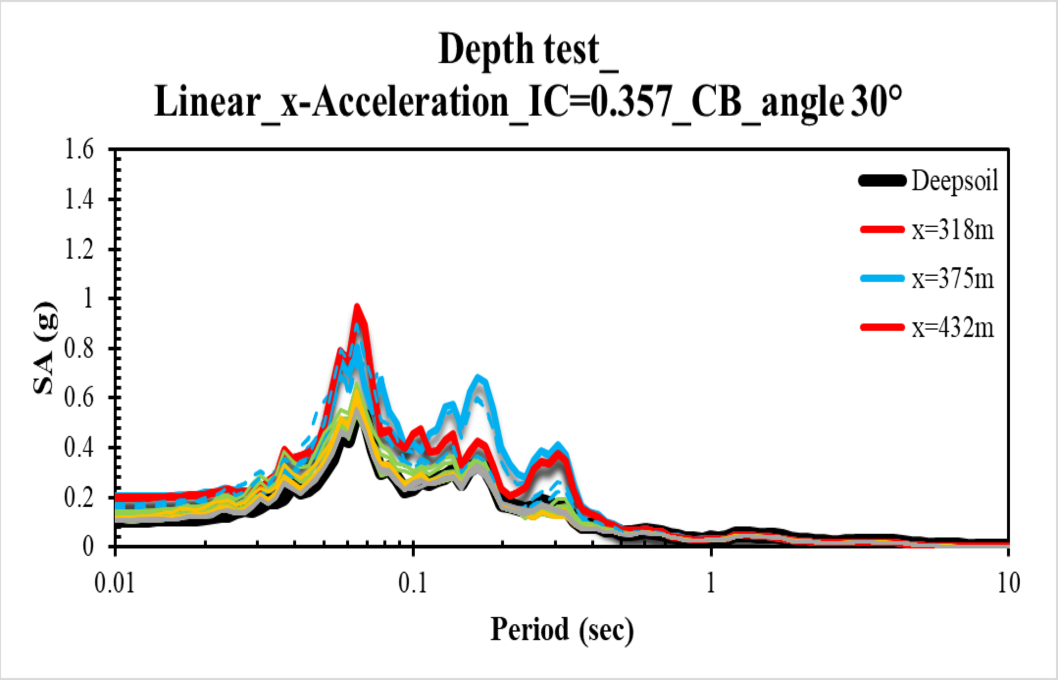

**Figure 4.43** *Depth test of compliant base with shear-wave velocity 760 m/s in linear cases*

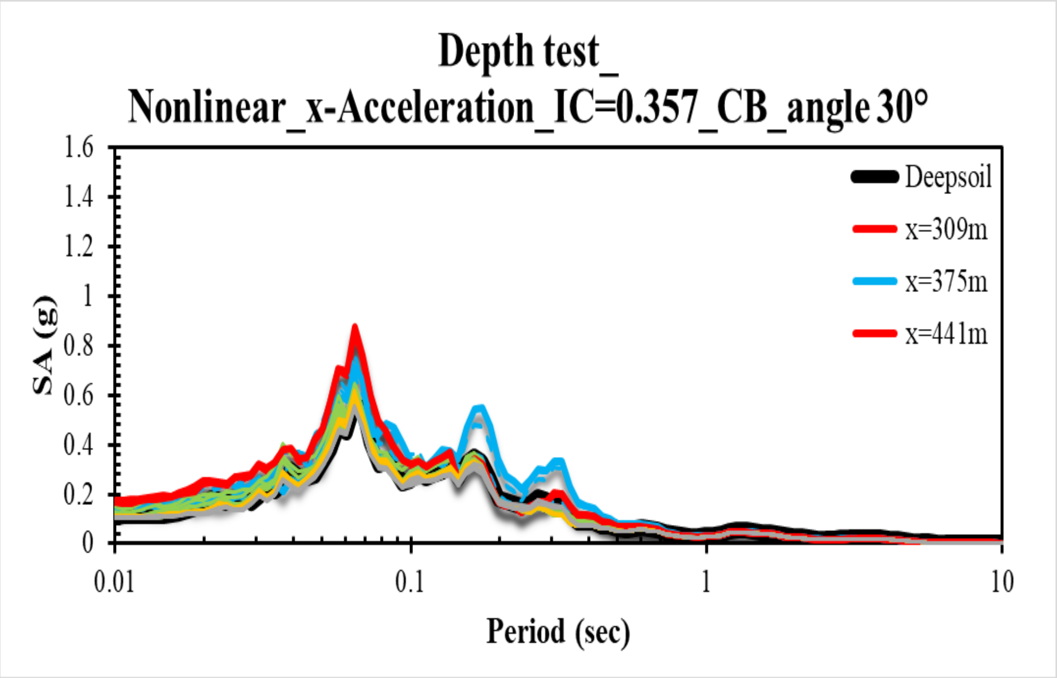

**Figure 4.44** *Depth test of compliant base with shear-wave velocity 760 m/s in nonlinear cases*

doi:10.6342/NTU201903794

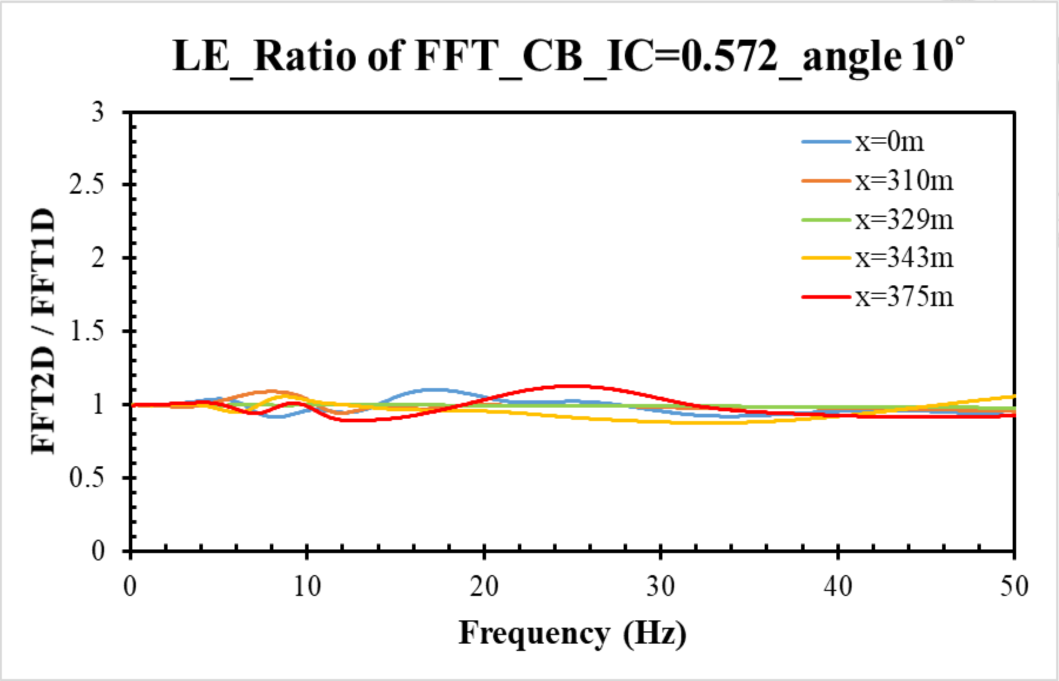

**(a)** *Linear case of compliant base, Vs=500 m/s*

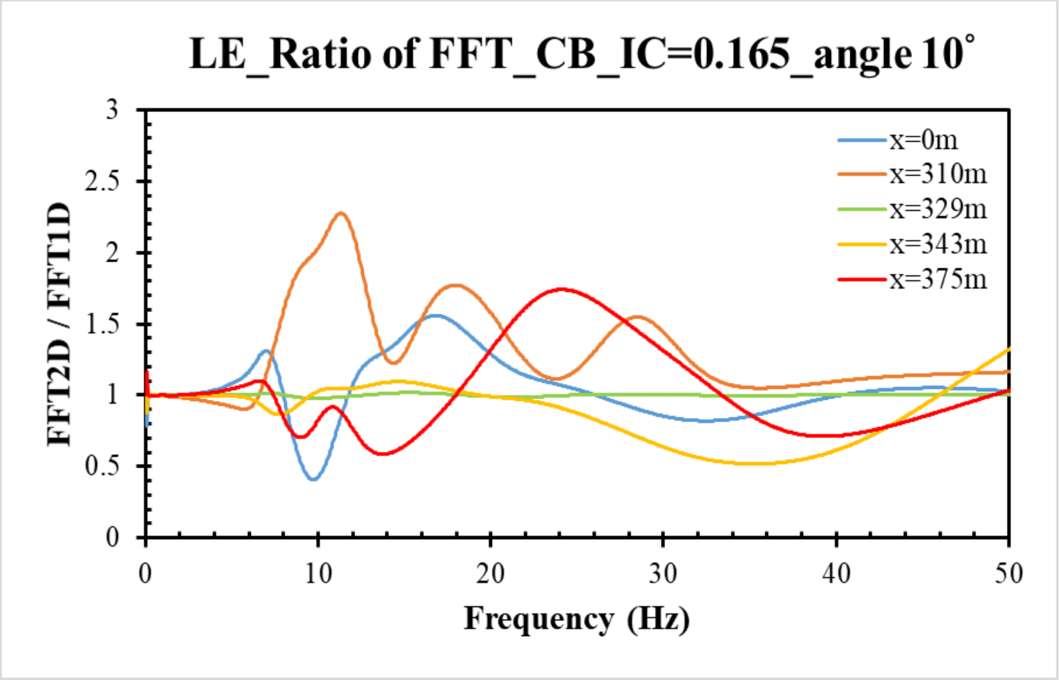

**(b)** *Linear case of compliant base, Vs=1500 m/s*

**Figure 4.45** *Comparison in compliant base with different shear-wave velocities*

doi:10.6342/NTU201903794

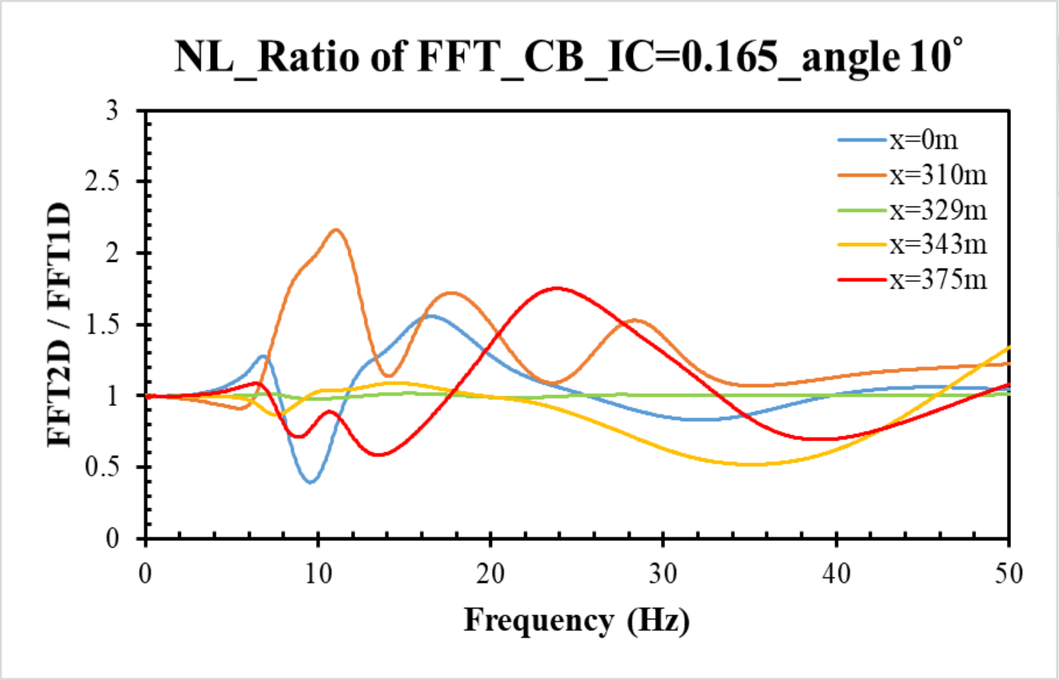

(a) Nonlinear case of compliant base, Vs=1500 m/s, inclined angle 10°

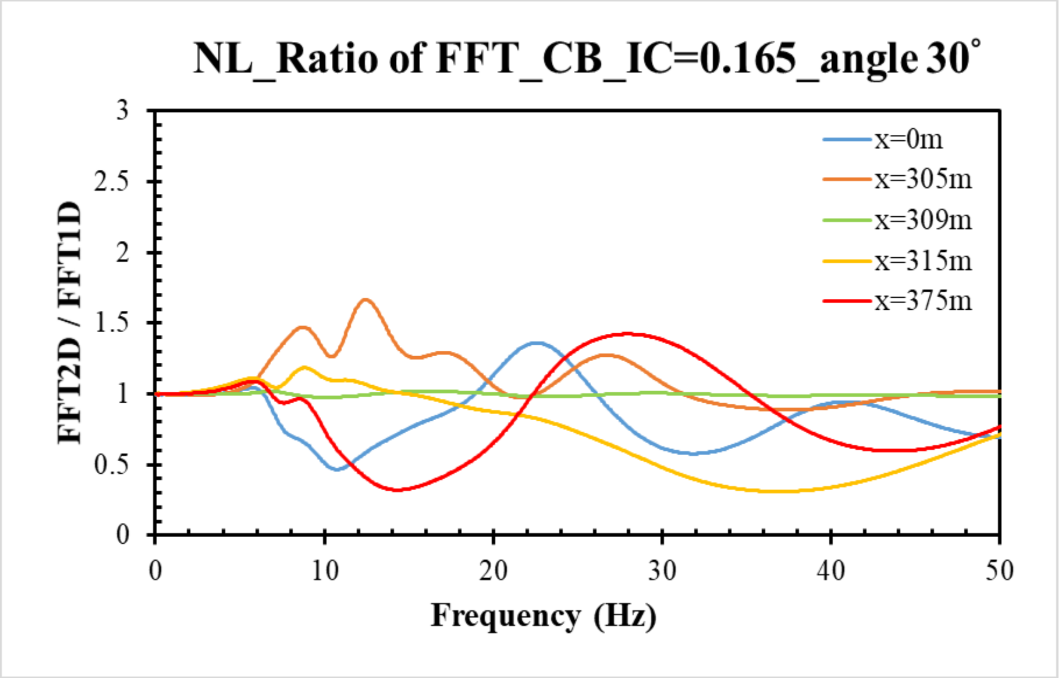

(b) Nonlinear case of compliant base, Vs=1500 m/s, inclined angle 30°

**Figure 4.46** *Influence of variation of tilt angles*

doi:10.6342/NTU201903794

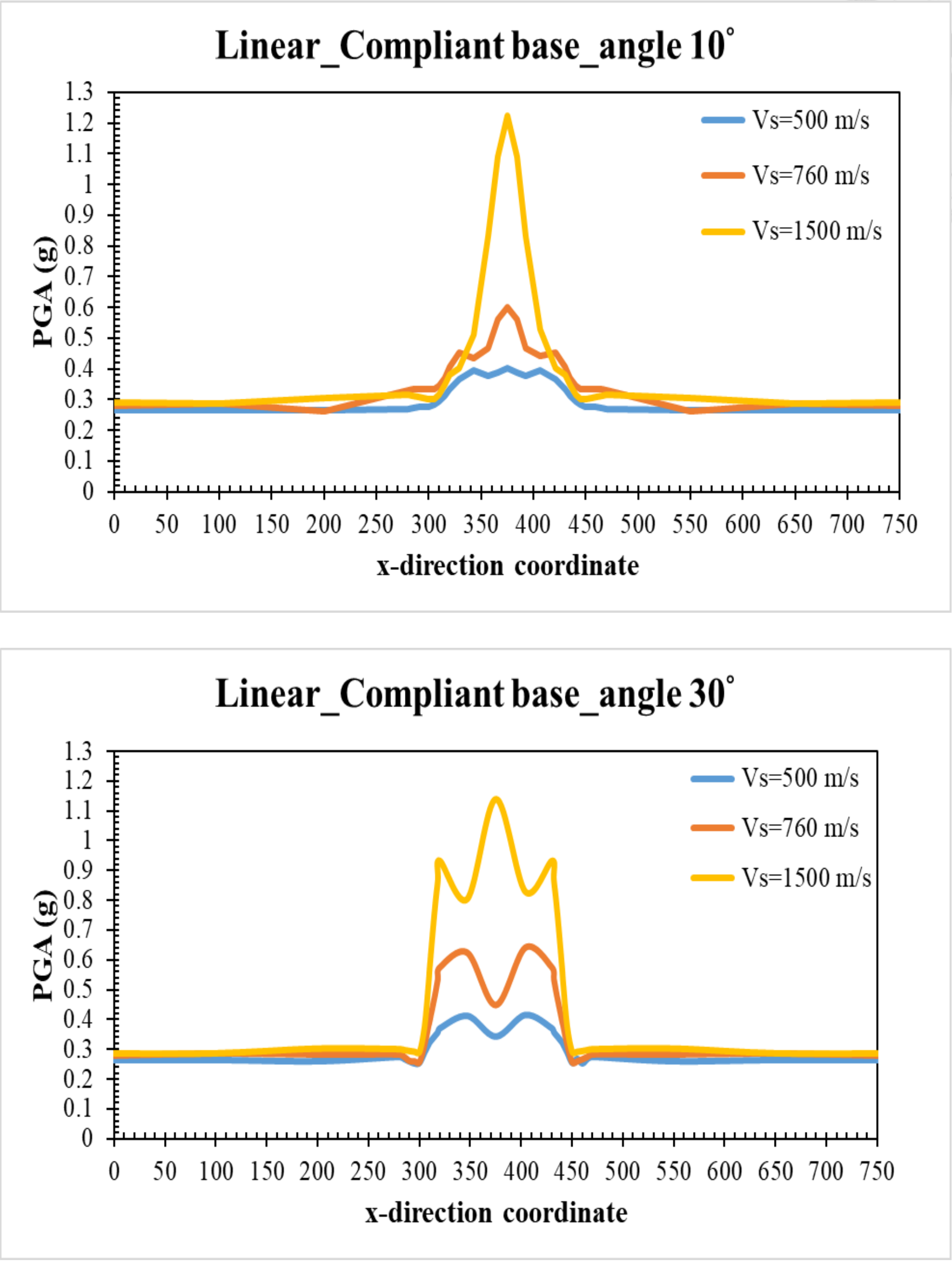

**Figure 4.47** *Trend of PGA due to tilt angles variation at x-direction coordinate at period 0.1 second*

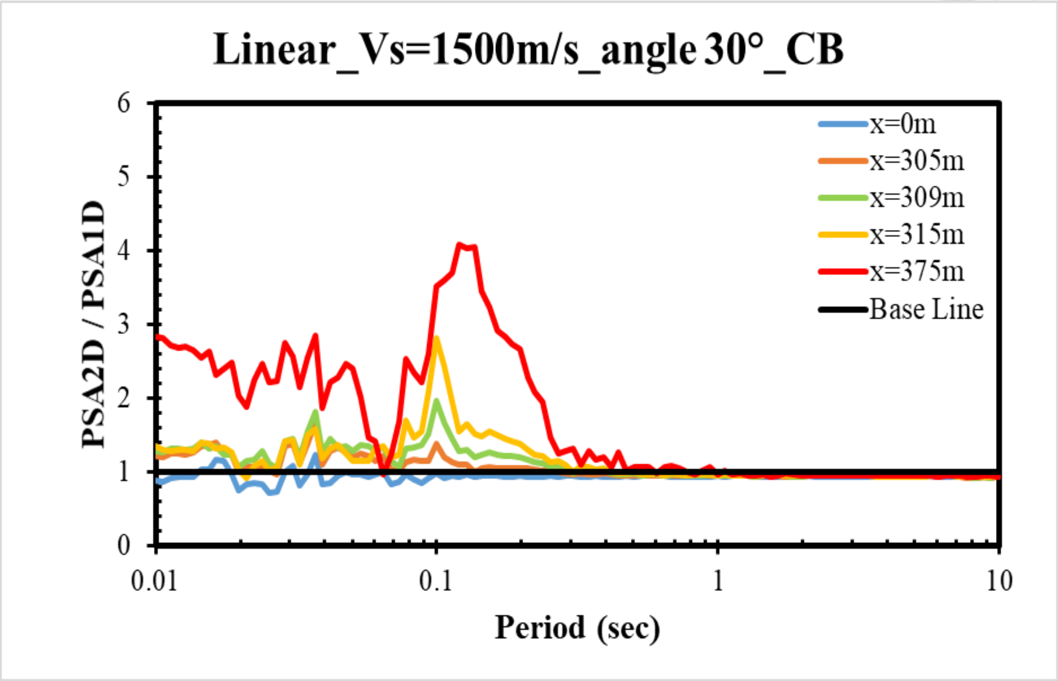

(a) *Linear case, compliant base with 1500 m/s shear-wave velocity*

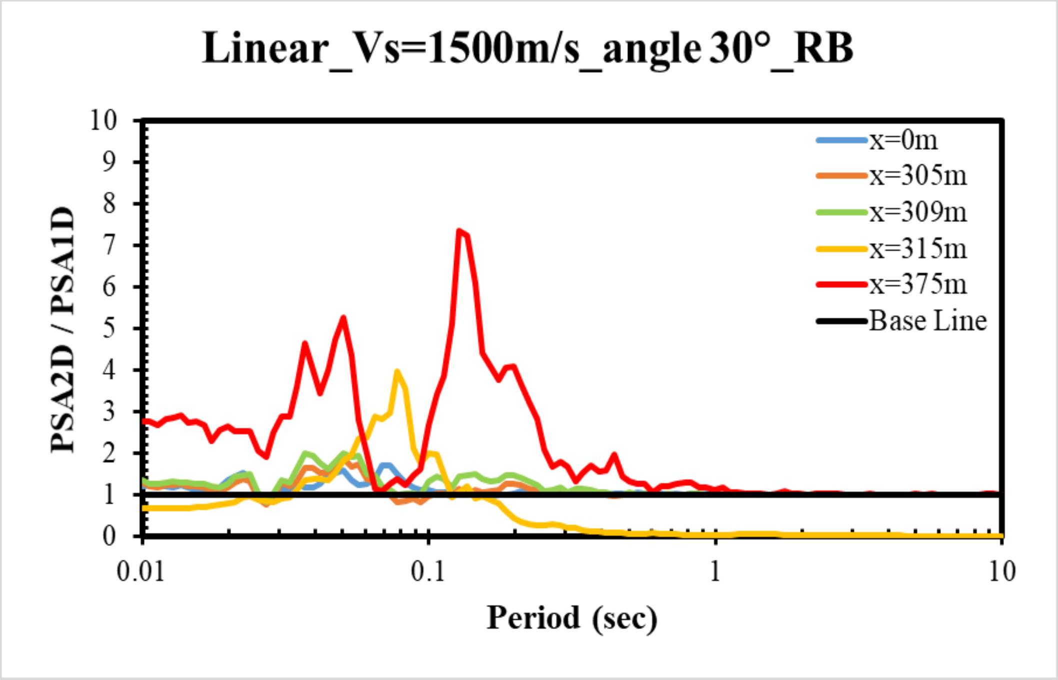

(b) *Linear case, rigid base with 1500 m/s shear-wave velocity*

**Figure 4.48** *Comparison of different boundary condition in PSA ratio curves*

doi:10.6342/NTU201903794

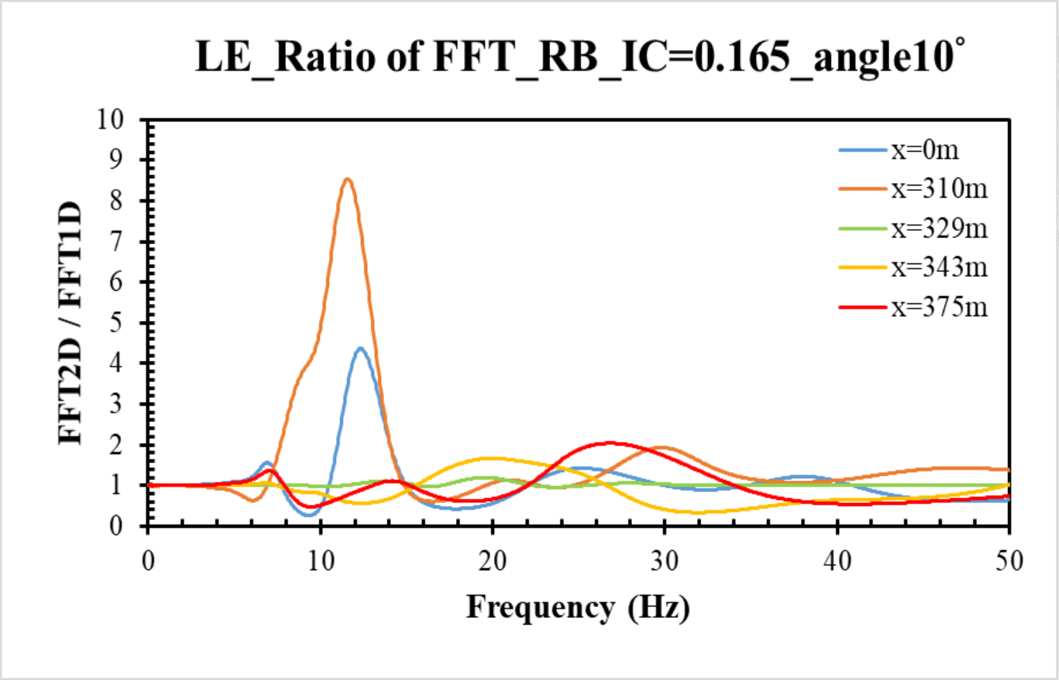

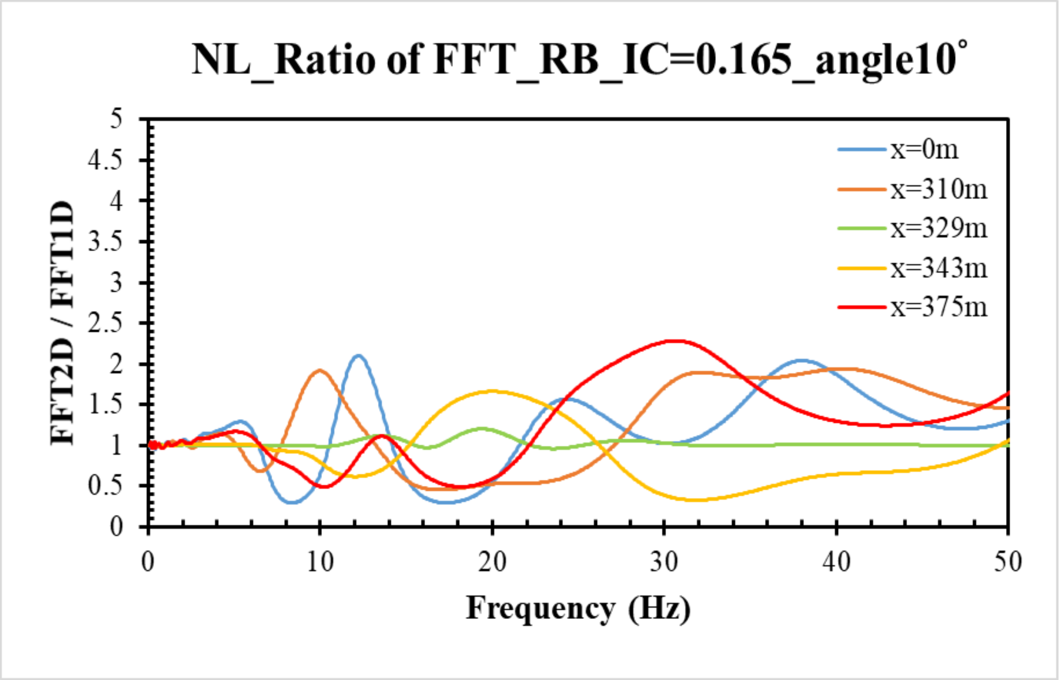

**Figure 4.49** *Influence of soil linearity and nonlinearity on Fourier transform ratio*

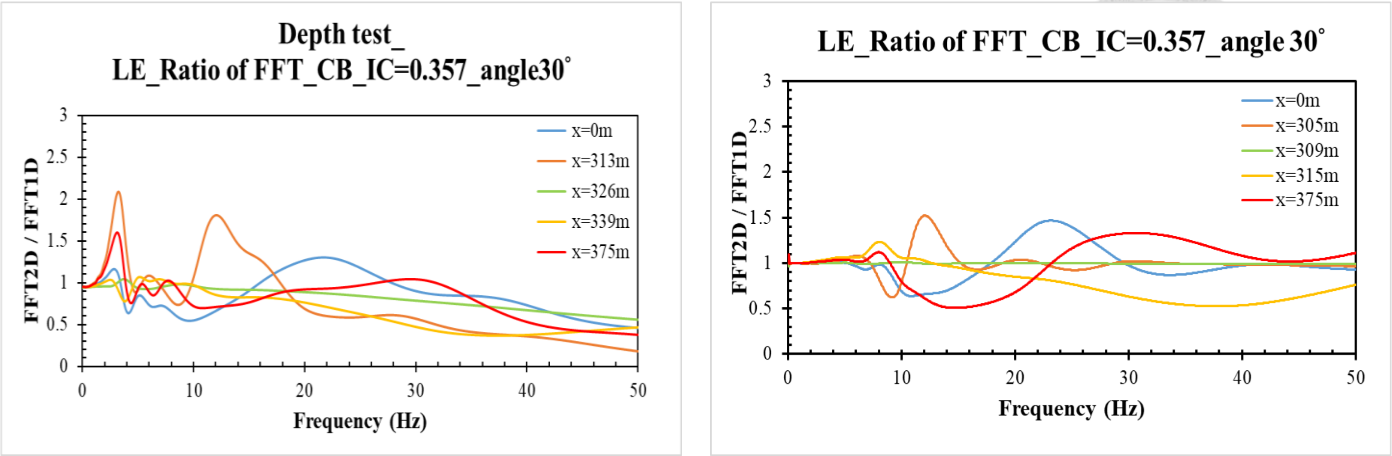

(a) 30m depth case, compliant base, Vs=760 m/s (b) 10m depth case, compliant base, Vs=760 m/s

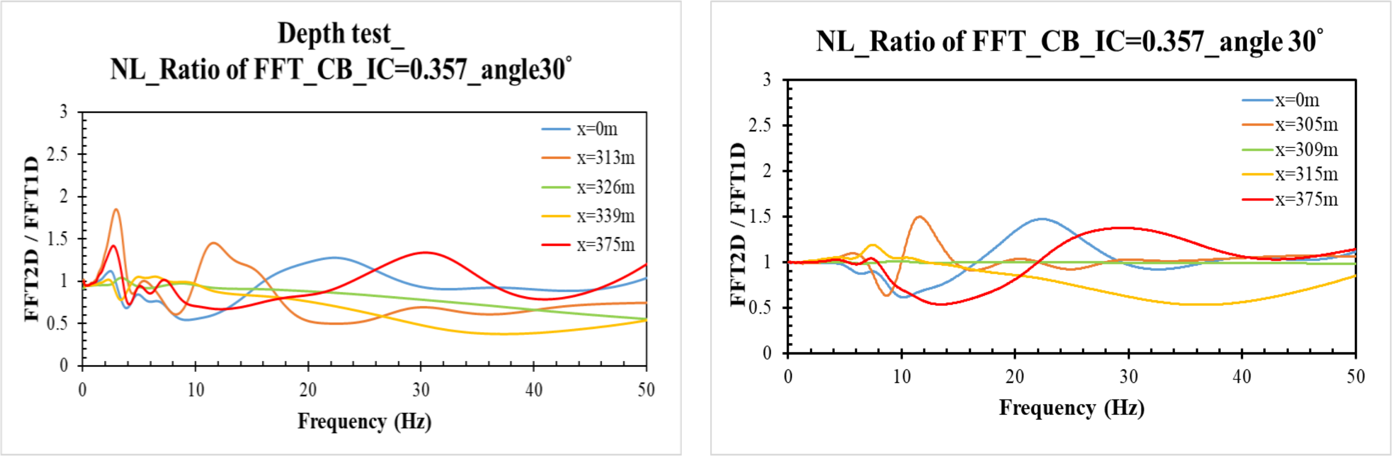

(c) 30m depth case, compliant base, Vs=760 m/s (d) 10m depth case, compliant base, Vs=760 m/s

**Figure 4.50** ***Comparison of Fourier transform ratio between cases for 10m and 30m thickness of the basin***

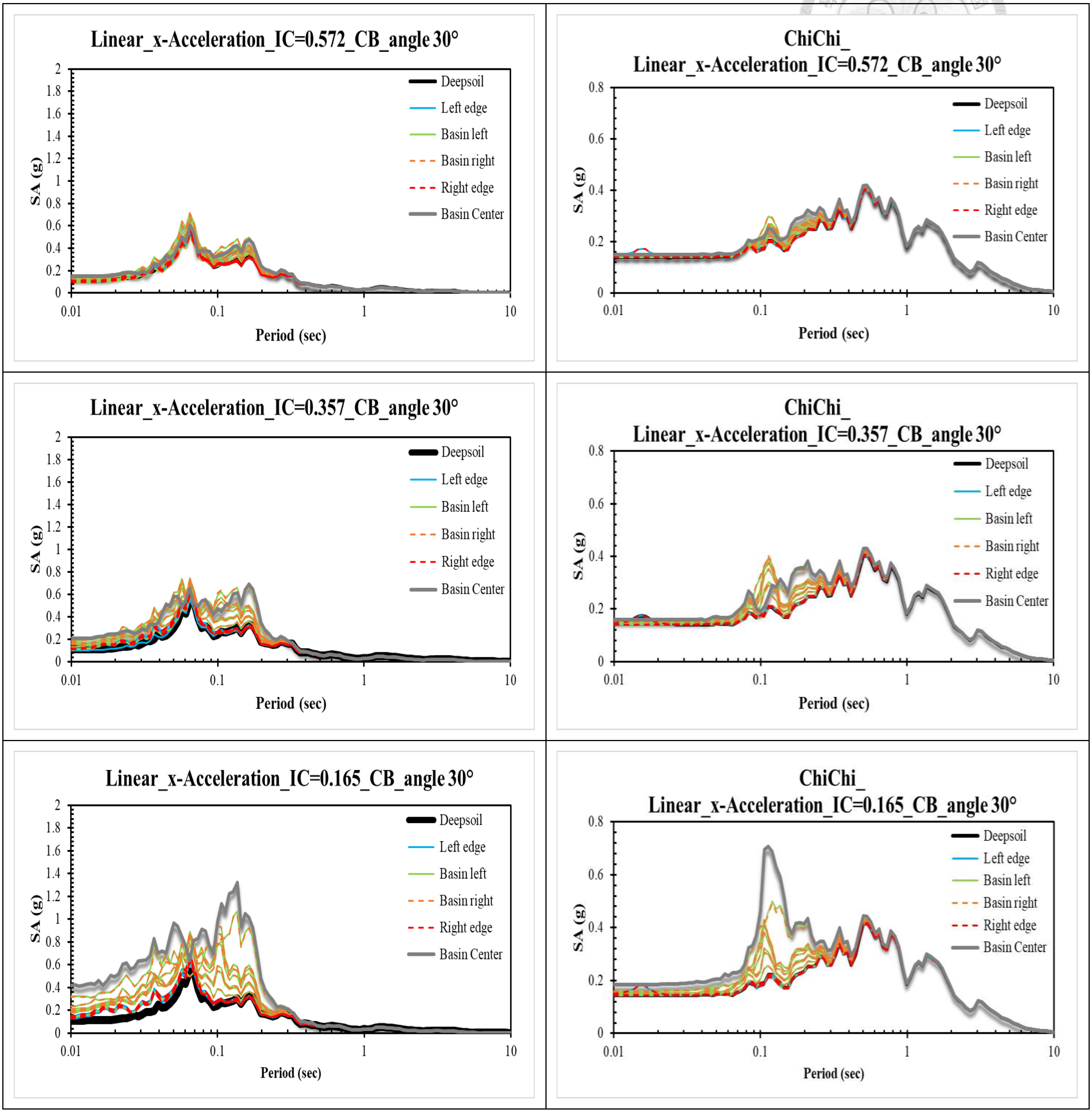

Figure 4.51 *Comparison of different input motion for linear compliant cases.*

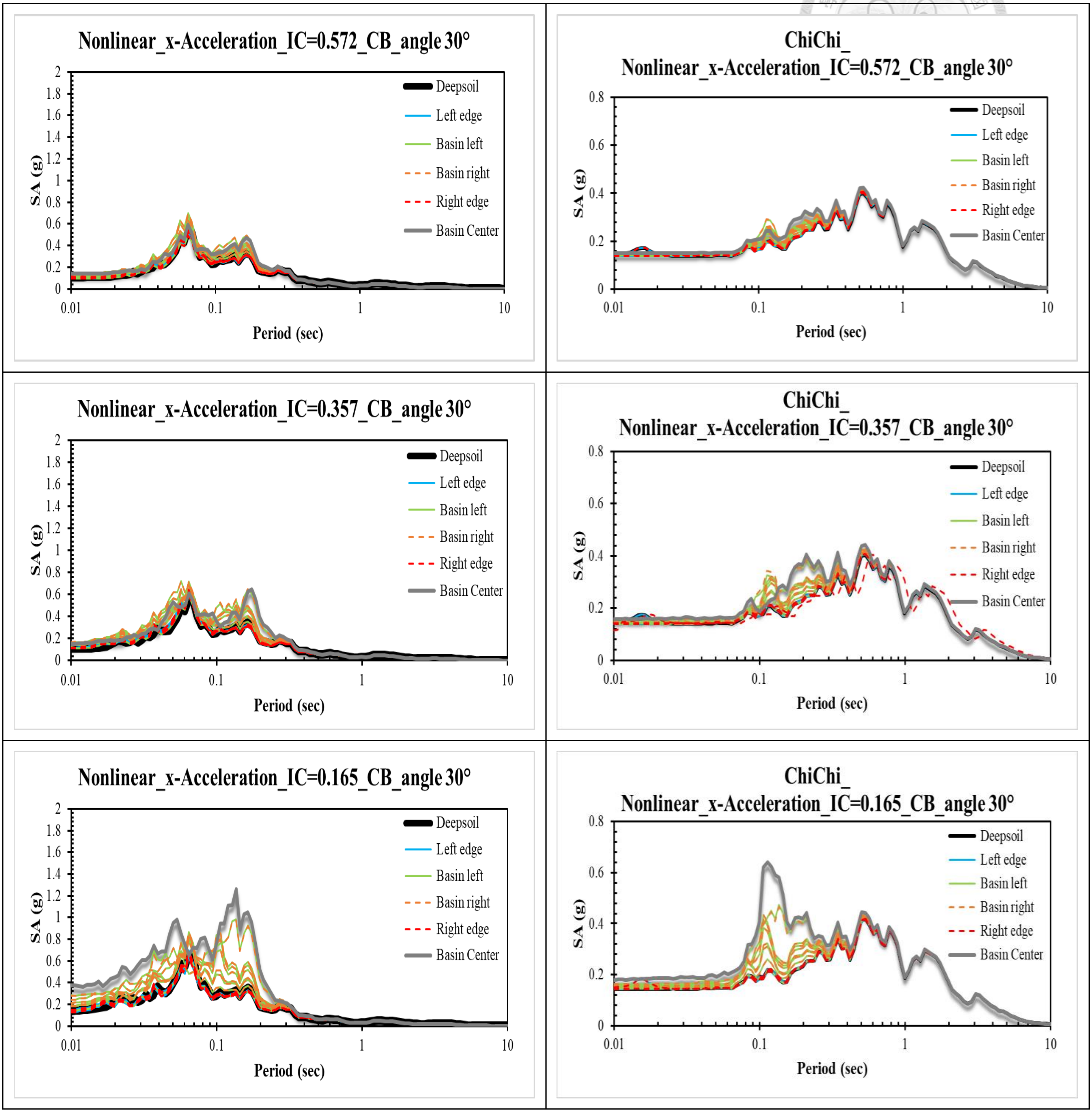

**Figure 4.52** *Comparison of different input motion for linear compliant cases.*

doi:10.6342/NTU201903794

**Table 4.1 Two-dimensional fundamental frequencies of the numerical models which estimated from Bard & Bouchon's empirical functions.**

| | **angle 10°** | **angle 20°** | **angle 30°** |
|---|---|---|---|
| **Vs=500 m/s** | $f^{SH} = 3.48693$ Hz | $f^{SH} = 3.454495$ Hz | $f^{SH} = 3.4479$ Hz |
| **Vs=760 m/s** | $f^{SH} = 4.2868$ Hz | $f^{SH} = 4.24694$ Hz | $f^{SH} = 4.2388$ Hz |
| **Vs=1500 m/s** | $f^{SH} = 5.47946$ Hz | $f^{SH} = 5.428493$ Hz | $f^{SH} = 5.4181$ Hz |

doi:10.6342/NTU201903794

# Chapter 5 Conclusions and Recommendations

In this study, the numerical program FLAC 2D 7.0 is utilized to simulate the ground site response dependent on different geological conditions. The software DEEPSOIL is also used to validate the accuracy of two-dimensional model edge. By using the one-dimensional results in DEEPSOIL, we could fit the response spectrum at edge of the numerical model where 2D effect eliminated in FLAC 2D 7.0. The spectral acceleration spectrum, Fourier smoothed transform, the ratio of peak spectral acceleration, and PGA curves are evaluated in this study to discuss the trend of site effect on each case. There are several summaries expressed as below

## 5.1 Conclusions

(1) Site effect might amplify or decline the intensity of site response. As impedance contrast of soil medium decreases, meaning shear-wave velocity increasing, the stiffness of soil layers becomes larger. The response spectrum induced by directly wave propagation is magnified, causing much more severe damage of ground surface.

(2) Due to fully wave reflection, the site response with rigid base always intense than that with compliant base. Therefore, shear-wave velocity becomes higher, the condition of soil material would much more similar to rigid boundary. And the wave

doi:10.6342/NTU201903794

refraction propagating parts of seismic energy to the complaint half-space, leading to smaller response of ground motion.

(3) For increasing depth of the basin while remaining same thickness of under layering, the proportion of the soft components would be higher. The site response would be amplified stronger than prediction.

(4) As peak ground acceleration of input motion increases, the site response would be amplified. Nevertheless, the results shown in three times intensity of input motion demonstrate the fact that the magnification of site response wouldn’t be equal as magnification of input motion. The maximum response induced by Nahanni and three times intensity input motion locates at same site for both cases in soil linearity. As the condition of soil nonlinearity, the maximum response would occur nearby the edge of basin.

(5) The amplitude of maximum site response would as strengthened as increasing tilt angles. The reason for this phenomenon might be attributed to the interacted combination of boundaries conditions, inclination and impedance contrast etc.

(6) With larger shear-strain of geological components, the behavior of material turned from elasticity to plasticity. The shear modulus might be smaller and damping is higher. More seismic energy is being damped, therefore, the resulting response should be smaller. The tendency in SA spectrum, Fourier transform ratio,

doi:10.6342/NTU201903794

amplification factors etc., expresses the influence of variation of soil behavior on ground response.

(7) Even though the geometry of numerical model is symmetric, the site response of the results might not be equal at the symmetric location of model. Therefore, we couldn’t assign symmetric boundary to simplify the model size. The reason for that phenomenon is because of applying asymmetric input motion, Nahanni. However, the results performed similar response but not exactly same.

(8) The geological properties are much more like compliant base in numerical model. Therefore, the results of different geological conditions with compliant base are significant for expressing the tendency of site effect on ground motion.

(9) The most damaging region would occur at the location between ground surface of symmetric location of 1/2 intersection slope. As the region of basin increased, the maximum response would be distributed far from central region of the basin.

## 5.2 Recommendations

(1) More inclined angle of the intersection slope should be applied to the numerical model, like angle 15°, angle 25° etc. By this method, we could distinctly distinguish the influence of different geological conditions on site effect, and develop a series of complete tendency of variation of site response.

doi:10.6342/NTU201903794

(2) In this study, only few shear-wave velocities are applied. Other values of shear-wave velocity can be considered in future work.

doi:10.6342/NTU201903794

# References

1. Antonio Carlos Siqueira de Lima, Member, IEEE, and Carlos Portela, Life Senior Member, IEEE, (2007, January), Inclusion of Frequency-Dependent Soil Parameters in Transmission-Line Modeling, *IEEE TRANSACTIONS ON POWER DELIVERY, (VOL. 22, NO. 1:* 492-499).

2. Borja, R. I., Chao-Hua L., Samat , K. M. and Masadat, G. M., (2000). Modelling non-linear ground response of non-liquefiable soils. *Earthquake Engineering and Structure Dynamic, 29,* pp.63-83.

3. Ching, J. Y., and Glaser, S. D. (2001, January). 1D TIME-DOMAIN SOLUTION FOR SEISMIC GROUND MOTION PREDICTION. *JOURNAL OF GEOTECHNICAL AND GEOENVIRONMENTAL ENGINEERING, 127*(1): 36-47.

4. Dey, A. K. and Stewart, R. R., (1997). Predicting density using Vs and Gardner's relationship. *CREWES Research Report, Vol. 9.*

5. Düzgün, O. A., and Budak, A. (2015). Effects of surface shapes and geotechnical conditions on the ground motion. *KSCE Journal of Civil Engineering*, *19*(5), 1336

6. F. Gouveia, R.C. Gomes & I.F. Lopes (2012, September), Influence of Stiffness Contrast in Non-horizontally Layered Ground on Site Effects, *Proceedings of World Conference on Earthquake Engineering, Lisboa.*

doi:10.6342/NTU201903794

7. James, K., Baise, L. G., Eric, M., Dorfmann, T. L., (2015). Comparison of 1D linear, equivalent-linear, and nonlinear site response models at six KiK-net validation sites. *Soil Dynamics and Earthquake Engineering, 69,* pp.207-219.

8. Jones, S., and Hunt, H. (2011, December). Effect of Inclined Soil Layers on Surface Vibration from Underground Railways Using the Thin-Layer Method. *JOURNAL OF ENGINEERING MECHANICS © ASCE, 137*(12): 887-900. .

9. Kim, M. K., Lee, J. S., and Kim, M. K. (2003, January). Two-Dimensional Seismic Response Analysis of Basin Effects. *KSCE Journal of Civil Engineering, (Vol. 7, No. 1*: 33-39 *)*

10. Lee, S. J., Chen, H. W., Liu, Q., Komatitsch, D., Huang, B. S. and Tromp, J.,(2008, February), Three-Dimensional Simulations of Seismic-Wave Propagation in the Taipei Basin with Realistic Topography Based upon the Spectral-Element Method, *Bulletin of the Seismological Society of America, (Vol. 98, No. 1*: 253–264).

11. Miller, S.L.M., Stewart, R.R., (1991). The relationship between elastic-wave velocities and density in sedimentary rocks, a proposal: 260-273.

12. Papageorgiou, A. S. and Kim, J., (1991, December), Study of the Propagation and Amplification of Seismic Waves in CARACAS Valleys with Reference to The 29 JULY 1967 Earthquake: SH Waves, *Bulletin of the Seismological Society of America, Vol. 81, No. 6*: 214-2233.

doi:10.6342/NTU201903794

13. Pavlenko O. V., (2001, April). Nonlinear Seismic Effects in Soils: Numerical Simulation and Study. *Bulletin of the Seismological Society of America, 91(2),* pp.381-396.

14. Phillips, C., Hashash, Y. M. A., (2009). Damping formulation for nonlinear 1D site response analyses. *Soil Dynamics and Earthquake Engineering 29,* pp.1143-1158.

15. Pitilakis, K.D., Makea, K.A., & Raptakis, D.G., (2001), 2D vs 1D site effects with potential applications to seismic norms: The cases of EUROSEISTEST and Thessaloniki, Aristotle University of Thessaloniki, Thessaloniki, Greece.

16. Scott, A. A., Nicholas, S., John, L., and Nan, D. (1997, June). Topographic Effects on the Seismic Response of Steep Slopes. *Bulletin of the Seismological Society of America, (Vol. 87, No. 3*: 701-709).

17. Semblat, J.F., Kham, M., Parara, E., Bard, P. Y., Pitilakis, K., Makra, K., and Raptakis, D. (2005). Seismic wave amplification: Basin geometry vs soil layering. *Soil Dynamics and Earthquake Engineering 25,* pp.529-538.

18. Wen Kuo-Liang & Dravinski Marijan. (1995, December). Effect of the 2D semi-circular basin on ground motions under the incident body wave. *TAO, (Vol. 6, No. 4*: 511-525).

19. 曾美綺（2017）。「地表地形對地震震波反應影響之數值模擬」，國立臺灣大學土木工程學系，碩士論文。

doi:10.6342/NTU201903794

# Appendix

## (1) Ratio of PSA2D and PSA1D in x-direction

### (a) Cases for compliant base analysis, shear-wave velocity 500 m/s

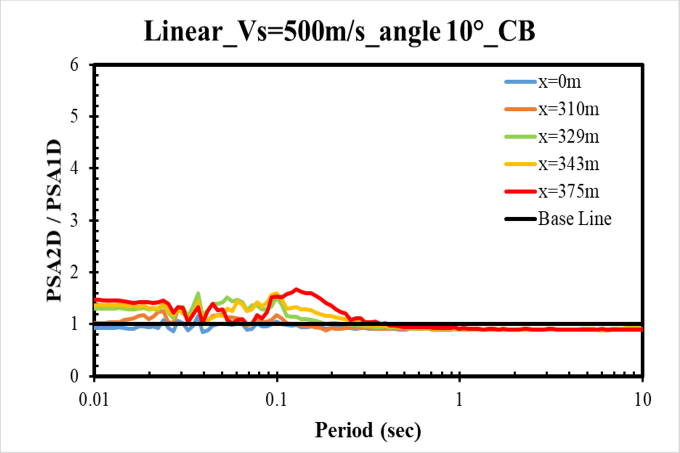
Linear_Vs=500m/s_angle 10°_CB

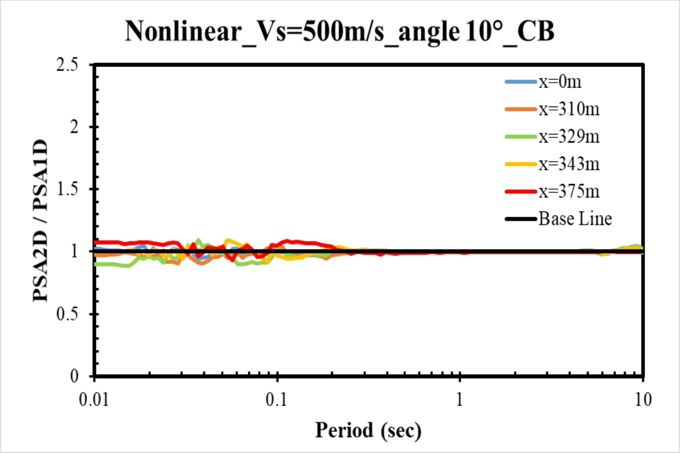
Nonlinear_Vs=500m/s_angle 10°_CB

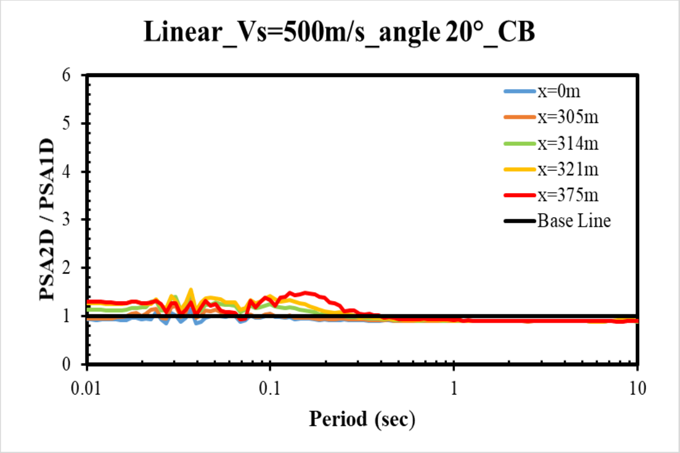
Linear_Vs=500m/s_angle 20°_CB

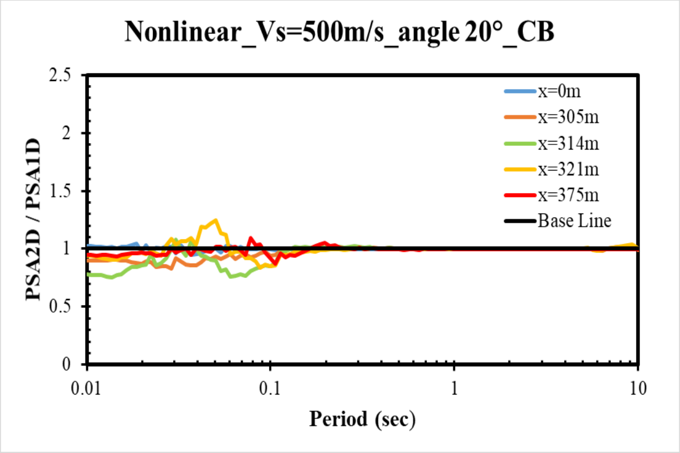
Nonlinear_Vs=500m/s_angle 20°_CB

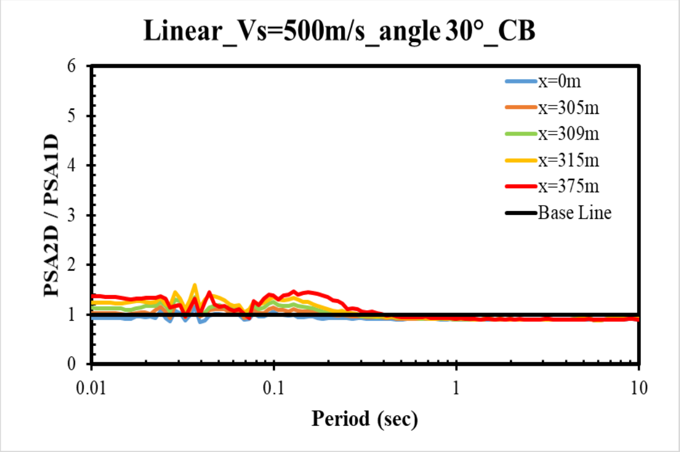
Linear_Vs=500m/s_angle 30°_CB

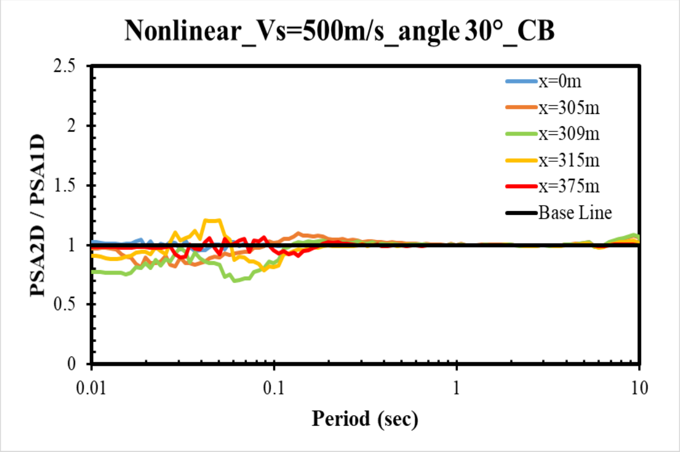
Nonlinear_Vs=500m/s_angle 30°_CB

(b) Cases for compliant base analysis, shear-wave velocity 760 m/s

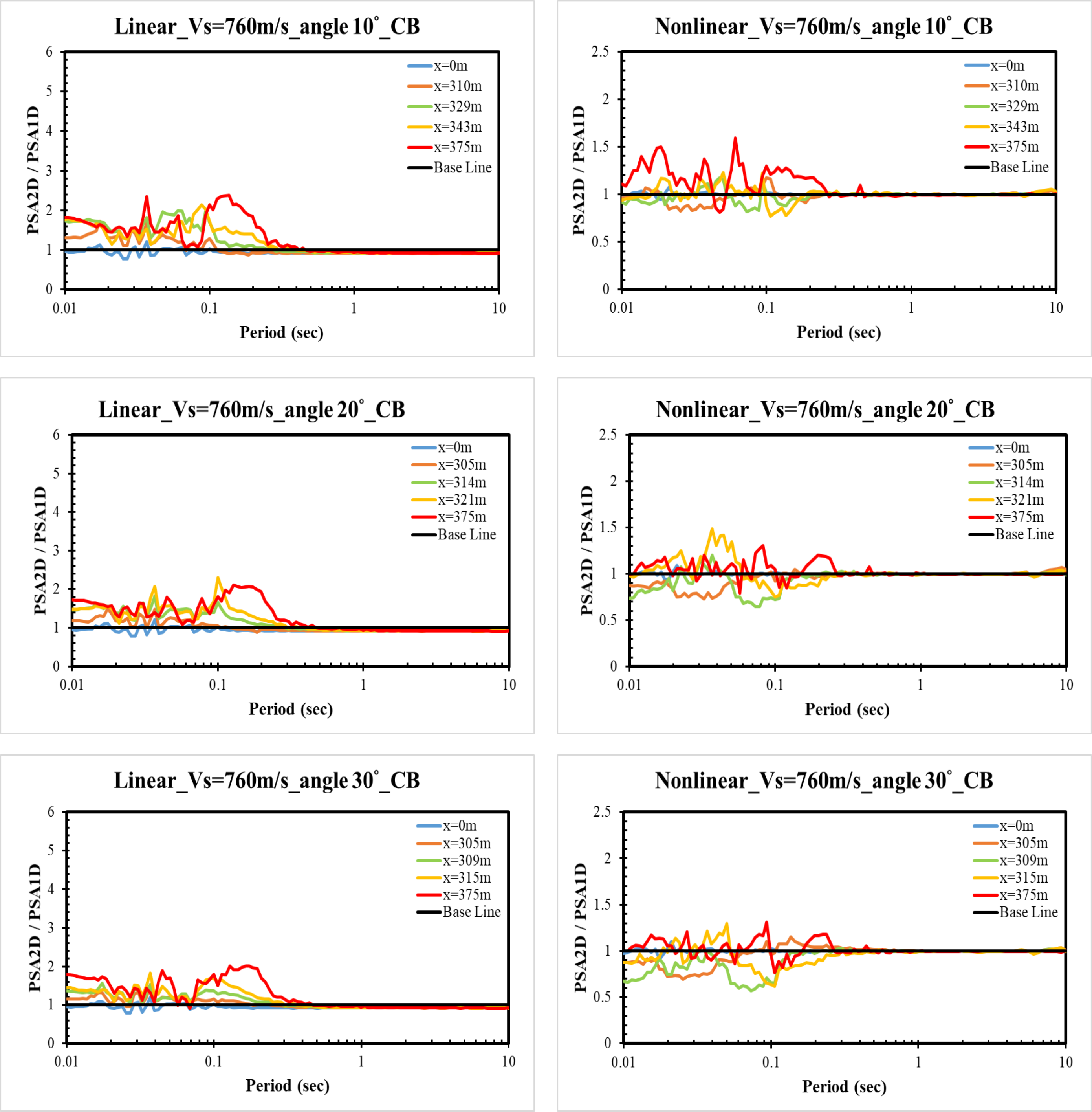

Linear_Vs=760m/s_angle 10˚_CB

Nonlinear_Vs=760m/s_angle 10˚_CB

Linear_Vs=760m/s_angle 20˚_CB

Nonlinear_Vs=760m/s_angle 20˚_CB

Linear_Vs=760m/s_angle 30˚_CB

Nonlinear_Vs=760m/s_angle 30˚_CB

doi:10.6342/NTU201903794

(c) Cases for compliant base analysis, shear-wave velocity 1500 m/s

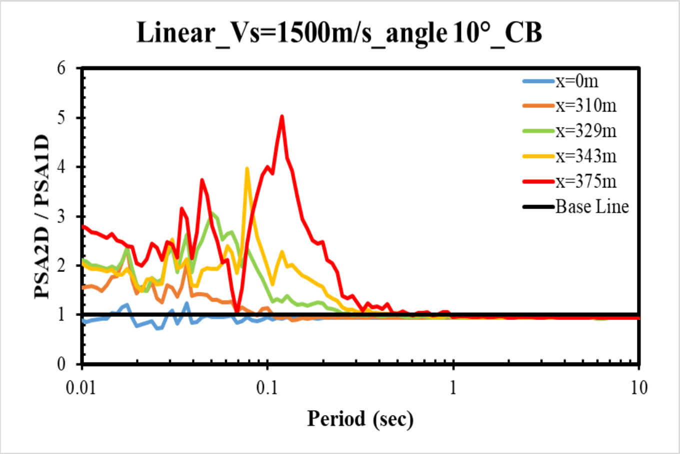

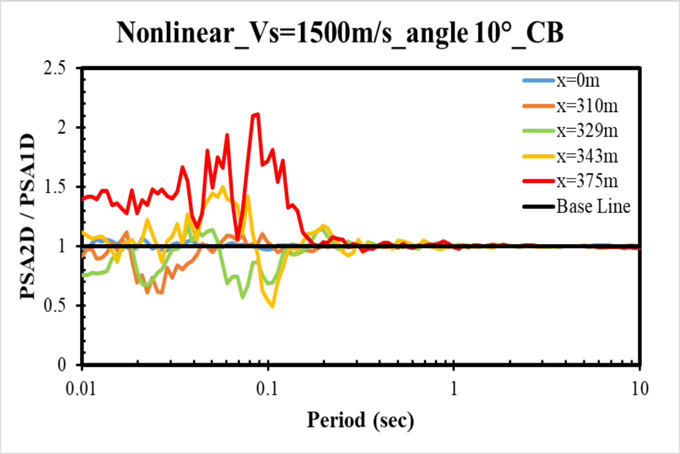

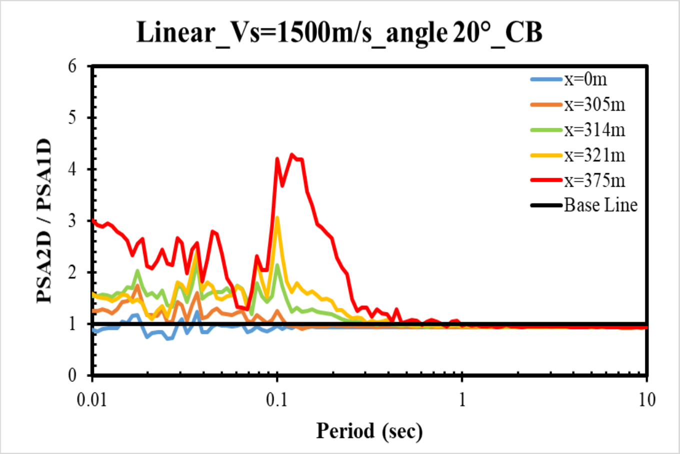

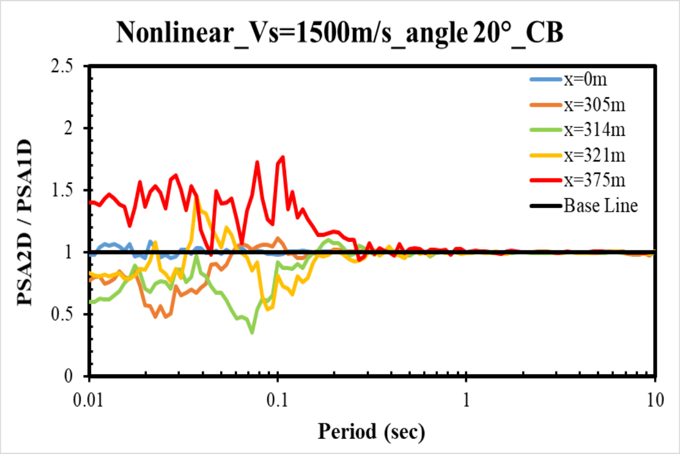

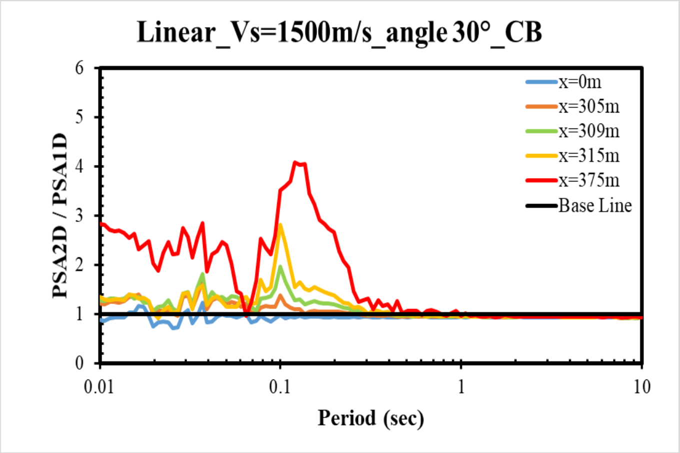

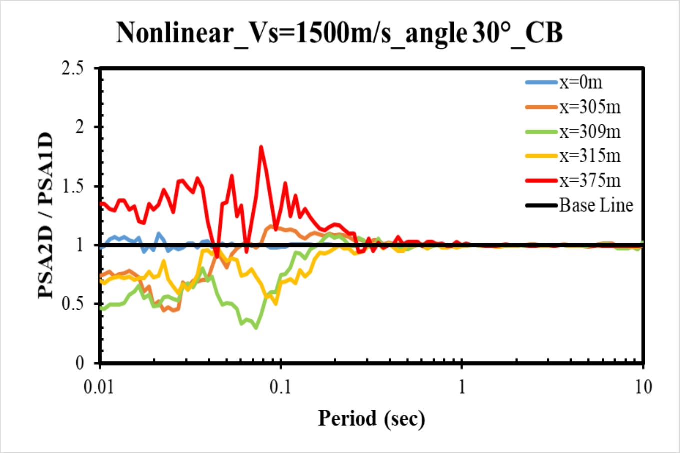

(d) Cases for rigid base analysis, shear-wave velocity 500 m/s

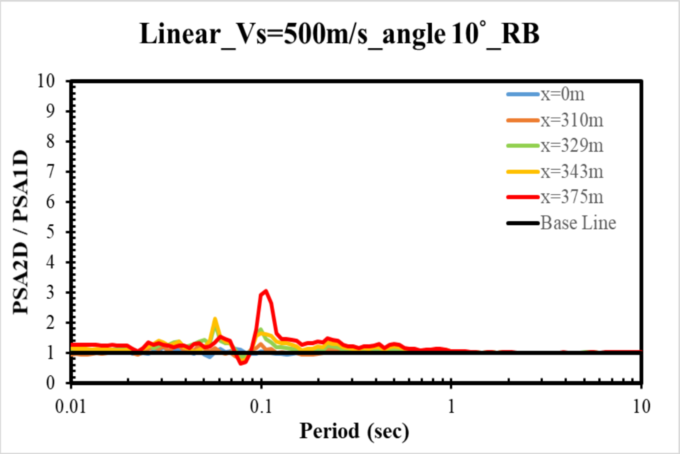

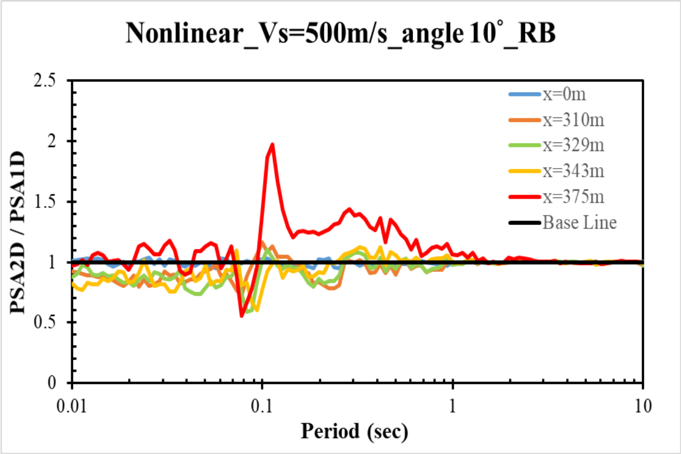

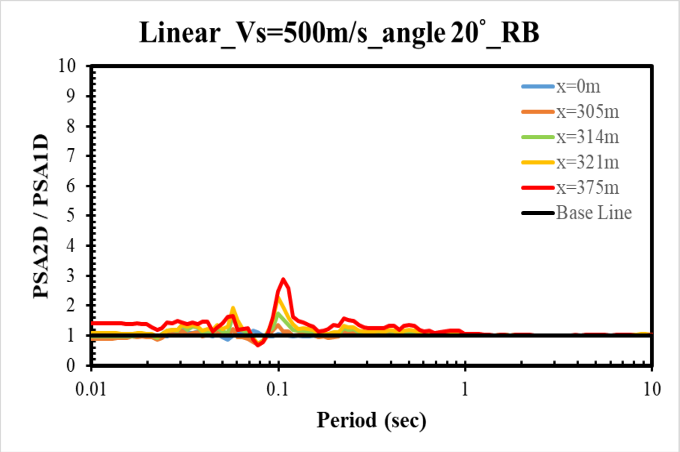

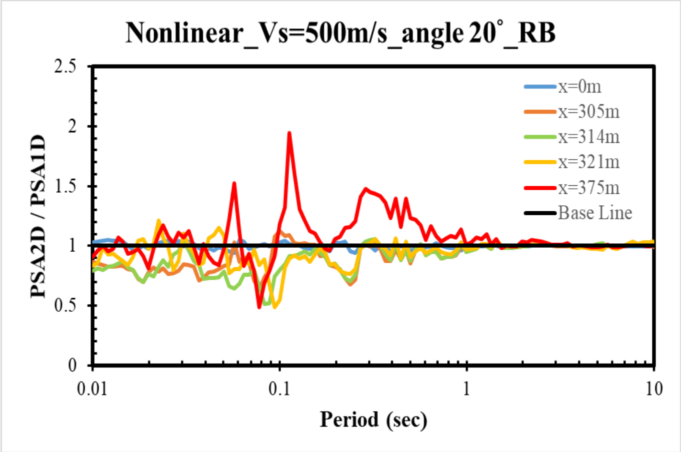

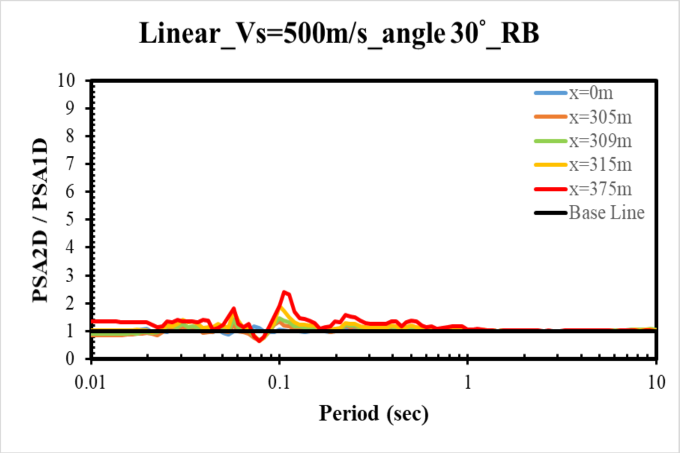

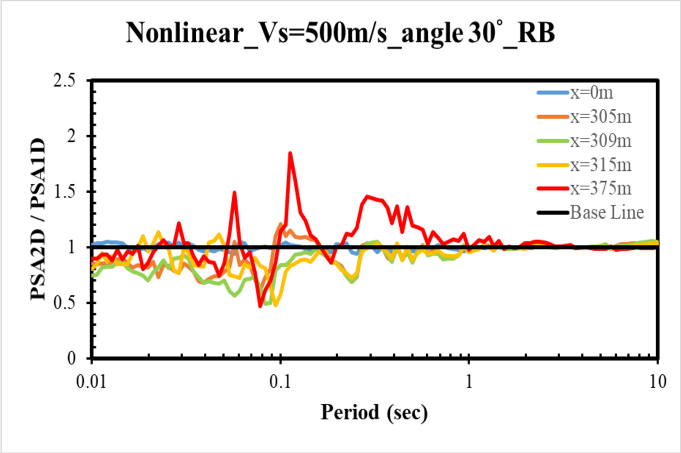

doi:10.6342/NTU201903794

(e) Cases for rigid base analysis, shear-wave velocity 760 m/s

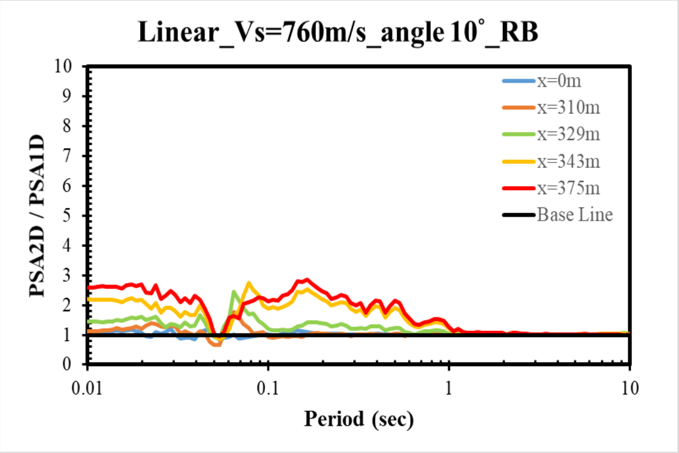

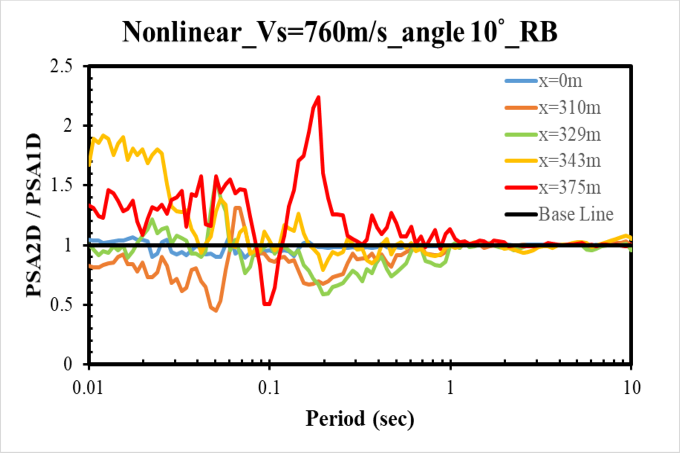

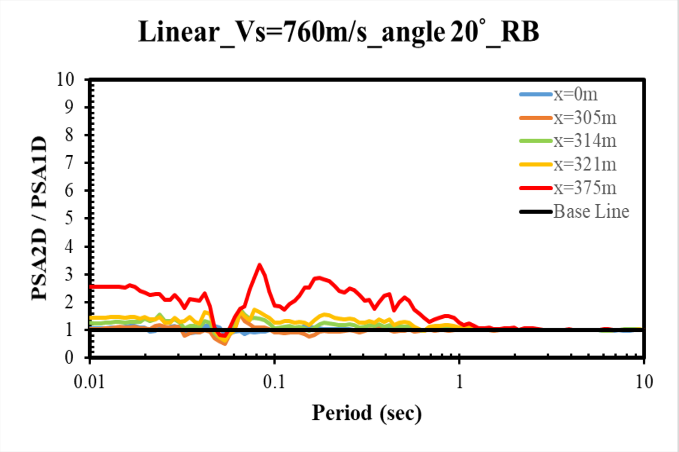

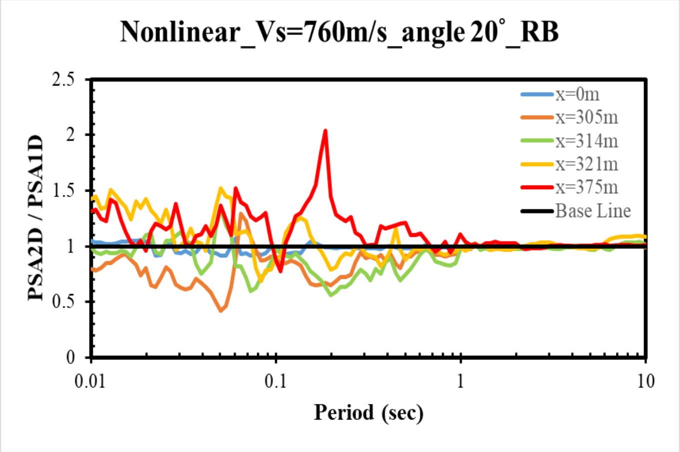

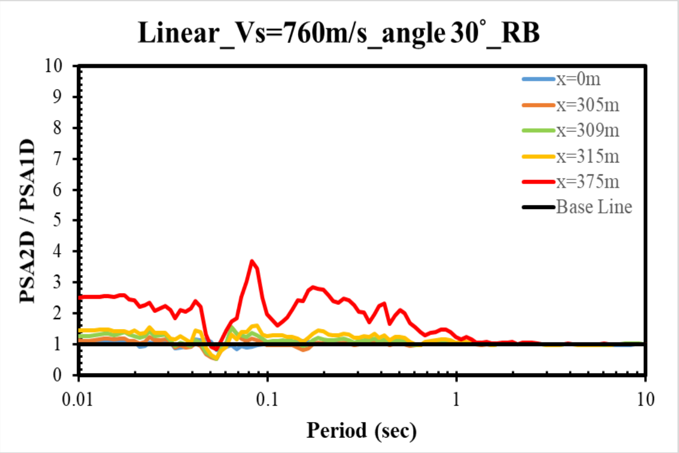

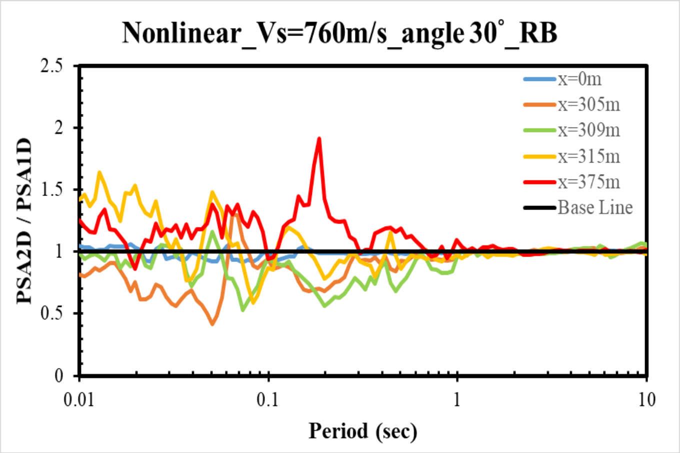

(f) Cases for rigid base analysis, shear-wave velocity 1500 m/s

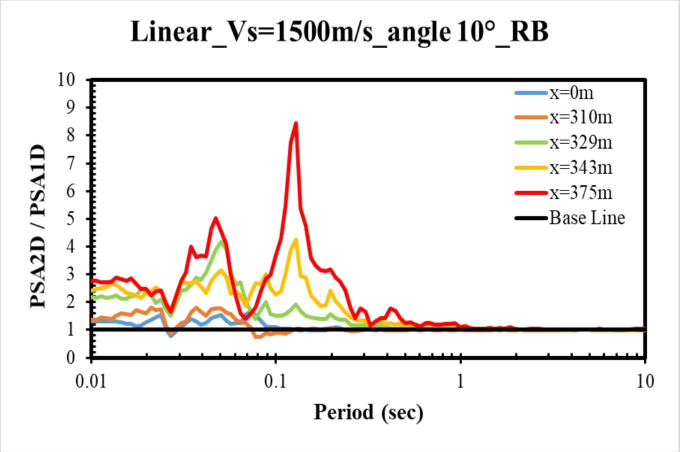

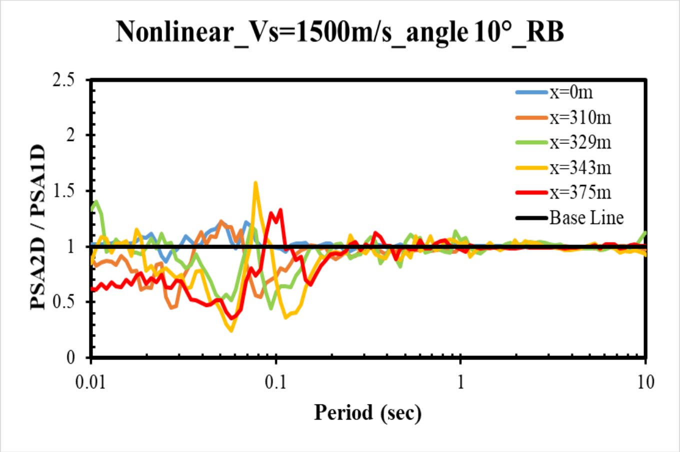

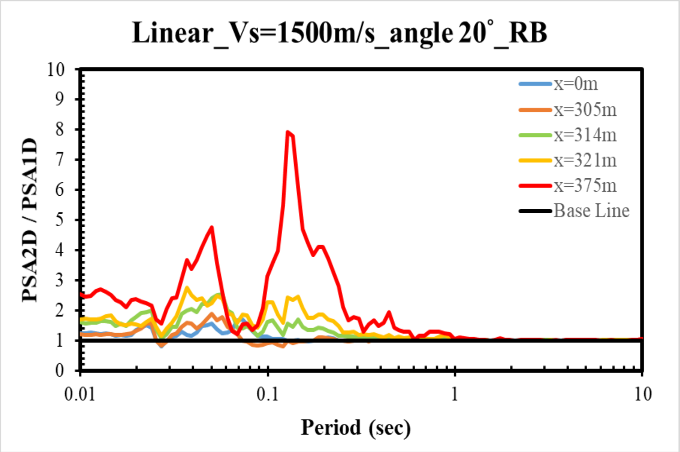

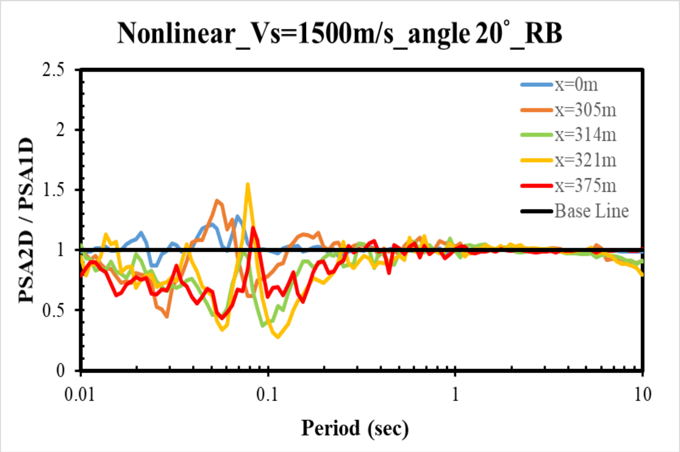

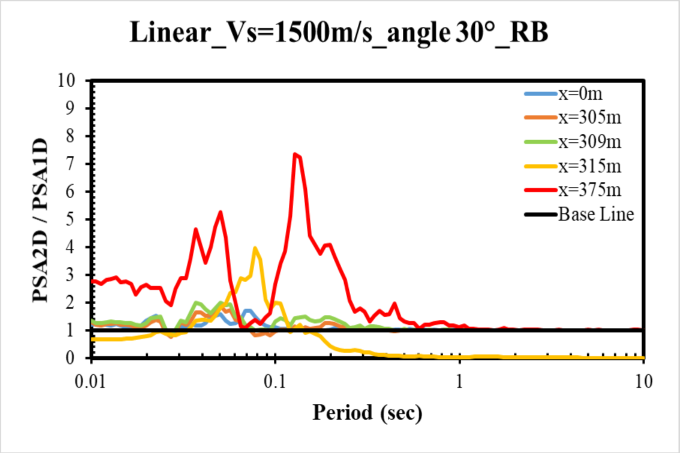

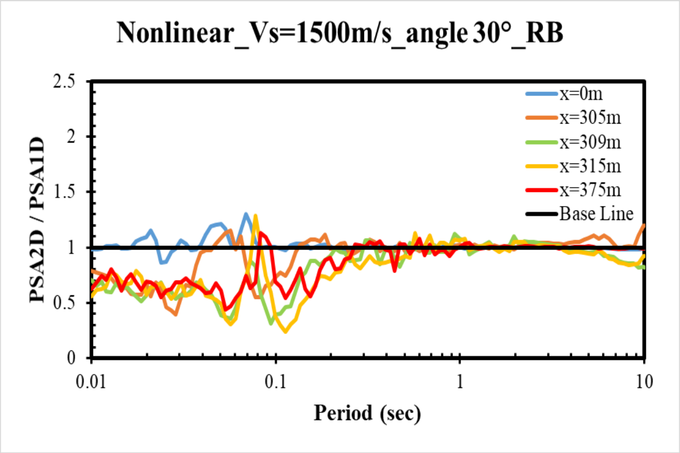

(2) Ratio of the smooth results for 2D Fourier transform and 1D Fourier transform in x-direction

(a) Cases for compliant base analysis, shear-wave velocity 500 m/s, impedance contrast 0.572

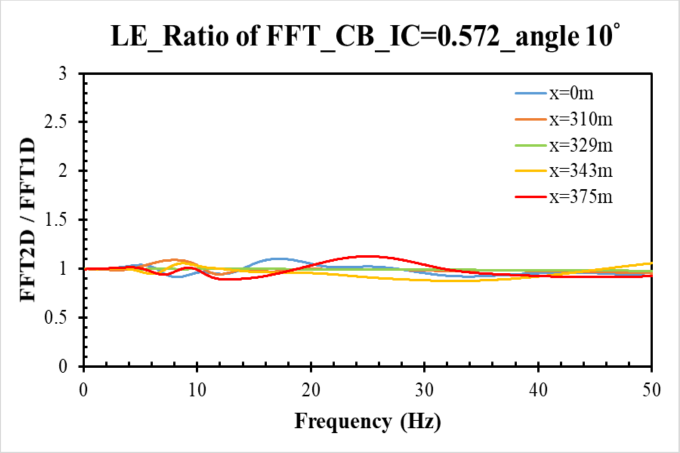

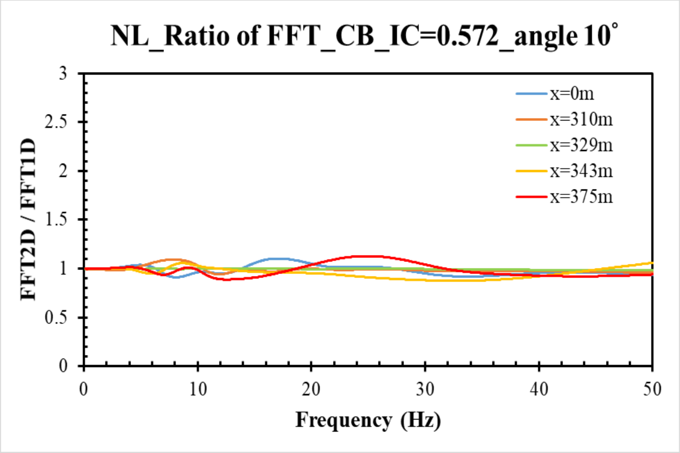

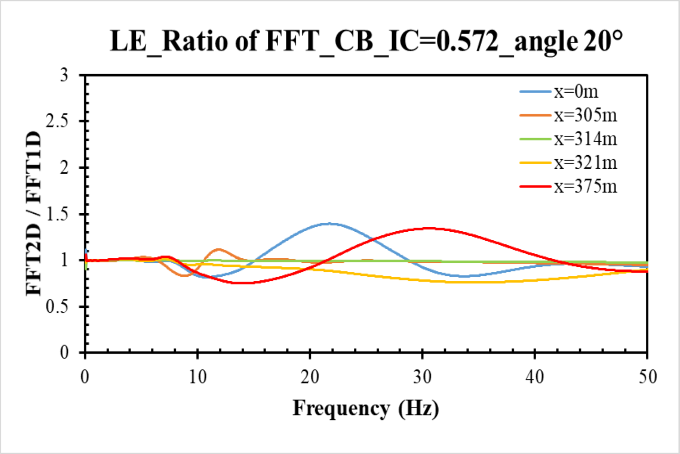

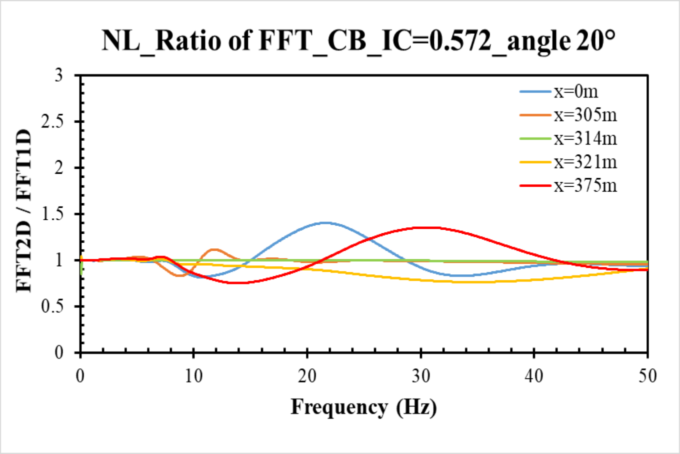

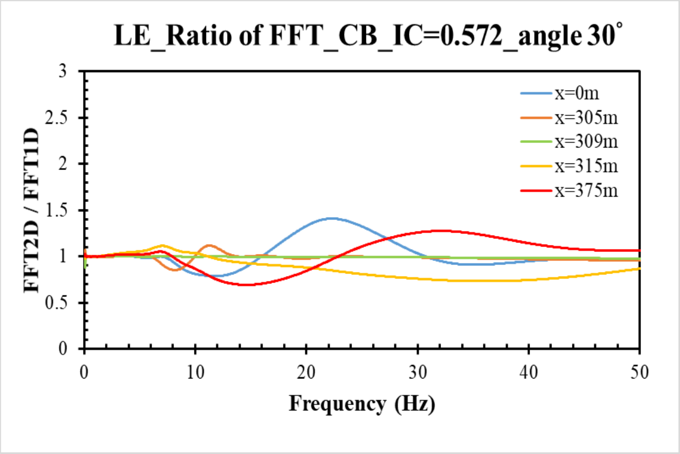

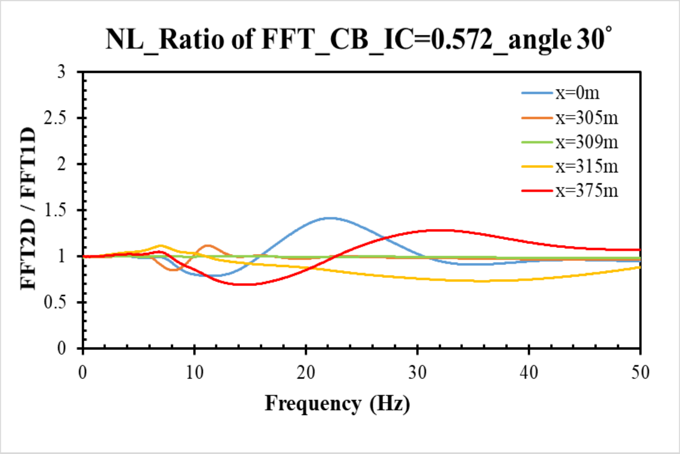

(b) Cases for compliant base analysis, shear-wave velocity 760 m/s, impedance contrast 0.357

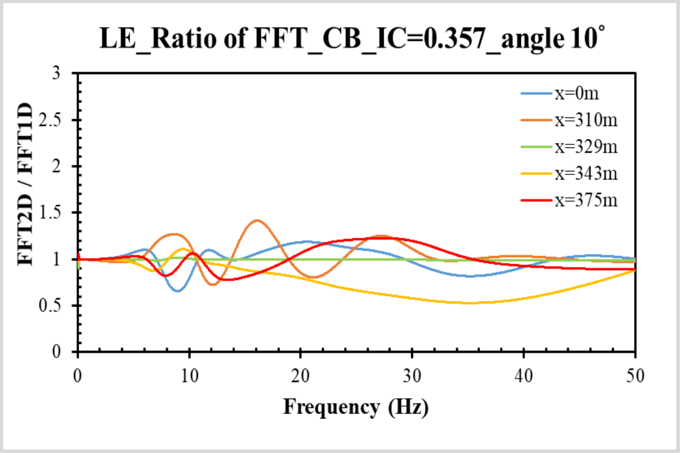

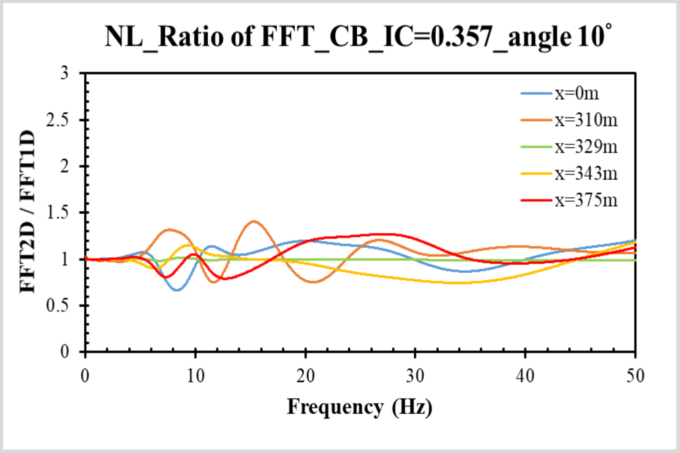

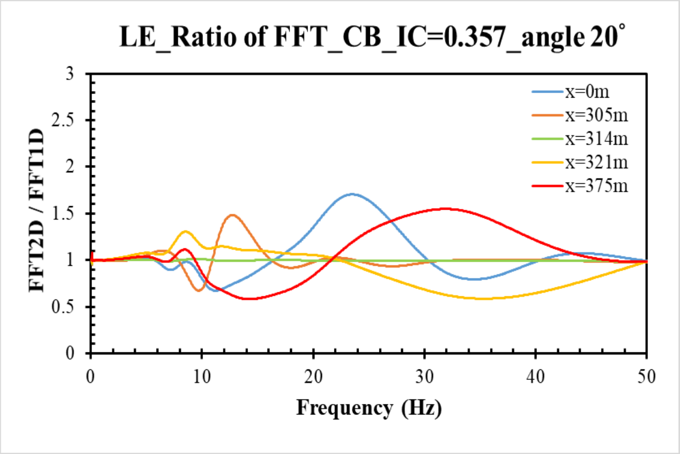

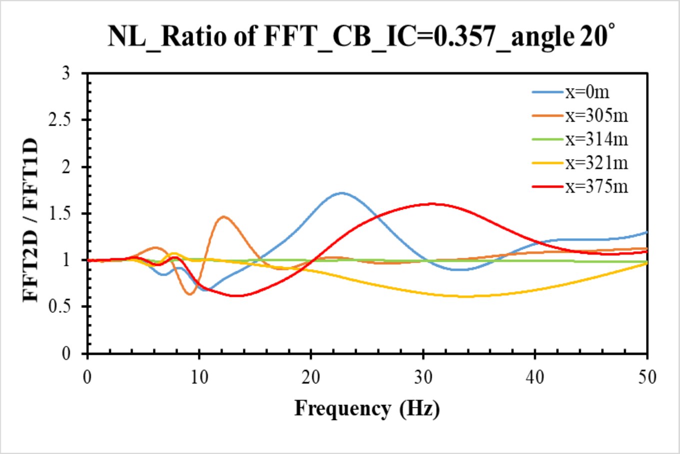

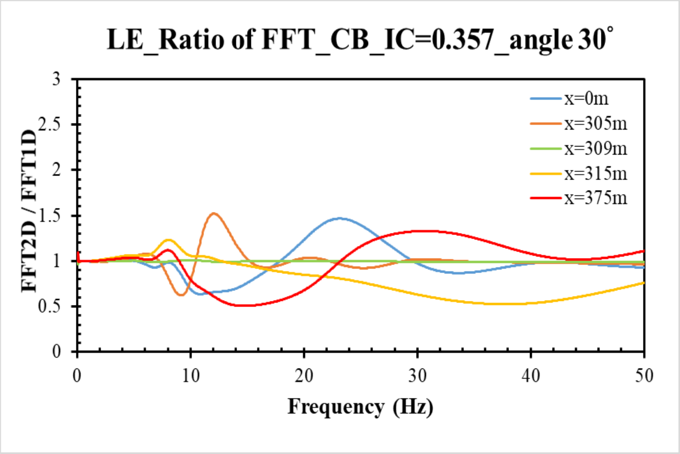

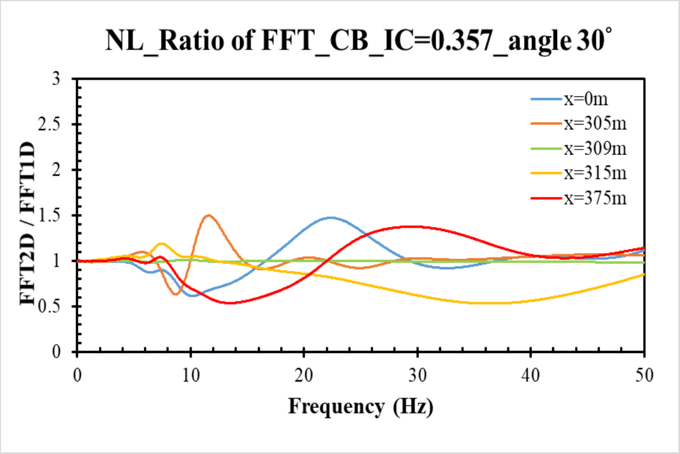

doi:10.6342/NTU201903794

(c) Cases for compliant base analysis, shear-wave velocity 1500 m/s, impedance contrast 0.165

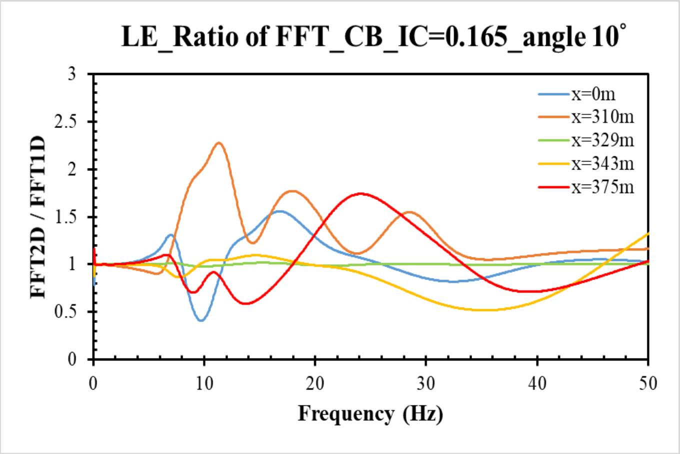

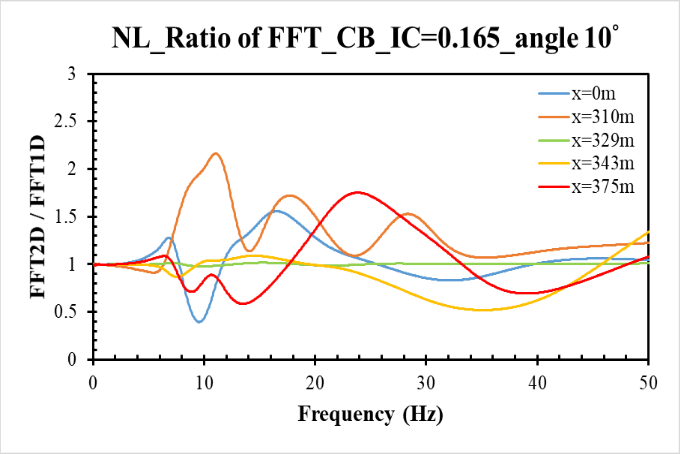

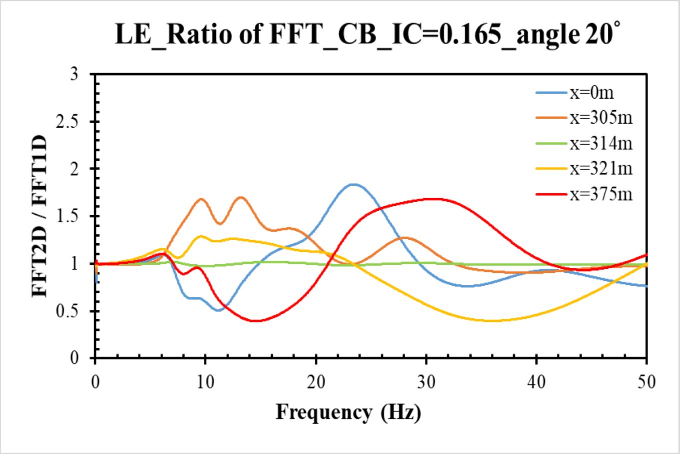

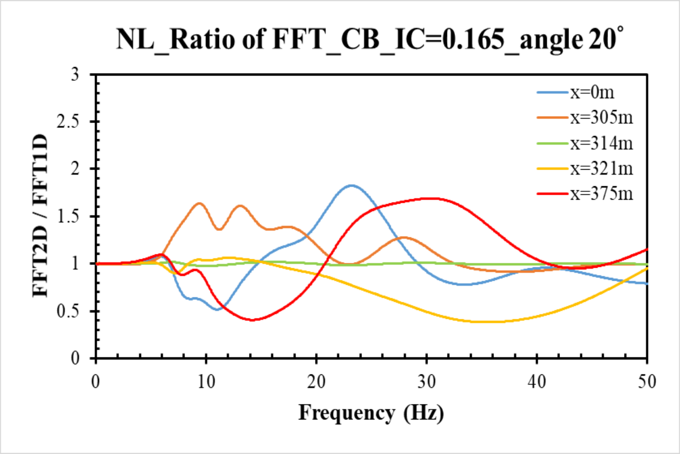

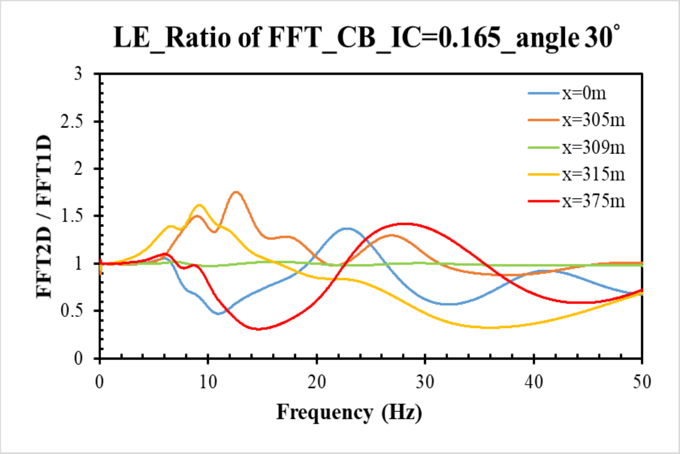

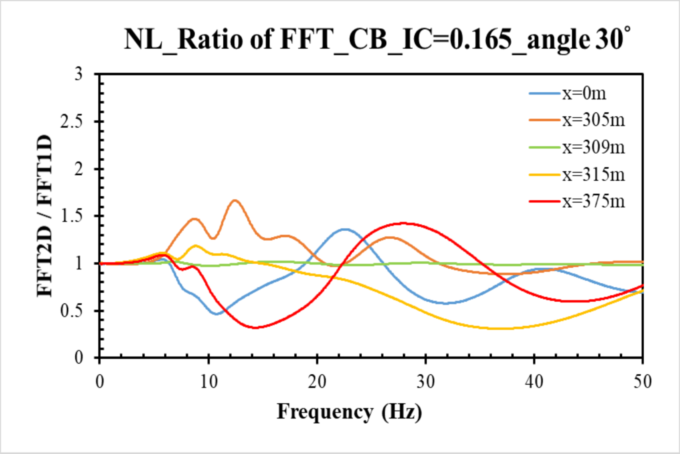

doi:10.6342/NTU201903794

(d) Cases for rigid base analysis, shear-wave velocity 500 m/s, impedance contrast 0.572

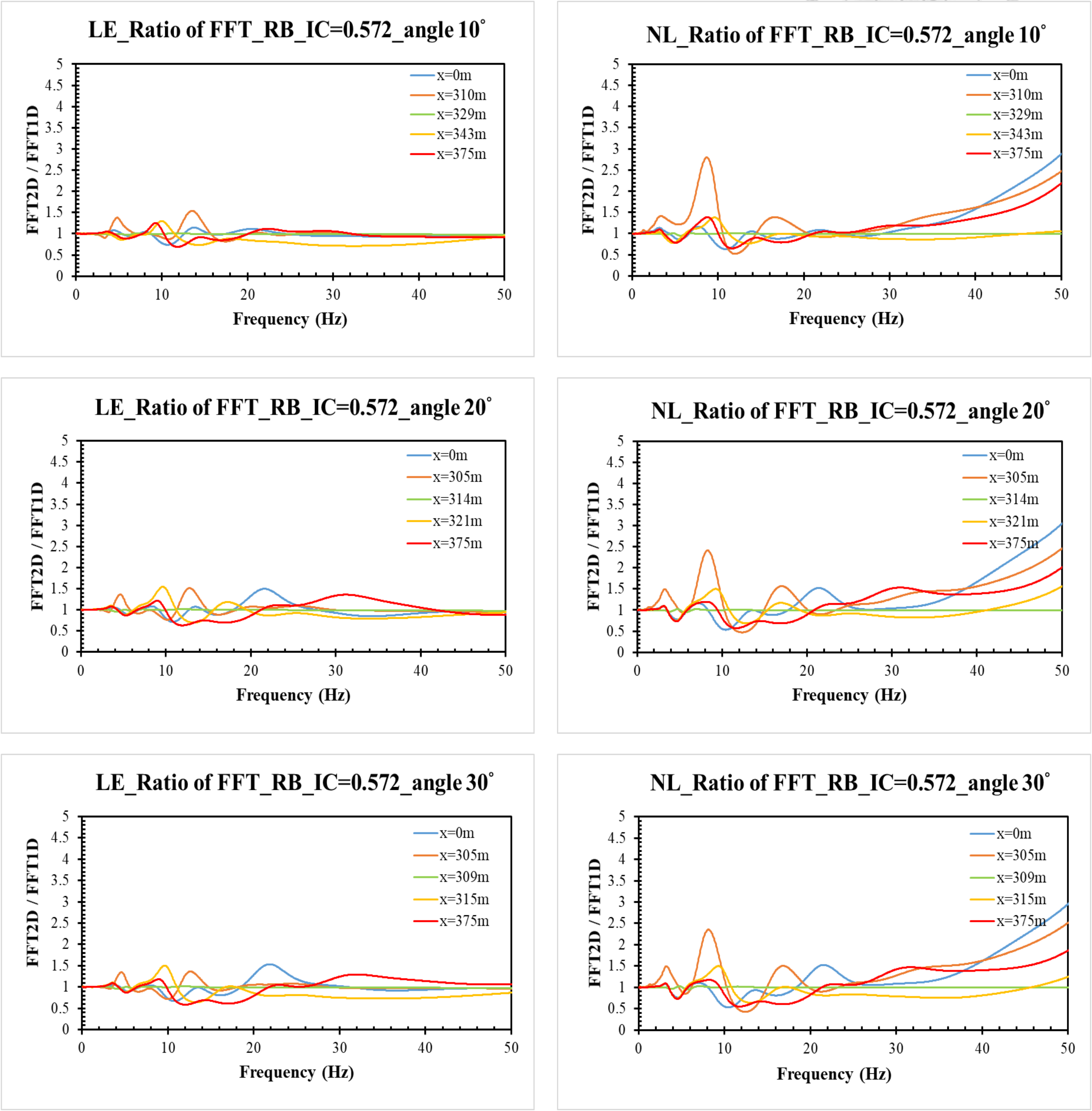

doi:10.6342/NTU201903794

(e) Cases for rigid base, shear-wave velocity 760 m/s, impedance contrast 0.357

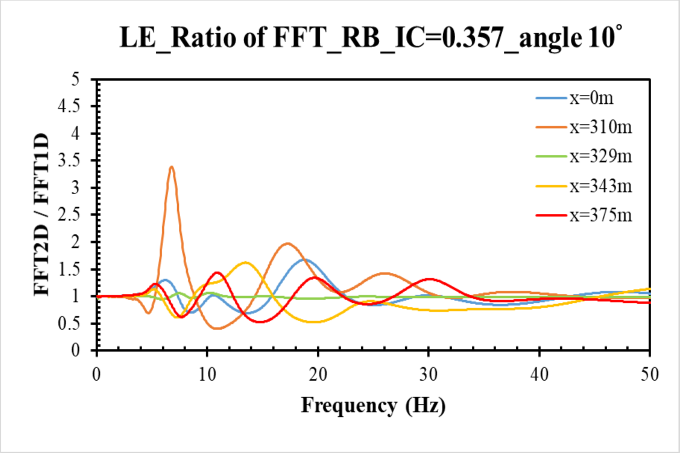

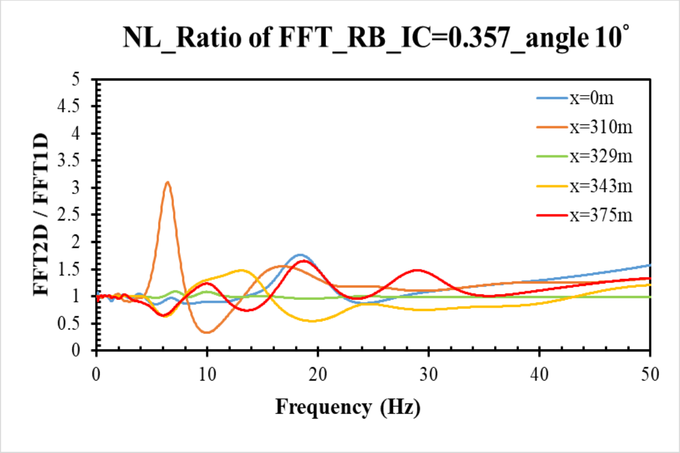

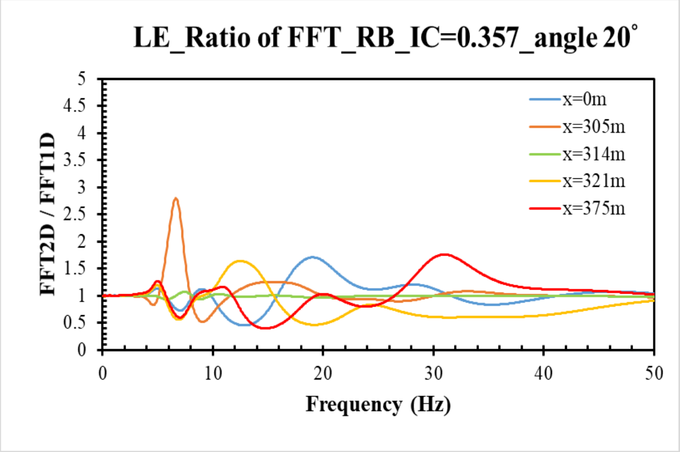

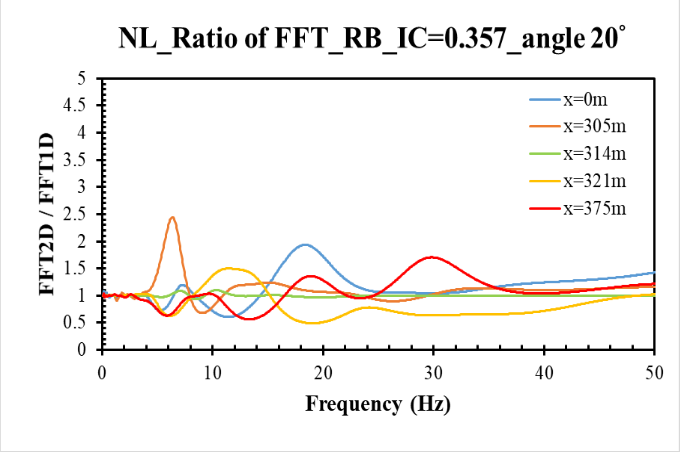

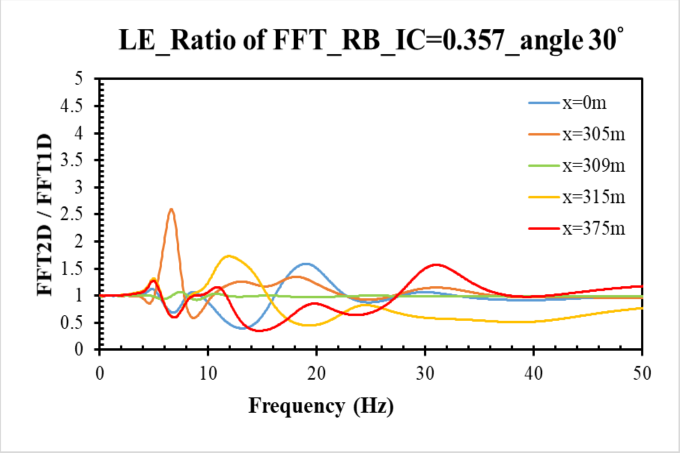

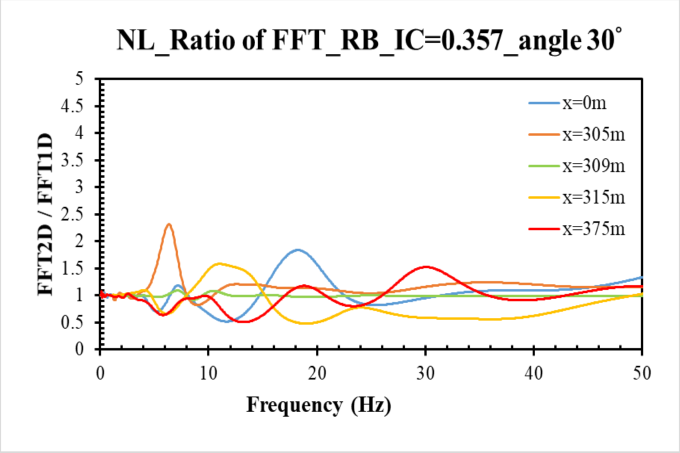

doi:10.6342/NTU201903794

(f) Cases for rigid base, shear-wave velocity 1500 m/s, impedance contrast 0.165

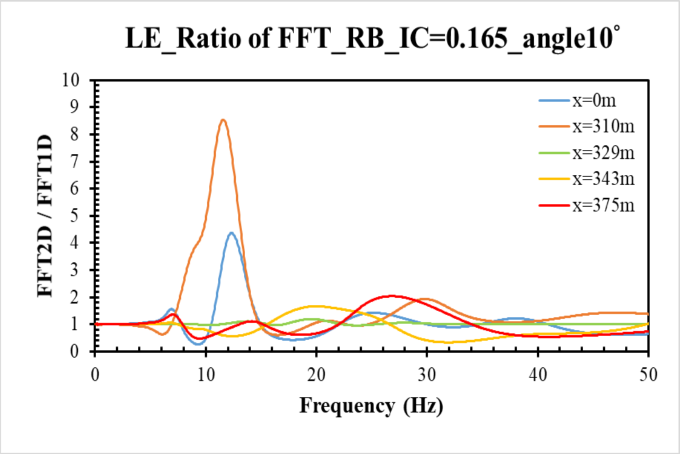

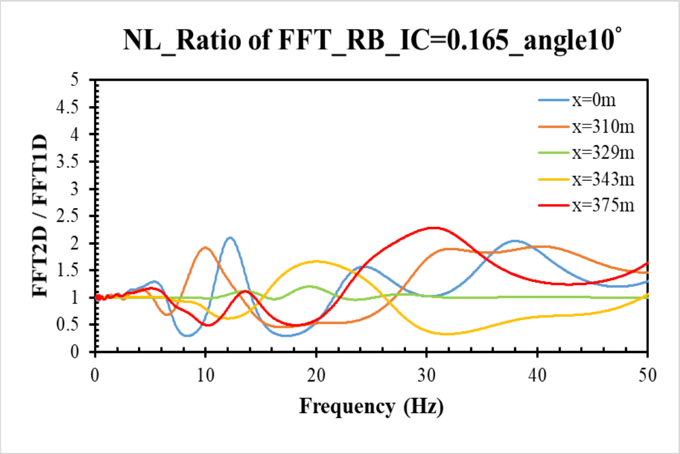

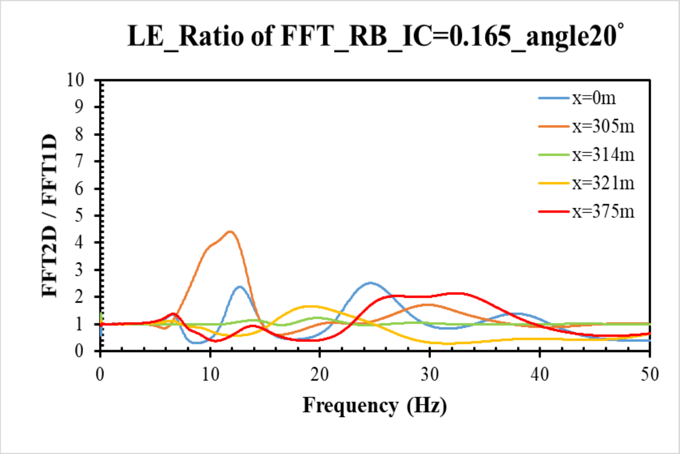

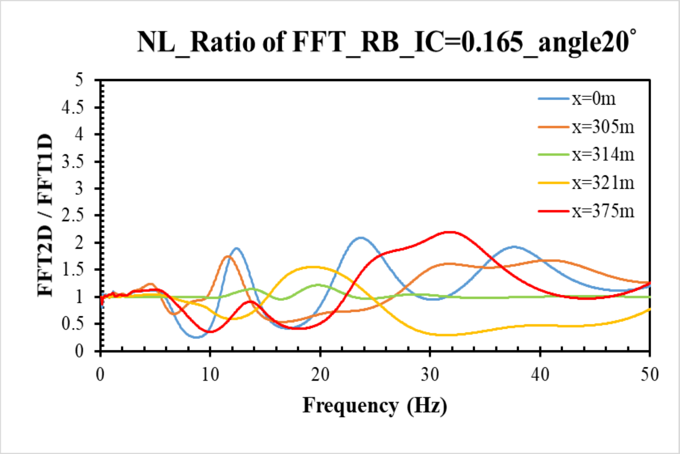

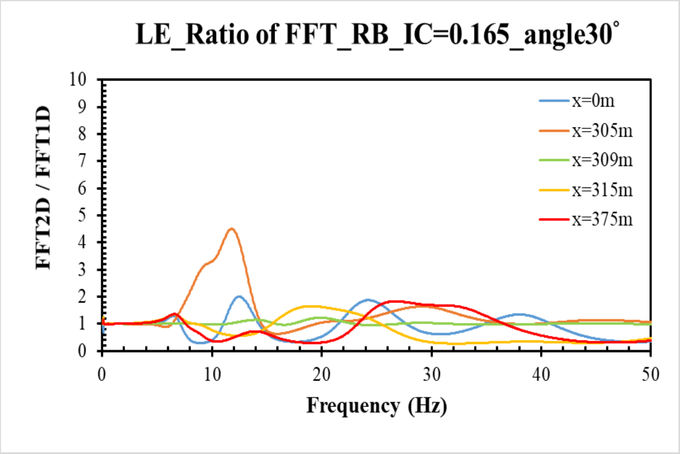

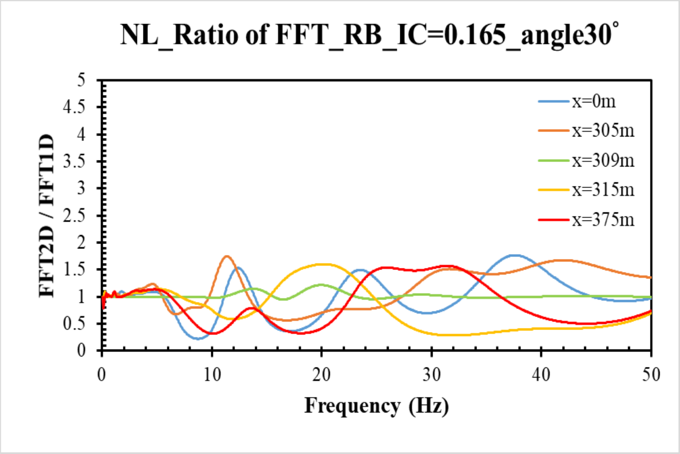

(3) Amplification factors, ratios of output motions to the input motions in x-direction

(a) Cases for compliant base, shear-wave velocity 500 m/s, impedance contrast 0.572

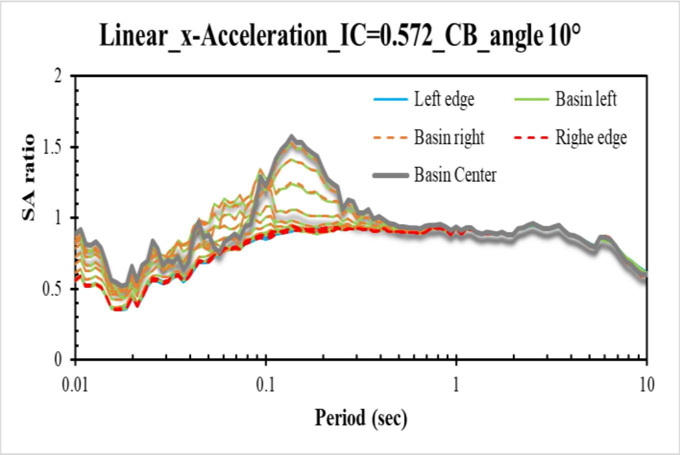

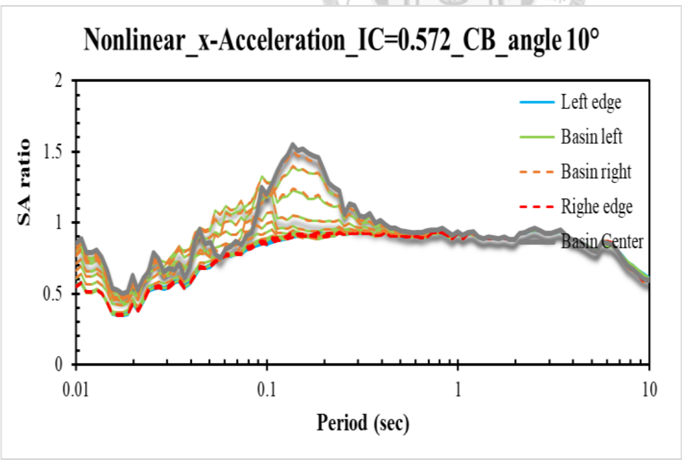

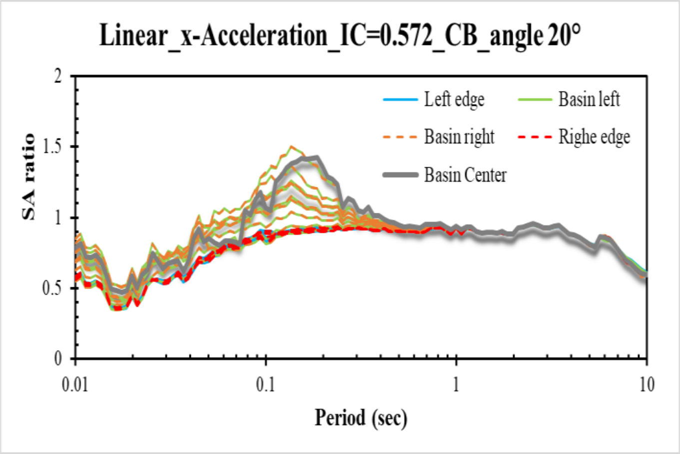

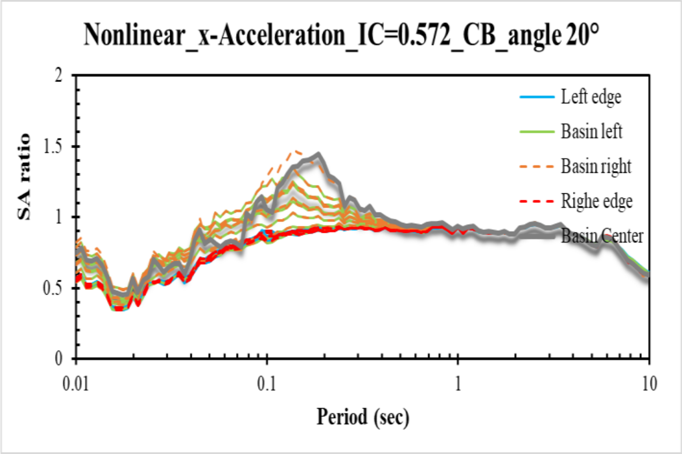

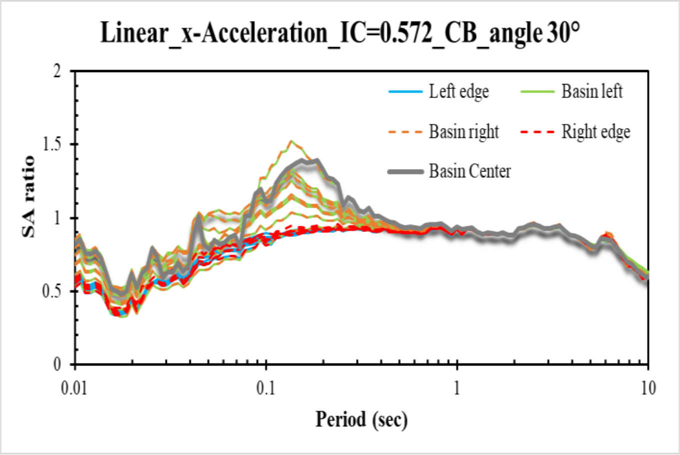

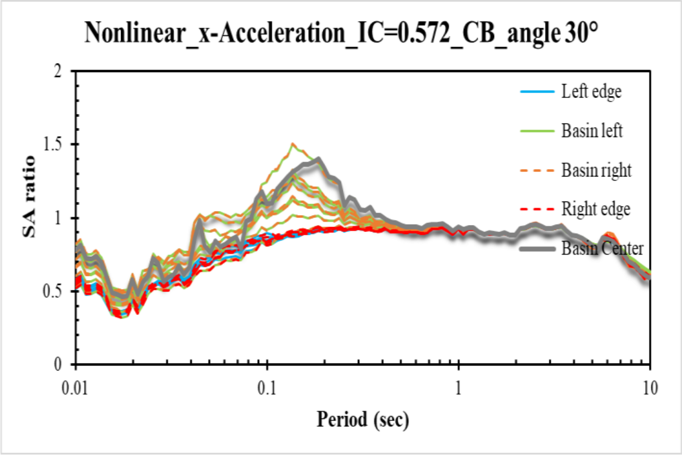

doi:10.6342/NTU201903794

(b) Cases for compliant base, shear-wave velocity 760 m/s, impedance contrast 0.357

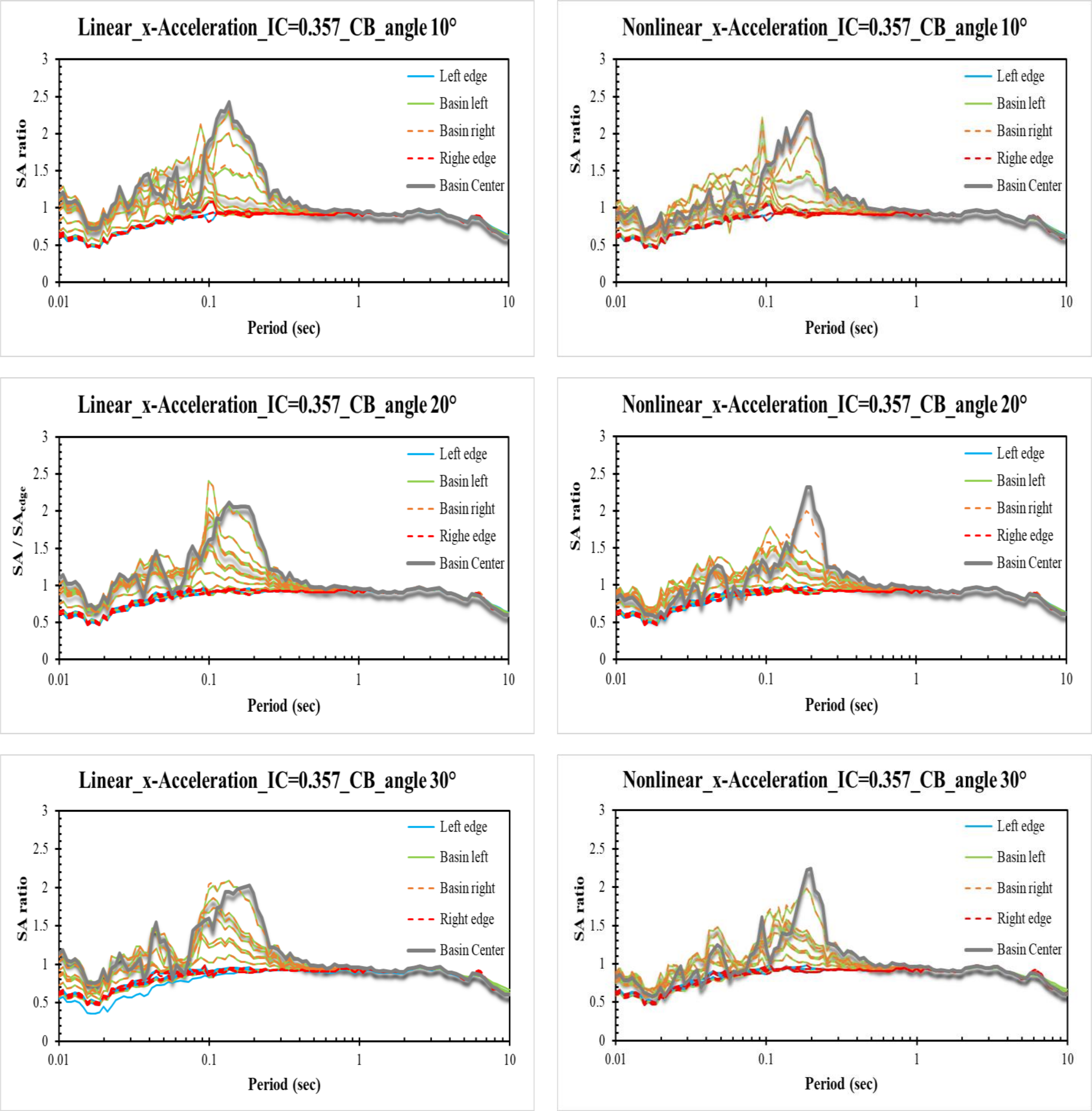

(c) Cases for compliant base, shear-wave velocity 1500 m/s, impedance contrast 0.165

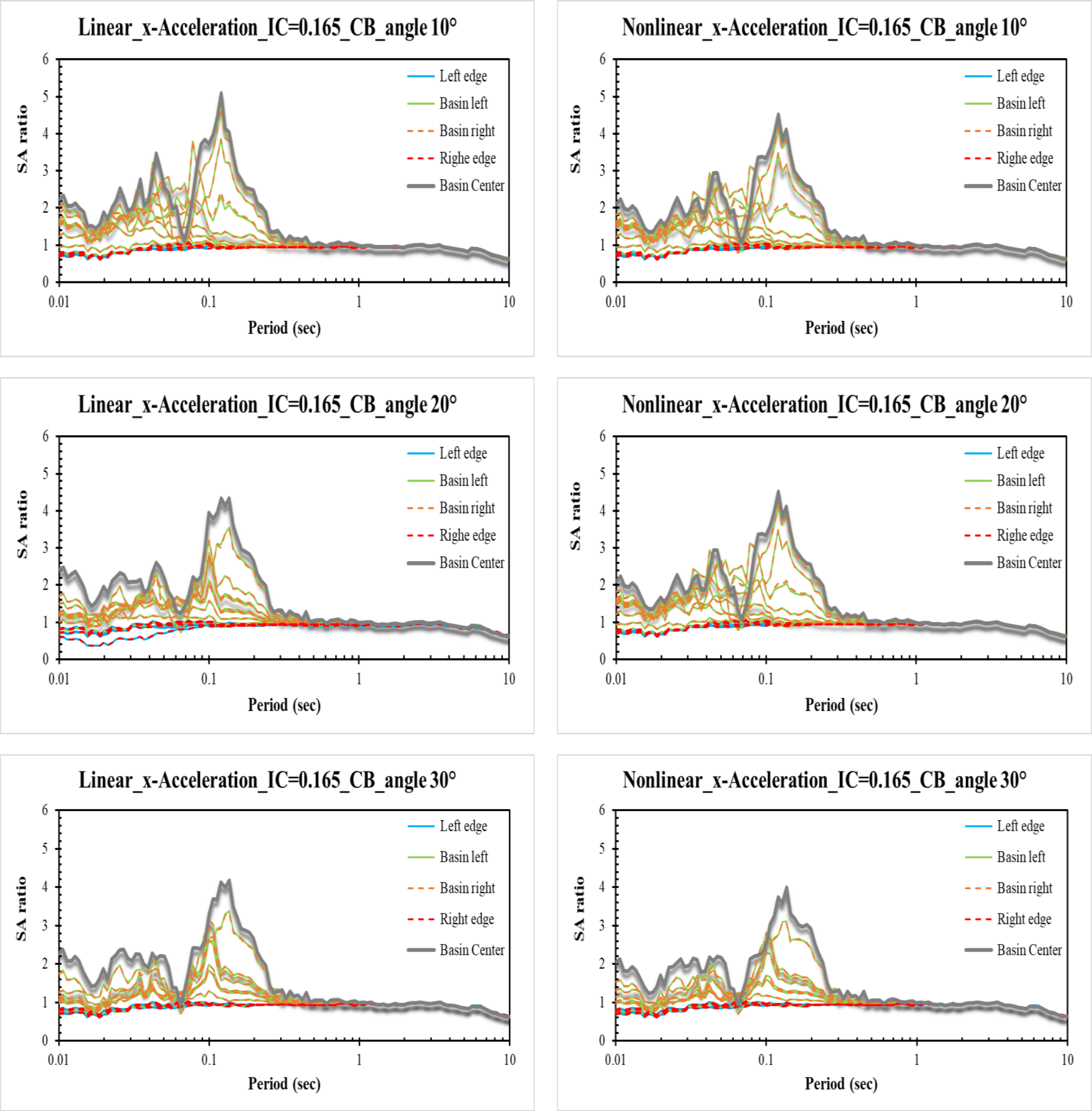

doi:10.6342/NTU201903794

(d) Cases for rigid base, shear-wave velocity 500 m/s, impedance contrast 0.572

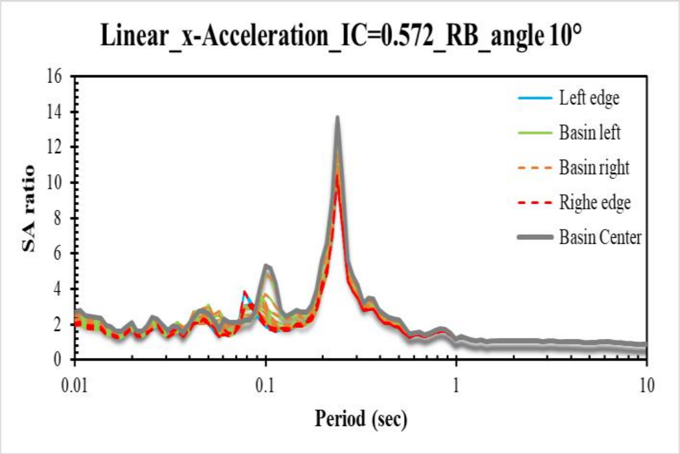

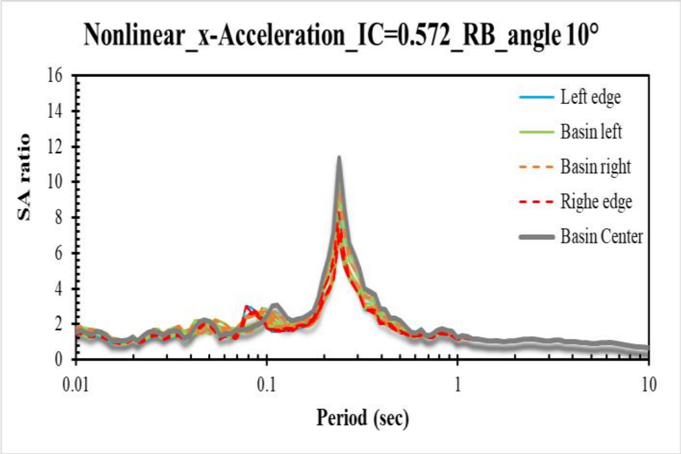

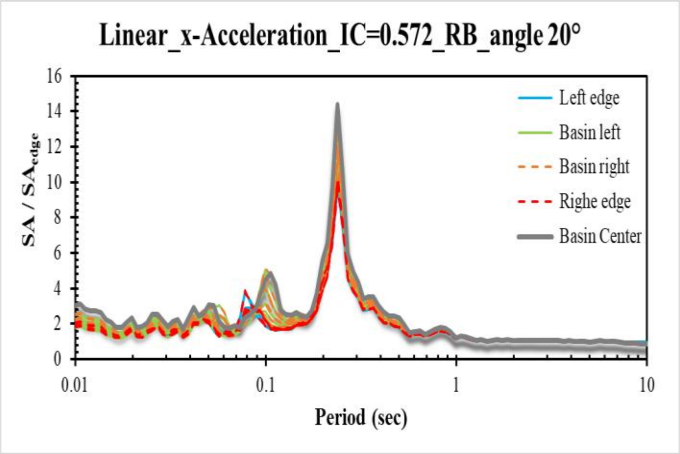

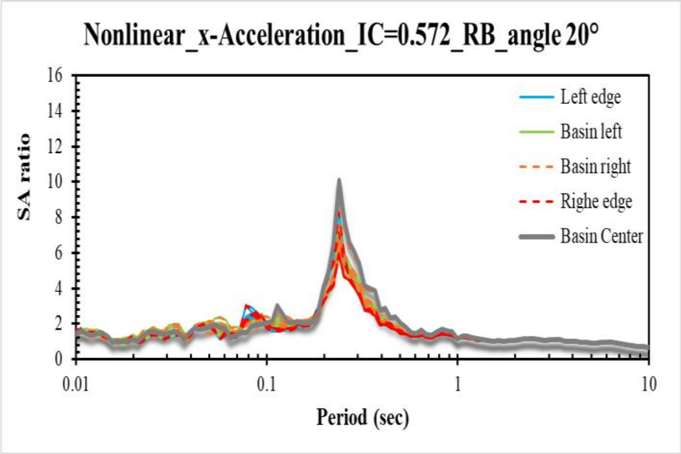

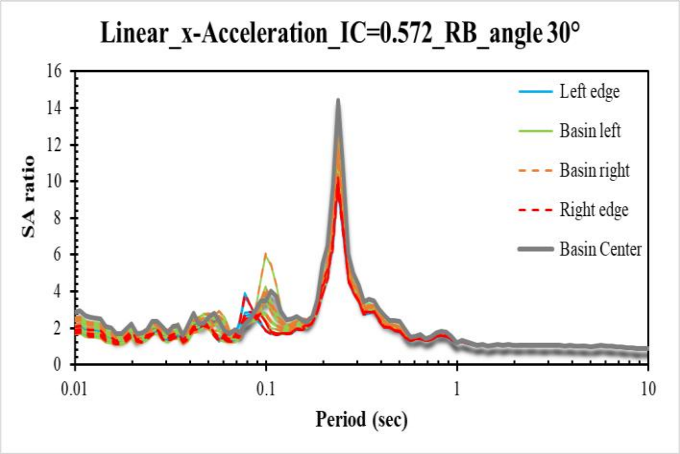

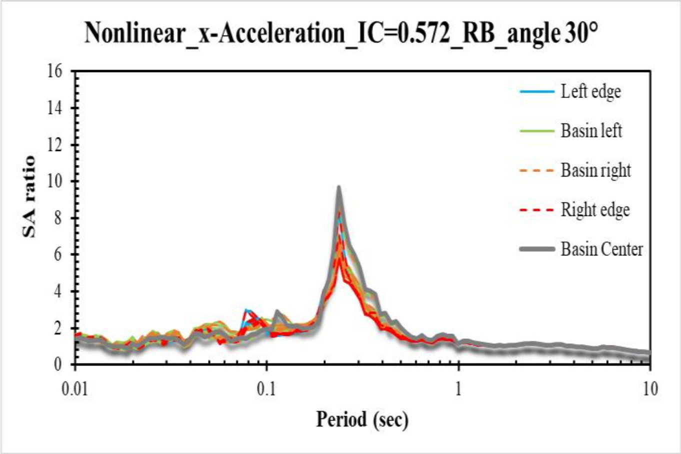

(e) Cases for rigid base, shear-wave velocity 760 m/s, impedance contrast 0.357

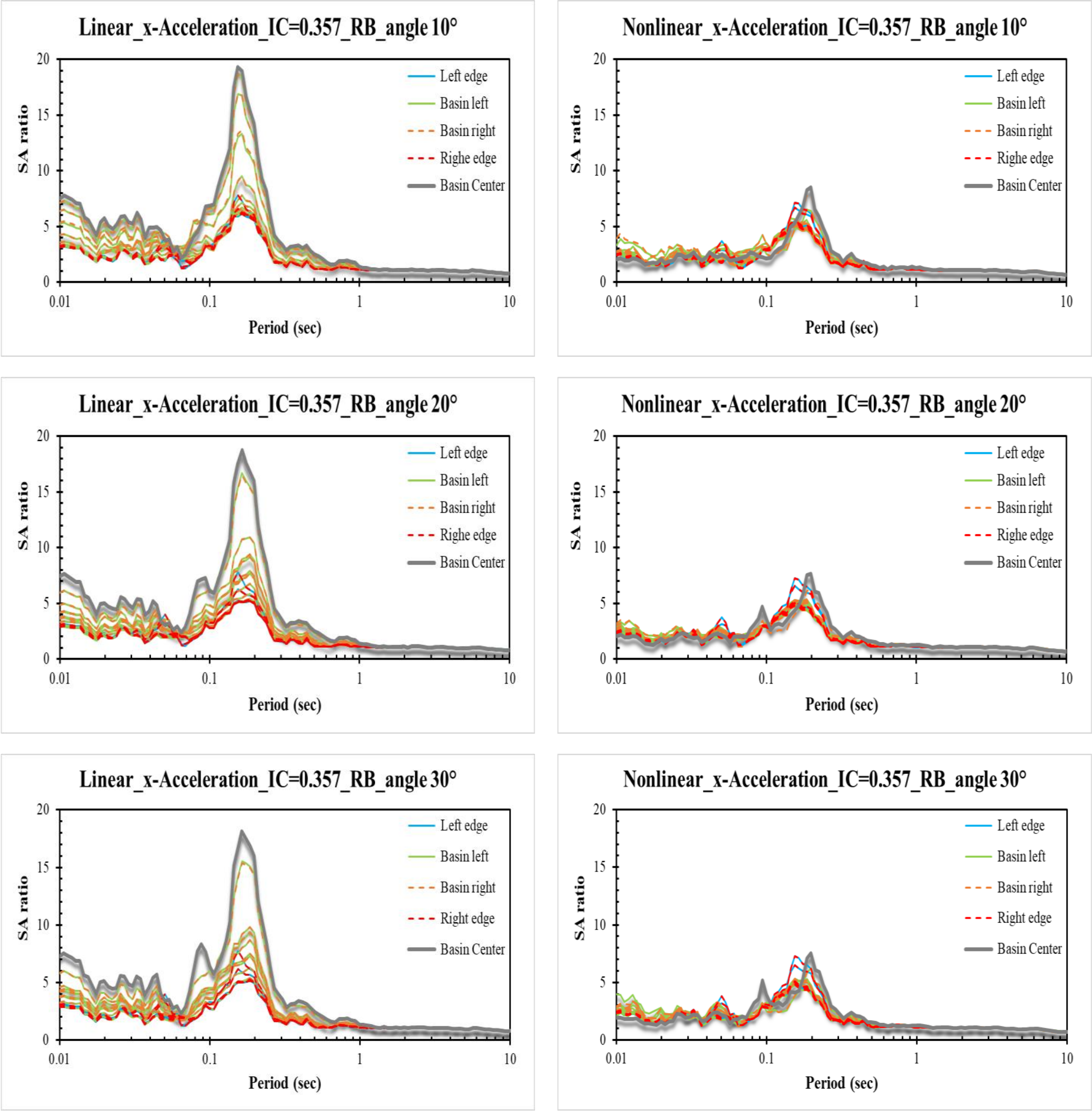

(f) Cases for rigid base, shear-wave velocity 1500 m/s, impedance contrast 0.165

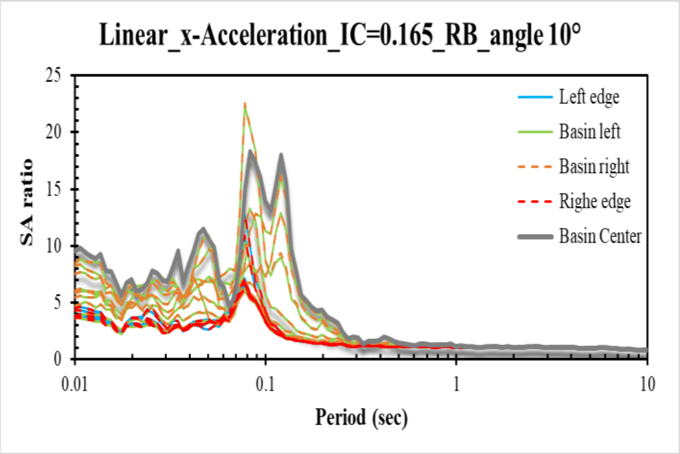

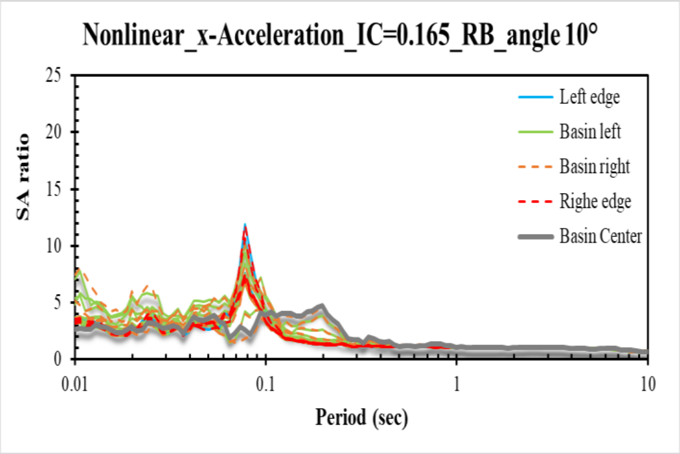

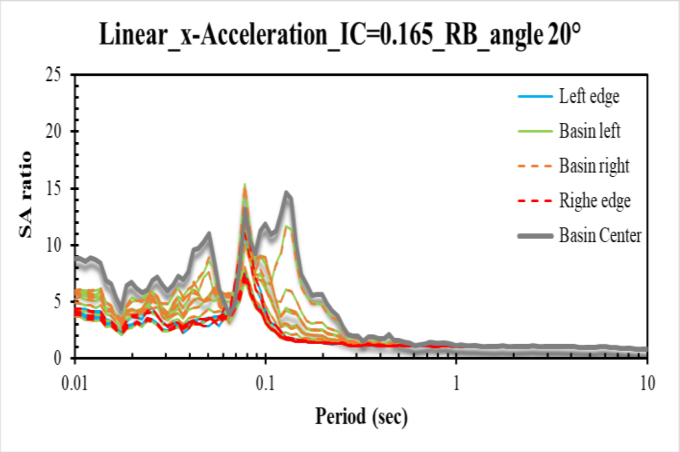

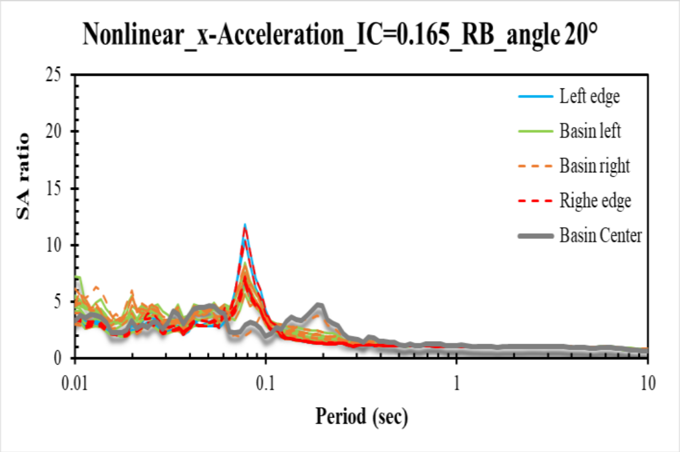

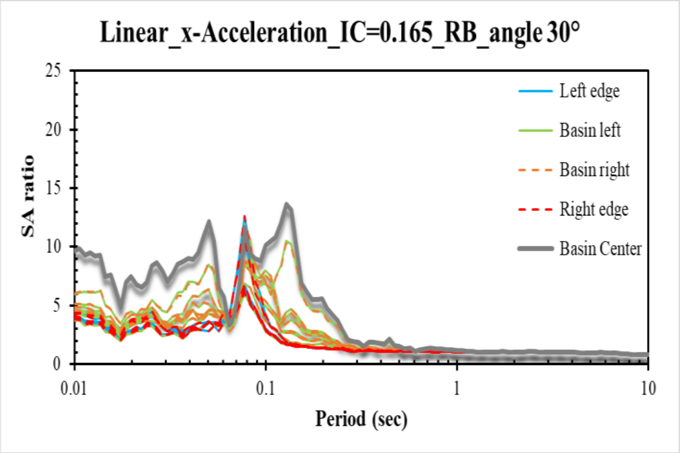

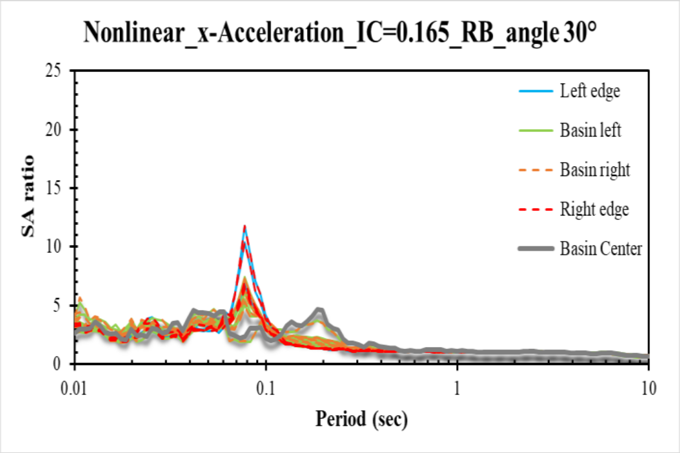

doi:10.6342/NTU201903794

### (4) PGA of x-acceleration in different periods for both compliant and rigid base

#### (a) PGA with compliant base, period 0.01 sec

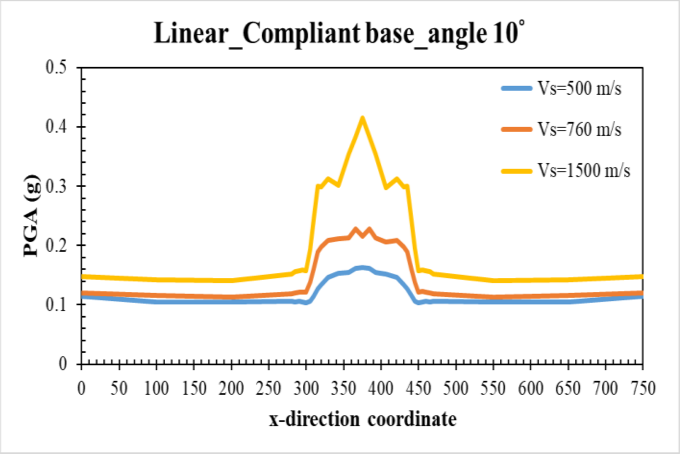

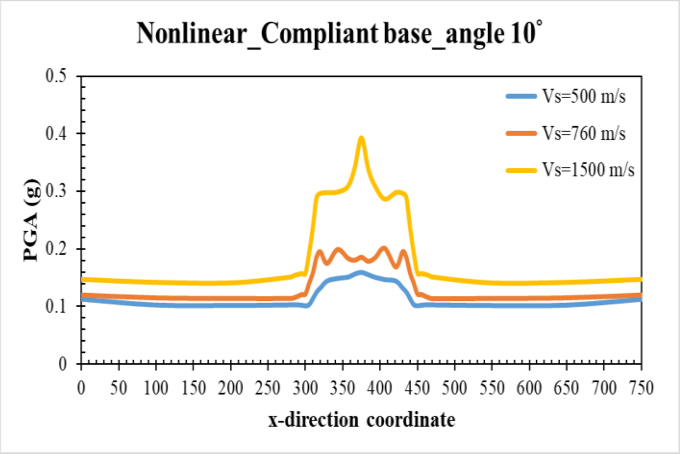

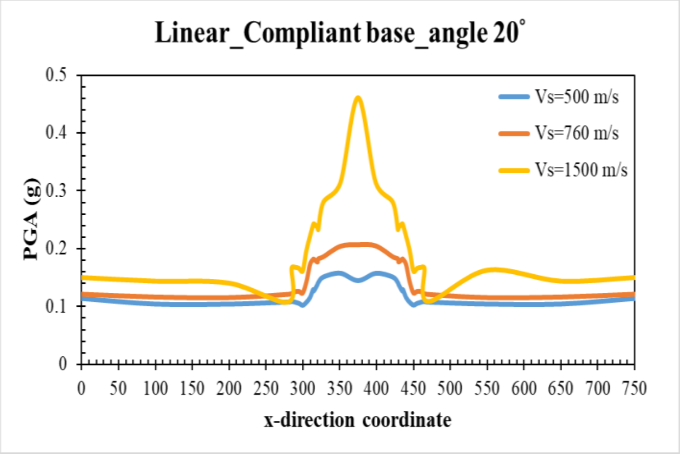

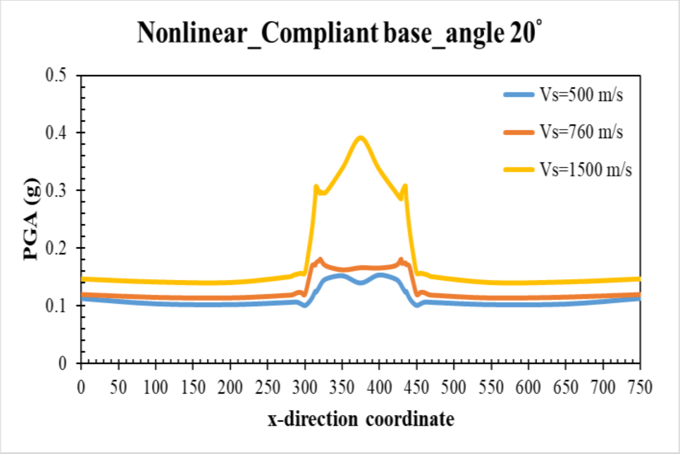

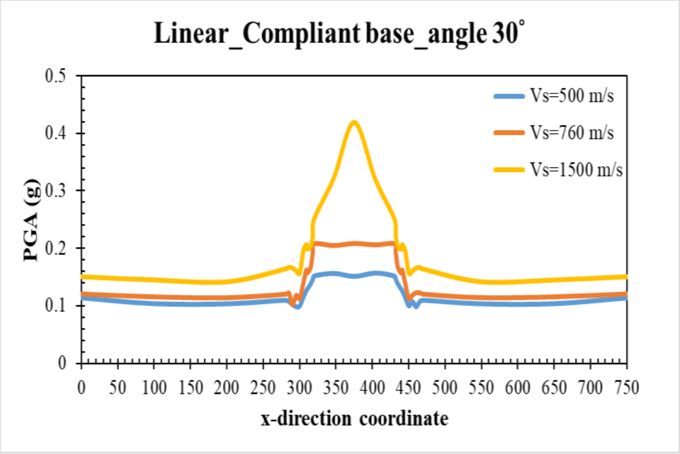

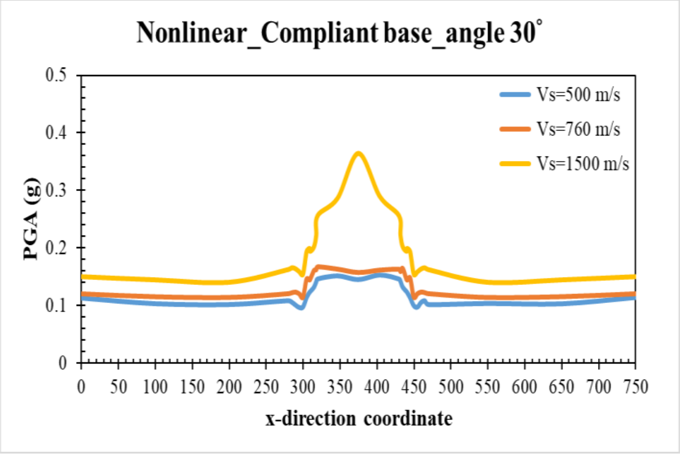

doi:10.6342/NTU201903794

(b) PGA with rigid base, period 0.01 sec

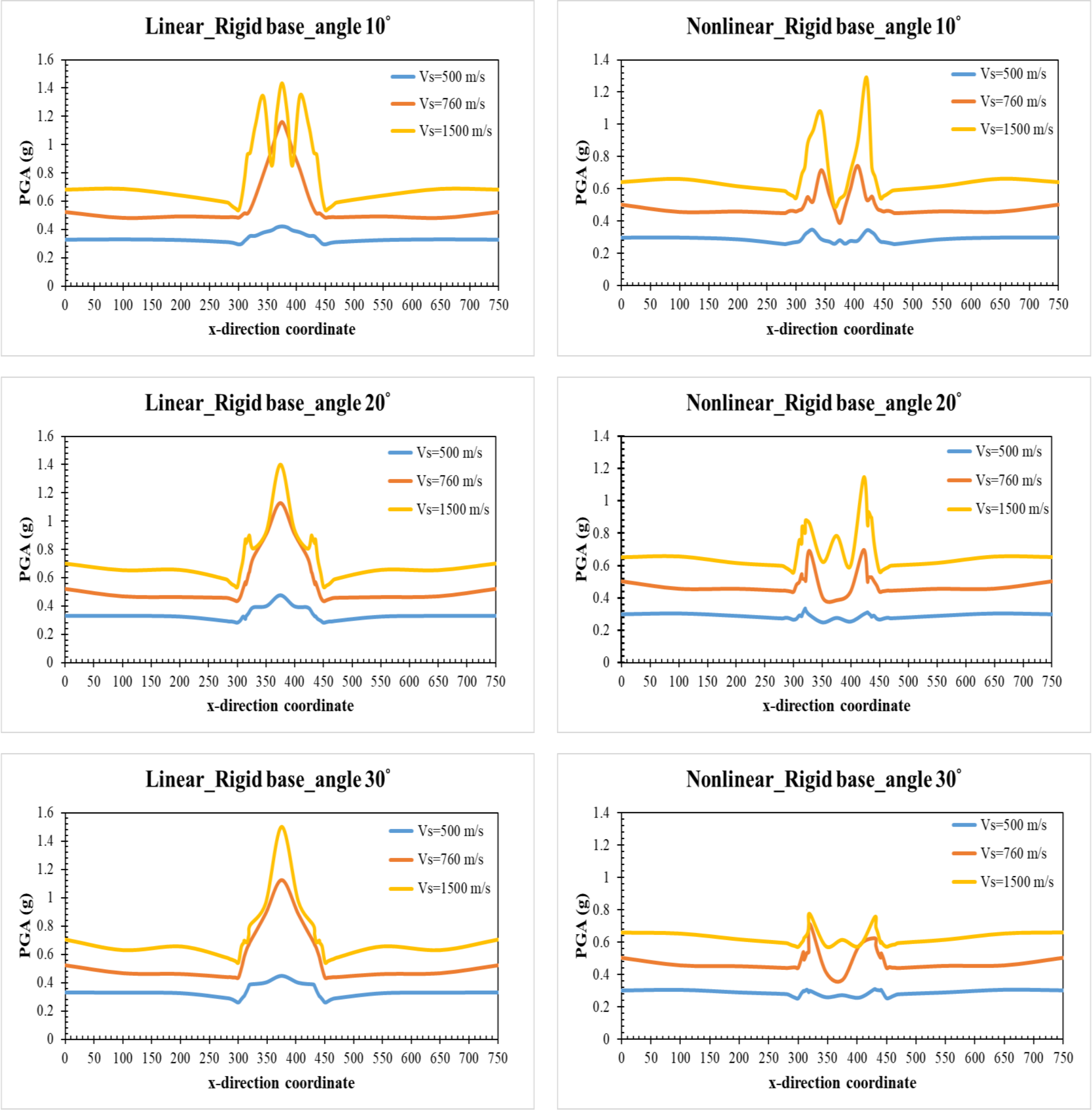
Linear_Rigid base_angle 10°

Nonlinear_Rigid base_angle 10°

Linear_Rigid base_angle 20°

Nonlinear_Rigid base_angle 20°

Linear_Rigid base_angle 30°

Nonlinear_Rigid base_angle 30°

(c) PGA with compliant base, period 0.1 sec

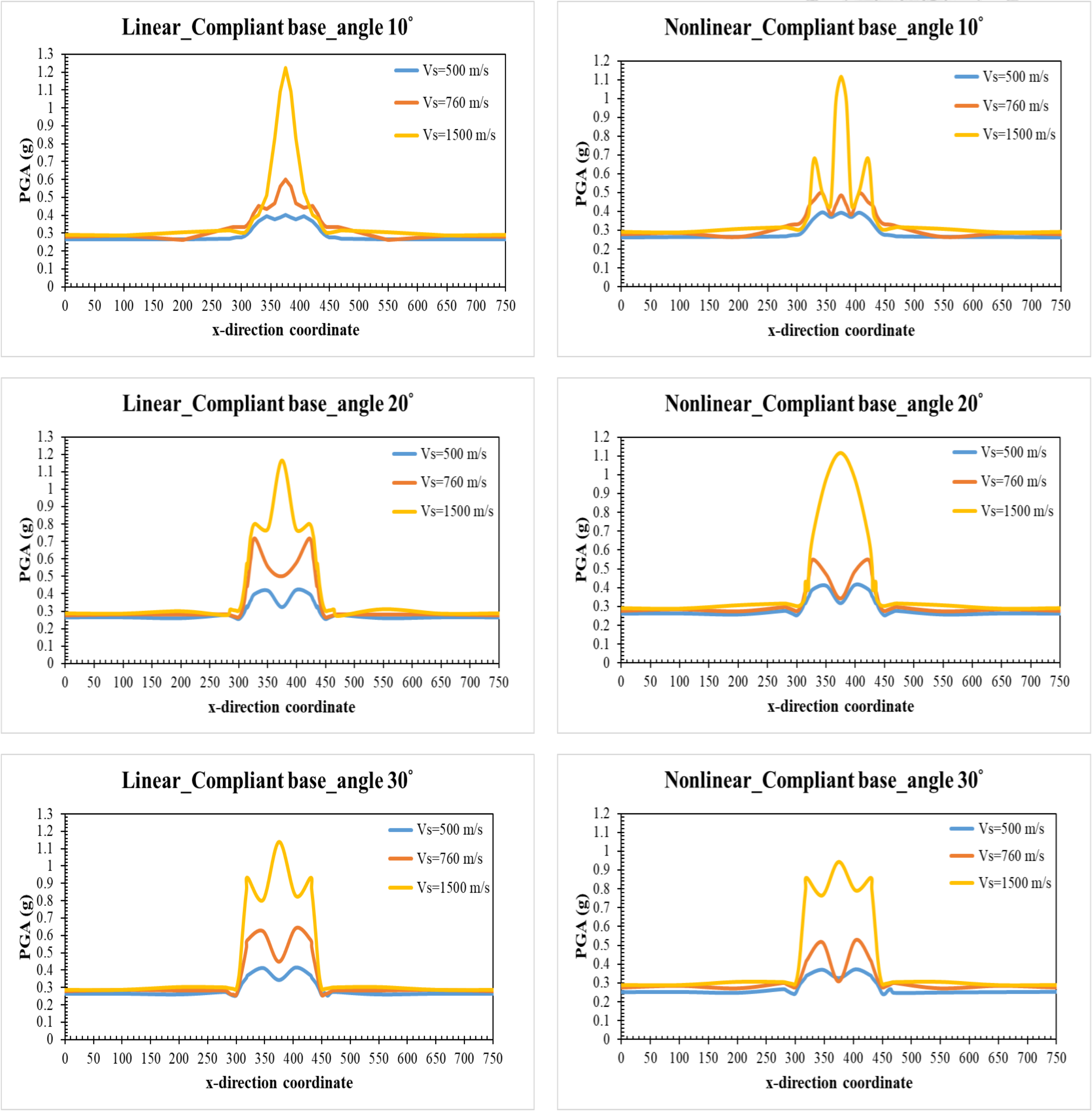

(d) PGA with rigid base, period 0.1 sec

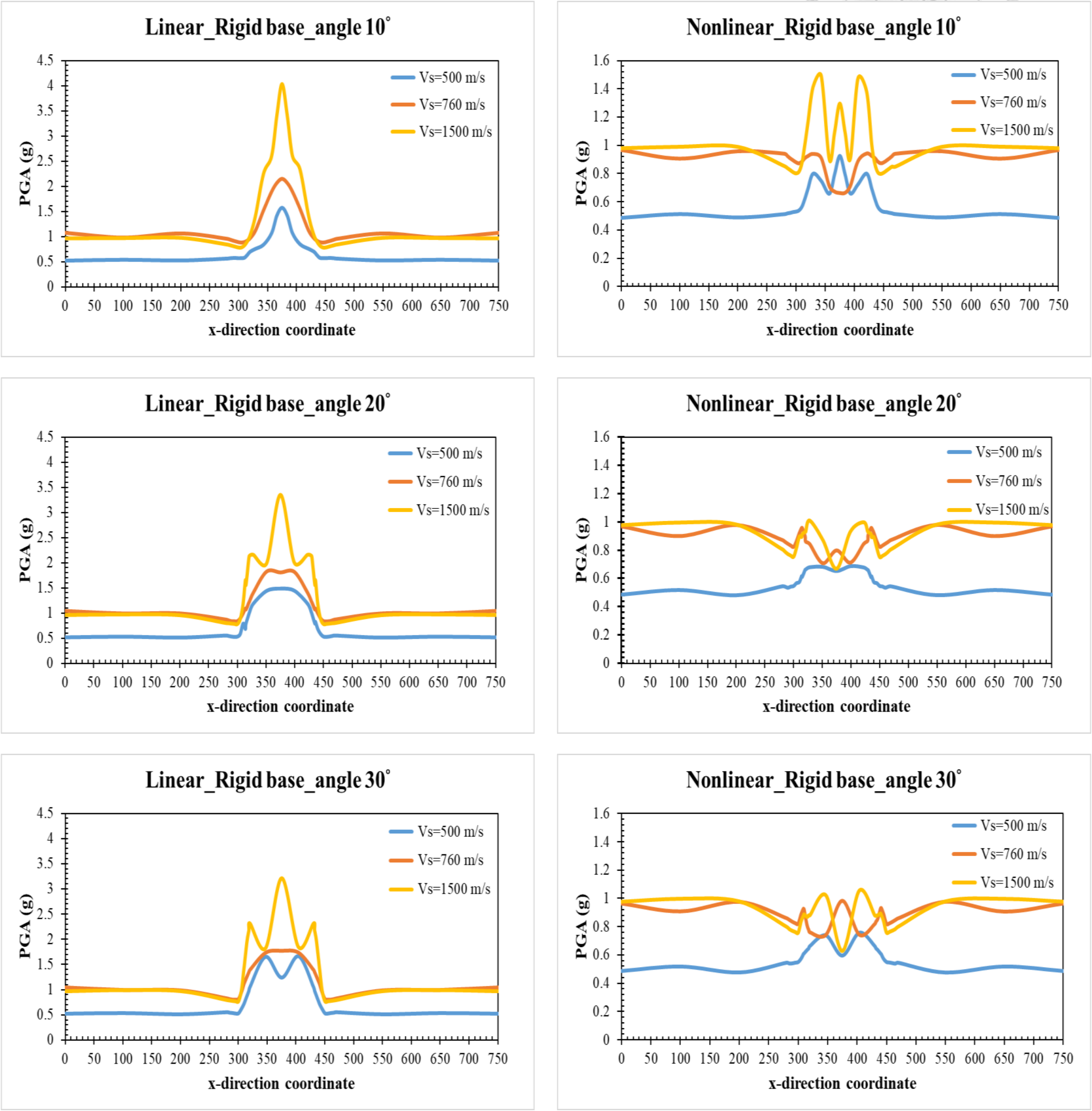

Linear_Rigid base_angle 10°

Nonlinear_Rigid base_angle 10°

Linear_Rigid base_angle 20°

Nonlinear_Rigid base_angle 20°

Linear_Rigid base_angle 30°

Nonlinear_Rigid base_angle 30°

doi:10.6342/NTU201903794

(e) PGA with compliant base, period 1 sec

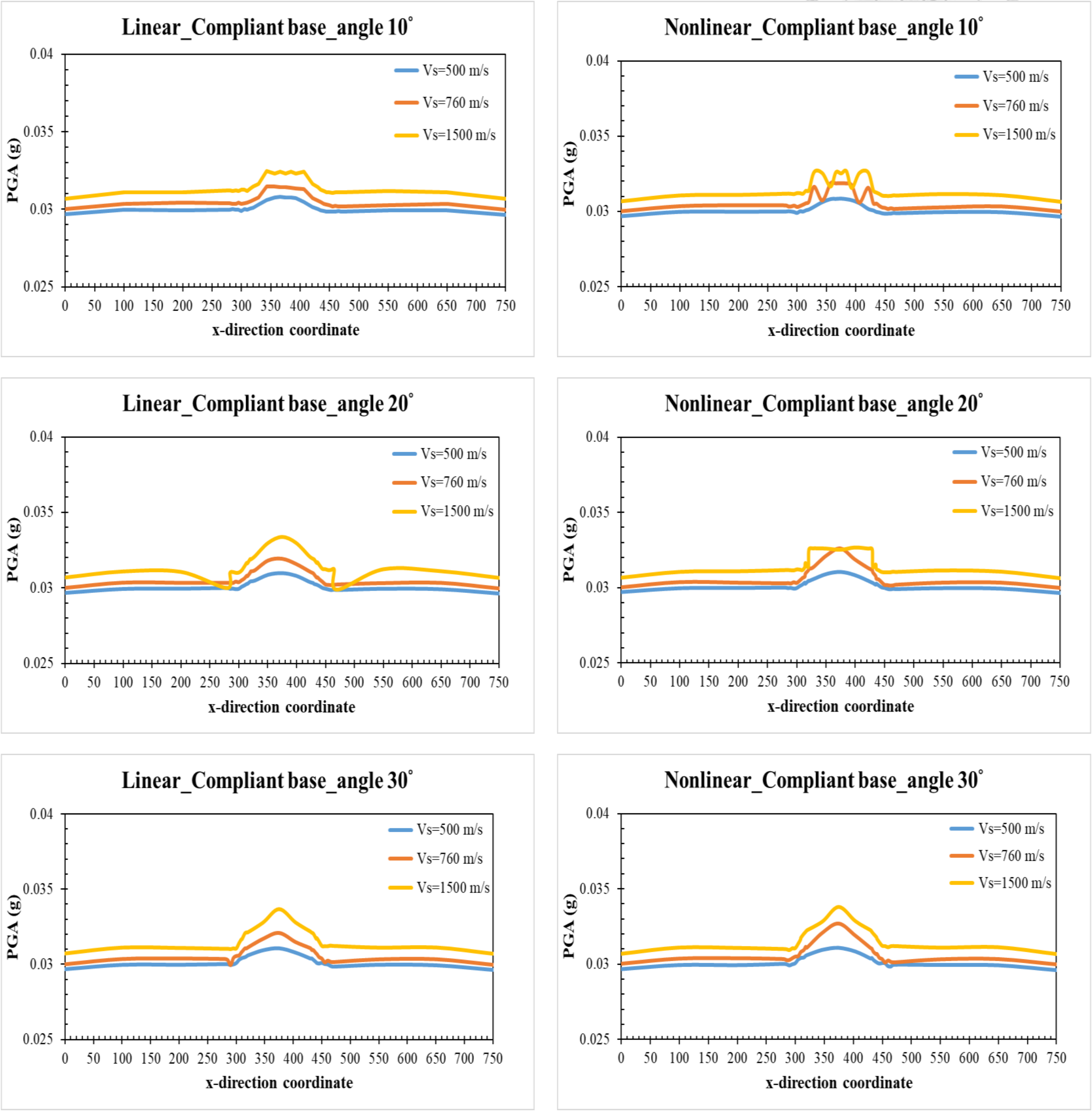

doi:10.6342/NTU201903794

(f) PGA with rigid base, period 1 sec

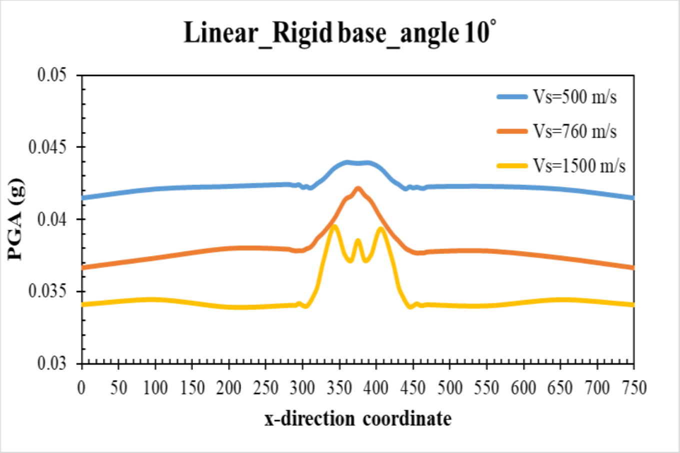

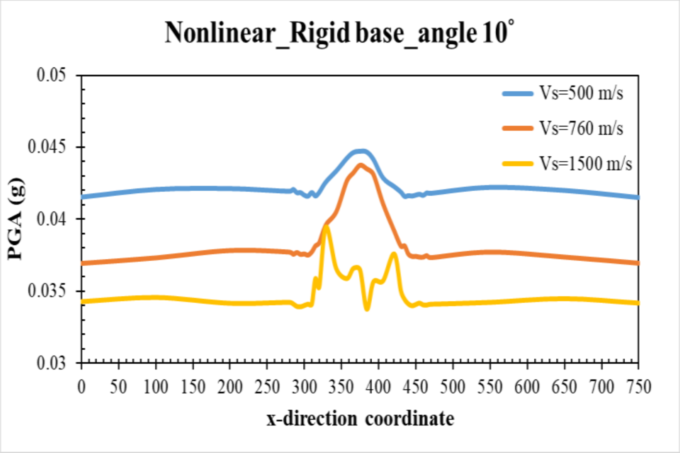

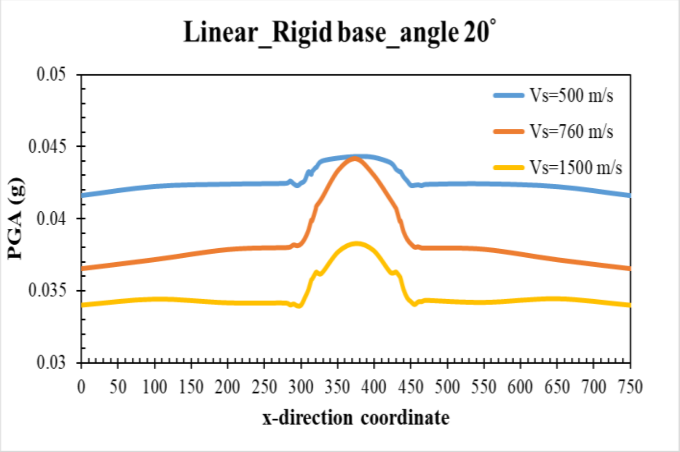

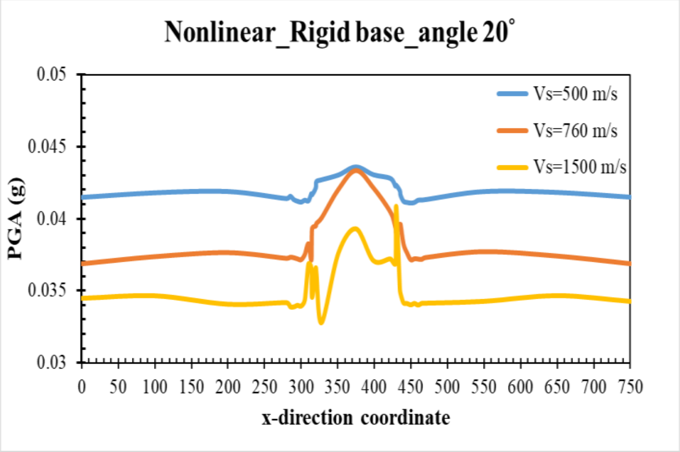

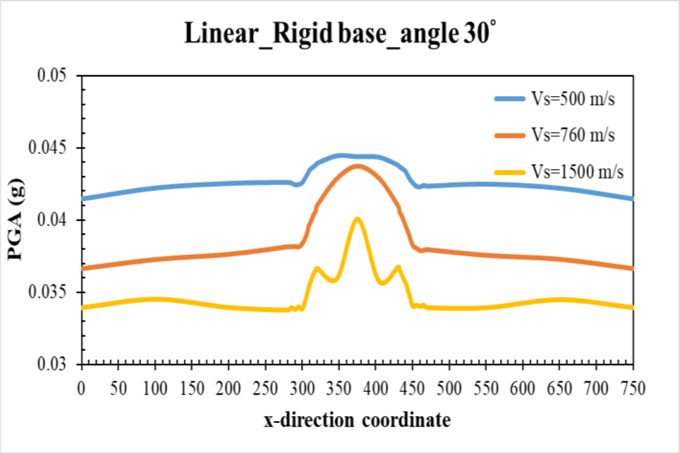

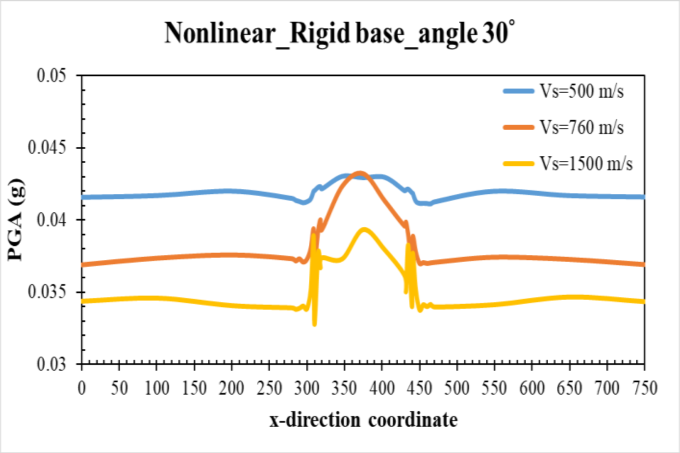

### (5) Lagged coherency in x-direction of different geological conditions

#### (a) Cases for compliant base, shear-wave velocity 500 m/s

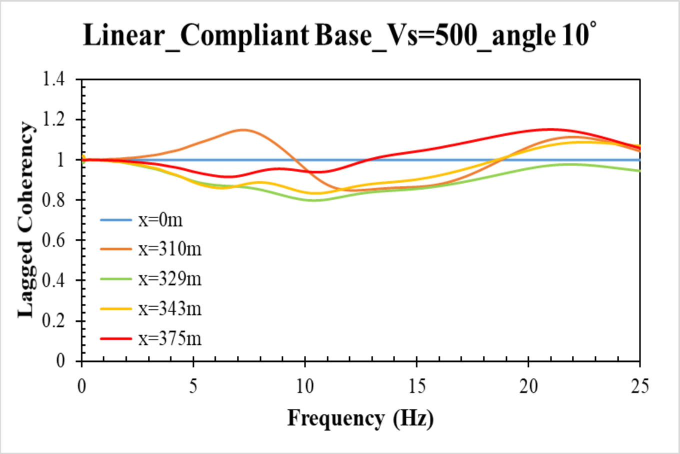

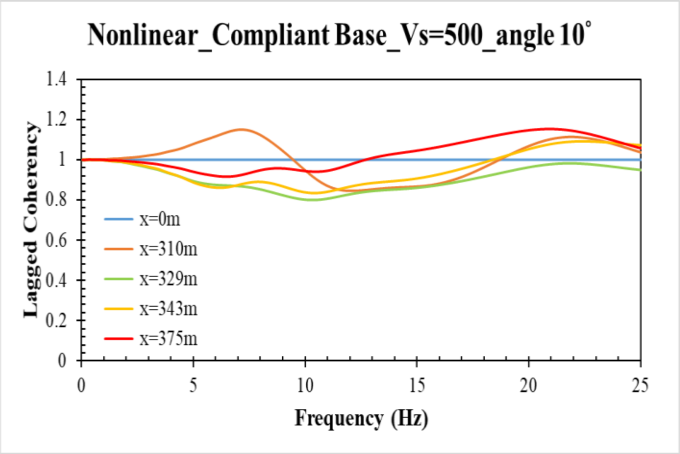

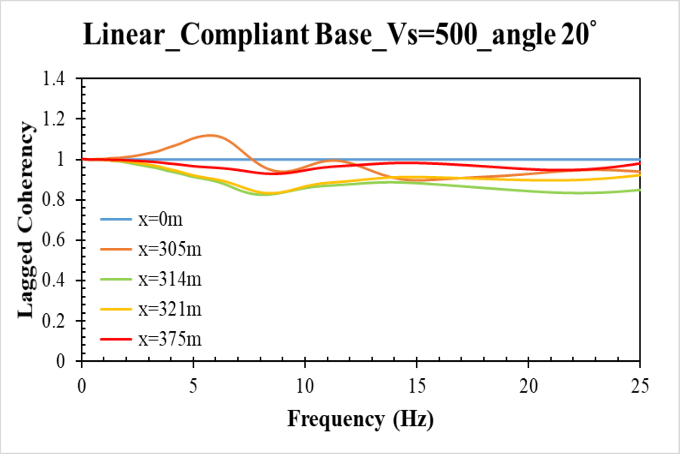

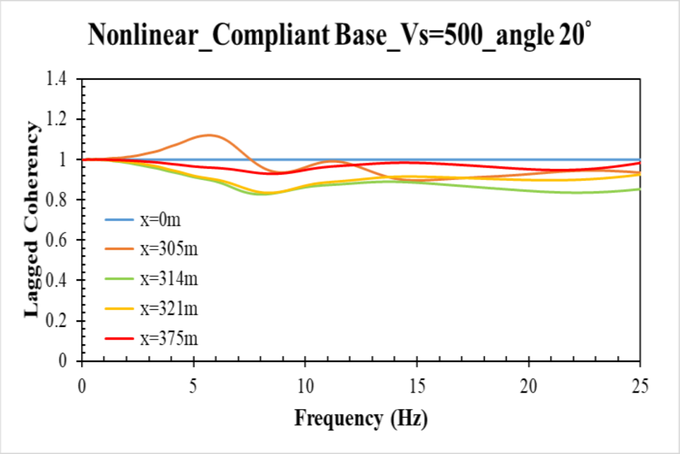

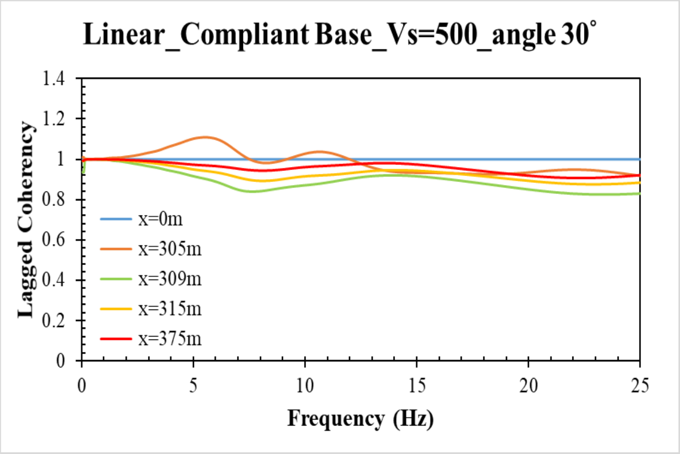

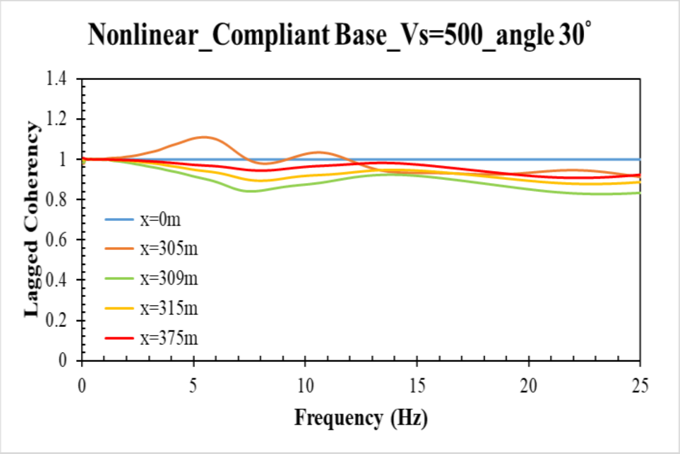

doi:10.6342/NTU201903794

(b) Cases for compliant base, shear-wave velocity 760 m/s

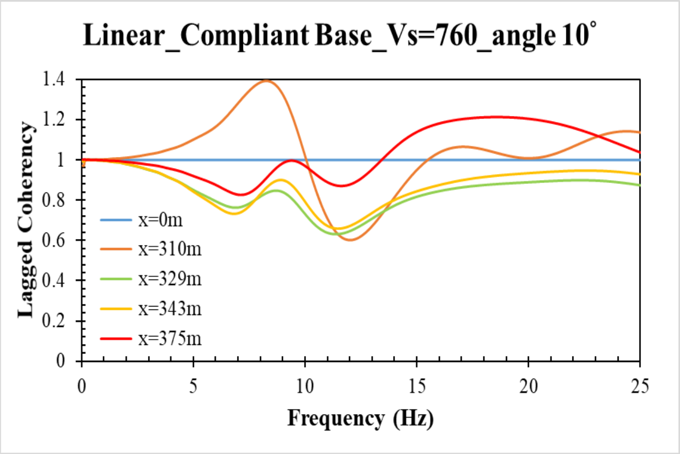

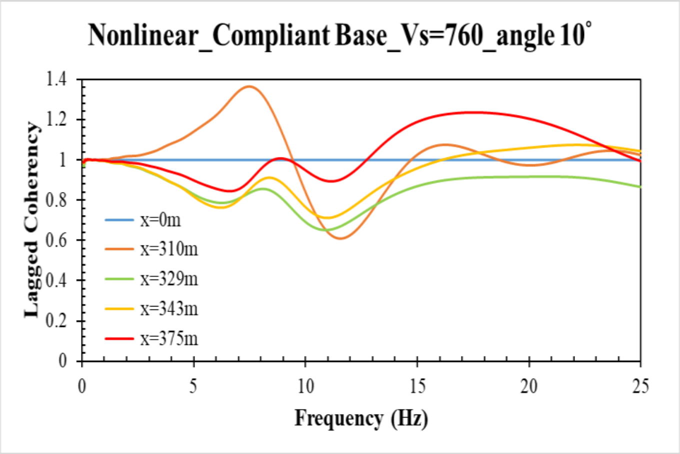

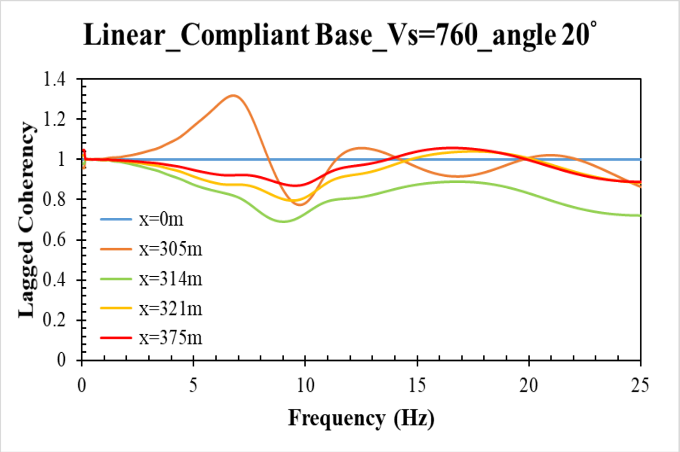

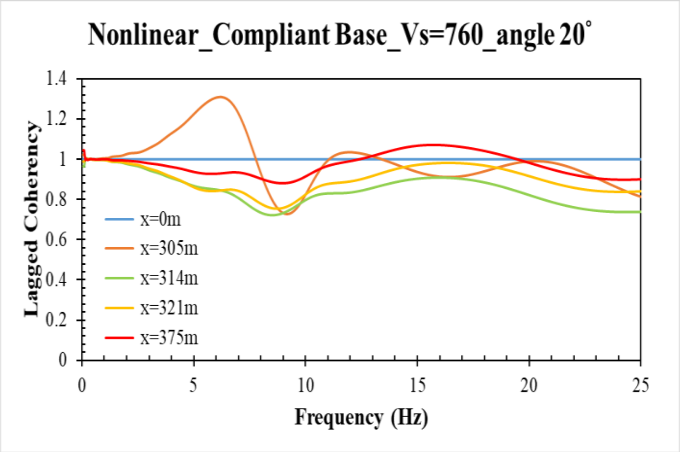

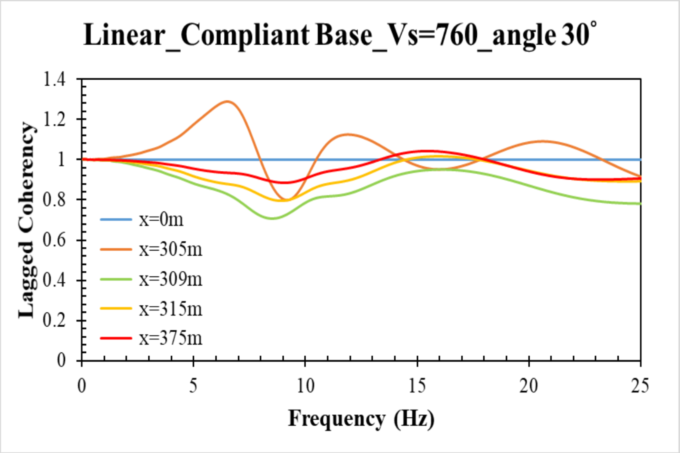

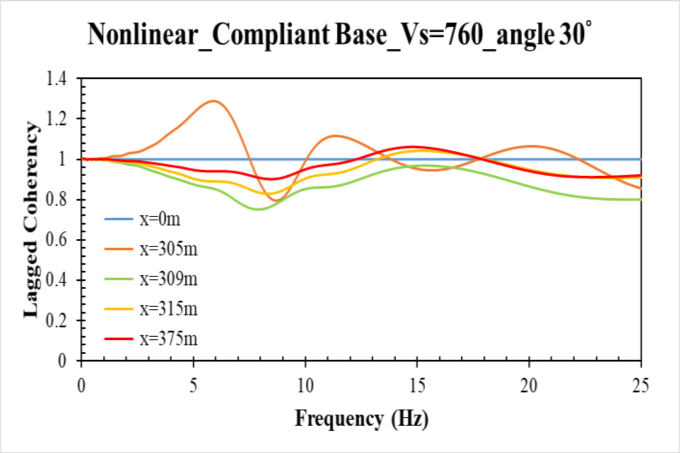

doi:10.6342/NTU201903794

(c) Cases for compliant base, shear-wave velocity 1500 m/s

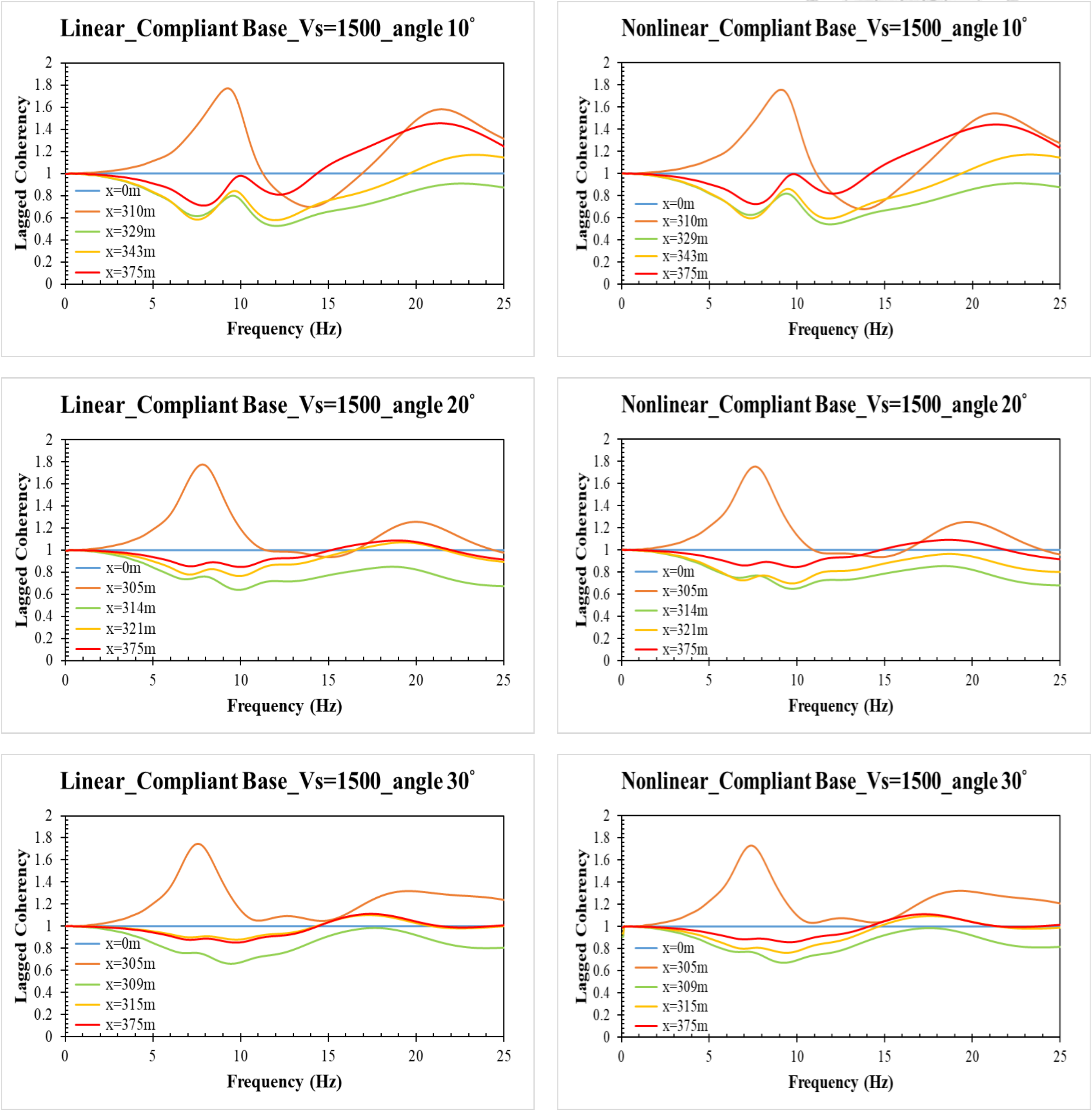

doi:10.6342/NTU201903794

(d) Cases for rigid base, shear-wave 500 m/s

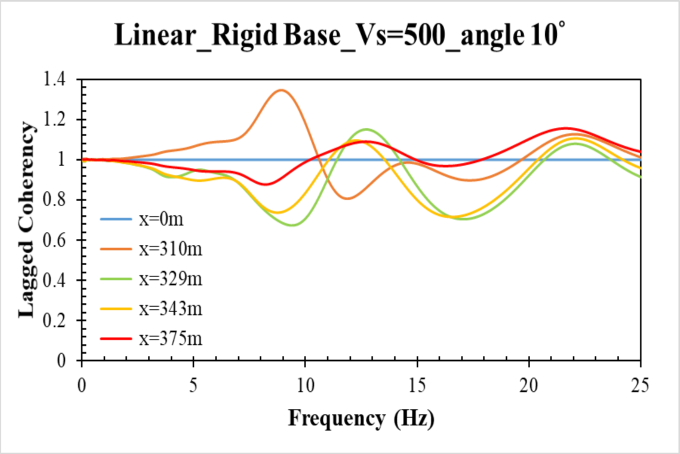

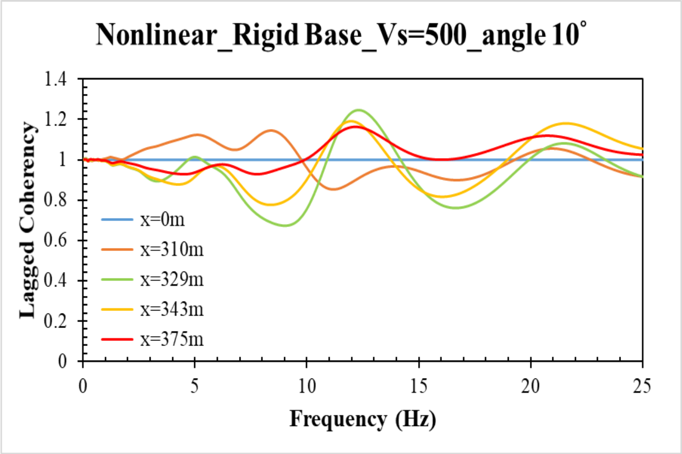

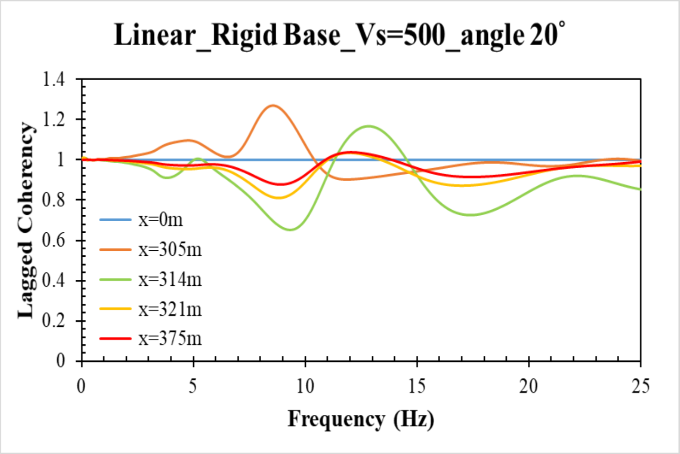

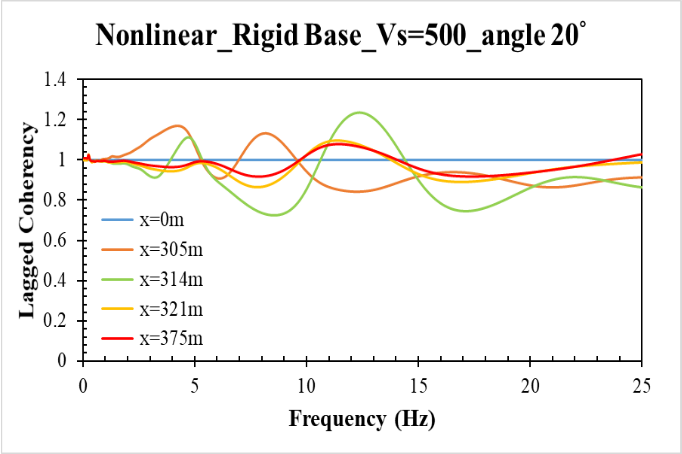

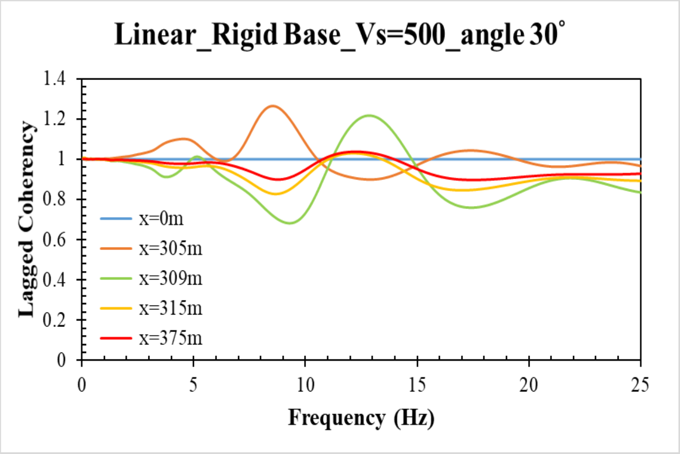

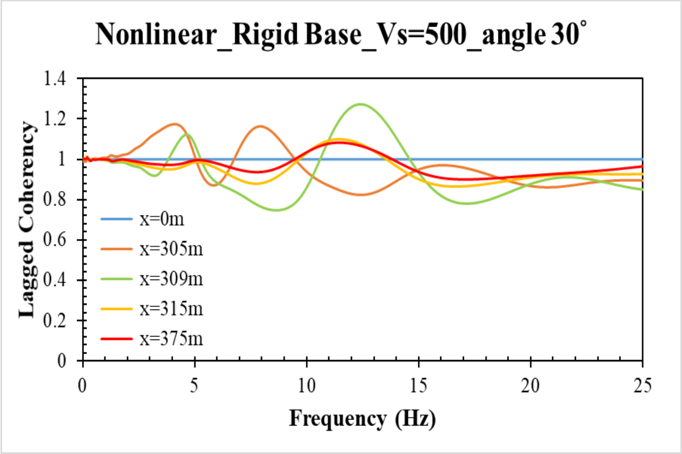

doi:10.6342/NTU201903794

(e) Cases for rigid base, shear-wave velocity 760 m/s

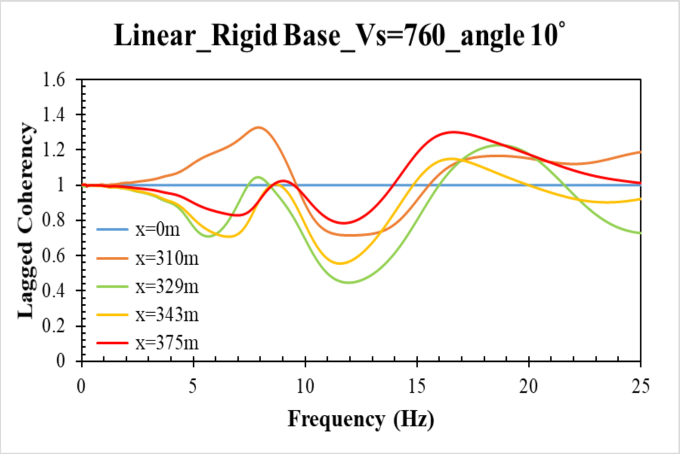

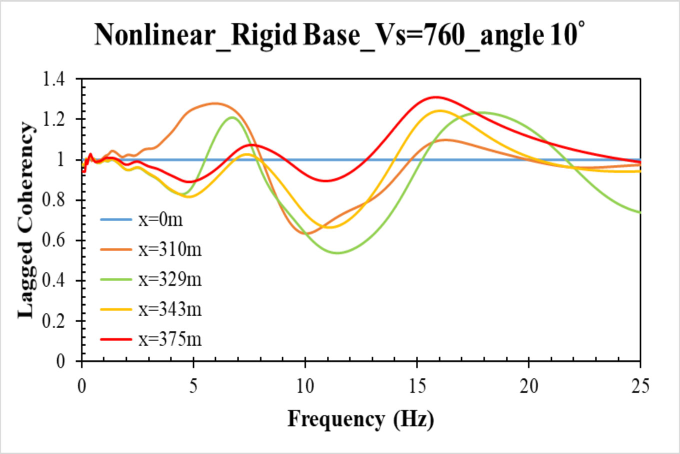

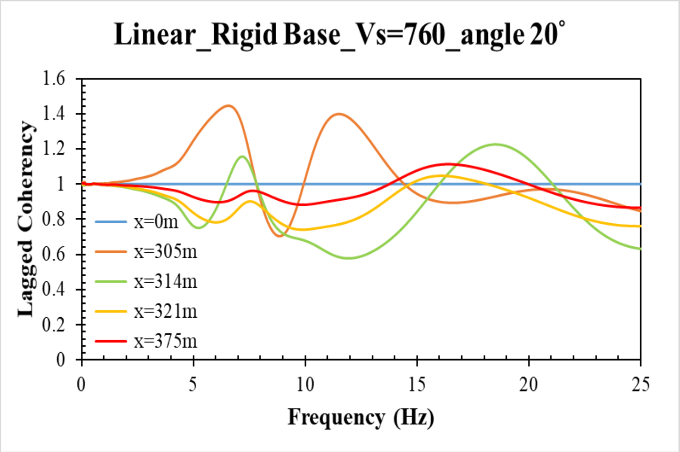

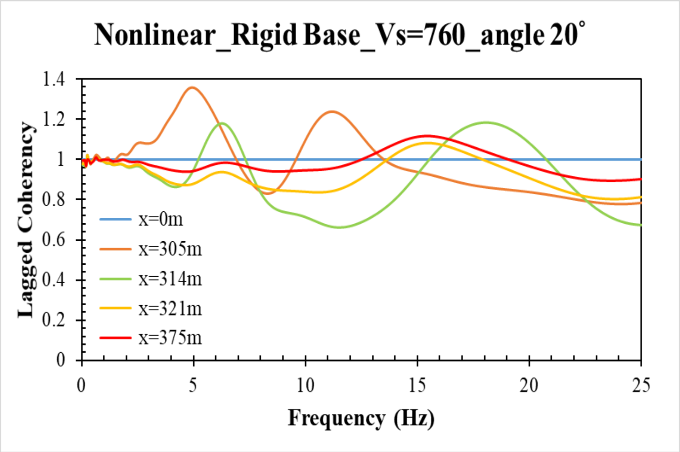

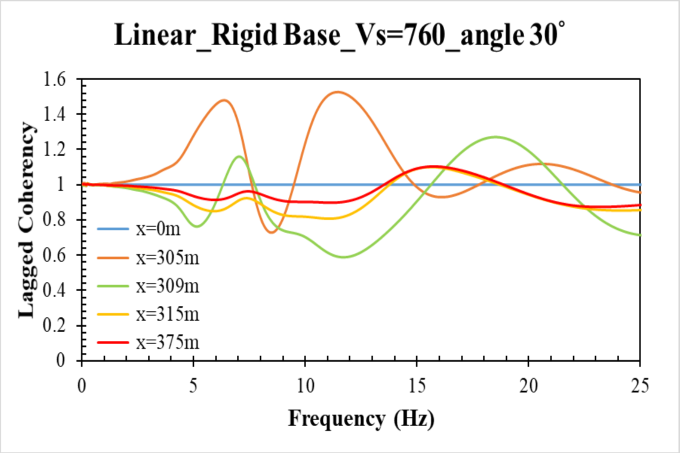

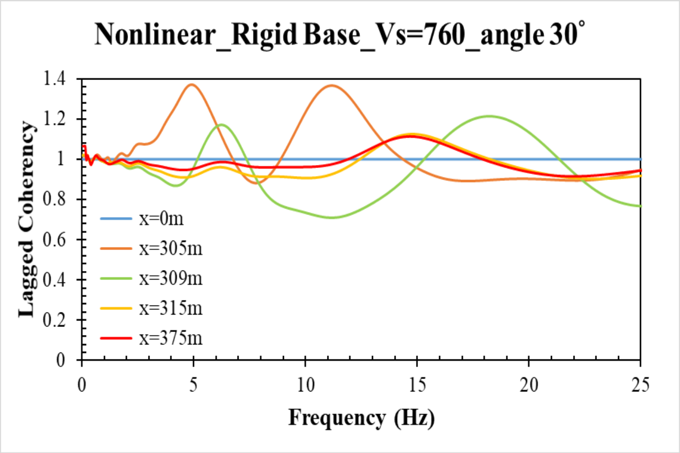

doi:10.6342/NTU201903794

(f) Cases for rigid base, shear-wave velocity 1500 m/s

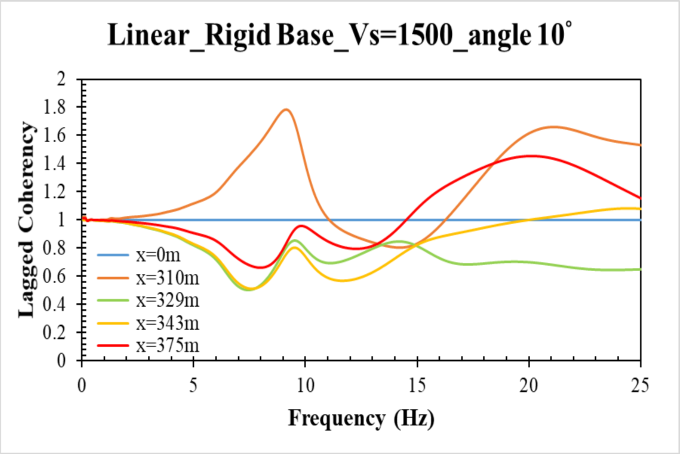

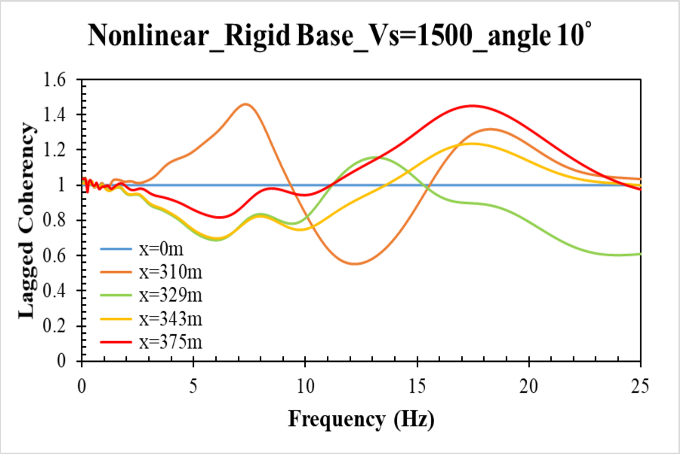

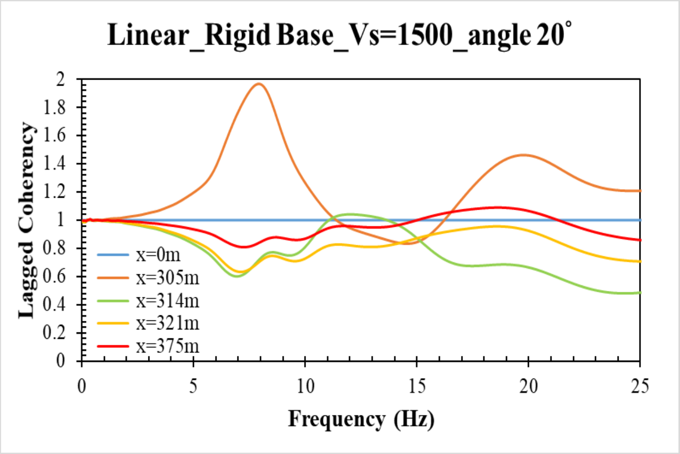

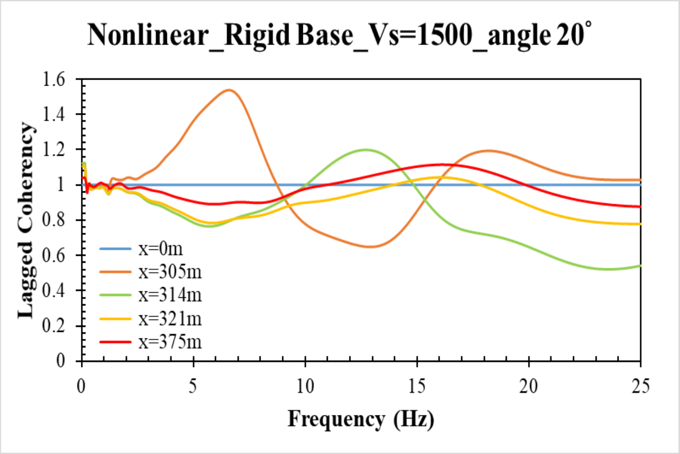

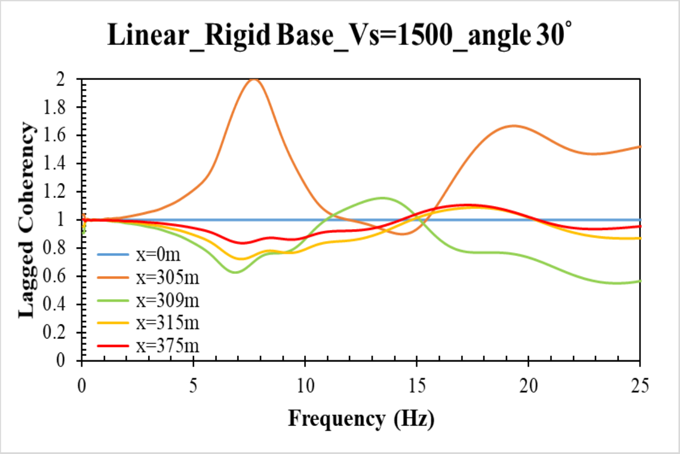

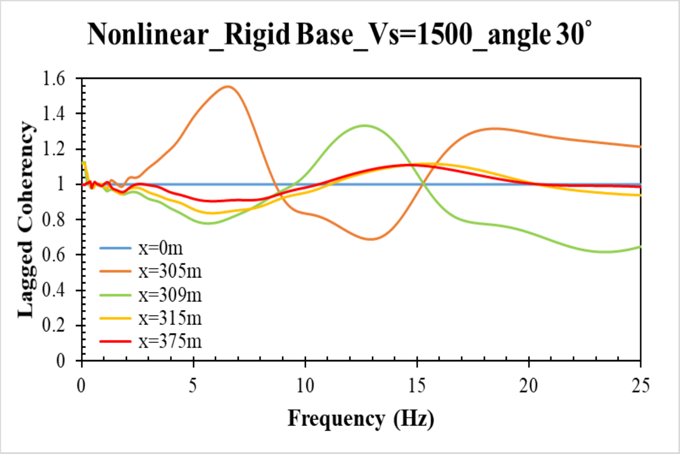

(6) Spectral acceleration spectrum in y-direction

(a) Y-SA with compliant base, Vs=500 m/s for both linear and nonlinear cases

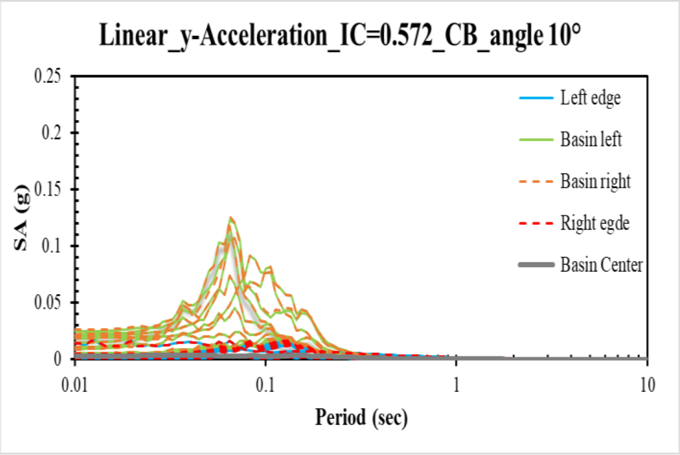

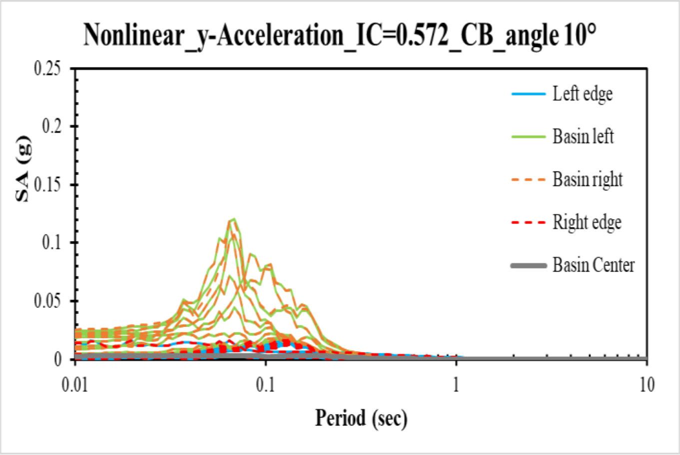

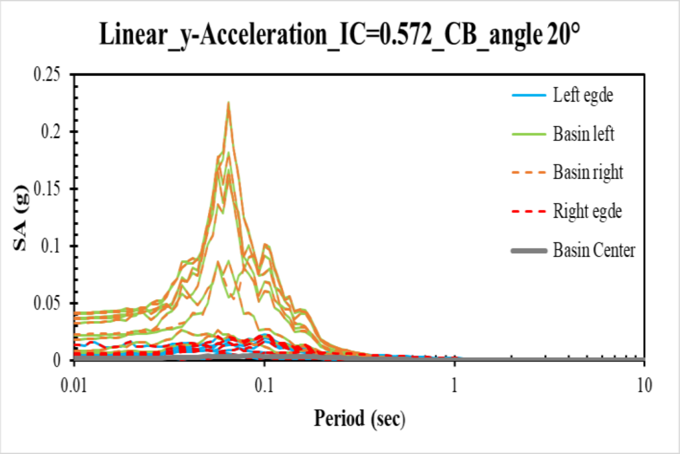

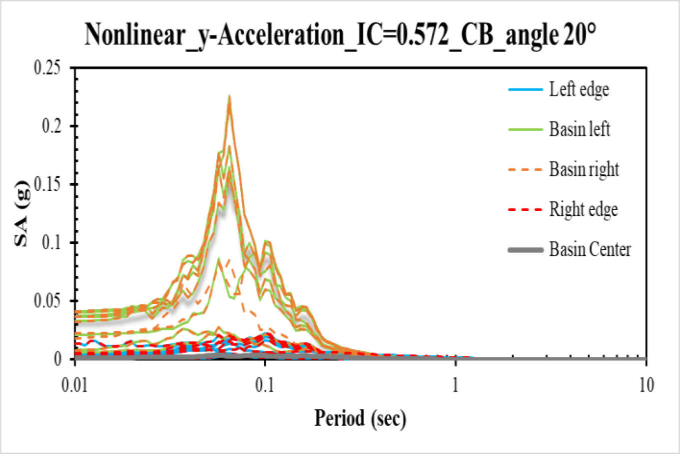

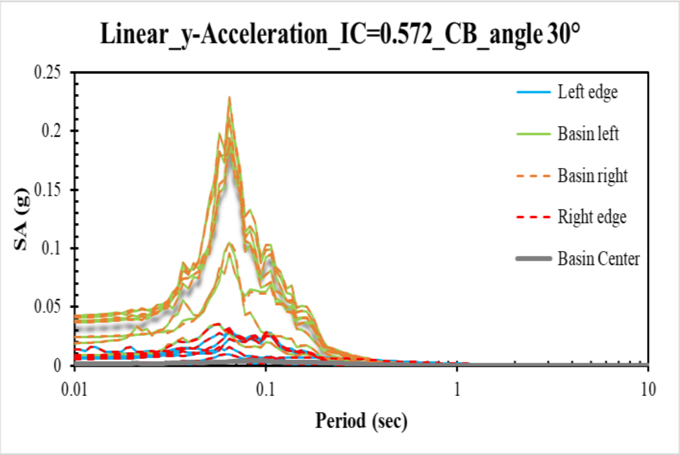

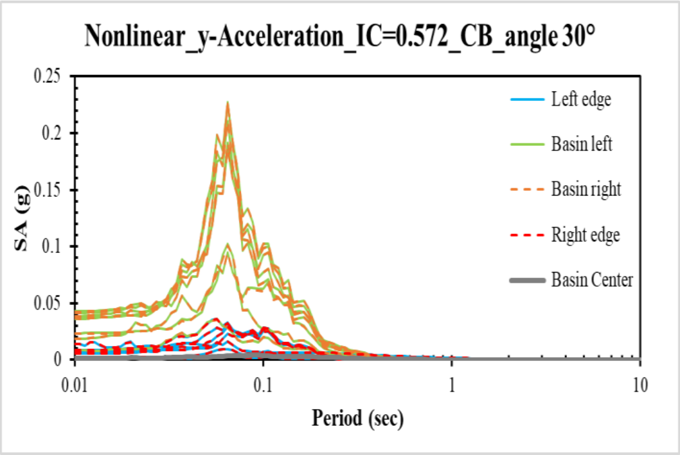

doi:10.6342/NTU201903794

(b) Y-SA with compliant base, Vs=760 m/s for both linear and nonlinear cases

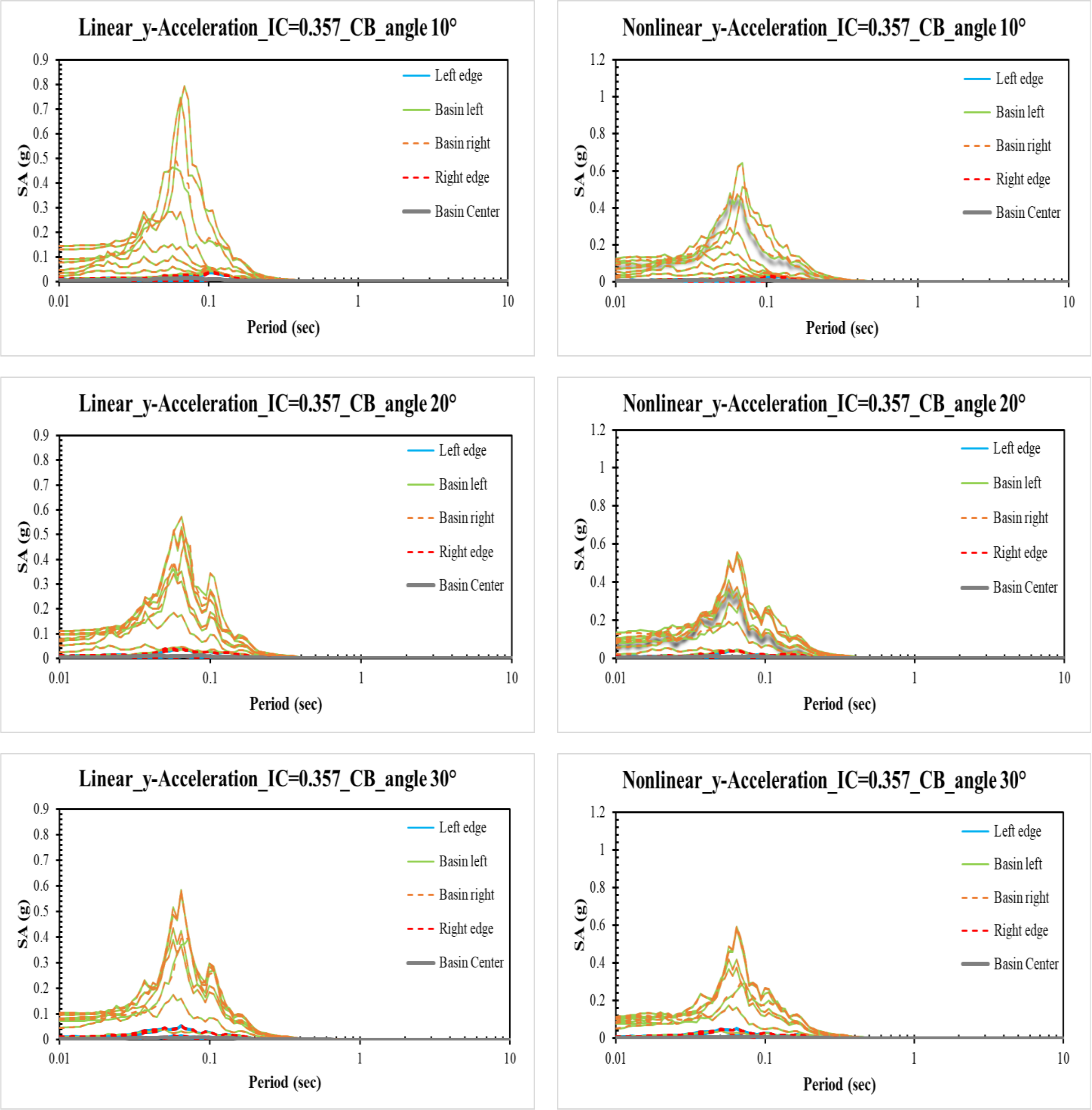

(c) Y-SA with compliant base, Vs=1500 m/s for both linear and nonlinear cases

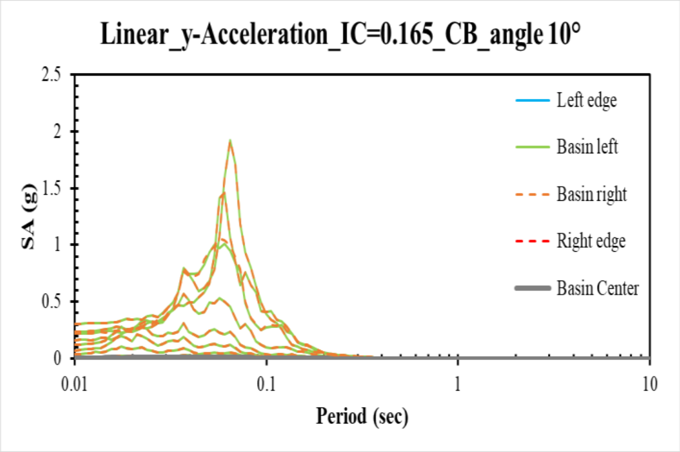

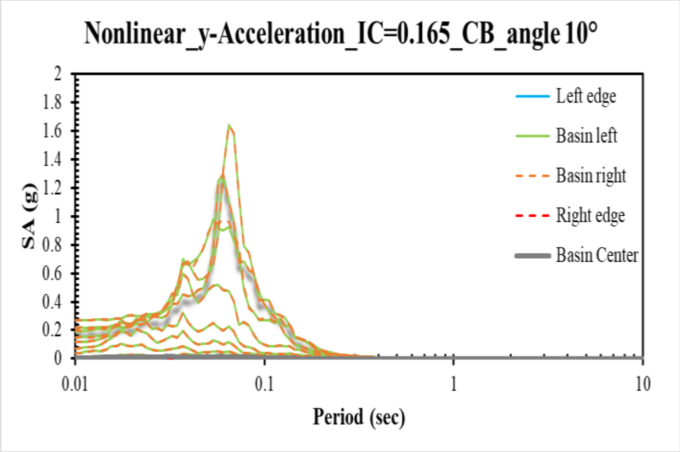

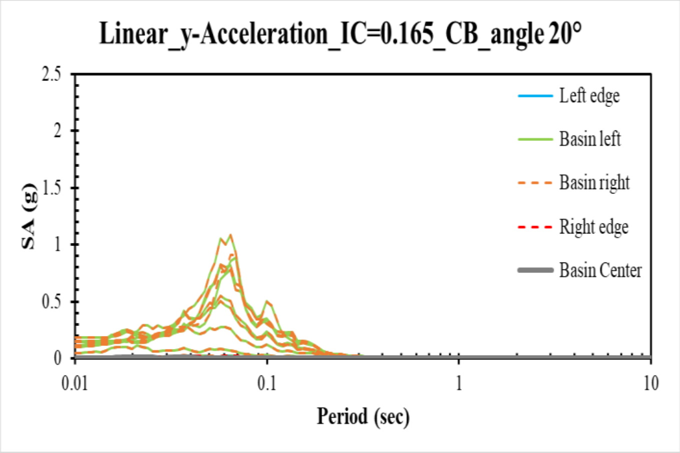

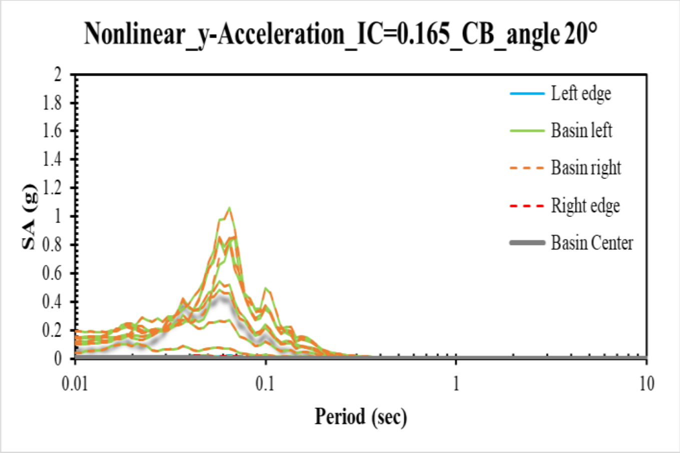

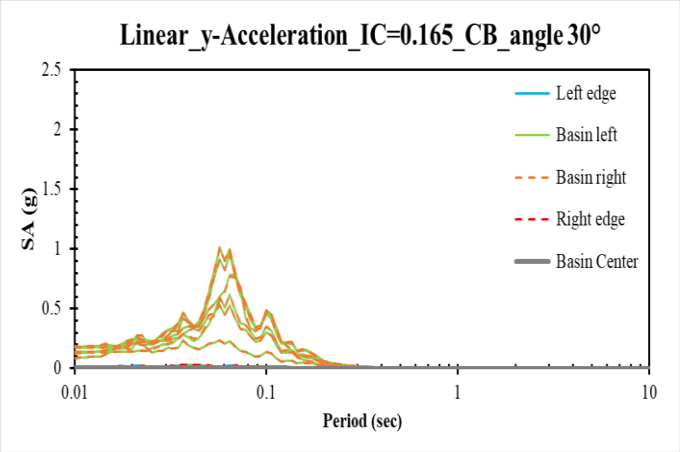

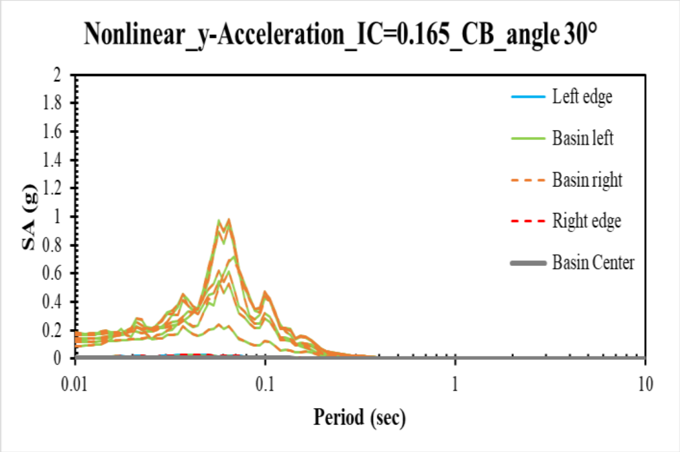

doi:10.6342/NTU201903794

(d) Y-SA with rigid base, Vs=500 m/s for both linear and nonlinear cases

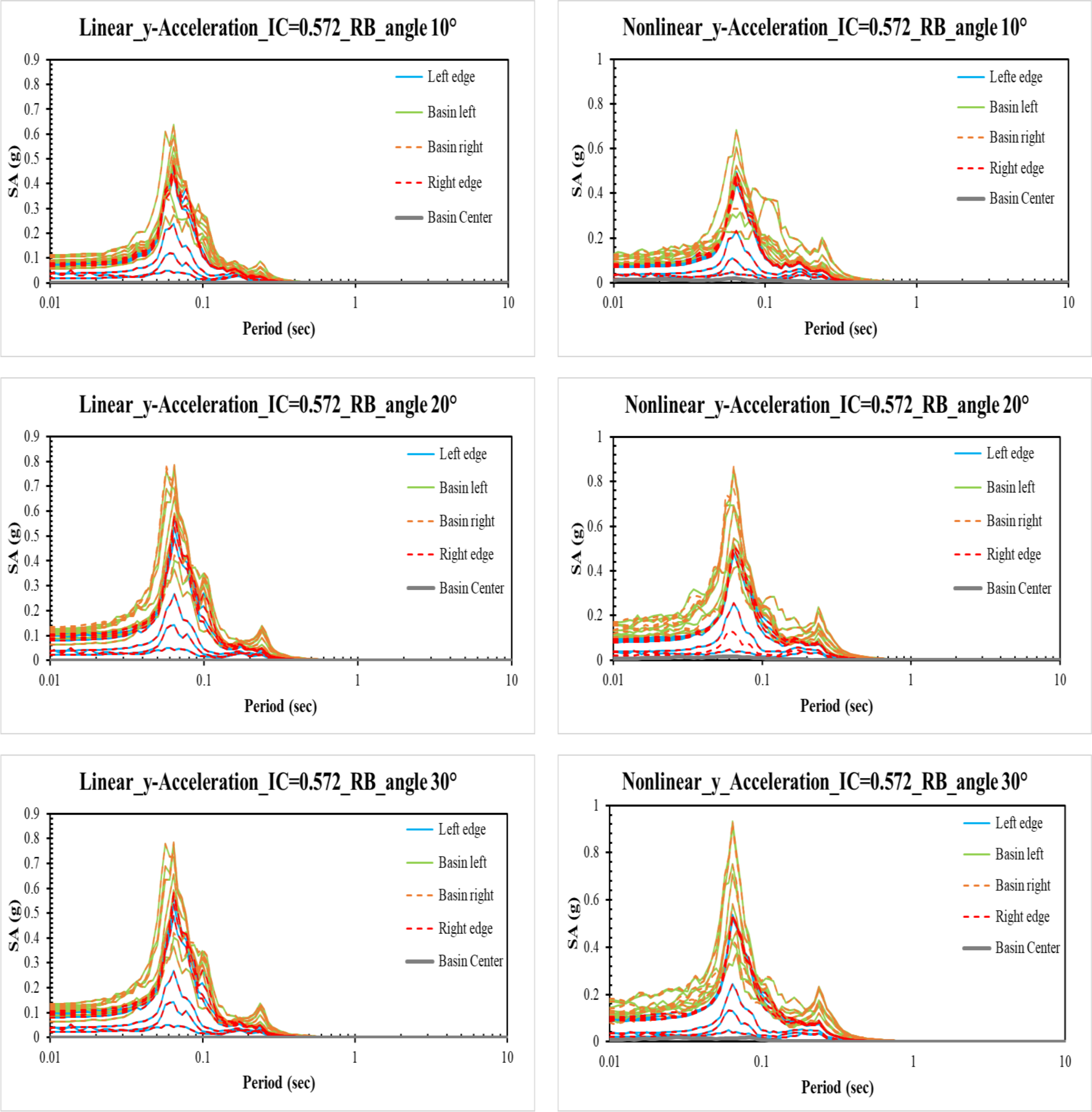

(e) Y-SA with rigid base, Vs=760 m/s for both linear and nonlinear cases

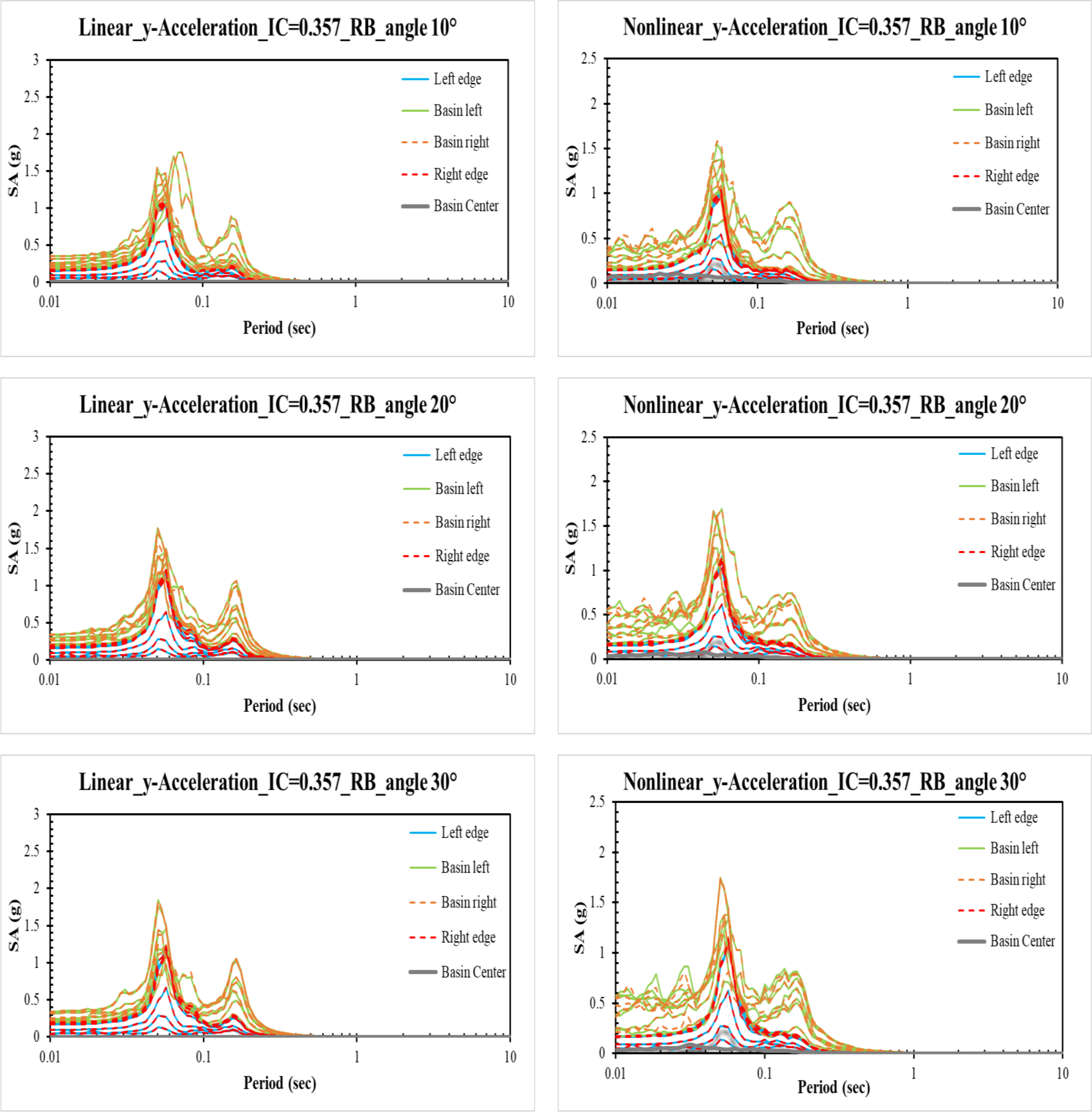

doi:10.6342/NTU201903794

(f) Y-SA with rigid base, Vs=1500 m/s for both linear and nonlinear cases

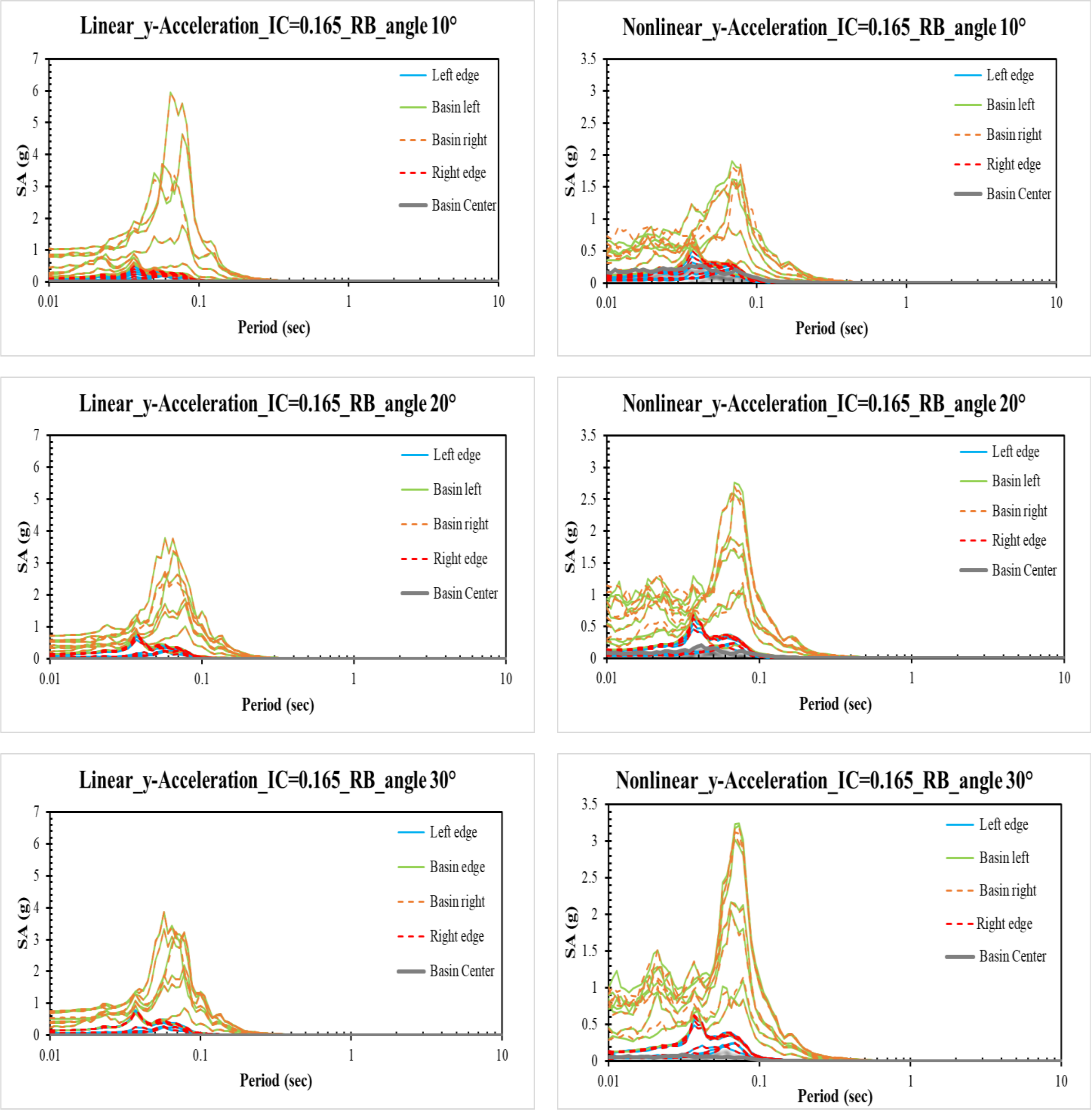

doi:10.6342/NTU201903794

### (7) Y_SA / Y_SA$_{edge}$

(a) Cases for compliant base, shear-wave velocity 500 m/s, impedance contrast 0.572

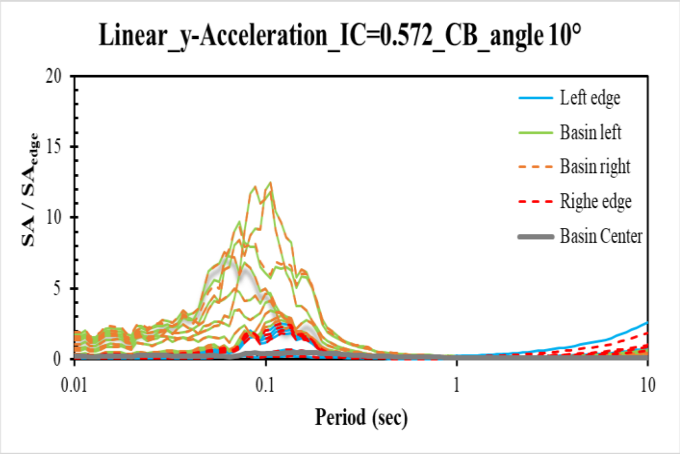

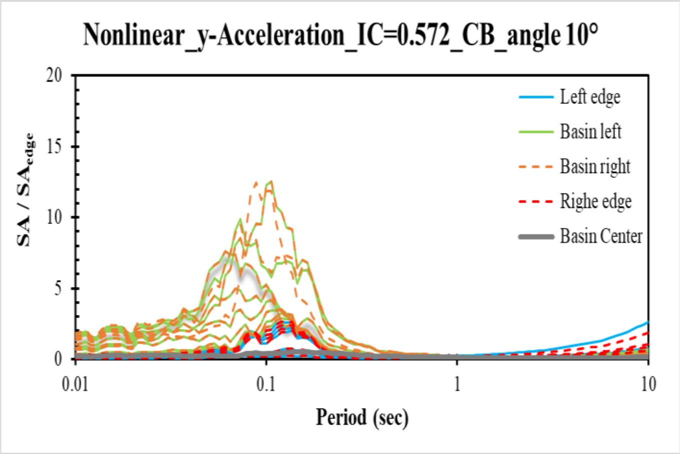

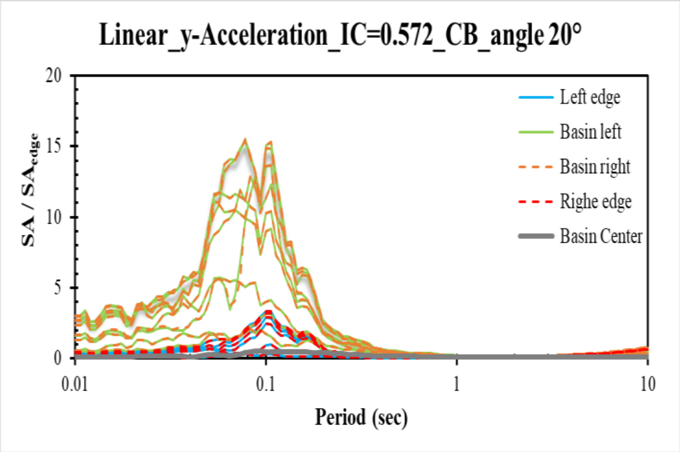

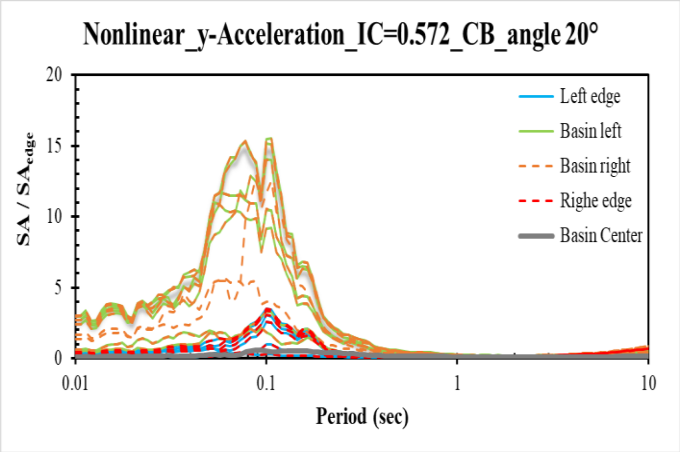

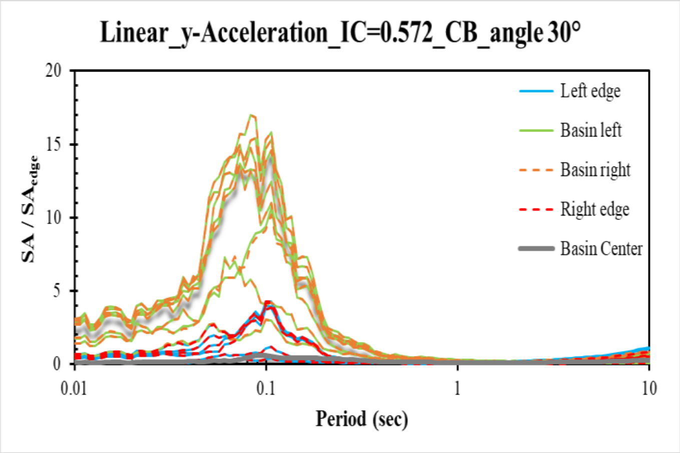

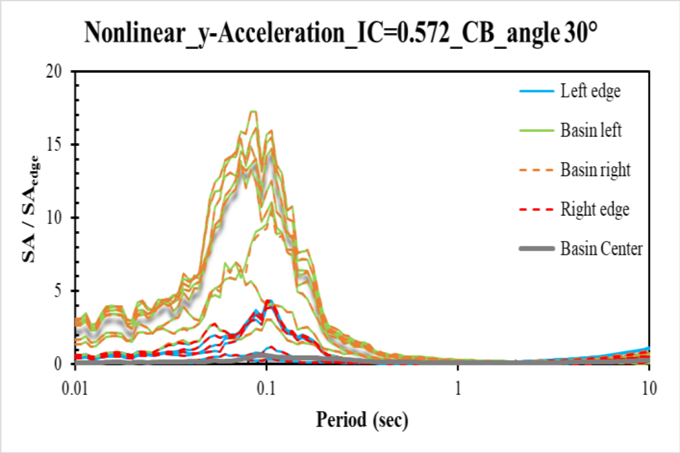

(b) Cases for compliant base, shear-wave velocity 760 m/s, impedance contrast 0.357

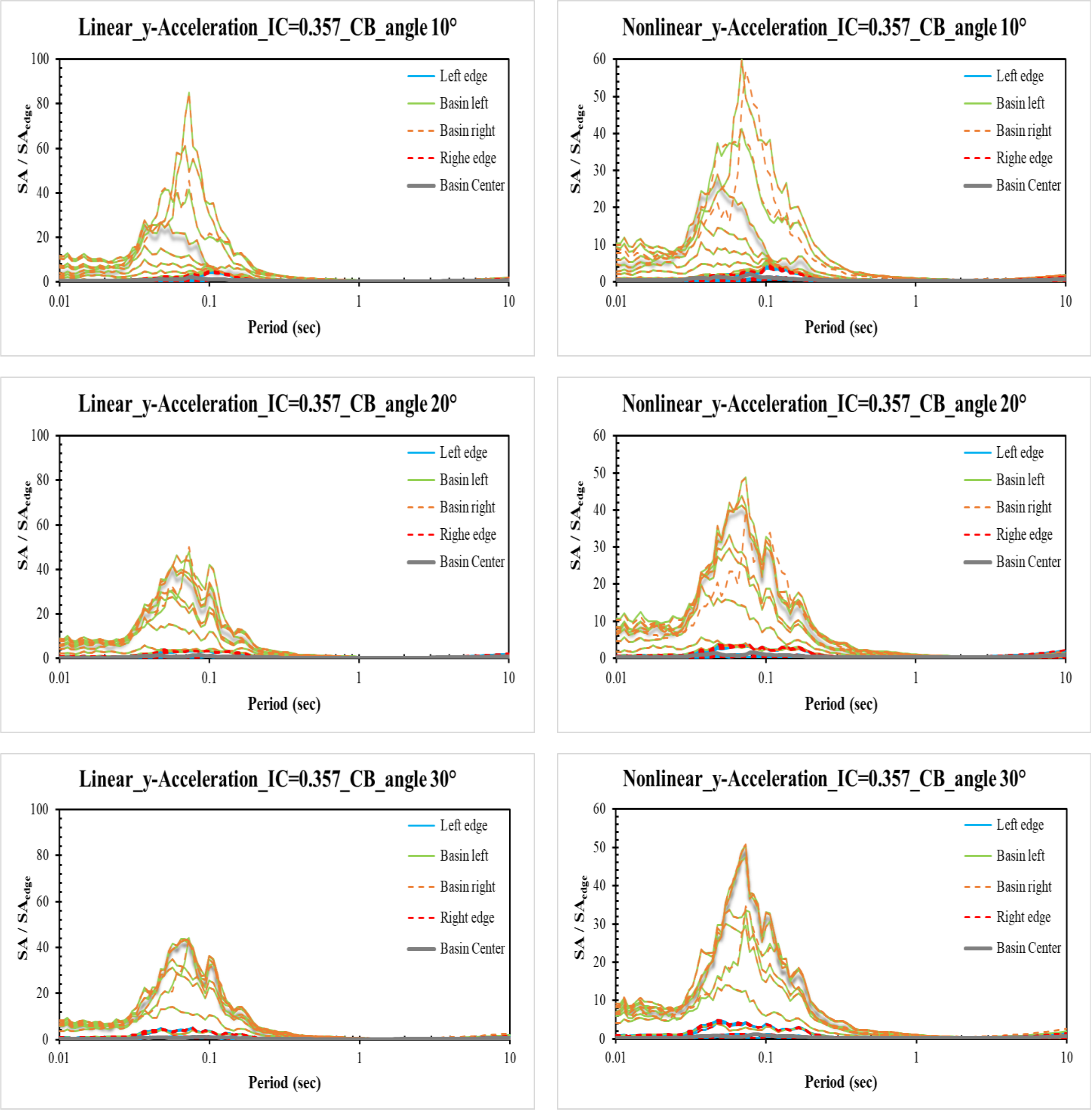

doi:10.6342/NTU201903794

(c) Cases for compliant base, shear-wave velocity 1500 m/s, impedance contrast 0.165

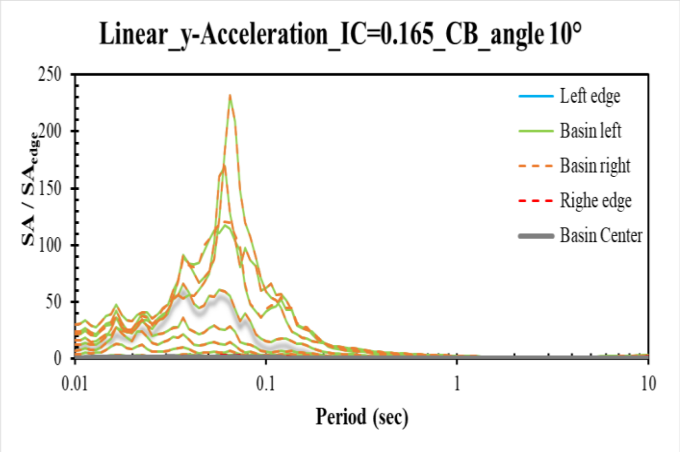

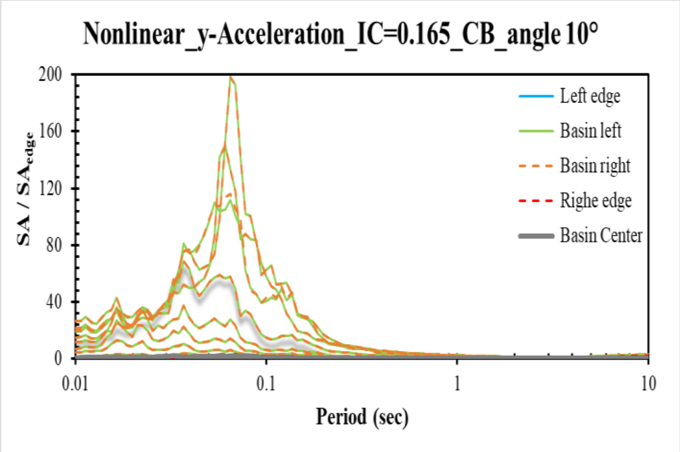

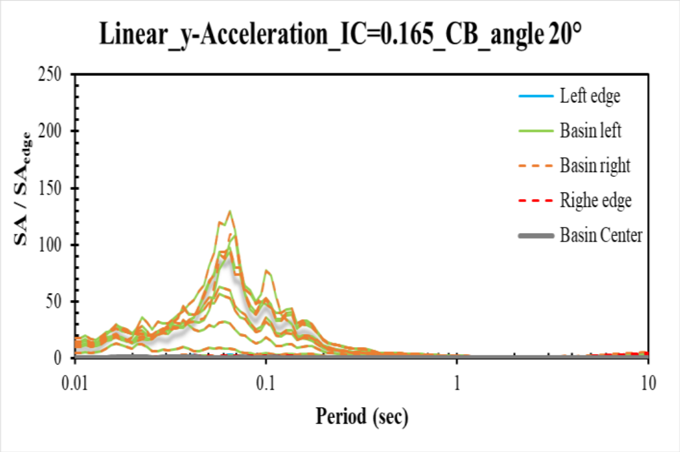

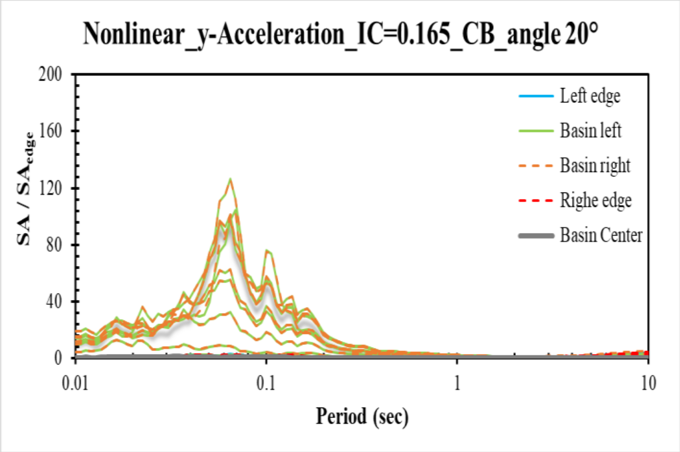

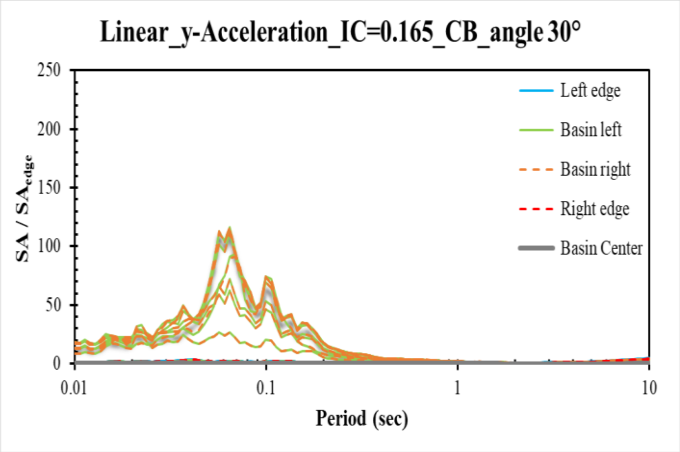

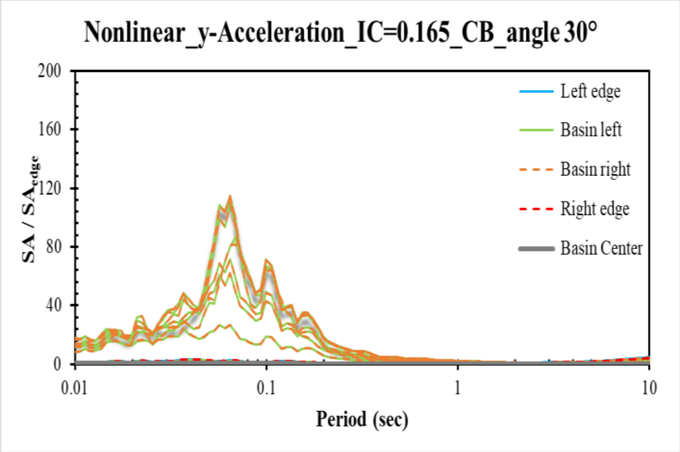

(d) Cases for rigid base, shear-wave velocity 500 m/s, impedance contrast 0.572

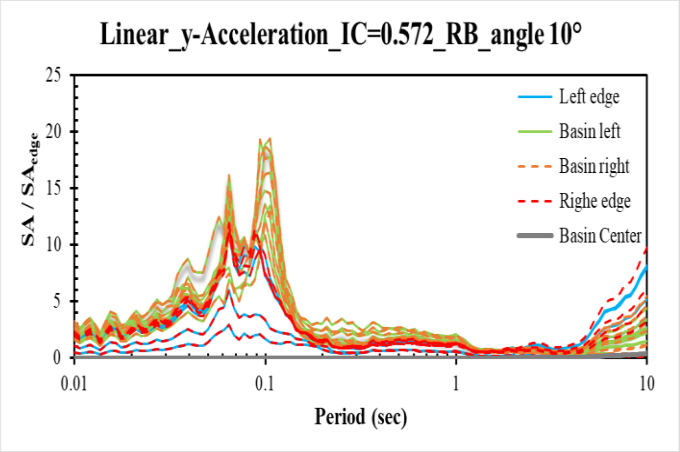
Linear_y-Acceleration_IC=0.572_RB_angle 10°

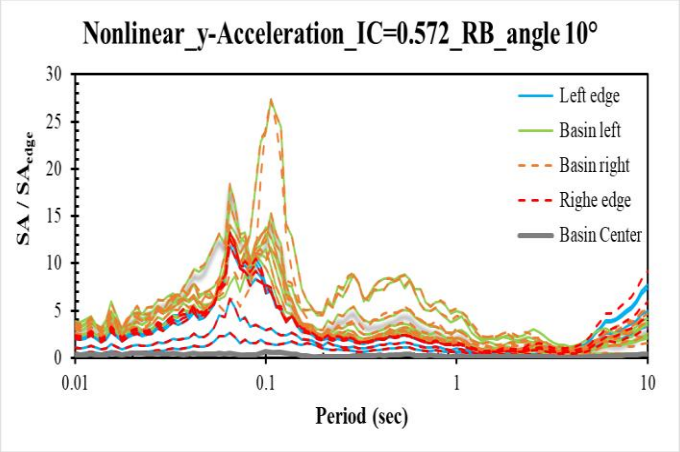
Nonlinear_y-Acceleration_IC=0.572_RB_angle 10°

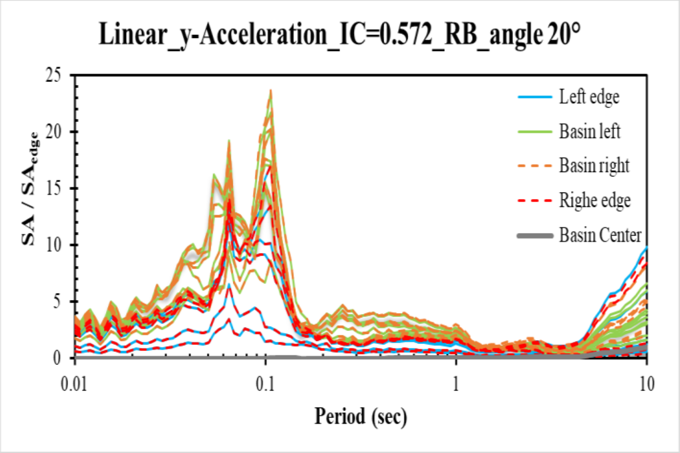
Linear_y-Acceleration_IC=0.572_RB_angle 20°

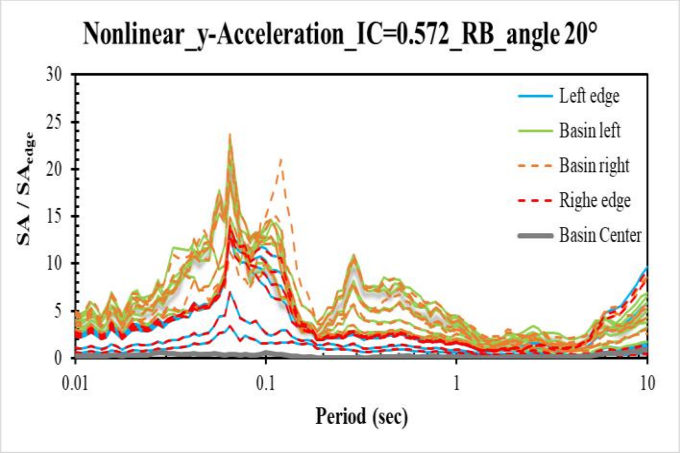
Nonlinear_y-Acceleration_IC=0.572_RB_angle 20°

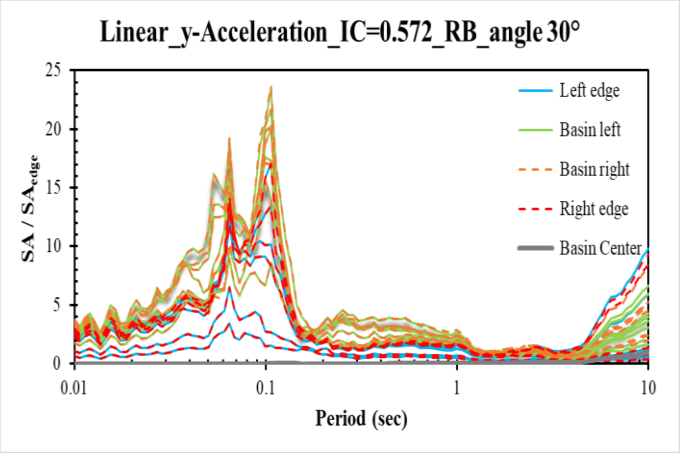
Linear_y-Acceleration_IC=0.572_RB_angle 30°

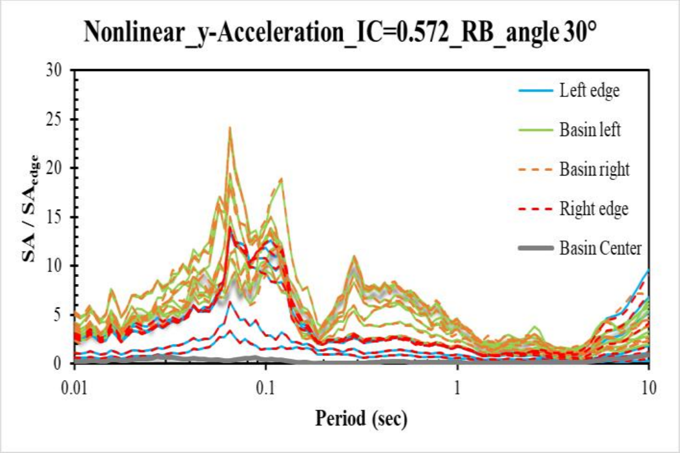
Nonlinear_y-Acceleration_IC=0.572_RB_angle 30°

(e) Cases for rigid base, shear-wave velocity 760 m/s, impedance contrast 0.357

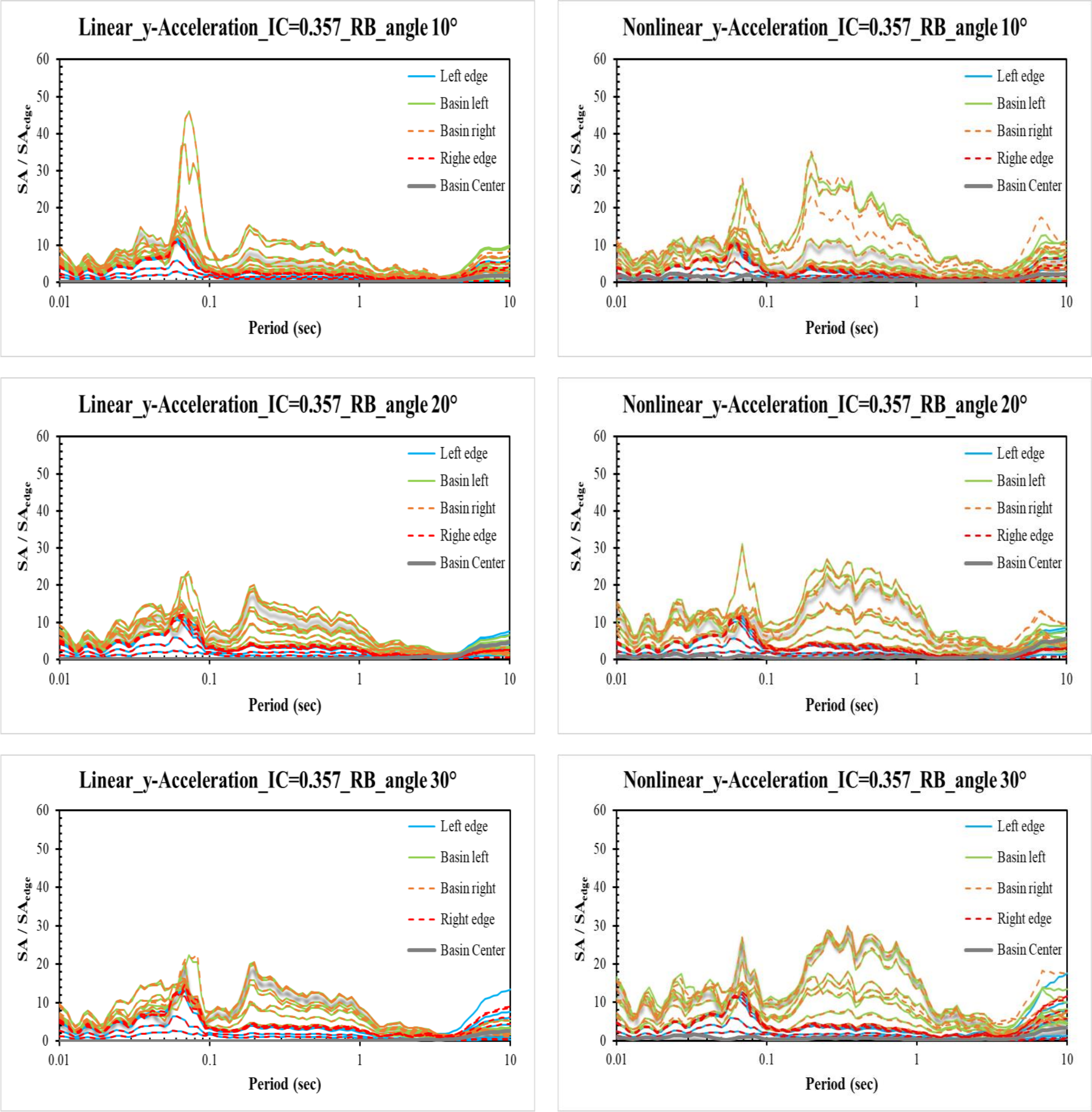

(f) Cases for rigid base, shear-wave velocity 1500 m/s, impedance contrast 0.165

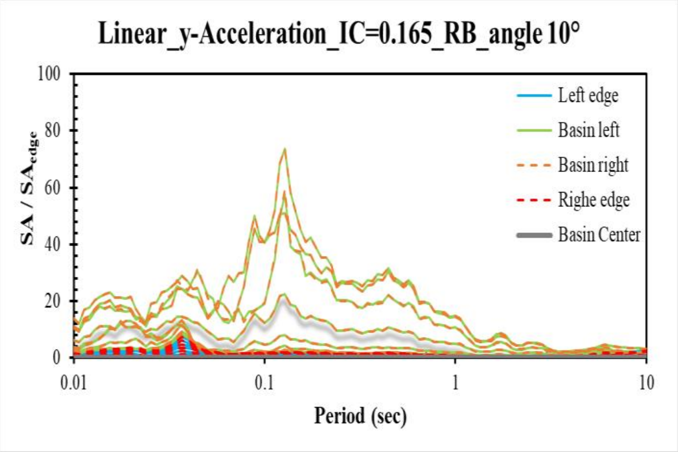
Linear_y-Acceleration_IC=0.165_RB_angle 10°

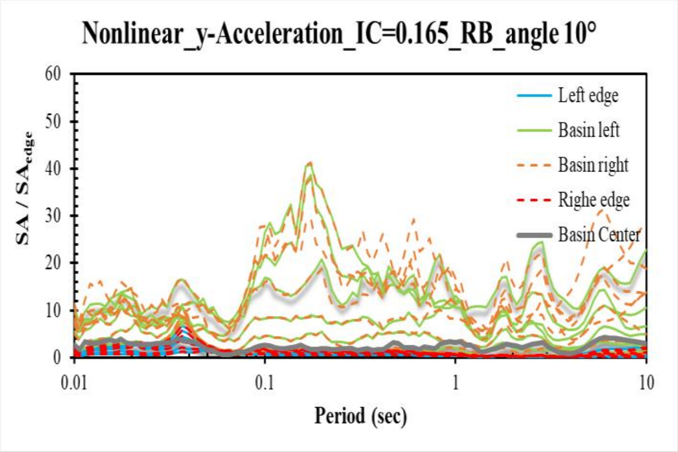
Nonlinear_y-Acceleration_IC=0.165_RB_angle 10°

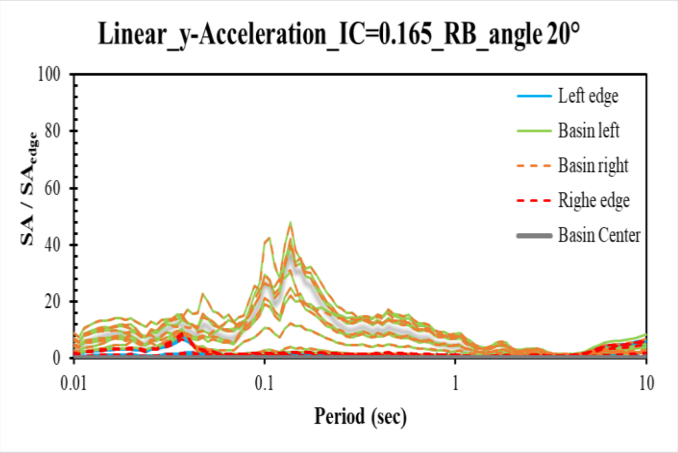
Linear_y-Acceleration_IC=0.165_RB_angle 20°

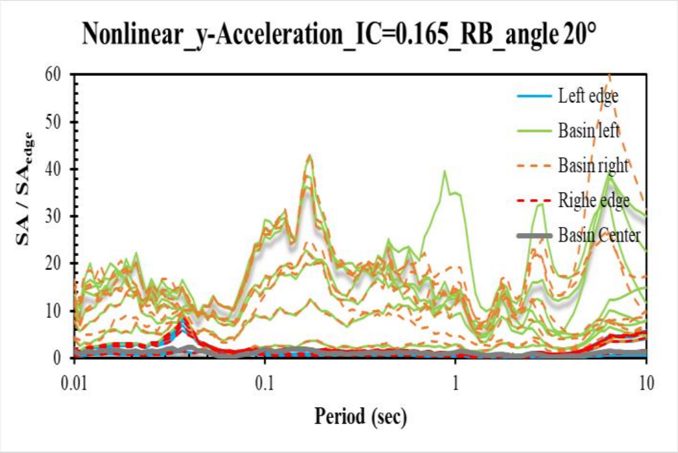
Nonlinear_y-Acceleration_IC=0.165_RB_angle 20°

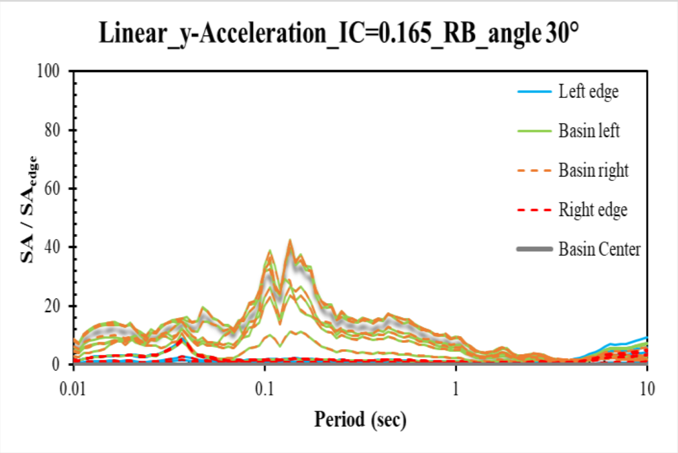
Linear_y-Acceleration_IC=0.165_RB_angle 30°

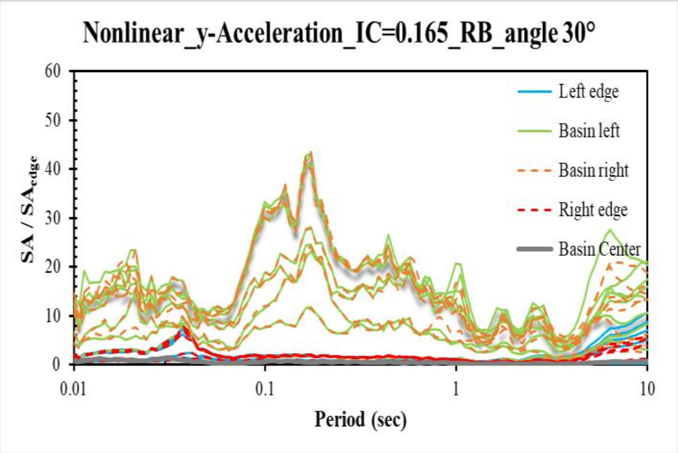
Nonlinear_y-Acceleration_IC=0.165_RB_angle 30°

doi:10.6342/NTU201903794

(8) PGA of y-acceleration in different periods for both compliant and rigid base

(a) PGA with compliant base, period 0.1 sec

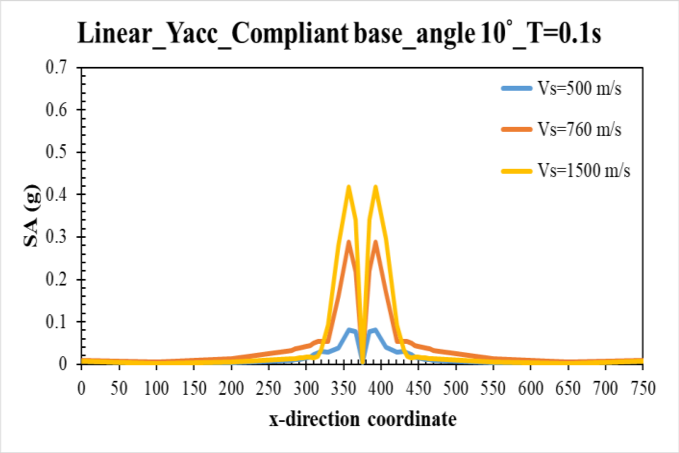

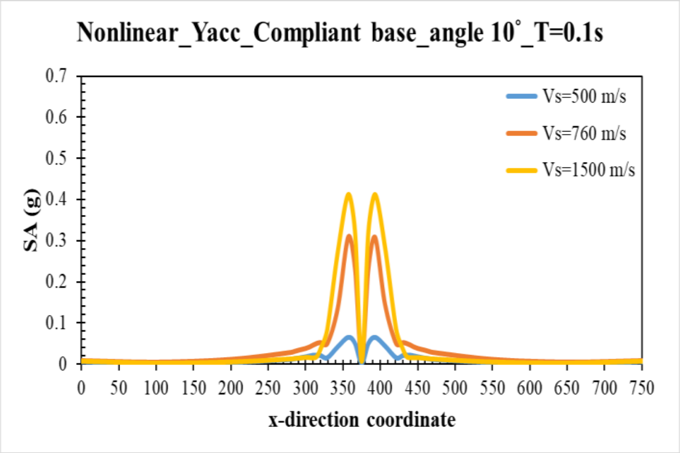

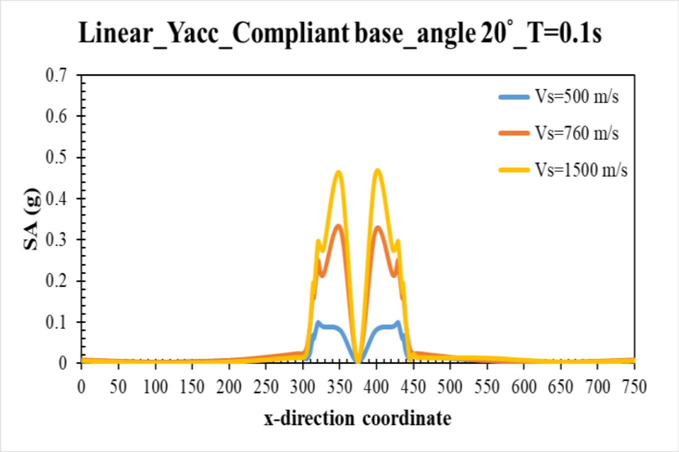

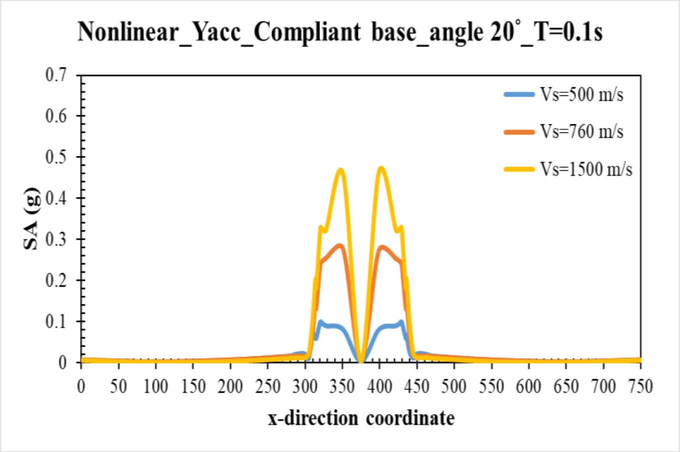

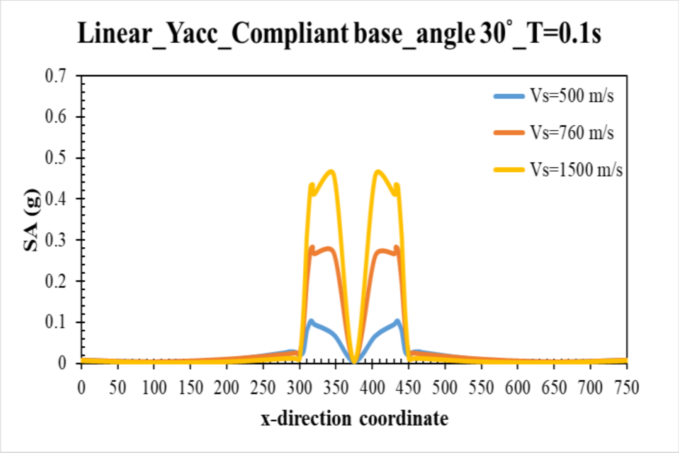

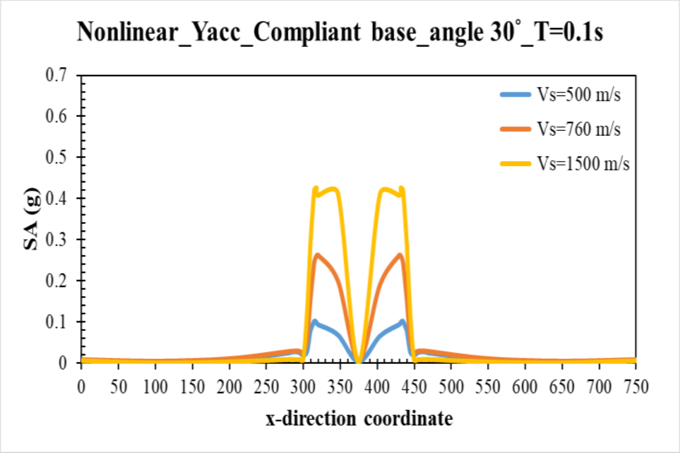

(b) PGA with rigid base, period 0.1 sec

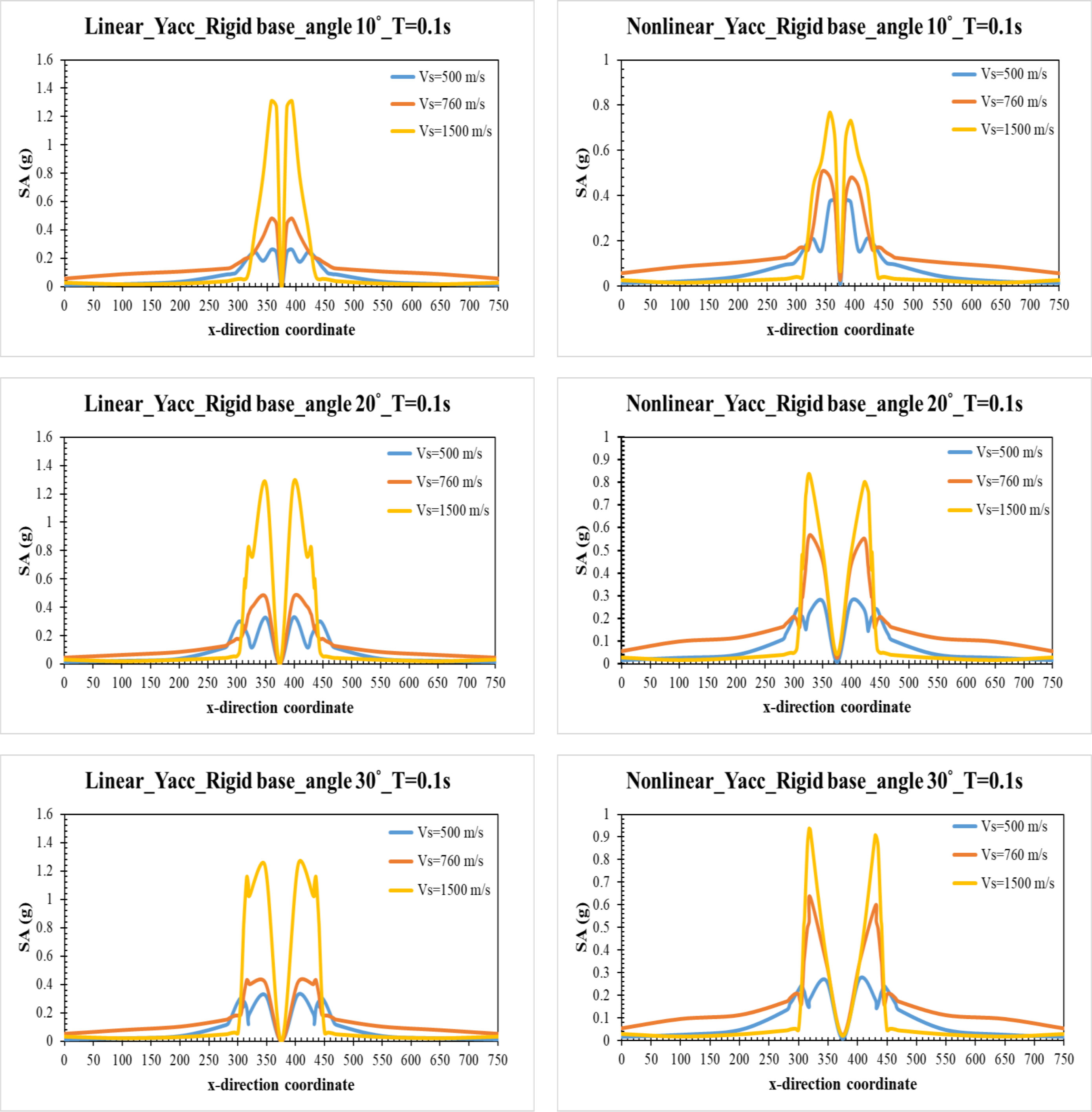

doi:10.6342/NTU201903794

(c) PGA with compliant base, period 0.3 sec

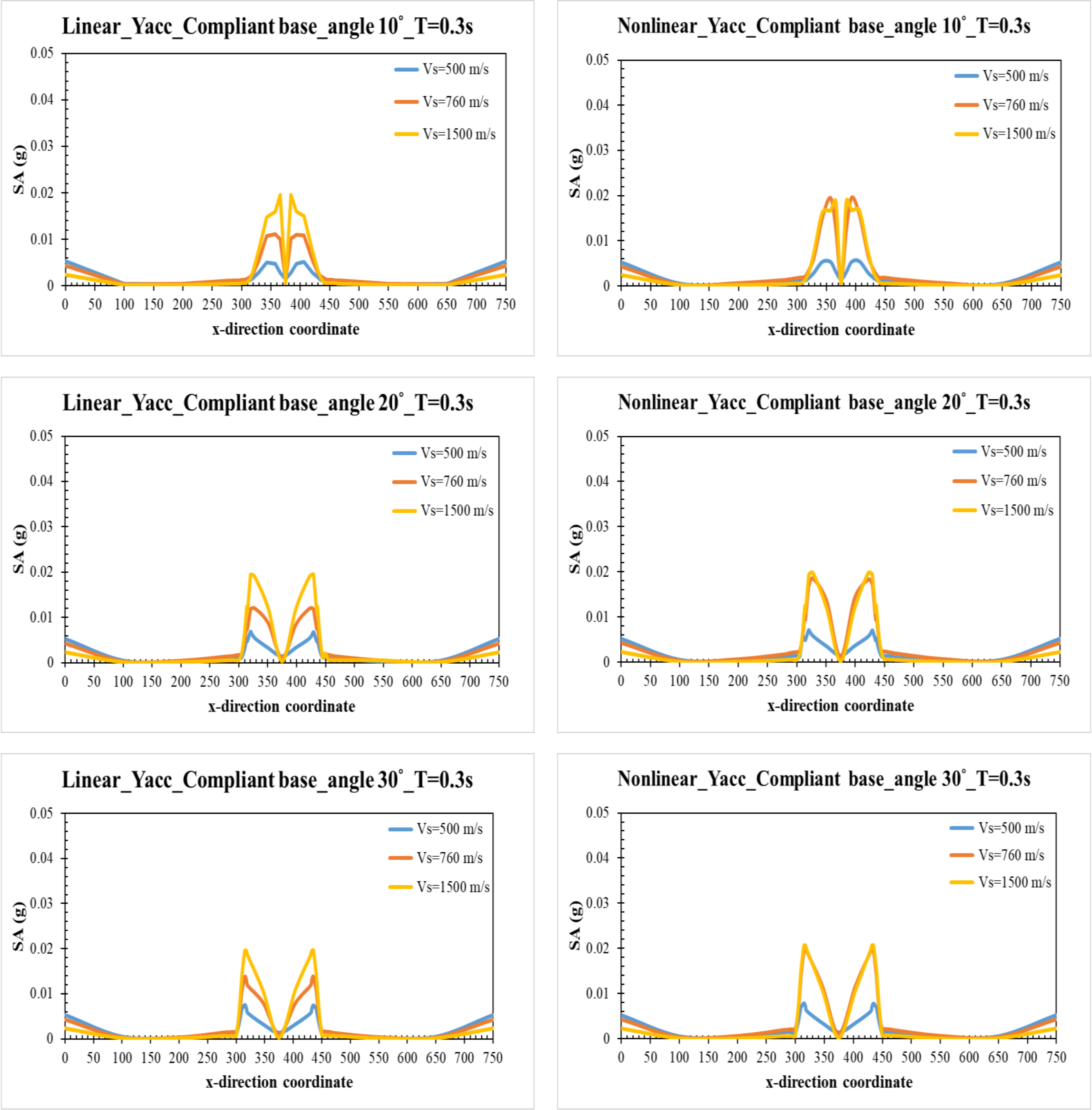

doi:10.6342/NTU201903794

(d) PGA with rigid base, period 0.3 sec

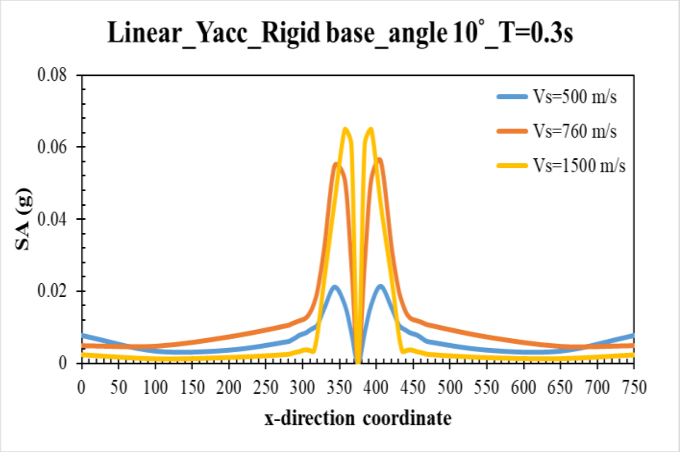
Linear_Yacc_Rigid base_angle 10°_T=0.3s

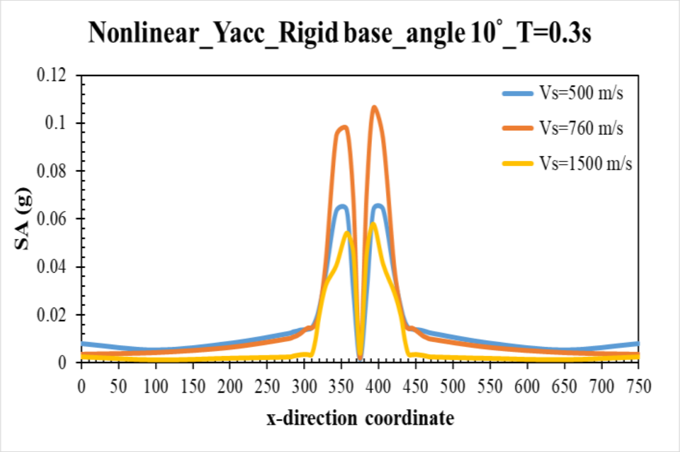
Nonlinear_Yacc_Rigid base_angle 10°_T=0.3s

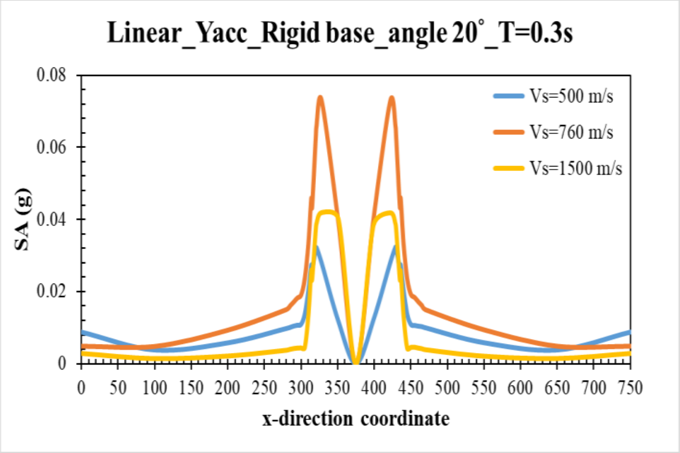
Linear_Yacc_Rigid base_angle 20°_T=0.3s

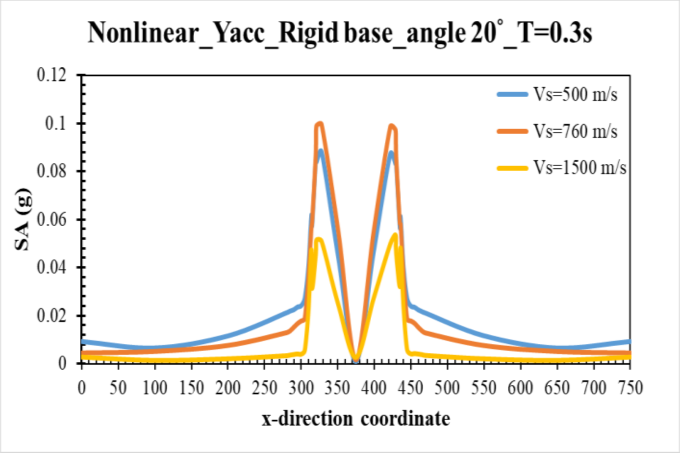
Nonlinear_Yacc_Rigid base_angle 20°_T=0.3s

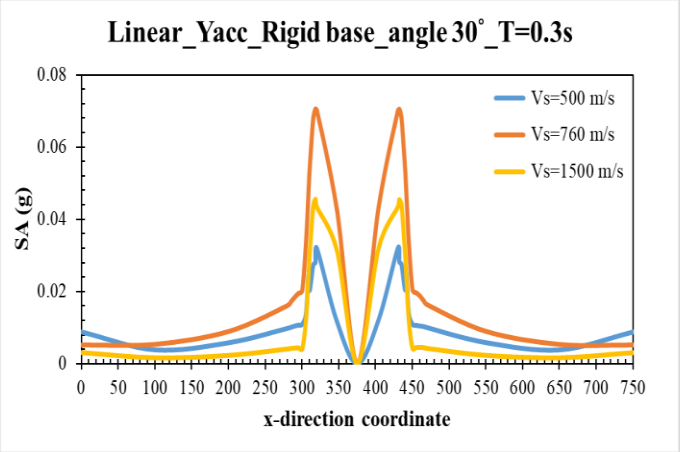
Linear_Yacc_Rigid base_angle 30°_T=0.3s

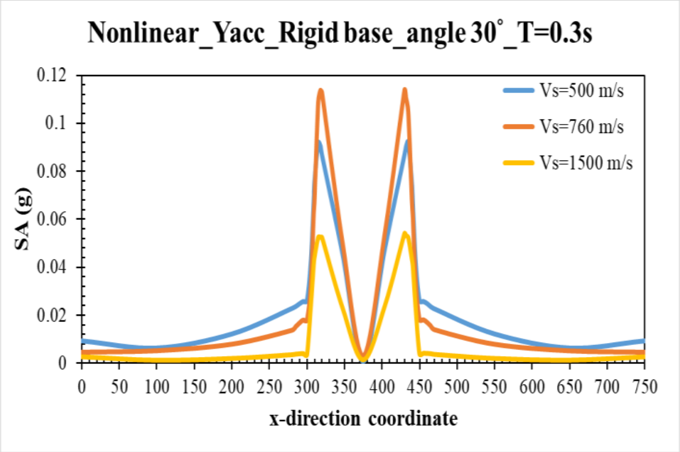
Nonlinear_Yacc_Rigid base_angle 30°_T=0.3s

### (9) Ratio of x-PGA and y-PGA at specific period

#### (a) PGA ratio with compliant base, period 0.1 sec

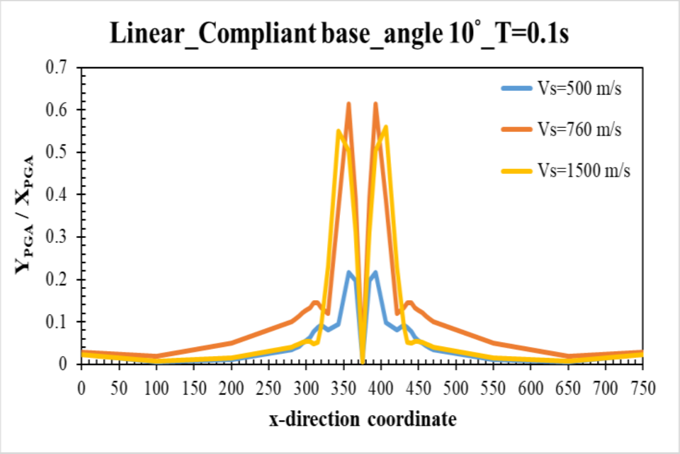

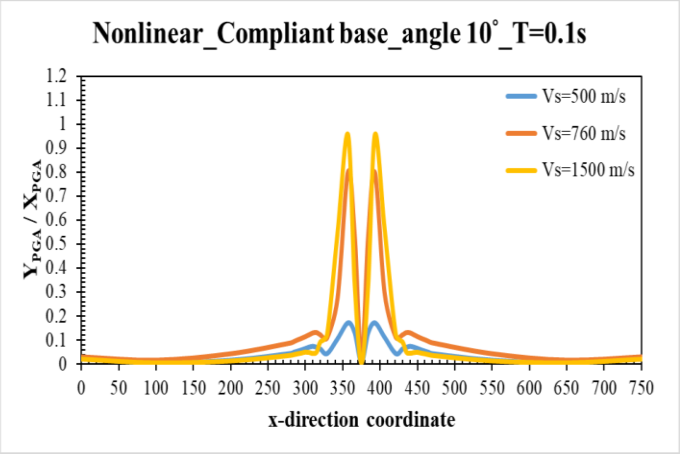

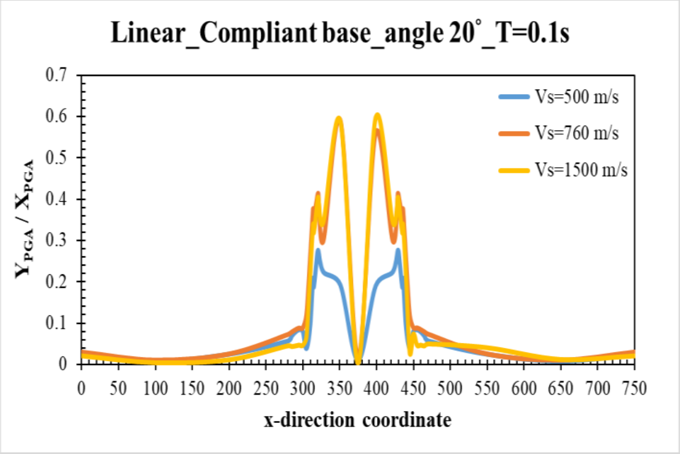

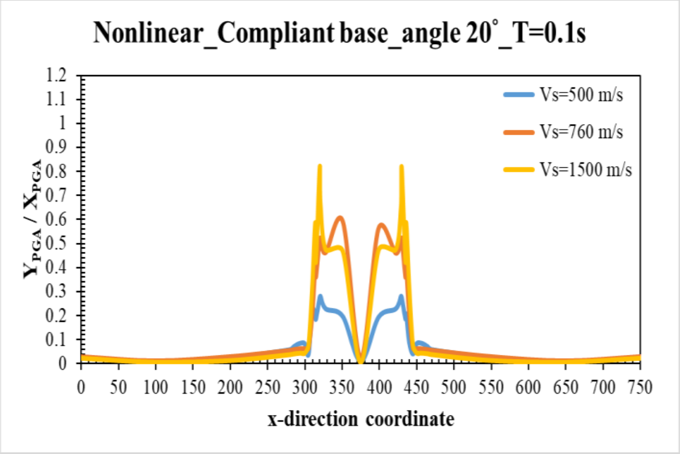

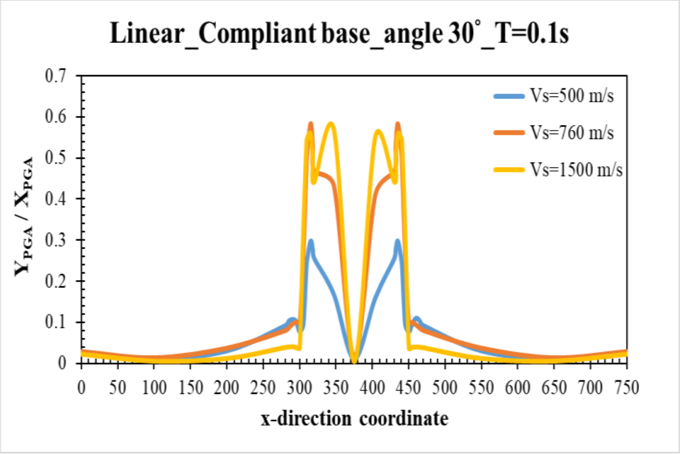

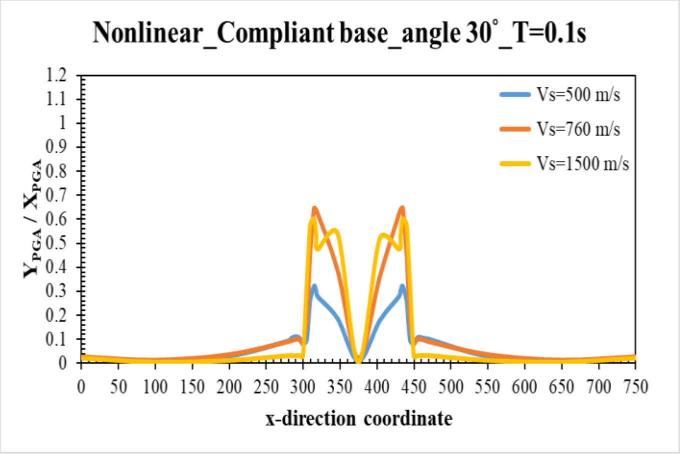

doi:10.6342/NTU201903794

(b) PGA ratio with rigid base, period 0.1 sec

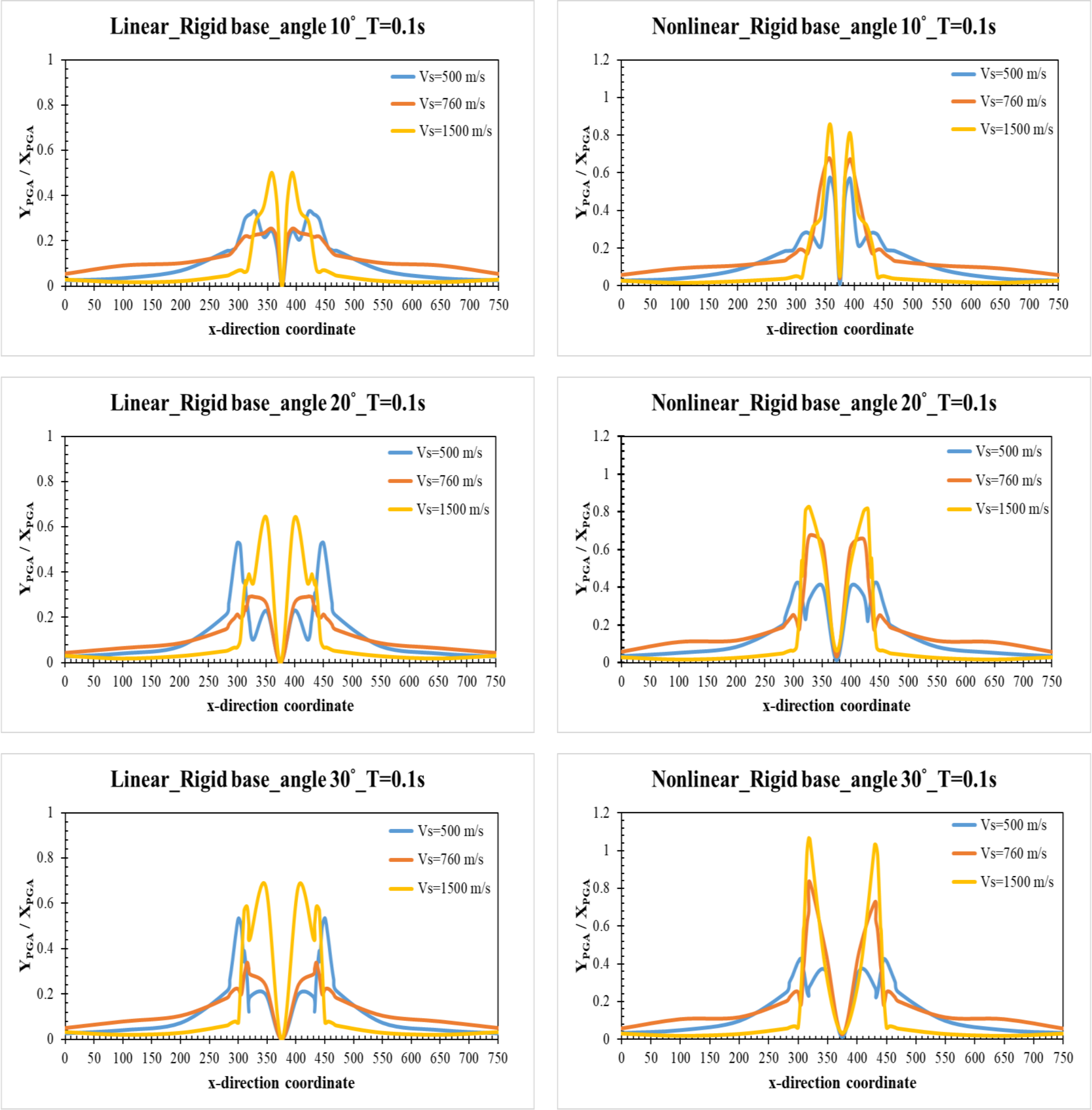

(c) PGA ratio with compliant base, period 0.3 sec

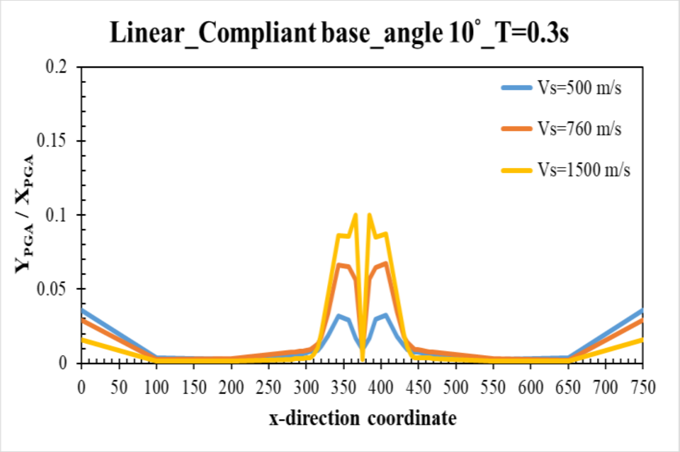
Linear_Compliant base_angle 10°_T=0.3s

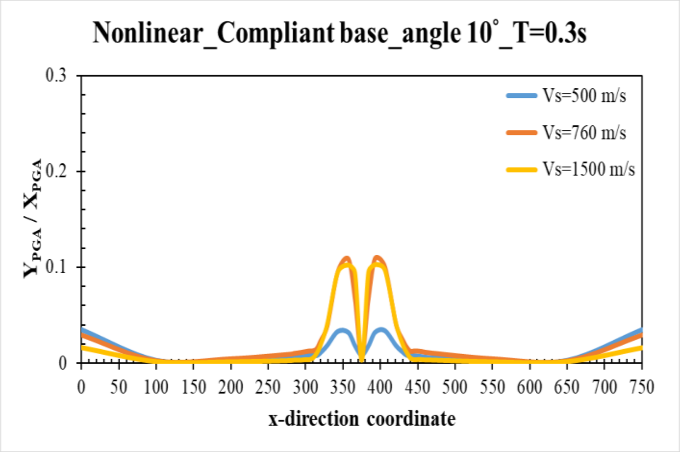
Nonlinear_Compliant base_angle 10°_T=0.3s

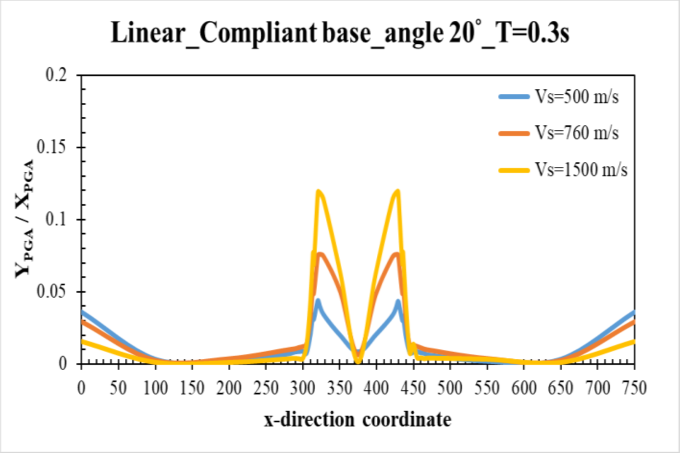
Linear_Compliant base_angle 20°_T=0.3s

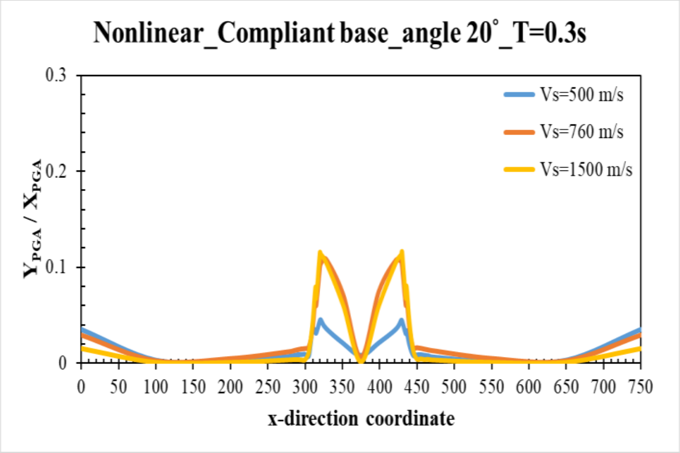
Nonlinear_Compliant base_angle 20°_T=0.3s

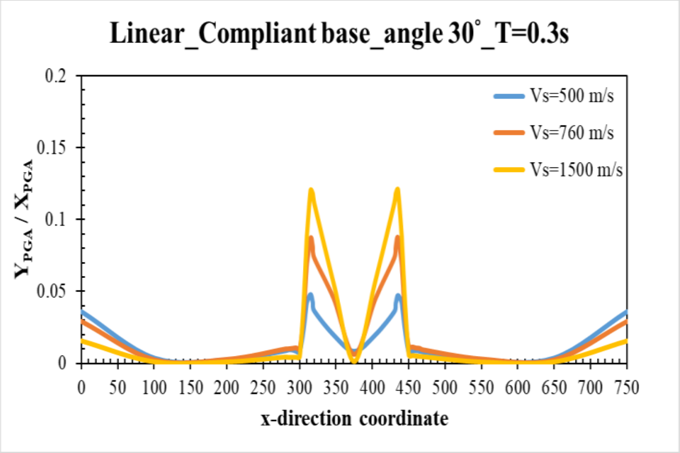
Linear_Compliant base_angle 30°_T=0.3s

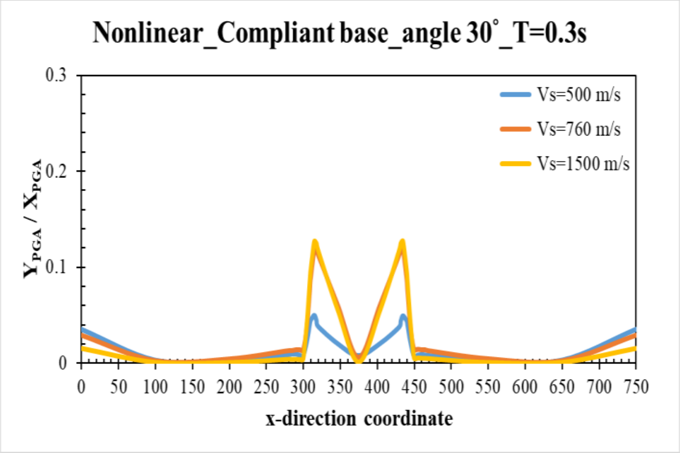
Nonlinear_Compliant base_angle 30°_T=0.3s

doi:10.6342/NTU201903794

(d) PGA ratio with rigid base, period 0.3 sec

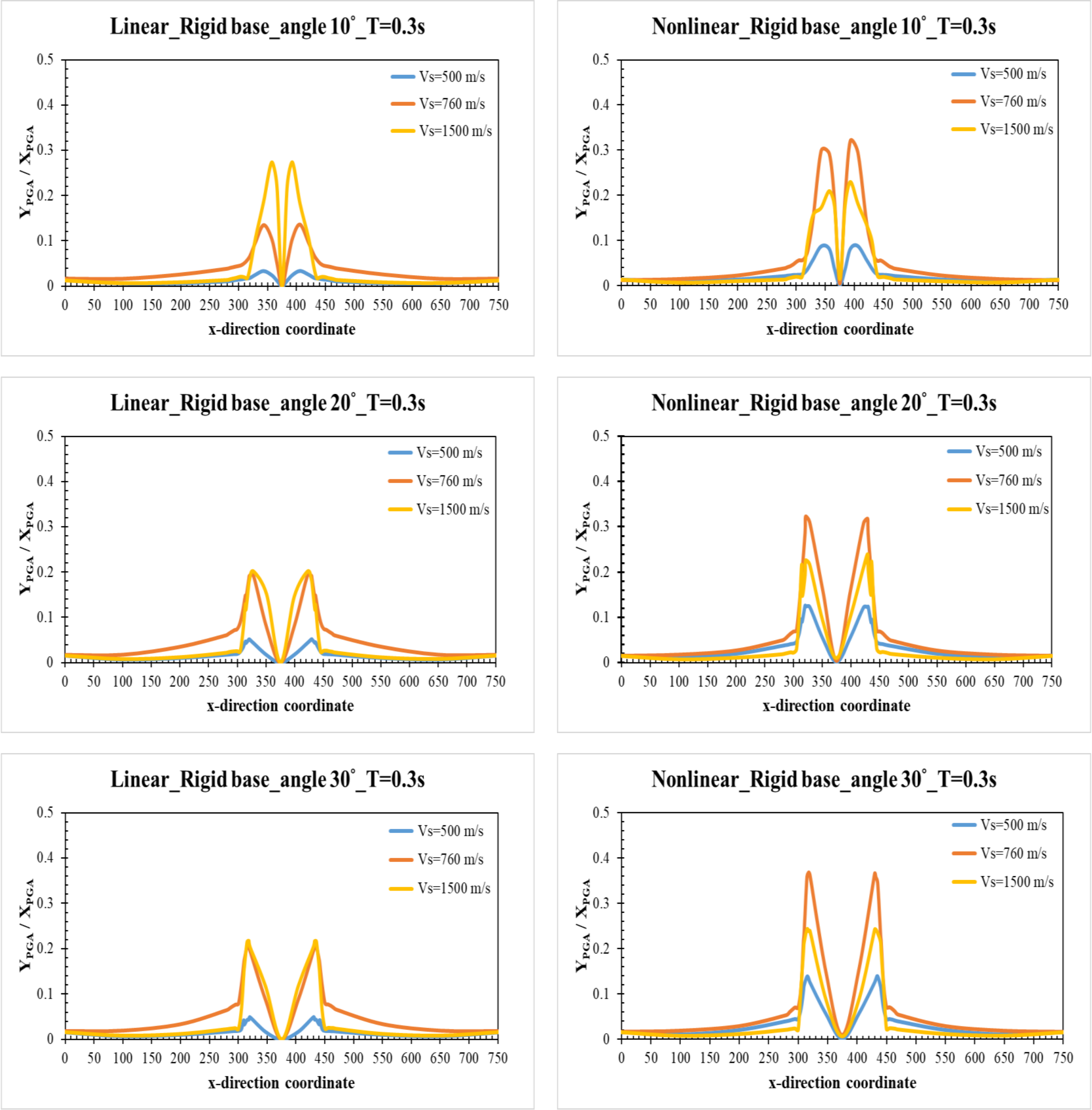

doi:10.6342/NTU201903794